

Transportation
Kentucky Transportation Center Research
Report

University of Kentucky

Year 1998

Experimental Analysis and Analytical
Modeling of Bridges With and Without
Diaphragms

James J. Griffin* Issam E. Harik[†]
David L. Allen[‡]

*LJB, Inc.

[†]University of Kentucky, harik@uky.edu

[‡]University of Kentucky, dallen@engr.uky.edu

This paper is posted at UKnowledge.

https://uknowledge.uky.edu/ktc_researchreports/365

Research Report
KTC-98-12

**EXPERIMENTAL ANALYSIS AND
ANALYTICAL MODELING OF BRIDGES
WITH AND WITHOUT DIAPHRAGMS
(FRT-66 and FRT-67)**

by

James J. Griffin
Structural Engineer
CON/STEEL Tilt-Up Systems
LJB Group, Inc. Engineers and Architects

Issam E. Harik
Professor of Civil Engineering and Head, Structures Section,
Kentucky Transportation Center

and

David L. Allen
Transportation Engineer V, Kentucky Transportation Center

Kentucky Transportation Center
College of Engineering, University of Kentucky
Lexington, Kentucky

in cooperation with

Transportation Cabinet
Commonwealth of Kentucky

and

Federal Highway Administration
U.S. Department of Transportation

The contents of this report reflect the views of the authors who are responsible for the facts and accuracy of the data presented herein. The contents do not necessarily reflect the official views or policies of the University of Kentucky, the Kentucky Transportation Cabinet, nor the Federal Highway Administration. This report does not constitute a standard, specification or regulation. The inclusion of manufacturer names or trade names are for identification purposes and are not to be considered as endorsement.

July 1998

1. Report No. KTC-98-12		2. Government Accession No.		3. Recipient's Catalog No.	
4. Title and Subtitle EXPERIMENTAL ANALYSIS AND ANALYTICAL MODELING OF BRIDGES WITH AND WITHOUT DIAPHRAGMS (FRT-66 and FRT-67)				5. Report Date July 1998	
				6. Performing Organization Code	
				8. Performing Organization Report No. KTC-98-12	
7. Author(s) J.J. Griffin, I.E. Harik, and D.L. Allen				10. Work Unit No. (TRAVIS)	
9. Performing Organization Name and Address Kentucky Transportation Center College of Engineering University of Kentucky Lexington, Kentucky 40506-0281				11. Contract or Grant No. FRT-66 and FRT-67	
				13. Type of Report and Period Covered Final	
12. Sponsoring Agency Name and Address Kentucky Transportation Cabinet State Office Building Frankfort, Kentucky 40622				14. Sponsoring Agency Code	
				15. Supplementary Notes Prepared in cooperation with the Kentucky Transportation Cabinet and the U.S. Department of Transportation, Federal Highway Administration	
16. Abstract Two prestressed concrete (P/C) I-girder bridges along the coal haul route system of Southeastern Kentucky were constructed with a 50 degree skew angle. One of the bridges has concrete intermediate diaphragms, while the other bridge has no intermediate diaphragms. Bridges of similar design along coal haul routes have experienced unusual concrete spalling at the interface of the diaphragms and the bottom flange of the girders. The purpose of this report is to identify the cause of the damage, and to evaluate the effectiveness of intermediate diaphragms. Experimental static and dynamic field testing was conducted on both bridges. All field tests were completed prior to the opening of the bridges. Once the calibration of the finite element models was completed using the test data, analyses were conducted with actual coal haul truck traffic to investigate load distribution and the cause of the spalling at the diaphragm-girder interface. Based on the results obtained in this research study, a significant advantage in structural response is generally not noted due to the presence of intermediate diaphragms. Although large differences were noted percentage wise between the responses of the two bridges, analyses suggested the bridge without intermediate diaphragms will experience displacements and stresses well within AASHTO and ACI design requirements. Finite element analyses also revealed the cause of concrete spalling witnessed in the diaphragm-girder interface region. The tendency of the girders to separate as the bridge was loaded played a large role in generating high stress concentrations in the interface region. Other mitigating factors were the presence of the diaphragm anchor bars and the fact the bridge is subjected to the overloads of coal trucks. Resolving this problem would in some measure require the removal of the concrete intermediate diaphragm. However, the total elimination of intermediate diaphragms is not recommended since they are required during construction and in the event the deck is to be replaced. The use of temporary steel diaphragms, therefore, is recommended as substitutes for the concrete intermediate diaphragms.					
17. Key Words Slab-on-Girder Load Distribution Experimental Testing			18. Distribution Statement Unlimited with approval of Kentucky Transportation Cabinet		
19. Security Classif. (of this report) Unclassified		20. Security Classif. (of this page) Unclassified		21. No. of Pages 186	22. Price

Experimental Analysis and Analytical Modeling of Bridges with and Without Diaphragms (FRT-66 and FRT-67)

EXECUTIVE SUMMARY

Research Objectives

The objectives of this study are to evaluate the effectiveness of intermediate diaphragms in prestressed concrete I-girder bridges subjected to vehicle overload common among coal haul trucks. In order to achieve these objectives, the following tasks were performed: 1) field testing of the Southbound bridge (with intermediate diaphragms) and Northbound bridge (without intermediate diaphragms) on US 23 over KY 40 (Figs. E-1 to E-3); 2) three-dimensional, static and dynamic finite element analyses of the US 23 bridges; 3) calibration of the finite element models with the field test data; and 4) analysis of the influence of intermediate diaphragms.

Background

Bridges of prestressed concrete I-girder design along coal haul routes have been experiencing unusual distress (concrete spalling) at the interface of the diaphragms and the bottom flange of the girders. The intermediate diaphragms appear to be contributing more to the increased rate of deterioration and damage than reducing the moment coefficient and distributing the traffic loads as expected.

AASHTO recommends the use of diaphragms at points of maximum moment for spans greater than 40-ft (12.21-m). Kentucky exceeds the AASHTO guidelines by specifying diaphragms at points of maximum moment for spans between 40 ft and 80 ft (12.21 m and 24.41 m), and diaphragms at third points for spans greater than 80 ft (24.41 m). The Southbound US 23 bridge, investigated in this research study, exceeds even the Kentucky requirements since diaphragms are located at the quarter points in Spans 2 and 3 (Figs. E-2 and E-4). The Northbound bridge was constructed with temporary intermediate diaphragms (Fig. E-3) or Z-bracing that were loosened after construction.

It should be noted that Section 9.10.1 of the *Standard Specifications for Highway Bridges* (AASHTO 1996) allows for diaphragms to be omitted when adequate strength is determined through testing or structural analysis.

Field Testing

Dynamic and static tests were conducted on the Northbound and Southbound US 23 bridges over KY 40. Static testing was accomplished by using two fully-loaded, tandem coal haul trucks to induce the displacements and strains on the Southbound and Northbound bridges. Static testing provided an opportunity to determine the deflections and stresses induced by normal traffic and coal truck loading.

Dynamic testing was accomplished by using a single fully-loaded, tandem coal haul truck. Dynamic testing provided an opportunity for the natural frequencies and mode shapes of the structures to be determined. The results from each test were used to calibrate finite element models of the US 23 bridges.

Experimental Results

The maximum concrete stresses in the deck of the Northbound bridge (without diaphragm) were 0.97 ksi (6.66 MPa) in compression and 0.28 ksi (1.94 MPa) in tension. Comparable maximum concrete stress values in the deck of the Southbound bridge (with diaphragm) were 0.15 ksi (1.21 MPa) in compression and 0.08 ksi (0.57 MPa) in tension. Since the stress values are within acceptable design criteria, the absence of intermediate diaphragms in the Northbound bridge does not seem to pose a threat to the serviceability and load capacity of the deck in the transverse direction under the static test loads. Similarly, the presence of intermediate diaphragms does not seem to impose excessive stresses on the Southbound bridge deck. Small strains were generally recorded from the gages placed around the diaphragm on the girder. In fact, the largest strain value recorded at the diaphragm-girder interface was 91.59 microstrain, corresponding to a tensile stress in the girder of 0.417 ksi (2.880 MPa).

Two conclusions were drawn from the experimental results of the girder out-of-plane displacements: 1) out-of-plane displacements were prevalent only when the load was in the span where deflections were being measured, and 2) although the absence of intermediate diaphragms leads to a large difference between out-of-plane displacements in the Southbound and Northbound bridges percentage-wise, the magnitude of the out-of-plane displacement is not sufficient to cause any concern.

Finite Element Model

Having completed the static and dynamic test phases, finite element models of the US 23 bridges were constructed and calibrated to correlate with the experimentally measured data. Local responses in the form of stresses around the diaphragm-girder interface were examined through the use of a smaller, more refined three-dimensional finite element model.

Effectiveness of Intermediate Diaphragms

Based on the results for vertical deflections, out-of-plane displacements, and girder stresses, a significant advantage in structural response is generally not noted due to the presence of intermediate diaphragms. Analyses completed using legal weight coal trucks suggest the Northbound bridge (bridge without intermediate diaphragms) will experience displacements and stresses well within the design parameters outlined by AASHTO and ACI. The single exception was noted in the load case where a tridem coal truck was located at the midspan of Spans 1 and 3 in both traffic lanes (Fig. E-4). The reduction in displacements and stresses of the Southbound bridge (with intermediate diaphragms) seemed to be advantageous percentage-wise, but the magnitudes of these two parameters were insufficient to suggest mandatory use of intermediate diaphragms.

Finite element analyses focusing on the diaphragm-girder interface region demonstrated that the concrete spalling witnessed in these locations was a result of girder stresses in excess of the concrete compressive strength. The tendency of the girders to separate as the bridge was loaded played a large role in generating these high stress concentrations. Other mitigating factors were the presence of the diaphragm anchor bars and the fact the bridge is subjected to the heavy loads of coal trucks.

Conclusions

Given the spalling associated with the presence of concrete intermediate diaphragms in bridges subjected to overloads, an alternative course of action seems advisable. Intermediate diaphragms on the whole do provide some load distribution among the adjacent girders, but the cost of construction and maintenance of this type of diaphragm outweighs the gain. However, the total elimination of intermediate diaphragms is not recommended since they are required during the construction phase (prior to the placement of the deck) and if the deck is to be replaced ("re-decking").

Recommendations

The use of steel diaphragms, such as the Z-type bracing (Fig. E-3), is recommended as substitutes for the concrete intermediate diaphragms. The steel diaphragms should be loosened after the deck and girders have achieved composite action (i.e., after the deck has cured).



Figure E-1. Southbound and Northbound (foreground) US 23 Bridges Over KY 40

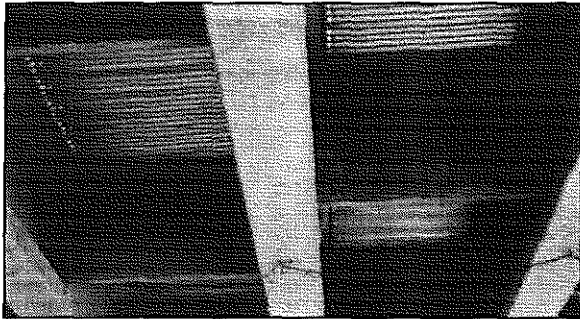


Figure E-2. Concrete Intermediate Diaphragms in Southbound Bridge on US 23.

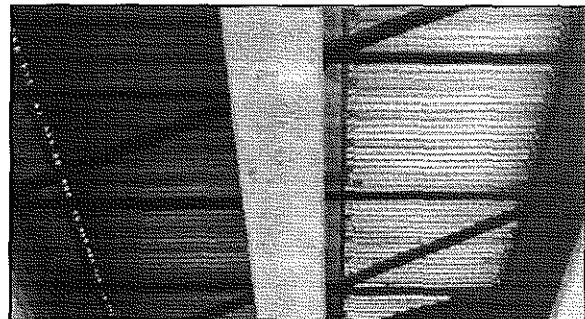


Figure E-3. Steel Intermediate Diaphragms in Northbound Bridge on US 23

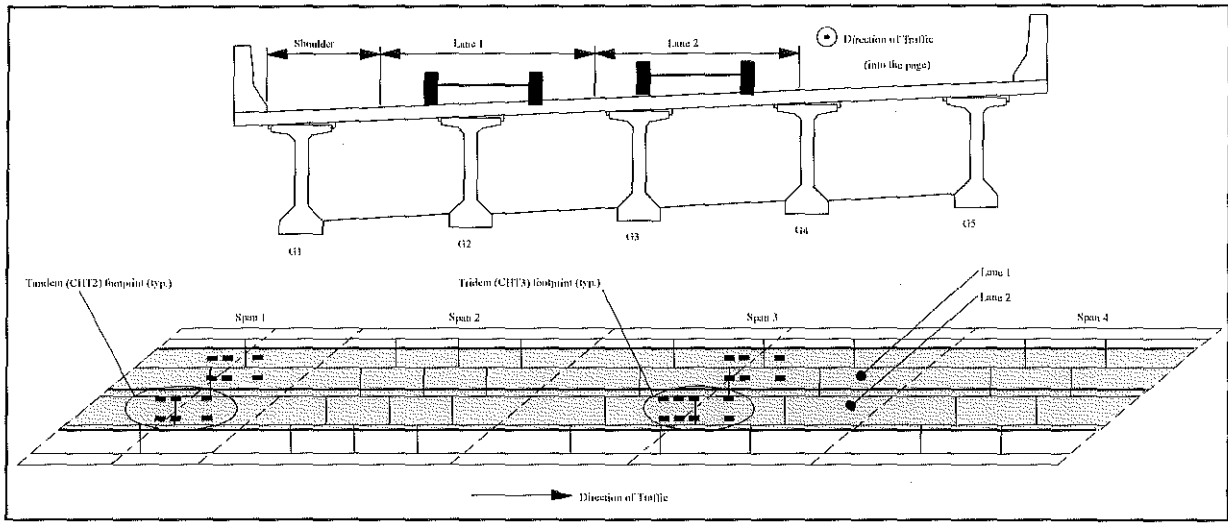


Figure E-4. Orientation of Coal Trucks on US 23 Bridges over KY 40

ACKNOWLEDGMENTS

The financial support for this project was provided by the Kentucky Transportation Cabinet and the Federal Highway Administration. Their cooperation, suggestions, and advise are appreciated.

TABLE OF CONTENTS

	PAGE
EXECUTIVE SUMMARY	ii
ACKNOWLEDGMENTS	vii
LIST OF TABLES	xi
LIST OF FIGURES	xiii
CHAPTER 1: INTRODUCTION	1
1.1. Bridge Diaphragms	1
1.1.1. Description of Diaphragms	1
1.1.2. Code Requirements	2
1.2. Literature Review	2
1.2.1. Intermediate Diaphragms	3
1.2.2. Load Distribution and Design	5
1.2.3. Experimental Testing	6
1.2.4. Analytical Modeling	8
1.2.5. Miscellaneous	10
1.3. Bridges Along Coal Haul Routes	11
1.4. Scope of Research	12
1.4.1. Location of the Bridges	12
1.4.2. Bridge Descriptions	12
1.4.3. Traffic Loading Profile	15
1.4.4. Research Objectives	15
1.5. Research Significance	16
CHAPTER 2: INSTRUMENTATION AND EXPERIMENTAL TESTING	17
2.1. Introduction	17
2.2. Static Testing Instrumentation	18
2.2.1. Instrumentation in the Deck	19
2.2.2. Instrumentation on the Girders	23
2.2.3. Instrumentation in the Diaphragm Region	27
2.3. Dynamic Testing Instrumentation	30
2.4. Experimental Testing	32

2.4.1. Total Instrumentation	32
2.4.2. Static Testing	34
2.4.3. Dynamic Testing	35
CHAPTER 3: DATA ACQUISITION AND EXPERIMENTAL RESULTS	36
3.1. Data Acquisition	36
3.1.1. Static Testing	36
3.1.2. Dynamic Testing	41
3.2. Calibration Factors	42
3.2.1. Static Testing	42
3.2.2. Dynamic Testing	44
3.3. Experimental Results	44
3.3.1. Static Testing	44
3.3.2. Dynamic Testing	59
3.3.3. Repeatability of Testing	63
CHAPTER 4: FINITE ELEMENT MODELING OF THE BRIDGES	64
4.1. Introduction	64
4.2. Finite Element Model of the Bridges	64
4.2.1. Frame Elements	65
4.2.2. Shell Elements	65
4.2.3. Solid Elements	66
4.2.4. Spring Specification	69
4.2.5. Joint Constraint Specification	71
4.2.6. Mass Specification	73
4.2.7. Joint Load Specification	74
4.3. Calibration of the Bridge Models	75
4.3.1. Dynamic Calibration	75
4.3.2. Static Calibration	79
CHAPTER 5: ANALYSIS OF DIAPHRAGM EFFECTIVENESS	84
5.1. Truck Loading	84
5.1.1. AASHTO Trucks	84
5.1.2. Coal Trucks	85
5.2. Parametric Study	91
5.3. Analysis Results	92
5.3.1. Midspan Vertical Deflections	92
5.3.2. Midspan Out-of-Plane Displacements	95
5.3.3. Midspan Bottom Flange Girder Stresses	98
5.4. Conclusions	102

CHAPTER 6: ANALYSIS OF DIAPHRAGM-GIRDER INTERFACE	104
6.1. Diaphragm-Girder Interface	104
6.2. Finite Element Model	104
6.2.1. Solid Elements	105
6.2.2. Joint Constraint Specification	107
6.2.3. Displacement Specification	109
6.3. Analysis Results	109
6.4. Conclusions	112
CHAPTER 7: CONCLUSIONS AND RECOMMENDATIONS	114
7.1. General Summary	114
7.1.1. Coal Truck Loading	114
7.1.2. Research Objectives	114
7.1.3. Research Significance	115
7.1.4. Experimental Testing	115
7.1.5. Experimental Results	117
7.1.6. Finite Element Model	119
7.2. Effectiveness of Intermediate Diaphragms	119
7.3. Future Research Needs	120
7.3.1. Alternate Diaphragm Types	121
7.3.2. Skewed <i>Versus</i> Non-skewed Bridges	121
7.3.3. Bridges of Various Construction	121
7.3.4. Other Analysis Techniques	122
BIBLIOGRAPHY	123
APPENDIX A: STATIC TEST INSTRUMENTATION	136
APPENDIX B: COMPUTER PROGRAM TO PROCESS STATIC TEST FILES ..	148
APPENDIX C: STATIC TEST EXPERIMENTAL RESULTS	153

LIST OF TABLES

	PAGE
Table 2.2.1a: Instrumentation on the Transverse Reinforcement in the Bridge Deck	21
Table 2.2.1b: Instrumentation on the Longitudinal Reinforcement in the Bridge Deck	22
Table 2.2.2a: Vertical and Transverse Displacement Instrumentation on the Girders	25
Table 2.2.2b: Strain Gage Instrumentation on the Girders	26
Table 2.2.3a: Instrumentation on the Threaded Diaphragm Anchor Bars	28
Table 2.2.3b: Instrumentation on the Diaphragms and Girders in the Diaphragm Region	30
Table 2.3.1a: Accelerometer Colors and Wire Lengths	32
Table 2.4.1: Total Instrumentation Required for Structural Testing of the Bridges	33
Table 3.1.1: File Names for the Northbound and Southbound Static Tests	38
Table 3.1.2: File Names for the Northbound and Southbound Dynamic Tests	41
Table 3.2.1: Reusable Strain Gage Calibration Factors	43
Table 3.3.1a: Maximum Strain and Stress Values Encountered During Static Testing	46
Table 3.3.1b: Strain and Stress on Transverse Reinforcement Bars in the US 23 Bridge Decks	47
Table 3.3.1c: Strain and Stress on Longitudinal Reinforcement Bars in the US 23 Bridge Decks	49
Table 3.3.1d: Vertical and Out-of-Plane Displacements of the US Bridge Girders	52
Table 3.3.1e: Strain and Stress Values Obtained From Girder Strain Gages	56
Table 3.3.2: Frequencies of the Northbound and Southbound Bridges Identified by the Experimental Data	62
Table 4.2: Components of the Bridge Models	65
Table 4.2.3: Comparison of Solid Element Model of Girder With Beam Formulas	68
Table 4.2.4: Spring Stiffness Substituted for the Piers in the Finite Element Models	71
Table 4.2.6: Lumped Masses Used to Simulate the Presence of Bridge Piers	73
Table 4.3.1a: Comparison of Experimental and Analytical Frequencies Obtained for the Southbound Bridge (Bridge With Intermediate Diaphragms)	78
Table 4.3.1b: Comparison of Experimental and Analytical Frequencies	

	Obtained for the Northbound Bridge (Bridge Without Intermediate Diaphragms)	79
Table 4.3.2a:	Static Calibration Factors for the US 23 Bridge Models	81
Table 4.3.2b:	Comparison of the Experimental and Analytical Results for Deflections and Stresses in the Southbound Bridge (Bridge With Intermediate Diaphragms)	82
Table 4.3.2c:	Comparison of the Experimental and Analytical Results for Deflections and Stresses in the Northbound Bridge (Bridge Without Intermediate Diaphragms)	83
Table 5.1a:	Load Combinations Applied to the Finite Element Models in Single Lane	89
Table 5.1b:	Load Combinations Applied to the Finite Element Models in Both Lanes	90
Table 5.2:	Summary of Span Lengths and Diaphragm Location on the US 23 Bridges	91
Table 5.3.1:	Maximum Vertical Deflection of the US 23 Bridges	95
Table 5.3.2:	Maximum Out-of-Plane Displacements of the US 23 Bridges	98
Table 5.3.3:	Maximum Longitudinal Stresses in the Bottom Flange of the Girders in the US 23 Bridges	102
Table 6.1:	Components of the Girder-Diaphragm Model	105
Table 6.2:	Nodal Deflections Imposed on Diaphragm-Girder Interface Model	109
Table A.1:	Transverse Bar Color Coding and Placement in the Southbound Bridge	138
Table A.2:	Transverse Bar Color Coding and Placement in the Northbound Bridge	139
Table A.3:	Longitudinal Bar Color Coding and Placement in the Southbound Bridge	140
Table A.4:	Longitudinal Bar Color Coding and Placement in the Northbound Bridge	140
Table A.5:	Anchor Bar Color Coding and Orientation in the Southbound Bridge	141
Table A.6:	Southbound Bridge Static Testing Schedule	142
Table A.7:	Northbound Bridge Static Testing Schedule	145
Table A.8:	Southbound and Northbound Bridge Dynamic Testing Schedule	147

LIST OF FIGURES

		PAGE
Figure E-1.	Southbound and Northbound US 23 Bridges Over KY 40	v
Figure E-2.	Concrete Intermediate Diaphragms in Southbound Bridge on US 23.	v
Figure E-3.	Steel Intermediate Diaphragms in Northbound Bridge on US 23	v
Figure E-4.	Orientation of Coal Trucks on US 23 Bridges over KY 40	vi
Figure 1.1.1a.	Concrete Intermediate Diaphragms	1
Figure 1.1.1b.	Steel Intermediate Diaphragms	2
Figure 1.3.	Concrete Spalling at Diaphragm-Girder Interface	11
Figure 1.4.1.	Map of Kentucky Highlighting Johnson County	12
Figure 1.4.2a.	Skew Angle of the Girders	12
Figure 1.4.2b.	Modified AASHTO Type IV I-Girder Used on the US 23 Bridges	12
Figure 1.4.2c.	Bird's Eye View of the US 23 Bridges: Southbound (Left - Bridge With Intermediate Diaphragms) and Northbound (Right - Bridge Without Intermediate Diaphragms)	14
Figure 1.4.2d.	Side View of the Southbound US 23 Bridge (Bridge With Intermediate Diaphragms)	14
Figure 2.1.	Span 3 of the US 23 Bridges	17
Figure 2.2.	US 23 Bridge Over KY 40	18
Figure 2.2.1a.	Transverse Strain Gage Placement in the Southbound Deck (Bridge With Intermediate Diaphragms)	19
Figure 2.2.1b.	Transverse Strain Gage Placement in the Northbound Deck (Bridge Without Intermediate Diaphragms)	20
Figure 2.2.1c.	Strain Gage on Rebar Prior to Protective Coatings	20
Figure 2.2.1d.	Longitudinal Strain Gage Placement in the Southbound Deck (Bridge With Intermediate Diaphragms)	21
Figure 2.2.1e.	Longitudinal Strain Gage Placement in the Northbound Deck (Bridge Without Intermediate Diaphragms)	22
Figure 2.2.2a.	LVDT Locations on Centerline of Southbound Span 3 (Bridge With Intermediate Diaphragms)	23
Figure 2.2.2b.	LVDT Locations on Centerline of Northbound Span 3 (Bridge Without Intermediate Diaphragms)	23
Figure 2.2.2c.	Out-of-Plane and Vertical LVDT Assemblies	24
Figure 2.2.2d.	Locations for Girder Strain Gage Placement in the Southbound Bridge (Bridge With Intermediate Diaphragms)	25
Figure 2.2.2e.	Locations for Girder Strain Gage Placement in the Northbound Bridge (Bridge Without Intermediate Diaphragms)	26

Figure 2.2.3a.	Strain Gages on Diaphragm Anchor Bar Near Threaded End	27
Figure 2.2.3b.	Locations of Diaphragm Anchor Bars Instrumented With Strain Gages in the Southbound Bridge (Bridge With Intermediate Diaphragms)	28
Figure 2.2.3c.	Strain Gage Placement Near the Flange-Diaphragm Interface	29
Figure 2.2.3d.	Locations of Diaphragm Regions Instrumented With Strain Gages in Span 3 of the Southbound Bridge	29
Figure 2.2.3e.	Strain Gages on the Face of Southbound Bridge Diaphragms	30
Figure 2.3.1a.	Accelerometers in Triaxial Arrangement	31
Figure 2.3.1b.	Moveable Accelerometer Locations on the US 23 Bridges	31
Figure 2.4.2a.	Tandem Coal Haul Trucks Used During Static Testing	33
Figure 2.4.2b.	Footprints and Axle Weights of Static Test Trucks	34
Figure 2.4.2c.	Locations of Static Test Lanes and Stations on the US 23 Bridges	34
Figure 2.4.2d.	Footprint and Axle Weights of Dynamic Test Truck	35
Figure 3.1.	Data Acquisition System	36
Figure 3.1.1a.	Data Record N2-9CH32.DAT	39
Figure 3.1.1b.	Data File N2-9CH.SUM Obtained From Processing N2-9CH#.DAT Through the Computer Program of Appendix B	40
Figure 3.1.2.	Data Record L2CH2.DAT	42
Figure 3.3.1a.	Locations of Static Test Lanes and Stations on the US 23 Bridges	44
Figure 3.3.1b.	Transverse Strain Gage Locations in the Southbound Deck (Bridge With Intermediate Diaphragms)	45
Figure 3.3.1c.	Transverse Strain Gage Locations in the Northbound Deck (Bridge Without Intermediate Diaphragms)	45
Figure 3.3.1d.	Strain on the Top Transverse Rebar at Location S1B3T/N1B3T: Trucks Side-by-Side	46
Figure 3.3.1e.	Longitudinal Strain Gage Locations in the Southbound Deck (Bridge With Intermediate Diaphragms)	48
Figure 3.3.1f.	Longitudinal Strain Gage Locations in the Northbound Deck (Bridge Without Intermediate Diaphragms)	48
Figure 3.3.1g.	Strain on the Longitudinal Rebar at Location S2F/N2F: Trucks Bumper-to-Bumper in Lane 1	49
Figure 3.3.1h.	Vertical (●) and Transverse (◆) LVDT Locations on Centerline of Southbound Span 3 (Bridge With Intermediate Diaphragms)	50
Figure 3.3.1i.	Vertical (●) and Transverse (◆) LVDT Locations on Centerline of Northbound Span 3 (Bridge Without Intermediate Diaphragms)	50
Figure 3.3.1j.	Out-of-Plane Displacement at Location S7D/N4D: Trucks Bumper-to-Bumper in Lane 1	51

Figure 3.3.1k.	Vertical Deflection at Location S7C/N4C: Trucks Bumper-to-Bumper in Lane 1	51
Figure 3.3.1l/	Strain Gage Location on Girder Cross Section and Deck	52
Figure 3.3.1m.	Girder Strain Gage Locations in the Southbound Bridge (Bridge With Intermediate Diaphragms)	53
Figure 3.3.1n.	Girder Strain Gage Locations in the Northbound Bridge (Bridge Without Intermediate Diaphragms)	53
Figure 3.3.1o.	Strain Across Girder Cross Section at Location S5C: Trucks Bumper-to-Bumper in Lane 1, Truck 1 at Station 9	53
Figure 3.3.1p.	Strain Across Girder Cross Section at Location N3A: Trucks Bumper-to-Bumper in Lane 1, Truck 1 at Station 9	53
Figure 3.3.1q.	Strain Along Bottom of Girder at Location S5B/N3B: Trucks Bumper-to-Bumper in Lane 1	54
Figure 3.3.1r.	Strain Along Bottom of Girder at Location S5D/N3D: Trucks Bumper-to-Bumper in Lane 1	55
Figure 3.3.1s.	Strain Gages Located Near the Girder Flange-Diaphragm Interface	57
Figure 3.3.1t.	Locations of Diaphragm Regions Instrumented With Strain Gages in Span 3 of the Southbound Bridge	57
Figure 3.3.1u.	Strain Gages on the Face of the Southbound Bridge Diaphragm D1 and Diaphragm D2	58
Figure 3.3.1v.	Strain on Girder at Locations S4A1 and S4A2 of the Diaphragm-Girder Interface With Trucks Bumper-to-Bumper in Lane 1	58
Figure 3.3.1w.	Strain on Face of Diaphragms D1 and D2	58
Figure 3.3.1x.	Strain on Girder at Locations S4A5 and N3E With Trucks Bumper-to-Bumper in Lane 2	59
Figure 3.3.2a.	Fast Fourier Transform of Acceleration Record L2CH2.DAT	59
Figure 3.3.2b.	Vertical Mode Shape of Northbound Bridge at 4.71 Hz Obtained from Experimental Data	60
Figure 3.3.2c.	Vertical Mode Shape of Southbound Bridge at 4.61 Hz Obtained from Experimental Data	61
Figure 3.3.3a.	Example of Dynamic Test Repeatability - Station 8E	63
Figure 3.3.3b.	Example of Static Test Repeatability - Gage N3CM	63
Figure 4.2.3a.	Solid Element Model of the Modified AASHTO Type IV Girder66	
Figure 4.2.3b.	Elements With Suppressed Incompatible Bending Modes	67
Figure 4.2.3c.	Illustration of a Girder Haunch	67
Figure 4.2.3d.	Cross Section of the Southbound Bridge Finite Element Model69	
Figure 4.2.3e.	Cross Section of the Northbound Bridge Finite Element Model69	
Figure 4.2.4.	Finite Element Model of Pier Used to Obtain Spring Stiffnesses	71
Figure 4.2.5.	Diaphragm Anchor Bar in Place at the Abutment	72
Figure 4.2.6.	Lumped Mass Locations for Steel Diaphragms in Northbound Bridge Finite Element Model	74

Figure 4.2.7.	Determination of Equivalent Nodal Loads in a Parallelogram Element After Chen (1995a)	74
Figure 4.3.1a.	Flow Chart of Iterative Procedure Used to Calibrate the US 23 Bridge Models With the Dynamic Test Data	76
Figure 4.3.1b.	Overlapping Regions Due to Solid Element Modeling of the Girder Haunches and Barrier Walls	77
Figure 4.3.1c.	Vertical Mode Shape of the Southbound Bridge (4.6406 Hz) and Northbound Bridge (4.7152 Hz)	77
Figure 4.3.1d.	Torsional Mode Shape of the Southbound Bridge (5.9545 Hz) and Northbound Bridge (5.8681 Hz)	77
Figure 5.1.1a.	Equivalent Lane Loadings Substituted for the Truck Trains of the 1935 AASHTO Specifications (AASHTO 1996)	84
Figure 5.1.1b.	Footprint of the AASHTO H and HS Trucks (AASHTO 1996)	85
Figure 5.1.2a.	Footprint of the Tandem and Tridem Coal Haul Trucks	86
Figure 5.1.2b.	Cross Section of Northbound US 23 Bridge (Bridge Without Intermediate Diaphragms) Illustrating Location of Traffic Lanes and Girder Number	87
Figure 5.1.2c.	Cross Section of Southbound US 23 Bridge (Bridge With Intermediate Diaphragms) Illustrating Location of Traffic Lanes and Girder Number	87
Figure 5.1.2d.	Orientation of Tridem Coal Trucks in Load Case 1	88
Figure 5.3.1a.	Vertical Deflection at Midspan of Span 3 - Load Case 10	92
Figure 5.3.1b.	Vertical Deflection at Midspan of Span 2 - Load Case 31	92
Figure 5.3.1c.	Orientation of Coal Trucks in Load Case 10	92
Figure 5.3.1d.	Orientation of Coal Trucks in Load Case 31	93
Figure 5.3.1e.	Maximum Vertical Deflection at Midspan of Span 3 - Load Case 35	94
Figure 5.3.1f.	Orientation of Coal Trucks in Load Case 35	94
Figure 5.3.2a.	Out-of-Plane Displacement at Midspan of Span 3 - Load Case 10	96
Figure 5.3.2b.	Out-of-Plane Displacement at Midspan of Span 2 - Load Case 31	96
Figure 5.3.2c.	Orientation of Coal Trucks in Load Case 10	96
Figure 5.3.2d.	Orientation of Coal Trucks in Load Case 31	97
Figure 5.3.3a.	Bottom Flange Girder Stresses at Midspan of Span 3 - Load Case 10	98
Figure 5.3.3b.	Bottom Flange Girder Stresses at Midspan of Span 2 - Load Case 31	99
Figure 5.3.3c.	Orientation of Coal Trucks in Load Case 10	99
Figure 5.3.3d.	Orientation of Coal Trucks in Load Case 31	100
Figure 5.3.3e.	Maximum Girder Tensile Stresses	101
Figure 5.3.3f.	Maximum Girder Compressive Stresses	101
Figure 6.1.	Concrete Spalling at Diaphragm-Girder Interface	104

Figure 6.2.	Longitudinal Dimensions of Diaphragm-Girder Interface Model	105
Figure 6.2.1a.	Solid Element Model of the Modified AASHTO Type IV Girder	106
Figure 6.2.1b.	Cross Section of Diaphragm-Girder Finite Element Model	106
Figure 6.2.2a.	Location of Diaphragm Anchor Bars on Actual Girder	107
Figure 6.2.2b.	Diaphragm Anchor Bar in Place at the Abutment	108
Figure 6.2.2c.	Illustration of Double Node Scheme Employed at the Location of Diaphragm Anchor Bar Insert	108
Figure 6.3a.	Stress Distribution at Diaphragm-Girder Interface - Load Case 35 (Legal Weight)	110
Figure 6.3b.	Girder Locations Reported in Figure 6.3a	110
Figure 6.3c.	Orientation of Coal Trucks in Load Case 35	111
Figure 6.3d.	Principal Stress Distribution at Diaphragm-Girder Interface - Load Case 35 (Legal Weight)	111
Figure 6.3e.	Stress Distribution at Diaphragm-Girder Interface - Load Case 35 (Overweight)	111
Figure 6.3f.	Principal Stress Distribution at Diaphragm-Girder Interface - Load Case 35 (Overweight)	112
Figure 6.3g.	Concrete Spalling at Diaphragm-Girder Interface	112
Figure 7.1.3.	Span and Diaphragm Locations in the Southbound US 23 Bridge	115
Figure A.1.	Grinding of Rebar	136
Figure A.2.	Polishing of Rebar	136
Figure A.3.	Surface Preparation and Strain Gage Mounting Materials	136
Figure A.4.	Liquid Polymer Protective Coating	137
Figure A.5.	Reusable Strain Gages Mounted on the Side of a Bridge Girder	137

CHAPTER 1

INTRODUCTION

1.1. BRIDGE DIAPHRAGMS

1.1.1. DESCRIPTION OF DIAPHRAGMS

In the *Standard Specifications for Highway Bridges* (AASHTO 1996), a diaphragm is defined to be a transverse stiffener which is provided between girders in order to maintain section geometry. For many years, intermediate diaphragms (i.e., diaphragms not located over piers or abutments) have been thought to contribute to the overall distribution of live loads in bridges. Consequently, most bridges constructed in Kentucky have intuitively included intermediate diaphragms.

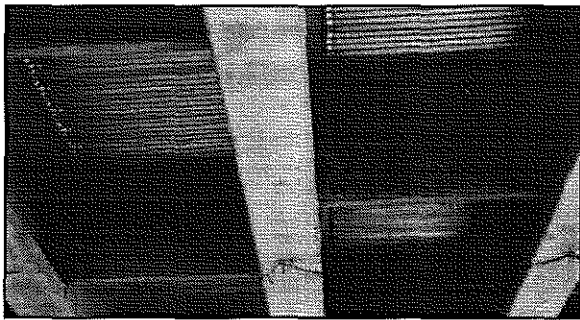


Figure 1.1.1a. Concrete Intermediate Diaphragms.

Depending on the type of bridge, the diaphragms may take different forms. The most common in prestressed concrete I-girder bridge construction is the concrete intermediate diaphragm pictured in Figure 1.1.1a. The diaphragm is cast-in-place and is said to be "full-depth" over the cross section of the girder. The diaphragm is generally integral with the deck through continuous reinforcement, tied to the girder through only four diaphragm anchor bars, and terminated at the end of the sloping portion of the girder bottom flange.

In steel girder bridge construction, however, a wide variety of intermediate diaphragms, also known as cross frames, are available. The most common types are K-bracing, X-bracing, and Z-bracing, the last of which is depicted in Figure 1.1.1b. As is indicated in Figure 1.1.1b, Z-bracing is an acceptable alternative to the cast-in-place concrete diaphragm for prestressed concrete I-girder bridges, as are the other steel type diaphragms. K-bracing may be modified with the presence of a top chord. Similarly, X-bracing may be modified by the presence of a top and/or bottom chord. All steel type diaphragms are bolted to an angle bracket attached to the girders, thereby offering a certain amount of rotational freedom not found in the concrete "full-depth" diaphragm.

1.1.2. CODE REQUIREMENTS

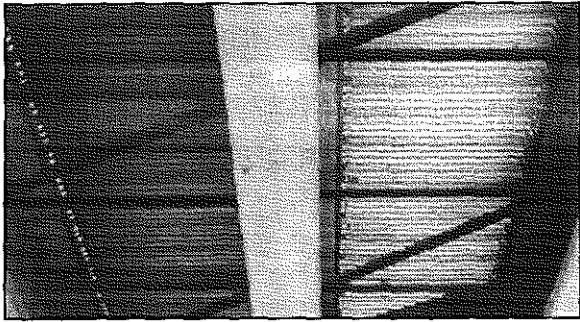


Figure 1.1.1b. Steel Intermediate Diaphragms.

The American Association of State Highway and Transportation Officials (AASHTO) requires the use of diaphragms in both of its design codes. Section 9.10 of the *Standard Specifications for Highway Bridges* (AASHTO 1996) requires the inclusion of diaphragms in prestressed concrete bridge design. Furthermore, Section 9.10.2 requires intermediate diaphragms to be placed between the girders at the points where maximum moments occur in spans in excess of 40 ft (12.19 m). Where tests or structural

analysis show adequate strength, though, diaphragms may be omitted. Similar recommendations are made in the *Load Resistance Factor Design (LRFD) Bridge Design Code* (AASHTO 1994). Article 5.13.2.2 requires the use of intermediate diaphragms to provide assistance in the distribution of live loads between the girders and to resist torsional forces. Article 5.14.1.1.4 indicates that in I-girder and T-girder construction, intermediate diaphragms are required at the points of maximum positive moments for spans in excess of 40 ft (12.19 m). Ironically, AASHTO does not incorporate the presence of intermediate diaphragms into the design equations for distribution of live load (AASHTO Subcommittee 1994), despite the fact that their inclusion is more or less mandated.

In a study at Auburn University, Stallings *et al.* (1993b) surveyed Departments of Transportation in all 50 states. The following responses were received from the Kentucky Transportation Cabinet in answer to the survey: 1) permanent intermediate diaphragms are required at midspan for spans greater than 40 ft (12.19 m) and at third points for spans in excess of 80 ft (24.38 m), 2) intermediate diaphragms when used are full depth cast-in-place concrete (see the description above), and 3) 80 percent of the bridges in Kentucky are constructed from prestressed concrete girders.

1.2. LITERATURE REVIEW

The objectives of this research were centered around an in-depth study into the behavior of concrete intermediate diaphragms in prestressed concrete I-girder bridges subjected to overloads common among coal trucks. An extensive literature review was conducted to investigate all aspects of the work that would be required to complete the study. The following four topics were identified as major areas where previous

research information would be important: 1) intermediate diaphragms, 2) load distribution and design of highway bridges, 3) experimental testing of bridges, and 4) analytical modeling. It should be noted that not one of the articles reviewed presented research on experimental testing and analytical modeling to conduct static as well as dynamic analyses of bridges with and without diaphragms using overloads (e.g., heavy coal trucks).

A summary of the articles/books for each topic is presented below, along with some additional information that proved useful throughout the course of the study. In the end, all of the references listed in the bibliography provided the author some assistance in completing this study.

1.2.1. INTERMEDIATE DIAPHRAGMS

In what seems to be the benchmark research in this area, Kostem and deCastro (1977) concluded that midspan diaphragms are not fully effective in the lateral distribution of live load for beam-slab bridges with typical dimensions and construction details such as those encountered in design and construction practice. When all design lanes are fully loaded, the diaphragms do not contribute noticeably to the lateral distribution of live load, i.e., the performance of the structure is comparable to one with no diaphragms. A recommendation was made that vehicle overload and large skew effects be considered before eliminating the use of intermediate diaphragms.

1.2.1.1. Prestressed Concrete Girder Bridges

Abendroth *et al.* (1991) summarized research conducted by various investigators. The primary objective of a study at the University of Illinois (Sithichaikasem and Gamble 1972) was to investigate the effects of diaphragms on load distribution characteristics in simple and continuous span prestressed concrete girder and slab highway bridges. In their theoretical analysis, the parameters studied included the number, stiffness, and location of diaphragms; the relative girder stiffness; the ratio of girder spacing to span; the girder torsional stiffness; the girder spacing; and the location and type of loading. For continuous span bridges with various diaphragm stiffnesses and bridge properties, the following conclusions were made: 1) diaphragms improve the load distribution characteristics of some bridges that have a large beam spacing to span length ratio; 2) the usefulness of diaphragms is minimal and they are harmful in most cases, and 3) on the basis of cost effectiveness, diaphragms are not recommended for highway bridges. Abendroth *et al.* (1991) also reported that Sengupta and Breen investigated the role of end and intermediate diaphragms in typical prestressed concrete girder and slab bridges in 1973. Experimental variables in that study included span length, skew angle of the bridge,

and number, location, and stiffness of the diaphragms. The elastic response of the bridge was studied under static, cyclic, and impact loads - with and without diaphragms. Overload and ultimate load behavior was also documented from various static load and impact load tests. Experimental results were used to verify a computer program, which in turn was used to generalize some of the results. Sengupta and Breen concluded that under no circumstances would the presence of intermediate diaphragms significantly reduce the design girder moments. In fact, in certain situations the presence of intermediate diaphragms might even increase the design moment. A recommendation that intermediate diaphragms be excluded in prestressed concrete girder and composite slab bridges was made. Abendroth *et al.* (1991) even cited other research by Kostem and deCastro which found that when all traffic lanes were loaded, diaphragms were ineffective in distributing loads laterally.

Based upon independent research work, Abendroth *et al.* (1991) concluded that diaphragms are more effective in reducing the girder moments when point loads are applied directly to the girder. However, the vertical loading of a bridge actually involves several point loads (i.e., truck loading). The function of diaphragms was found to have an insignificant difference under the action of dynamic loads (in the normal expected frequency range) as opposed to static loads. On average, diaphragms were less effective in terms of load distribution when dynamic loads occurred. Overall, Abendroth *et al.* (1991) noted that bridge response to vertical loads applied to prestressed concrete girders was not significantly affected by diaphragm type or location, and, in fact, diaphragms have minimal influence on the vertical load distribution within the bridge. A later publication (Abendroth *et al.* 1995) reiterated these conclusions.

1.2.1.2. Steel Girder Bridges

As regards steel bridges, Azizinamini *et al.* (1995) also evaluated the effectiveness of intermediate diaphragms. Steel girders are more susceptible to web cracking near the connection of cross frames to the girder, especially for details where stiffeners are not rigidly connected to top and bottom flanges. A summary of an experimental investigation was presented. Some of the major conclusions were as follows: 1) load distribution factors are only slightly affected by the presence of intermediate cross frames, 2) in the case of no intermediate cross frames the percent difference in deflection of girders compared to having X or K type cross frames is higher when only one lane is loaded or the load straddles the centerline. However, it should be noted that the resulting deflections for both interior and exterior girders in these cases are much lower than the case where both lanes are loaded, and 3) the distribution factors obtained experimentally for the case of no cross frames are still smaller than what those predicted by AASHTO or Imbsen formulas. In summary, cross frames not only are unnecessary, but are also, to a degree, harmful as they try

to prevent the small tendency of the girders to separate during elastic response, consequently transferring restraining forces to girder webs. A companion paper to this work (Kathol *et al.* 1995) sought to: 1) investigate the global and local behavior of steel bridges with and without diaphragms and 2) assess the ultimate load carrying capacity in the absence of diaphragms. Design, construction, and testing of a full scale steel girder bridge in the laboratory was completed to fulfill these objectives. As with Azizinamini *et al.* (1995), this study concluded that the contribution of diaphragms to load carrying capacity of steel girder bridges is minimal and also noted that corrosion problems are closely linked with the presence of diaphragms. Stallings *et al.* (1996a) and Stallings *et al.* (1996b) made the same case about the effectiveness of intermediate diaphragms. Evaluation of field measurements of girder stresses and deflections made before and after the diaphragms were taken out were the basis for the conclusions reported. The study cited Zokaie, Bakht and Moses, Walker, and Newmark in agreeing with the determination that the deck was responsible for transverse load distribution in multi-girder steel bridges. It was noted that the National Cooperative Highway Research Program (NCHRP) Project No. 12-26, which produced the truck load distribution factors for the AASHTO LRFD Specifications (AASHTO 1994), assumed diaphragms and cross frames had an insignificant effect on load distribution. Despite this acknowledgment, AASHTO still requires the inclusion of diaphragms at points of maximum moment for spans over 40 ft (12.19 m).

Cheung *et al.* (1986) reported on the apparent lack of previous research to deal with the actual increases or decreases of longitudinal moments due to diaphragms, i.e., most published papers concentrated on the alleged effectiveness, or lack thereof, of a particular *arrangement* of diaphragms. One point that was stressed heavily is the fact that three-dimensional models are essential when evaluating the effectiveness of intermediate diaphragms. Contrary to other research, this study found that the actual number of diaphragms do not affect the global distribution of moments provided that the total diaphragm stiffness remains unchanged and that there are at least two or more intermediate diaphragms present within the span. Kennedy and Soliman (1982) had reached similar conclusions four years earlier. Based on experimental findings and parametric studies using the finite element method, it was observed that the effective moments of resistance along failure yield lines in the positive and negative moment regions depend on the position of the load and on the nature of the connection between the transverse steel diaphragms and the longitudinal steel beams or girders. Tedesco *et al.* (1995) presented a comprehensive, three-dimensional, dynamic finite element analysis of a multi-girder steel bridge, both with and without diaphragms. Comparisons with field test results were made to verify the analysis.

1.2.2. LOAD DISTRIBUTION AND DESIGN

Background information on the development of wheel load distribution factors

can be found in Culham and Ghali (1997), Hays *et al.* (1986), Sanders and Elleby (1970), and Stanton and Mattock (1986). In work completed prior to the new AASHTO formulas, Tabsh (1994) presented a simple method for the computation of live load distribution factors for highway girder bridges, taking into account the longitudinal and transverse effect of the truck loads on the bridge. One significant aspect of the study was the concern with permit loading when developing the equations. Verification of the proposed equations was completed by comparing results on non-composite and composite steel girder bridges.

Chen (1995a and 1995b) studied load distribution in bridges with unequally spaced girders. AASHTO empirical formulas for estimating live load distribution factors were compared to results from the refined method. Parametric studies were conducted with a number of real bridge examples that were simply supported, non-skewed, and had no diaphragms. Refined load distribution equations were proposed. Subsequent work by Chen and Aswad (1996) sought to review the accuracy of the formulas for live load distribution for flexure contained in the LRFD Specifications (AASHTO 1994) for prestressed concrete I-girder bridges. It was concluded that the use of a refined method, namely finite element analysis, generally leads to a reduction of the lateral load distribution factor in I-beams when compared to the simplified LRFD guidelines. Fu *et al.* (1996) conducted comparable work by field testing four steel I-girder bridge structures under the effect of real moving truck loads. The results indicated that all the code methods (AASHTO, LRFD, and the Ontario Highway Bridge Design Code [OHBDC]) produced higher distribution factors.

Further revisions to load distribution equations were presented by Tarhini and Frederick (1995). Contrary to AASHTO assumptions, their finite element analysis revealed that the entire bridge superstructure acts as a unit rather than a collection of individual structural elements. The paper correlated distribution factor results obtained from published field test data with the proposed formulas as well as the AASHTO method. The effect of cross bracing on the wheel load distribution factor was found to be negligible.

1.2.3. EXPERIMENTAL TESTING

1.2.3.1. Static Testing

In recent years, several studies have been published on load testing of bridges using known weight trucks or ambient traffic loadings. However, the focus of the individual research efforts has been many and varied. For example, in research on nondestructive testing of a concrete slab bridge, Aktan *et al.* (1992) reported on the use of known weight trucks to obtain static bridge response as a basis for nondestructive bridge evaluation (NDE). Experimental data taken from the static and dynamic

testing of the bridge were used to calibrate a finite element model. A similar study was conducted by Cook *et al.* (1993) on a prestressed flat slab bridge. Experimental and analytical research was conducted with the primary objectives of: testing the bridge for service, fatigue, and ultimate loads; developing analytical models to predict the performance of the system; and verifying the analytical results by comparing them with those obtained from experimental data. In Helba and Kennedy (1995), equations for the design and analysis of skew bridges were developed from the analysis of a prototype composite bridge subjected to Ontario Highway Bridge Design Code (OHBDC) truck loading. One conclusion drawn from this study was that rigidly connected diaphragms produce a significant increase in the ultimate load capacity of the bridge.

Most researchers, though, tend to concentrate on a particular aspect or characteristic of a bridge, as is evident in tests conducted by Craig *et al.* (1994). This study noted that strains measured on fascia stringers under decks with integral curbs were significantly lower than those measured on the first interior beam, even when the wheel line was closer to the fascia stringer than to the first interior beam. Ebeido and Kennedy (1996a) conducted an experimental investigation on the effect of transverse diaphragms on the load distribution characteristics of simply supported skew composite steel bridges. The study revealed the importance of the presence of orthogonal intermediate transverse diaphragms joined to the longitudinal girders using moment connections. The study also reported results from tests done by Boyce in 1977 on actual bridges which demonstrated that such connections lead to improved bridge stiffness, better load distribution, and increased ultimate load capacity. Empirical formulas for span and support moment distribution factors were derived for a large class of bridge characteristics (e.g., bridges with more than two continuous spans, nonprismatic girders, etc.). Empirical formulas for both the reaction and the shear distribution factors were developed in later work (Ebeido and Kennedy 1996b).

Only one of the articles obtained in the literature review for experimental testing made mention of the effects of overload (neglecting the studies on railway bridges, of course). Dicleli and Bruneau (1995) investigated the effects of overload trucks on steel slab-on-girder bridges based on the growing concern that the cumulative effect of such overloads have never been assessed. Only bending moments were considered in investigating the potential negative impacts of heavy permit trucks. One conclusion drawn from this study was that none of the permit trucks considered produced detrimental effects on the interior girders since in bridges with more than one design lane, combinations of two or more design trucks could be used to produce moments much larger than those resulting from a single heavy permit truck.

1.2.3.2. Dynamic Testing

Studies into the dynamic characteristics of bridges were also helpful for the

research at hand. Some studies attempted to ascertain only the global response of a bridge for either categorization or calibration purposes. Dusseau and Dubaisi (1993) reported on the dynamic testing of 20 typical highway bridges in Washington. Empirical formulas for predicting the vibrational frequencies of other bridges in the Washington inventory were derived. Multi-girder steel bridges with varying span lengths and number of diaphragms were evaluated dynamically using design vehicles in a study conducted by Wang *et al.* (1993). Upon completion of the field tests, the dynamic responses of the bridges were analyzed with the finite element method.

On the other hand, some researchers completed dynamic tests to investigate the effect of varying bridge characteristics on mode shapes and vibrational frequencies. Law *et al.* (1995a) conducted a study whereby the effect of local damage in the diaphragm on the first modal frequency was examined. Three types of damage were studied that constituted a reduction in the stiffness of the diaphragm(s). The study concluded that there was no noticeable change in the first modal frequency in all three cases. Law *et al.* (1995b) furthered the work with model tests and measurements of 13 full scale bridges. Similarly, Paultre *et al.* (1995) initiated a study with the following main objectives: 1) evaluating the dynamic amplification factor for different highway bridges, 2) calibrating finite element models of the bridges being tested, and 3) examining the effects of changes in the stiffness of structural elements and the influence of secondary structural elements on the dynamic response. Data from the tests demonstrated that the dynamic amplification factor may be strongly influenced by variables such as the vehicle speed and the ratio of the vehicle weight to the total weight of the structure.

1.2.4. ANALYTICAL MODELING

Analytical studies involving the finite element method, skew effects in bridges and/or the presence of intermediate diaphragms in bridges were desired. Although several references concentrated on different bridge types than prestressed concrete slab-on-girder bridges, the general principles and theories outlined in each study were quite useful in the current research.

1.2.4.1. Static Analysis

Chen and Aswad (1994) investigated the differences between AASHTO, LRFD, and refined methods (finite element method, the grillage analogy method, or the harmonic [series] method) for bridge analysis. Bridge models were constructed using standard shell and beam finite elements. It was concluded that the refined methods yielded substantially smaller values for distribution factors than the two code procedures.

Bakht (1988) reported on a simple procedure by which skewed bridges could be analyzed to acceptable design accuracy using methods originally developed for the analysis of right bridges. The study concluded that beam spacing, in addition to skew angle, is an important criterion when analyzing a skew bridge as right. Results from an error analysis using experimental data indicated that the process of analyzing a skew bridge as equivalent right is safe as far as longitudinal moments are concerned, but is unsafe when dealing with longitudinal shears.

Ghosn and Moses (1996) reported on the capability of typical prestressed concrete I-beam bridge systems to continue to carry loads after the failure or the damage of one or more of the bridge's main load carrying members. The effect of heavy truck loads was considered. Analytical results from the study were compared to those obtained from full scale field tests.

1.2.4.2. Dynamic Analysis

Casas (1995) outlined a method to model bridges dynamically based on field test observations. Finite element models using beam elements in a frame or grillage assembly were employed. Difficulties in completing a dynamic analysis using a grillage analogy were addressed. Barker (1996) used the grillage analogy to conduct a study on a one-third scale composite bridge. Jaeger and Bakht (1982) initially discussed the use of grillage analogy to conduct bridge analyses. A very detailed explanation of its theory and application was included. Wilson (1996) also examines the use of finite element models in conducting three-dimensional dynamic analyses of structures. Special emphasis is placed on dynamic analysis for Earthquake Engineering.

In a work by Chan and O'Connor (1990b), vehicle models were developed to evaluate the dynamic impact factor used to design highway bridges. The proposed impact factors were based on numerous field studies on a composite steel and concrete bridge and on research previously conducted in 1988. Recommendations were made to consider a dynamic moment ratio (DMR) rather than the more popular impact factor. Since many aspects of dynamic bridge modeling involve the definition of design trucks, Nassif and Nowak (1995) attempted to quantify the dynamic load factor (DLF) associated with the current inventory of trucks using the results from previously published experiments. The same conclusions of Chan and O'Connor were reached - the DLF decreases as the static stress in each girder increases, i.e., the DLF decreases for heavier trucks. This latter work seems to be a generalization of the research on a steel girder bridge conducted by Nowak *et al.* (1993a).

Huang *et al.* (1992) conducted a parametric study on three span, continuous steel beam bridges subjected to dynamic loads. Analytical results indicated the

variation of wheel load distribution factors and impact factors were insignificant at most sections as transverse stiffness was varied, leading to the conclusion that very large transverse stiffness in the type of steel multi-girder bridge examined was unnecessary. Studies on thin-walled box girder bridges (Huang *et al.* [1995]) yielded similar results. Huang *et al.* (1993) conducted the same research on concrete girder bridges after the study of prestressed concrete bridges made by Wang *et al.* (1992). Variations in transverse stiffness were noted to have a significant effect on short span, concrete girder bridges. The significance of this effect dissipated as the span length was increased.

Theoretical studies also offered some insight to dynamic modeling considerations. Chompooming and Yener (1995) presented various algorithms for the moving mass problem. Several models of vehicles were proposed and evaluated. An alternate to the AASHTO impact factor was again offered in the form of a dynamic response factor (DRF) which represents the ratio of maximum live load dynamic deflections to maximum live load static deflections. Gbadeyan and Oni (1995) tackled the same moving mass problem with special emphasis on developing a formulation based on arbitrary end conditions, rather than only simple supports. Lee (1995) presented similar work in a study of a multi-span beam with one-sided point constraints subjected to a downward directed moving load. Lin *et al.* (1994) reported on dynamic modeling using Bernoulli-Euler's differential equation assuming small deformations to derive the dynamic equations of a bridge vibration system. Vibration control design was the focus of this research.

1.2.5. MISCELLANEOUS

Many additional references provided background information on topics not listed above, e.g., prestressed concrete girder design for continuous spans (Oesterle *et al.* [1989]). Some offered insight into material behavior (Ahlborn *et al.* [1995]), while others looked at a particular component of a bridge sub- or superstructure, e.g. Burke (1994) examined semi-integral abutments while Pentas *et al.* (1995) investigated joint movements.

Dunnicliff (1993) provided information on field testing instruments. Qualities such as accuracy, precision, and sensitivity were discussed. Methods to combat noise and error in data acquisition were presented. Detailed evaluations of different types of strain gages, transducers, and methods of data acquisition were valuable during the instrumentation phase of the current research study. A discussion on the use of temperature compensating, or "dummy", gages was also presented.

Although many authors discussed the finite element method (Aktan *et al.* [1995], Barker [1995a], Galambos *et al.* [1993], Klaiber *et al.* [1987], Moses and Verma

[1987]), their application was to steel girder bridges and did not concentrate on load distribution or the presence of intermediate diaphragms. Moses and Verma (1987) included prestressed concrete spans in their research in addition to incorporating weight-in-motion (WIM) data to define realistic truck loads. Barker (1995b) did propose a new method for the determination of load distribution factors for concrete bridges. However, this new method was not popular due to its site specific requirements. Mufti *et al.* (1994) evaluated the effectiveness of finite element programs to conduct structural assessments.

1.3. BRIDGES ALONG COAL HAUL ROUTES

The primary source for load distribution equations for engineers in the United States can be found in the *Guide Specifications for Distribution of Loads for Highway Bridges* (AASHTO Subcommittee 1994). However, this code points out that the simplified load distribution formulas have limitations. If two different truck types are considered simultaneously, e.g., one permit truck along with a design truck, the formulas are not applicable. Furthermore, the effects of intermediate diaphragms and cross frames are not included in the load distribution formulas. None of the AASHTO codes addresses the type of overload condition that exists with coal haul trucks on bridges with or without intermediate diaphragms.

Considering the extensive coal haul route system in the Commonwealth of Kentucky, these limitations on the design equations can be of great concern to engineers. It is interesting to note that some bridges of prestressed concrete I-girder construction which carry coal haul traffic in Southeastern Kentucky have experienced unusual concrete spalling at the interface of the intermediate diaphragms and the bottom flange of the girders (see Figure 1.3 - notice that the diaphragm anchor bars mentioned in Section 1.1.1 have been exposed). Conversely, bridges of similar design subjected to only normal traffic loading (i.e., no coal trucks) do not seem to incur the same damage. In these overload cases, the diaphragms appear to be contributing more to the increased rate of deterioration and damage than reducing the moment coefficient and distributing the traffic loads as expected. Since Dicleli and Bruneau (1995) examined overloads on steel

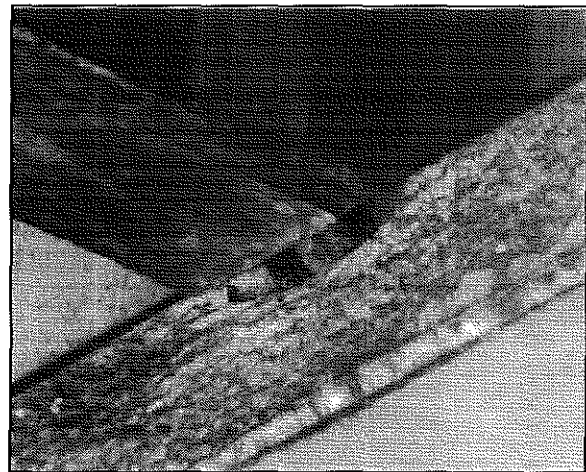


Figure 1.3. Concrete Spalling at Diaphragm-Girder Interface.

slab-on-girder bridges based on the growing concern that the cumulative effects of such overloads have never been assessed, it would appear to be expedient that a similar study be conducted on prestressed concrete I-girder bridges, including the effects of the intermediate diaphragms.

1.4. SCOPE OF RESEARCH

1.4.1. LOCATION OF THE BRIDGES

The newly constructed US 23 is a bypass around the city of Paintsville in Johnson County, Kentucky. This county is located in the coal rich Southeastern portion of the Commonwealth (see Figure 1.4.1). US 23 is officially recognized in the coal haul route system of Kentucky and accounts for approximately 20 percent of the total coal haul road mileage in Johnson County. The bypass is considered a major artery for the 2.1 million tons (18,682.4 MN) of coal shipped within the county each year (Kentucky 1994). Since the new route for US 23 intersected US 460 and KY 40, rather than establish traffic lights along these highly traveled roads, overpass bridges were constructed. The focus of this research is on the two US 23 bridges over KY 40.

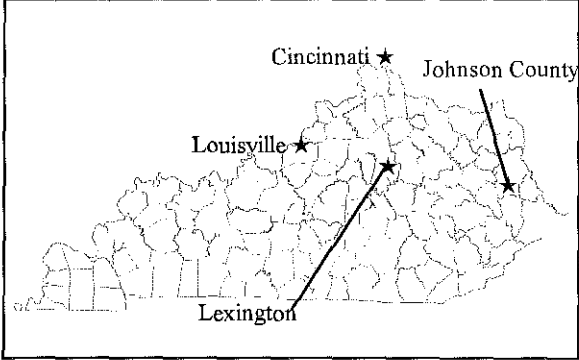


Figure 1.4.1. Map of Kentucky Highlighting Johnson County.



Figure 1.4.2a. Skew Angle of the Girders.

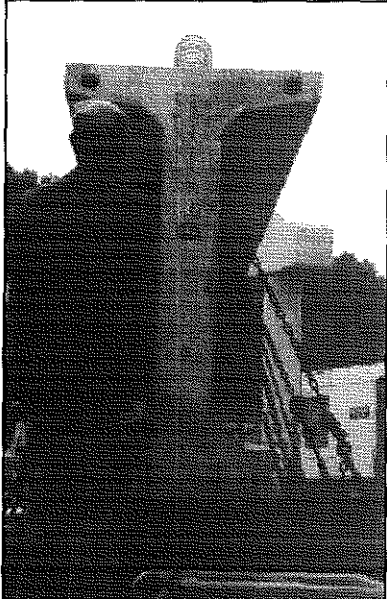


Figure 1.4.2b. Modified AASHTO Type VI I-Girder Used on the US 23 Bridges.

1.4.2. BRIDGE DESCRIPTIONS

The two bridges were constructed with four spans of lengths 58.875 ft (17.95 m), 82.5 ft (25.15 m); 118.5 ft (36.12 m); and 80.625 ft (24.58 m), respectively. The width of the bridge was such to accommodate two traffic lanes with an exterior shoulder 12 ft (3.66 m) wide and an interior shoulder 6 ft (1.83 m) wide. This led to an overall bridge width of 45.292 ft (13.81 m). Due to the orientation of KY 40, the bridges have a 50 degree skew angle. The skew is measured as the angle bounded by the centerline of the pier and a line perpendicular to the girders. Figure 1.4.2a illustrates the skew in the two bridges. A superelevation of 0.029 ft per foot (0.0345 m per meter) was provided on both bridges.

Each bridge superstructure is composed of five precast, prestressed concrete Modified AASHTO Type IV I-girders, pictured in Figure 1.4.2b, beneath an 8 in (203.2 mm) thick cast-in-place deck supported on stay-in-place metal deck forms. The AASHTO girders are 66 in (1676.4 mm) tall, and have a bottom flange width of 26 in (660.4 mm), a top flange width of 36 in (914.4 mm), and a web thickness of 8 in (203.2 mm). Shear stirrups were extended above the top flange to provide composite action once the concrete in the deck cured. The superstructure is continuous for live load through the use of the composite cross section and pier diaphragms. The substructure consists of two end abutments and three piers, each with four pier columns. Each pier column is 36 in (914.4 mm) in diameter and is bounded by a 42 in (1066.8 mm) square pier cap. Shear keys are provided on the abutments and pier caps to prevent lateral movement of the superstructure during loading. All substructure elements were erected on steel bearing piles.

The Southbound bridge, which will carry empty coal trucks, was constructed with 10 in (254 mm) thick cast-in-place concrete intermediate diaphragms (see Figure 1.1.1a). Conversely, the Northbound bridge carries loaded coal trucks and was constructed with temporary steel intermediate diaphragms (see Figure 1.1.1b). The diaphragms are in a "Z" formation and are attached to the girder via an angle bracket and bolt. After the deck achieved sufficient compressive strength, these bolts were loosened. From this point on, the Northbound bridge was considered to have no intermediate diaphragms. Diaphragms in both bridges were located at the midspan of Span 1, at the quarter points in Spans 2 and 3, and at the third points in Span 4. Figure 1.4.2c gives a bird's eye view of both bridges. Figure 1.4.2d is a side view of the Southbound bridge. In both pictures, Span 1 is in the foreground.

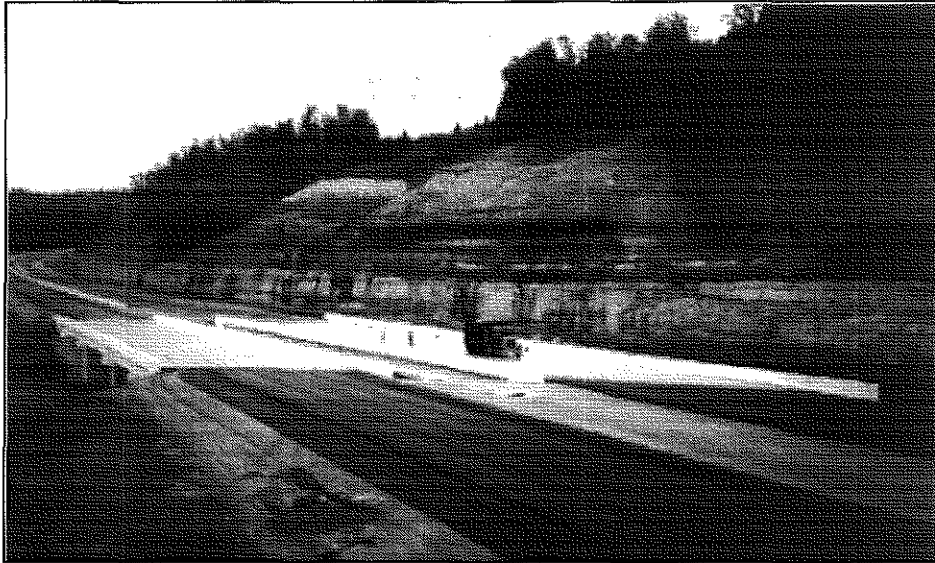


Figure 1.4.2c. Bird's Eye View of the US 23 Bridges: Southbound (Left - Bridge With Intermediate Diaphragms) and Northbound (Right - Bridge Without Intermediate Diaphragms).

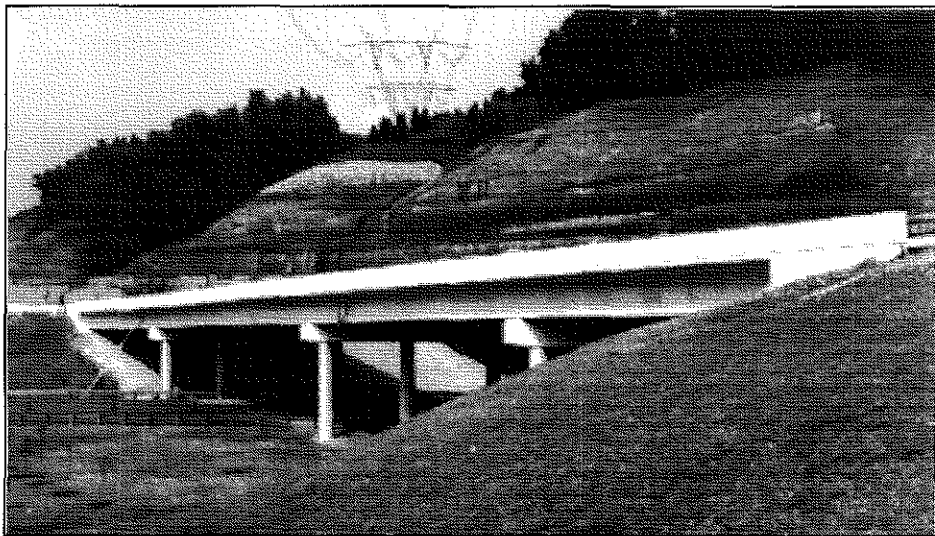


Figure 1.4.2d. Side View of the Southbound US 23 Bridge (Bridge With Intermediate Diaphragms).

1.4.3. TRAFFIC LOADING PROFILE

As mentioned previously, US 23 is a vital link in the coal haul route system of Johnson County in addition to being a heavily traveled bypass around Paintsville. As such, the US 23 bridges over KY 40 can be expected to experience normal and overload traffic patterns. Dump and tractor-trailer type trucks, which can legally haul up to 80,000 lbs (355.84 kN) in Kentucky, will be in the normal traffic loadings.

On the other hand, the extended-weight coal haul road system created by Kentucky's General Assembly in 1986 allows trucks hauling coal to weigh much more if a permit is obtained. Under this system, three-axle (tandem) dump trucks may haul 94,500 lbs (420.34 kN), four-axle (tridem) dump trucks may haul 105,000 lbs (467.04 kN), and the five to six-axle tractor-trailers may haul 126,000 lbs (560.45 kN) (Associated Press 1995, Breed 1995b). Although these limits seem quite generous, they are rarely followed. According to state records compiled between January 1993 and May 1996, 104 tickets were issued in Johnson County to permitted coal trucks for exceeding the legal weight limit. The vehicles cited were an average of 53,588 lbs (238.36 kN) overweight (Breed and Bridis 1996). Still, Chief of Field Operations and Training for the Division of Motor Vehicle Enforcement Major Steve Maffet tells of even worse violations. "A while back we weighed one, I think it was in Pike County, it weighed somewhere around 206,000 lbs [916.29 kN]," Maffet said (Breed 1995b). Engineers must be aware of these potential overload conditions when designing a bridge because consistent and uniform enforcement of the load limits does not exist. For instance, one trucker was caught 89,000 lbs (395.87 kN) overweight, but only paid a \$25 fine for not wearing his seat belt (Breed 1996b).

1.4.4. RESEARCH OBJECTIVES

Bridges of prestressed concrete I-girder design along coal haul routes have been experiencing unusual distress (concrete spalling) at the interface of the diaphragms and the bottom flange of the girders. The intermediate diaphragms appear to be contributing more to the increased rate of deterioration and damage than reducing the moment coefficient and distributing the traffic loads as expected. The objectives of this study are as follows: 1) complete three-dimensional, static and dynamic finite element analyses of both bridges, 2) conduct field testing on both bridges, 3) calibrate the finite element models with the field test data, and 4) analyze the influence of intermediate diaphragms on load distribution in prestressed concrete (P/C) I-girder bridges subjected to vehicle overload common among coal haul trucks.

1.5. RESEARCH SIGNIFICANCE

Previously, AASHTO has recommended the use of diaphragms at points of maximum moment for spans greater than 40 ft (12.19 m). Kentucky exceeds the AASHTO guidelines by specifying diaphragms at points of maximum moment for spans between 40 and 80 ft (12.19 and 24.38 m) and diaphragms at third points for spans greater than 80 ft (24.38 m). As has already been discussed, the two bridges in this study exceed even the Kentucky requirements since diaphragms are located at the quarter points in Spans 2 and 3.

It should be noted that Section 9.10.1 of the *Standard Specifications for Highway Bridges* (AASHTO 1996) allows for diaphragms to be omitted when adequate strength is determined through testing or structural analysis. By investigating the load distribution and the relative transverse displacement (or twisting) between the prestressed concrete girders, it will be possible to ascertain whether or not the intermediate diaphragms are performing as intended in bridges subjected to the severe overload of coal trucks. This research will be the first study to address the issues of overload (i.e., coal trucks) and the influence of intermediate diaphragms in bridges with and without diaphragms. This task will be accomplished through the use of finite element models calibrated with static and dynamic experimental test data. Additional emphasis will be placed on determining the cause of the concrete spalling in the diaphragm-girder interface region. The results obtained from investigating these issues could lead to significant reductions in the construction and maintenance costs of future bridge projects.

CHAPTER 2

INSTRUMENTATION AND EXPERIMENTAL TESTING

2.1. INTRODUCTION

Once the US 23 bridges over KY 40 had been identified as the experimental subjects of this study, an instrumentation plan was prepared so that the dynamic and static testing would be comprehensive and complete. Planning for the instrumentation began shortly after construction of the two bridges was started. In cooperation with the contractor and Kentucky Transportation Cabinet personnel, instrumentation was proposed which would take advantage of the opportunity to embed gages in the bridges as the construction progressed. The information in this chapter is a summary of the instrumentation plan and record of how this plan was implemented in the laboratory and/or field.

During the planning of the static testing phase, certain physical aspects of the bridge site had to be addressed. First, Span 3 of the respective US 23 bridges was located directly over KY 40 (see Figure 2.1). This road is a heavily traveled roadway which serves a large portion of the Paintsville community and, therefore, could not be closed for the duration of the testing. Consequently, personnel from the Kentucky Department of Highways at the Johnson County garage were contacted to coordinate traffic control as the static testing was conducted.



Figure 2.1. Span 3 of the US 23 Bridges.

Second, the relative height of the two US 23 bridges required mechanical assistance to access the superstructure. Two motorized man-lifts were used to reach the I-girders. A ladder was sufficient for instrumenting the girders near the pier at the end of Span 3 since the clearance height at this point was approximately 20 ft (6.10 m) and these locations did not pose a threat to personnel by passing traffic. The use of this equipment greatly reduced the preparation and instrumentation time required to complete the testing of the bridges.



Figure 2.2. US 23 Bridge Over KY 40 (Span Numbers Are Marked - Northbound Traffic Travels from Right to Left [←]).

Third, a trailer and canopy were used to house the test equipment and establish a data acquisition station. Both the trailer and canopy provided the necessary mobility to move the station from one bridge to another with minimal effort. Personnel spent the night on site to guard against vandalism and theft.

Finally, high-voltage, overhead power lines were a chief concern. Lead wire lengths were kept as short as possible and shielded wire was used for all the equipment. During the data acquisition phase, an effort was made to eliminate the static noise associated with the electro-magnetic field of these overhead power lines.

2.2. STATIC TESTING INSTRUMENTATION

As mentioned in Chapter 1, each US 23 bridge has four spans, is continuous for live load, and uses five precast, prestressed concrete (P/C) I-girders to support a cast-in-place deck. Concrete intermediate diaphragms were included in the Southbound bridge. The Northbound bridge was constructed with steel intermediate diaphragms that were loosened after the deck cured. Since the greatest response to loading could be expected in the longest span, Span 3 (see Figure 2.2), only this section had extensive

instrumentation during the static testing phase. Instrumentation for static testing was placed in the deck and on the girders of both bridges as well as on the diaphragms of the Southbound bridge.

2.2.1. INSTRUMENTATION IN THE DECK

2.2.1.1. Transverse Direction

By measuring the strains in the transverse deck reinforcement, a comparison of the stresses in the steel reinforcement bars (hereunto referred to as "rebars") in the deck could be made between bridges with and without intermediate diaphragms (Southbound and Northbound bridges, respectively). The measured strains would allow for the determination of whether or not a bridge deck would experience higher stresses in the absence of diaphragms. A secondary benefit these strain readings provided was to lend some insight into the bending behavior of the deck in bridges with and without diaphragms.

Epoxy coated rebars fitted with strain gages and measuring 20 ft (6.10 m) in length were placed in the bridge decks in the transverse direction (perpendicular to the girder line) at the locations indicated in Figures 2.2.1a and 2.2.1b on the Southbound and Northbound bridges, respectively. These bars were in addition to the reinforcement required by the original design. It is important to note that each location group (i.e., S1A, N1B, etc.) had one rebar in the top mat of deck reinforcement and, as a precaution, one rebar in the bottom mat of deck reinforcement. A code name system was developed to document the precise location of each gage. For example, in Figure 2.2.1a the code "S1A3" was obtained by taking the "S" to stand for the Southbound bridge, "1" to differentiate the bar as transverse reinforcement, the "A" to designate the transverse line on which the gages were mounted, and "3" to mark the

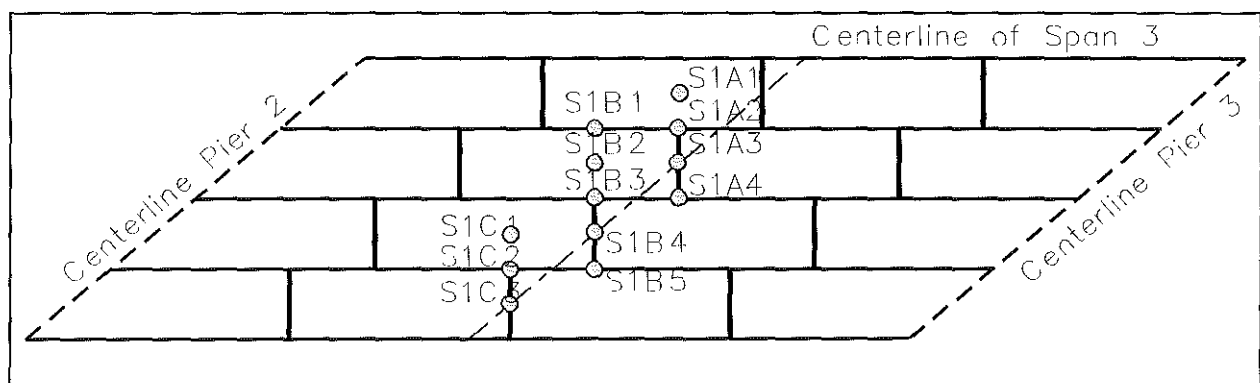


Figure 2.2.1a. Transverse Strain Gage Placement in the Southbound Deck (Bridge With Intermediate Diaphragms).

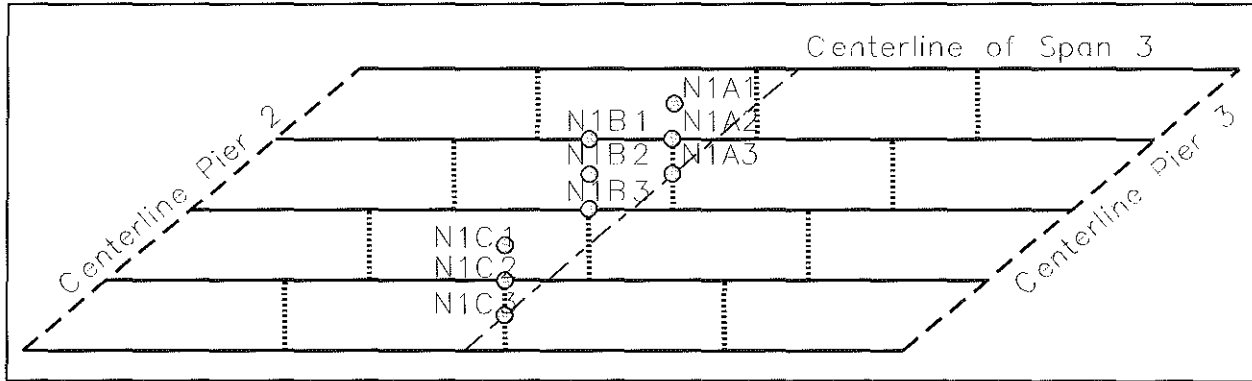


Figure 2.2.1b. Transverse Strain Gage Placement in the Northbound Deck (Bridge Without Intermediate Diaphragms).

position of the third gage on the rebar. The letter "T" or "B" was added to this code name to designate whether the rebar was in the top or bottom mat of the deck reinforcement.

The strain gages were mounted following the process described in Appendix A for the steel strain gages. An example of a strain gage mounted to the steel rebar is given in Figure 2.2.1c. The gages were aligned such that the end gages (gages 1, 3, 4, and 5 in Figure 2.2.1a and gages 1 and 3 in



Figure 2.2.1c. Strain Gage on Rebar Prior to Protective Coatings.

Figure 2.2.1b) were located at a distance from the end of the bar greater than the development length, l_d . For No. 6 epoxy coated rebar, Section 8.25 of the *Standard Specifications for Highway Bridges* (AASHTO 1996) gives equations to calculate the development length as 29.04 in (737.62 mm). In some instances No. 5 epoxy coated rebar were used. Development length requirements were still met in these cases. Strain gages 1 and 3 were placed at a distance of 63 in (1600.2 mm) from the end of the bar to the center of the gage. The additional locations illustrated in Figure 2.2.1a (i.e., S1A4, S1B4, and S1B5) indicate that additional transverse bars, 10 ft (3.05 m) in length, were placed in the bottom mat. The strain gages on these bars, gages 4 and 5, were placed at the center of the bar. Rebar with strain gages were not placed in locations comparable to these additional gages (i.e. S1A4, S1B4, and S1B5)

on the Northbound bridge since the deck had already been poured when these new gages were added to the instrumentation plan. Table 2.2.1a lists the number of strain gages and rebars used to instrument the respective bridge decks in the transverse direction.

Table 2.2.1a: Instrumentation on the Transverse Reinforcement in the Bridge Deck.

Bridge	Direction	Instruments/Materials Required	
		Strain Gages	Reinforcement Bars
Southbound	transverse	21	9
Northbound	transverse	18	6

2.2.1.2. Longitudinal Direction

The strain information obtained from gages mounted on longitudinal steel reinforcement in the deck was coupled with the information from the strain gages of Section 2.2.2.2. to allow for the determination of the neutral axis of the composite cross section. Strain comparisons between the bridges with and without intermediate diaphragms could then be made to investigate how forces/stresses are transferred by diaphragms.

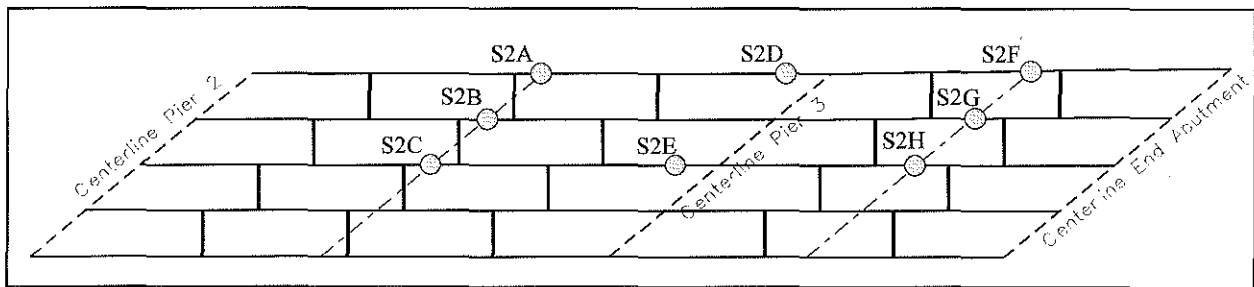


Figure 2.2.1d. Longitudinal Strain Gage Placement in the Southbound Deck (Bridge With Intermediate Diaphragms).

Epoxy coated rebars measuring 10 ft (3.05 m) in length and fitted with strain gages were placed in the deck in the longitudinal direction (parallel to the girder line) at the locations indicated in Figures 2.2.1d and 2.2.1e on the Southbound and

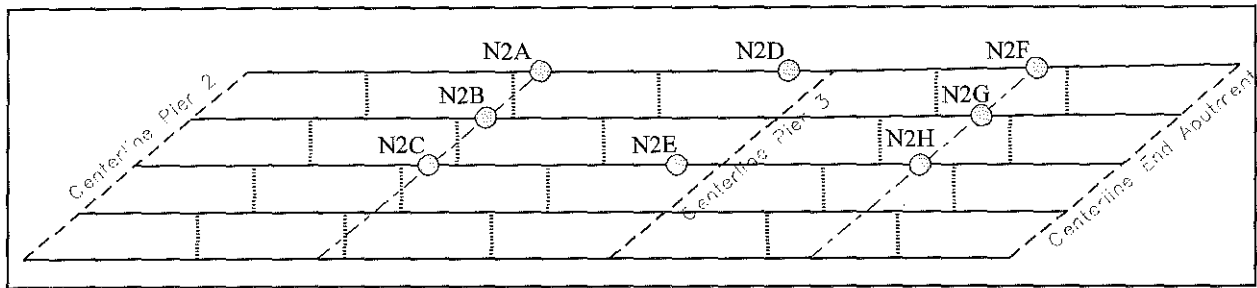


Figure 2.2.1e. Longitudinal Strain Gage Placement in the Northbound Deck (Bridge Without Intermediate Diaphragms).

Northbound bridges, respectively. These bars were in addition to the reinforcement required by the original design. Each rebar was instrumented with only one strain gage located at a distance greater than the development length, ℓ_d , from either end of the bar. The strain gage was placed at a distance of 60 in (1524 mm) from the end of the bar to the center of the gage. A similar code name as described above was applied to these longitudinal gages. The single exception to this was the fact that only one gage was mounted to a bar, thereby negating the need for the last number. For example, in the code name S2D in Figure 2.2.1d, "S" designates the bar as being in the Southbound bridge, "2" indicates that the bar is in the longitudinal reinforcement of the deck, and "D" gives the exact location. Table 2.2.1b lists the number of strain gages and rebars used to instrument the respective bridge decks in the longitudinal direction.

Table 2.2.1b: Instrumentation on the Longitudinal Reinforcement in the Bridge Deck.

Bridge	Direction	Instruments/Materials Required	
		Strain Gages	Reinforcement Bars
Southbound	longitudinal	8	8
Northbound	longitudinal	8	8

2.2.2. INSTRUMENTATION ON THE GIRDERS

2.2.2.1. Displacements

A comparison of girder out-of-plane displacements between bridges with and without intermediate diaphragms was essential in determining the effectiveness of diaphragms. Large out-of-plane displacements would be viewed as an indication that diaphragm use needed to be continued.

Linear Variable Differential Transformers (LVDTs) were placed at the locations indicated in Figures 2.2.2a and 2.2.2b for the Southbound and Northbound bridges, respectively. The LVDTs were used to measure the vertical deflections (locations marked by circles) and relative out-of-plane displacements (locations marked by diamonds) of the girders. A code name similar to those described above was applied to differentiate these measurements from the others. For example, in the code name

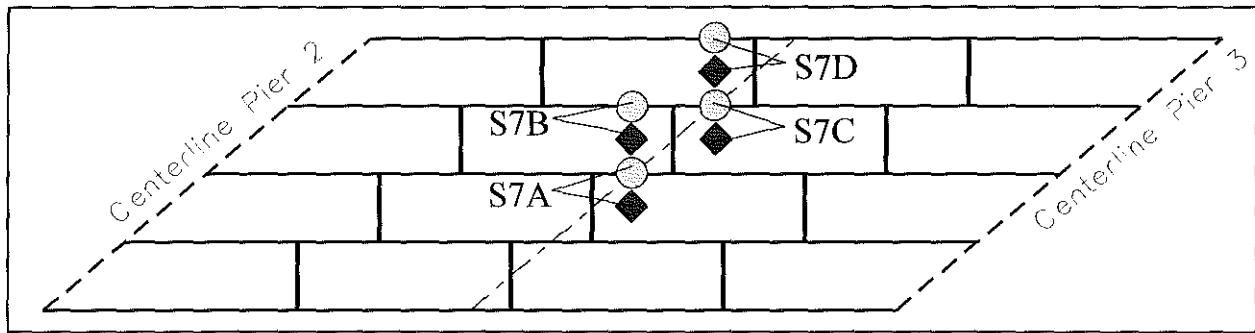


Figure 2.2.2a. LVDT Locations on Centerline of Southbound Span 3 (Bridge With Intermediate Diaphragms).

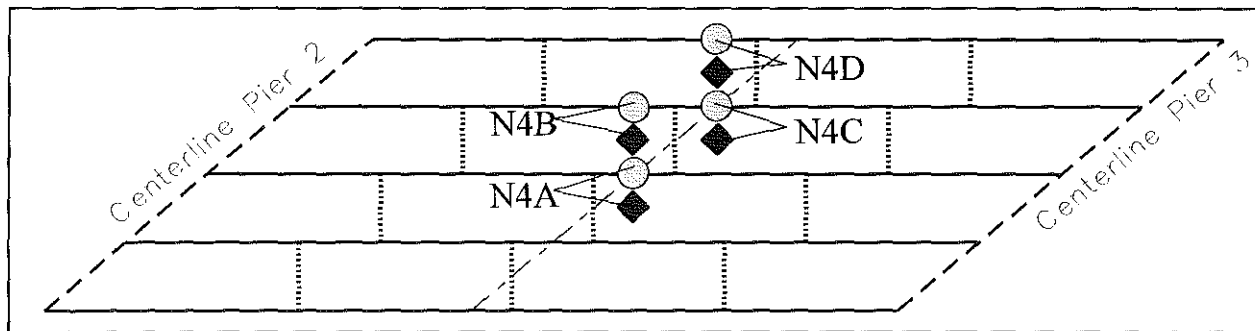


Figure 2.2.2b. LVDT Locations on Centerline of Northbound Span 3 (Bridge Without Intermediate Diaphragms).

S7D in Figure 2.2.2a, "S" represents the Southbound bridge, "7" indicates that the instrument is an LVDT (the code was "4" for the Northbound bridge), and "D" gives the exact location. The letters "V" and "T" were also added to the code name to designate whether the measurement was a vertical or transverse (out-of-plane) displacement.

Due to the relative height of the structure, a rigid mounting platform on which to mount the LVDTs was not feasible. Consequently, a cable-suspended weight system was developed to measure the vertical displacements. Threaded inserts were hammered into the bottom face of the girder. An eye hook was then screwed into the insert. Couplings and a steel cable were used to suspend a 50 lb (0.22 kN) cylinder slightly above a platform fitted with an LVDT. The weight and shape of the suspended cylinder were purposely chosen to reduce the effects of sway due to wind. This setup also allowed for easy transport to the next measurement location.

Obtaining absolute out-of-plane displacements was impossible since a rigid mounting platform was not available. Therefore, a spring-loaded rod, which is pictured in position in Figure 2.2.2c, was constructed to measure the relative out-of-plane displacement between two girders. A LVDT was mounted in parallel with the rod. An angle attached to the stationary portion of the rod provided the fixed end against which the LVDT measured displacement. Figure 2.2.2c also depicts the cable-suspended weight assembly described above. Table 2.2.2a lists the number of LVDTs used to instrument the respective bridges.

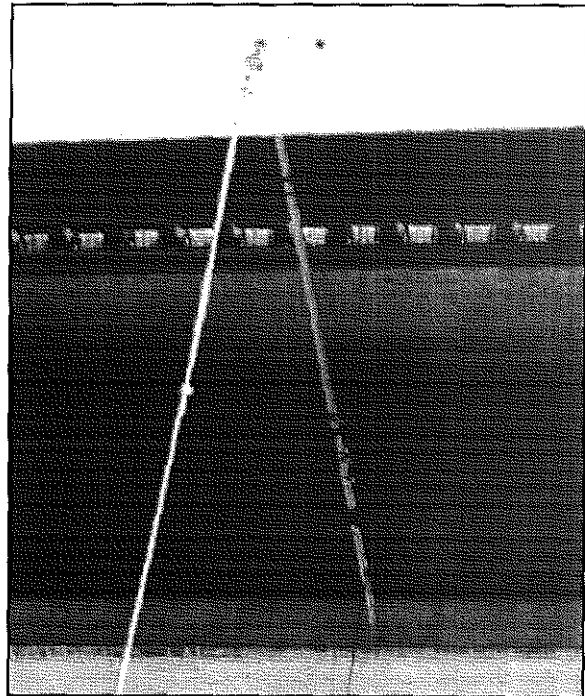


Figure 2.2.2c. Out-of-Plane and Vertical LVDT Assemblies.

Table 2.2.2a: Vertical and Transverse Displacement Instrumentation on the Girders.

Bridge	Instruments/Materials Required	
	Vertical LVDTs	Out-of-Plane LVDTs
Southbound	4	4
Northbound	4	4

2.2.2.2. Strains

Strain data across a girder cross section is essential for determining the neutral axis of the composite cross section under various loadings and how the neutral axis varies as the load traverses along the longitudinal axis of the bridge. Data obtained from this section coupled with the information obtained from the longitudinal bars of Section 2.2.1.2 would make these calculations possible. Strain comparisons between the bridges with and without intermediate diaphragms could then be made to investigate how forces/stresses are transferred among the girders by the presence of intermediate diaphragms.

Reusable strain gages were mounted on the prestressed concrete I-girders in Span 3 at the locations pictured in Figures 2.2.2d and 2.2.2e on the Southbound and

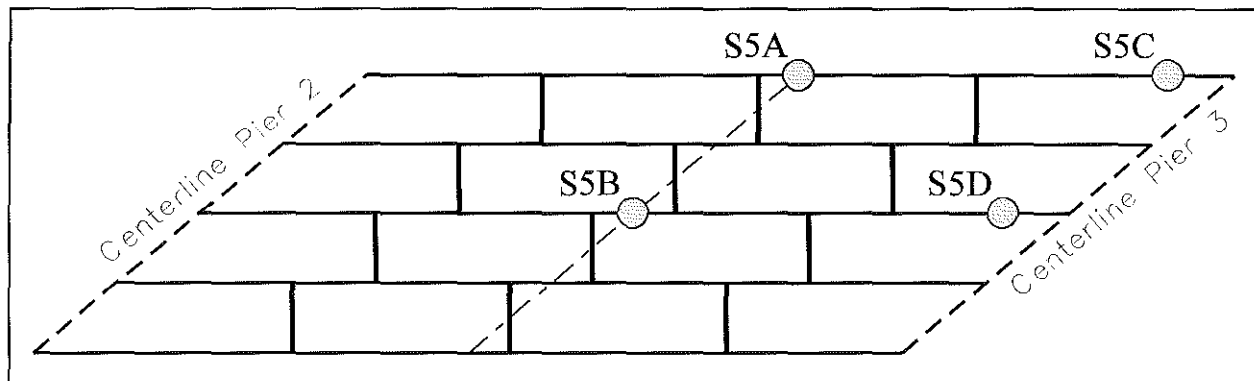


Figure 2.2.2d. Locations for Girder Strain Gage Placement in the Southbound Bridge (Bridge With Intermediate Diaphragms).

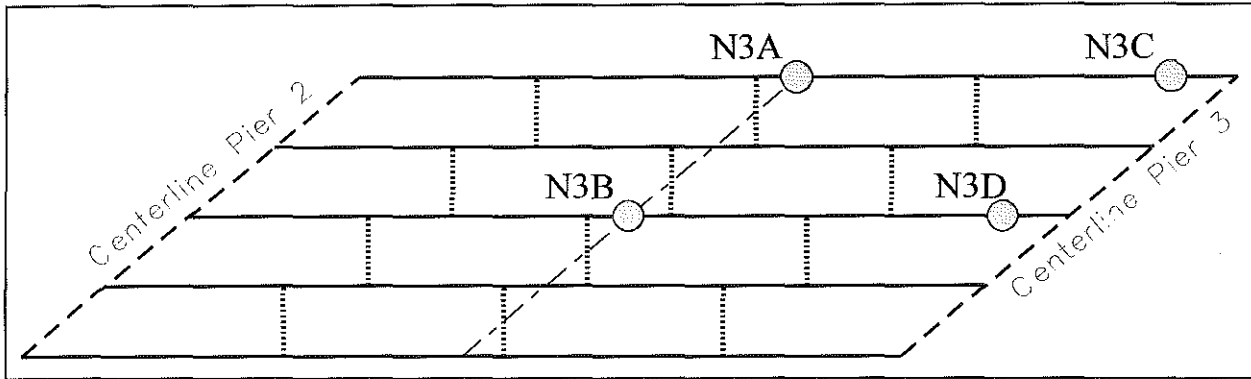


Figure 2.2.2e. Locations for Girder Strain Gage Placement in the Northbound Bridge (Bridge Without Intermediate Diaphragms).

Northbound bridges, respectively. The reusable strain gages placed on the girder were aligned with the longitudinal rebar instrumented with strain gages discussed in Section 2.2.1.2. Code names were used to designate the bridge and girder cross section considered. For example, in the code name S5A in Figure 2.2.2e, "S" designates the girder under consideration as being in the Southbound bridge, "5" indicates that reusable strain gages were aligned along the girder cross section (the code was "3" for the Northbound bridge), and "A" marks the exact location (i.e., centerline or end span on Girder 1 or 3). The letters "B", "M", and "T" were also used to indicate whether the reusable strain gage was located at the bottom, middle, or top of the girder. Table 2.2.2b lists the number of reusable strain gages required to complete this portion of the instrumentation.

Table 2.2.2b: Strain Gage Instrumentation on the Girders.

Bridge	Instruments/Materials Required
	Strain Gages
Southbound	12
Northbound	12

2.2.3. INSTRUMENTATION IN THE DIAPHRAGM REGION

2.2.3.1. Threaded Anchor Bars

Significant spalling of concrete has been noted at the interface of girder flanges and intermediate diaphragms on similar bridges along coal haul routes. It was assumed strain gages on the threaded anchor bars would provide some insight as to the nature of the bar stresses at these locations. These stresses may indicate the role the threaded anchor bars have in the intermediate diaphragms and what contribution they may lend to the concrete spalling, e.g., if bending in the threaded bars contributes to the spalling.

Steel strain gages were mounted on one of the two threaded diaphragm anchor bars (see Figure 2.2.3a) for the prestressed concrete I-girder locations indicated in Figure 2.2.3b. The bars had two gages mounted 90 degrees apart near the threaded end and were inserted such that one gage was oriented directly up, on a line perpendicular to the bottom face of the girder. Only the Southbound bridge could be instrumented as such. The code names in Figure 2.2.3b were applied to distinguish bridge and gage location. Table 2.2.3a summarizes the strain gages and materials required to instrument the Southbound bridge as such.

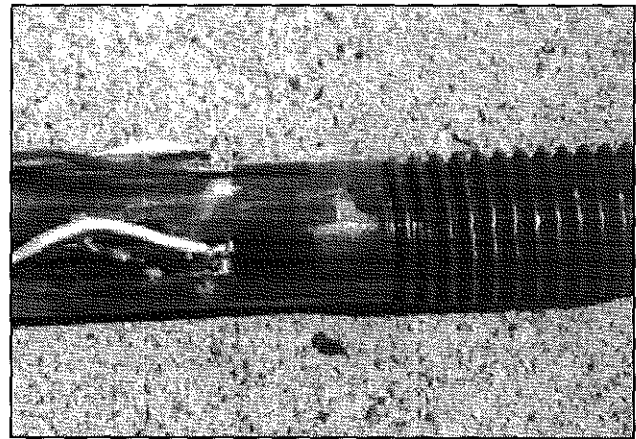


Figure 2.2.3a. Strain Gages on Diaphragm Anchor Bar Near Threaded End.

The reinforcement bars in the concrete intermediate diaphragms of the Southbound bridge typically extend into the deck. During construction, the reinforcement in the diaphragm marked in Figure 2.2.3b was cut low, i.e., not extended into the deck. It was critical that this situation be tested in order to ascertain the true behavior of concrete intermediate diaphragms in prestressed concrete I-girder bridges. With this diaphragm reinforcement cut low, three cases were tested: 1) bridges with diaphragms whose reinforcement extends into the deck, 2) bridges with diaphragms whose reinforcement does not extend into the deck, and 3) bridges without diaphragms (the Northbound bridge).

2.2.3.2. Diaphragms

Extensive instrumentation near the areas noted for significant concrete spalling was planned to provide some insight as to the nature of the stresses at these locations. These stresses may indicate the action of the intermediate diaphragm, i.e., whether the distress is a result of shear stresses, bearing forces, etc.

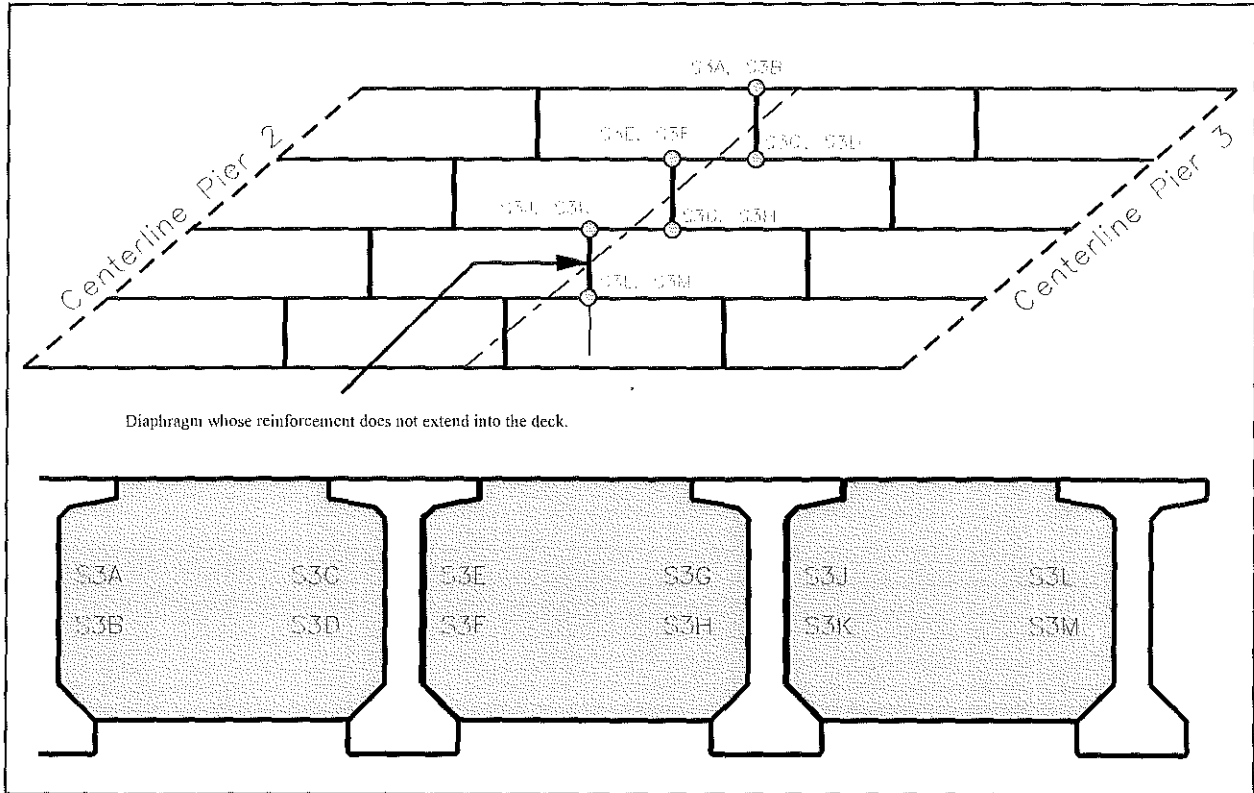


Figure 2.2.3b. Locations of Diaphragm Anchor Bars Instrumented With Strain Gages in the Southbound Bridge (Bridge With Intermediate Diaphragms).

Table 2.2.3a: Instrumentation on the Threaded Diaphragm Anchor Bars.

Bridge	Instruments/Materials Required	
	Steel Strain Gages	Threaded Diaphragm Anchor Bars
Southbound	12	6

Reusable strain gages were placed near the diaphragm-girder interface on the Southbound bridge girders as illustrated in Figure 2.2.3c at the locations indicated in Figure 2.2.3d. Since separating the girder, flexural strains from the strains causing concrete spalling would be difficult to do, a horizontal strain gage was also mounted a few feet from the diaphragm-girder interface (denoted by the "*" in Figures 2.2.3c and 2.2.3d). In order to obtain comparable strains in a bridge without diaphragms, the Northbound bridge was instrumented with a strain gage at the identical positions marked with an asterisk as indicated in Figures 2.2.3c and 2.2.3d. Code names for these gages were similar to those described above. For example S4A3 in Figure 2.2.3c can be broken down as follows: "S" denotes the Southbound bridge, "4" indicates the gages were near the diaphragm-girder interface, "A" designates the girder on which the gages were mounted, and "3" gives the gage number.

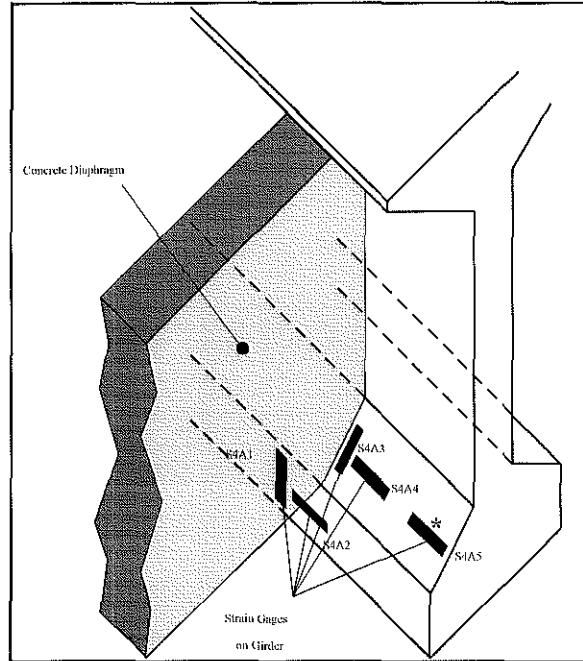


Figure 2.2.3c. Strain Gage Placement Near the Flange-Diaphragm Interface.

Strain gages were also mounted in a rosette pattern on the diaphragms as illustrated in Figure 2.2.3e on the diaphragms circled in Figure 2.2.3d. A

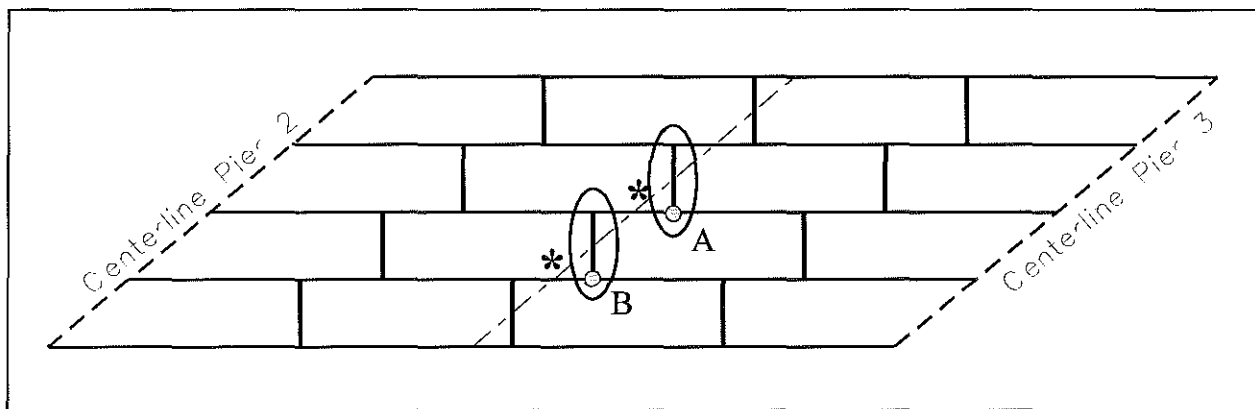


Figure 2.2.3d. Locations of Diaphragm Regions Instrumented With Strain Gages in Span 3 of the Southbound Bridge.

summary of the instruments used on the girders and diaphragms in this region is provided in Table 2.2.3b.

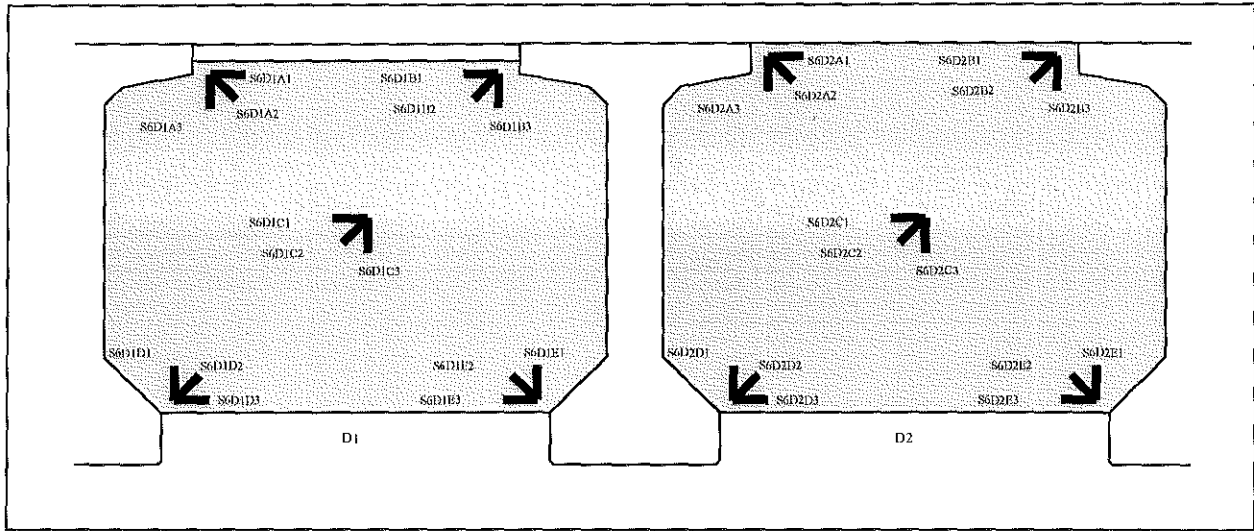


Figure 2.2.3e. Strain Gages on the Face of the Southbound Bridge Diaphragms (Note: Diaphragms 1 (D1) and 2 (D2) were instrumented on the opposite face of S3A-S3M).

Table 2.2.3b: Instrumentation on the Diaphragms and Girders in the Diaphragm Region.

Bridge	Instruments/Materials Required	
	Reusable Strain Gages on Girders	Reusable Strain Gages on Diaphragms
Southbound	10	30
Northbound	2	N/A

2.3. DYNAMIC TESTING INSTRUMENTATION

Dynamic testing was conducted on the Northbound and Southbound bridges in order to determine the mode shapes and frequencies associated with the two structures. Since results from the dynamic testing would be used to calibrate the finite element models of the two bridges, numerous recording stations were necessary to adequately define the acceleration characteristics of the bridges.

Moveable accelerometers (pictured in Figure 2.3.1a) were placed on the deck at the locations indicated in Figure 2.3.1b. A series of tests were conducted so that

accelerations at each station were measured while Stations 8E and 8W remained fixed as base stations. Accelerations in the vertical, longitudinal, and transverse directions were measured at each location. Tests were conducted in this manner on both the Southbound and the Northbound bridges. The triaxial arrangement of the accelerometers are illustrated in Figure 2.3.1a, while the color conventions and respective wire lengths for the accelerometers are given in Table 2.3.1a.



Figure 2.3.1a. Accelerometers in Triaxial Arrangement.

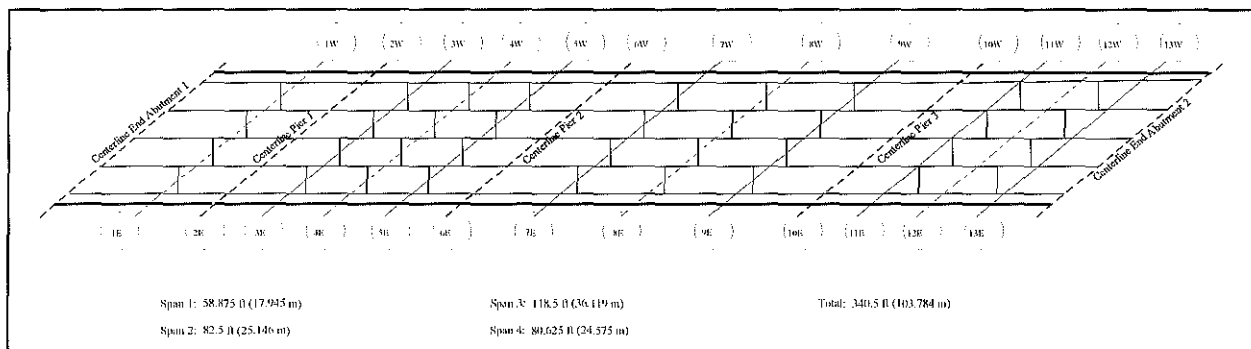


Figure 2.3.1b. Moveable Accelerometer Locations on the US 23 Bridges.

Table 2.3.1a: Accelerometer Colors and Wire Lengths.

Accelerometer Color	Code	Wire Length in ft (m)	Comments
Black	B/	210 (64.01)	Base Stations
Blue	B	235 (71.63)	
Green	G	250 (76.20)	Positioned as Necessary
Orange	O	255 (77.72)	
Red	R	260 (79.25)	
White	W	280 (85.34)	
Yellow	Y	300 (91.44)	

2.4. EXPERIMENTAL TESTING

Static testing provided an opportunity to determine the deflections and stresses induced by normal traffic and coal truck loading. Dynamic testing provided an opportunity for the natural frequencies and mode shapes of the structures to be determined. The results from each test were used to calibrate the finite element models of the US 23 bridges which will be discussed in later chapters.

2.4.1. TOTAL INSTRUMENTATION

Table 2.4.1 summarizes the instruments (gages, etc.) listed in the above sections. The cumulative number of instruments required for the entire testing procedure (i.e., both bridges) is reported. Color coding was essential for documenting the precise location of the strain gages mounted on rebar or diaphragm anchor bars once the deck and diaphragms were poured. Tables A.1 through A.5 in Appendix A list the color codes and orientation for each gage based upon the location codes defined in the figures and text of this chapter. Depth locations within the deck slab are also reported.

Limited data acquisition channels *versus* the number of instrument locations to be read required the static testing to be conducted in four different setups for the Southbound bridge and two different setups for the Northbound bridge. Tables A.6 and A.7 in Appendix A indicate the sequence in which the strain gages and LVDTs were read during the static testing. The fourth setup for the Southbound bridge was

conducted two months later and involved fully instrumenting the rosette patterns planned for the diaphragms (see Figure 2.2.3e). The number of stations where vibration data was to be recorded also made multiple tests necessary. Table A.8 in Appendix A demonstrates the sequence in which the accelerometers were positioned and read during the dynamic testing of both bridges.

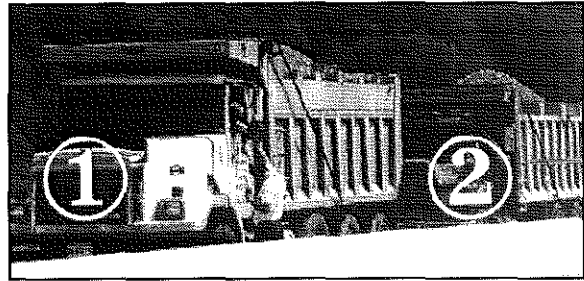


Figure 2.4.2a. Tandem Coal Haul Trucks Used During Static Testing.

Table 2.4.1: Total Instrumentation Required for Structural Testing of the Bridges.

Type of Instrument	Number of Instruments	
	Southbound Bridge	Northbound Bridge
Steel Strain Gages on Deck Reinforcement	29	26
Steel Strain Gages on Diaphragm Anchor Bars	12	-----
Steel Strain Gage Total	41	26
Concrete Strain Gages on Diaphragms	30	-----
Concrete Strain Gages on Girders	22	14
Concrete Strain Gage Total	52	14
LVDTs	8	8
Static Testing Total	101	48
Accelerometers	21	21
Dynamic Testing Total	21	21

2.4.2. STATIC TESTING

Static testing was accomplished by using two fully-loaded, tandem coal haul trucks (see Figure 2.4.2a) to induce the displacements and strains on the Southbound and Northbound bridges. The footprints and strains on the Southbound and Northbound bridges. The footprints of the respective truck tires are given in Figure 2.4.2b. For each test setup listed in Appendix A, the trucks were positioned three different ways in two "lanes". Trucks were either bumper-to-bumper in Lane 1, bumper-to-bumper in Lane 2, or side-by-side in Lanes 1 and 2 (Truck 1 was in Lane 1 while Truck 2 was staggered in Lane 2 to account for the skew angle of the bridges). Lane 1 was defined to be 2 ft (0.61 m) off the west curb (measured perpendicular to the barrier wall) and

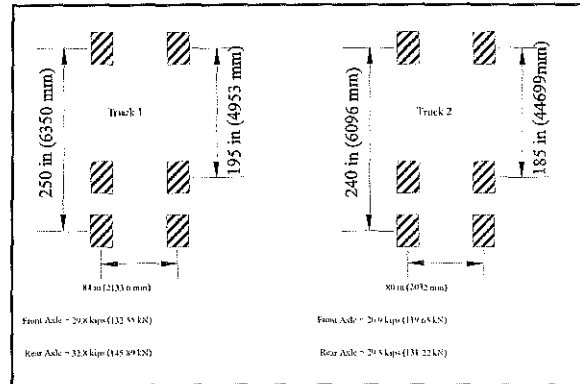


Figure 2.4.2b. Footprints and Axle Weights of Static Test Trucks.

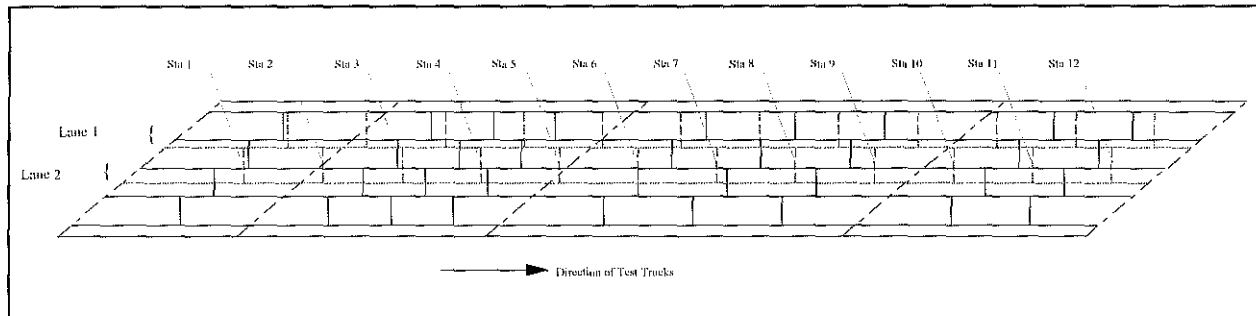


Figure 2.4.2c. Locations of Static Test Lanes and Stations on the US 23 Bridges.

Lane 2 was defined to be 14 ft (4.27 m) off the west curb. These lane definitions were chosen since the instrumentation on the girders was directly beneath these areas of the bridges. Stations were marked at 314 in (7975.6 mm) intervals in each lane. Figure 2.4.2c illustrates these "lane" and "station" locations. Strain gage and LVDT data were obtained for each station in each lane on the bridge for each test setup.

For example, in the Southbound Static Test 1 (SS1), Truck 1 was positioned at Station 2 in Lane 1 and Truck 2 was positioned at Station 1 in Lane 1 to complete a bumper-to-bumper test. All data acquisition channels were read for seven seconds using a sampling rate of 200 Hz while the trucks were positioned at these locations. Subsequent data readings were made by incrementing the truck positions to the next station. One static test setup was complete once bumper-to-bumper tests in each lane

and one side-by-side test was conducted. The process was repeated for two of the remaining three Southbound static test setups and all of the Northbound static test setups.

The fourth static test setup on the Southbound bridge was conducted two months later using a single fully-loaded, tandem coal haul truck. In fact, it was the same truck used to excite the bridges during the dynamic testing. The footprint of the tires on this third truck are given in Figure 2.4.2d. This truck was positioned such that the passenger-side, rear tandem straddled the center of the diaphragm instrumented with the rosette pattern. The two diaphragms on the Southbound bridge indicated in Figure 2.2.3c were tested using this procedure.

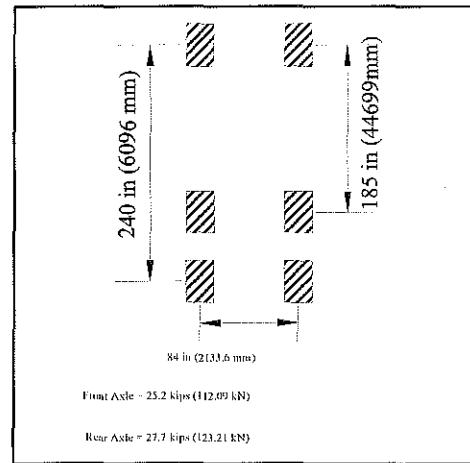


Figure 2.4.2d. Footprint and Axle Weights of Dynamic Test Truck.

2.4.3. DYNAMIC TESTING

Dynamic testing was accomplished by using a single fully-loaded, tandem coal haul truck whose footprint was given in Figure 2.4.2d. The truck traveled along the centerline of the respective bridges in order to excite the dynamic response. For each test the truck speed was 52 mph (83.69 km per hour). Due to the construction of the approach roadway, insufficient space was available to reach 55 mph (88.51 km per hour) with a fully-loaded truck. However, there was enough roadway so that the driver did not have to decelerate until the truck was clear of the bridge. Five setups for each bridge were completed to obtain all of the vibrational data required. Both bridges were tested dynamically with the truck traveling in the same direction. This was possible since the testing was completed prior to the bridges being opened to traffic.

CHAPTER 3

DATA ACQUISITION AND EXPERIMENTAL RESULTS

3.1. DATA ACQUISITION

As mentioned in Chapter 2, a limited number of data acquisition channels were available for completing the static and dynamic tests on the US 23 bridges. An IBM-compatible portable (laptop) computer with docking station was used to record the data from a Keithley-Metrobyte data acquisition system. Sixty-four channels were available with simultaneous sample and hold capability to ensure that all channels were sampled and recorded at the same time instead of sequentially. Signal conditioners from Sensotec were used for collecting data from the steel strain gages; the LVDTs and

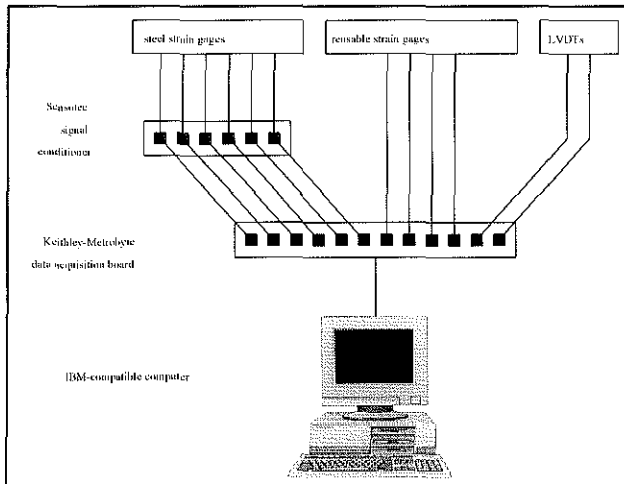


Figure 3.1. Data Acquisition System.

the reusable strain gages from Bridge Diagnostics, Inc., did not require signal conditioning. Figure 3.1 illustrates the data acquisition system used at the bridge site. Approximately 140 megabytes of data were obtained from the static and dynamic tests of the two bridges using the software VIEWDAC[®]. Since the data was stored in binary format, this corresponds to roughly 35 million data points to be analyzed (one point equals four bytes). Some particulars of the data acquisition process for the static and dynamic tests are given below.

3.1.1. STATIC TESTING

The steel strain gages were wired in series to "dummy" gages to compensate for any temperature variations throughout the testing process (a description of this procedure is given in Dunnichiff [1993]). By using this procedure the raw data obtained from the static tests did not include a contribution to strain due to temperature effects. An added advantage of connecting these "dummy" gages in series

was that it eliminated the necessity to match wire lengths of the "dummy" and real gages. Therefore, less interference from the overhead power lines would be encountered.

The same gages used on the deck rebar and diaphragm anchor bars were mounted on a steel bar. Wire leads with pin connectors were attached to the gages and the bar was encased in a 6 in (152.4 mm) square by 36 in (914.4 mm) long concrete beam poured in the Structures Laboratory at the University of Kentucky. In the field, the concrete beam was placed on the deck of the bridge being tested. The wire leads from the strain gages on the deck rebar and diaphragm anchor bars were soldered to a pin connector in the field. The other end of the "dummy" gage lead wires were attached to the data acquisition system. As different test setups were required, reorienting the "dummy" gages to the steel strain gages was just a matter of joining the appropriate male and female ends of the pin connectors. The reusable strain gages had self-contained temperature compensators and did not require the use of this "dummy" gage procedure.

To combat any influence by the overhead power lines at the US 23 bridge site, a sampling rate of 200 Hz was chosen. For the first static test (both trucks in lane 1 of the Northbound bridge), all gages and LVDTs were sampled at 200 Hz for 20 seconds. This proved to be too time consuming since the computer was required to read and store approximately one megabyte (200 points per second x 20 seconds x 4 bytes per point x 64 channels = 1,024,000 bytes) of information per station. A ten second sampling rate was adopted for the second test (both trucks in lane 2 of the Northbound bridge), but this also proved to be too time consuming. For all subsequent tests (Northbound and Southbound), the sampling rate was reduced to seven seconds, thereby requiring the computer to read and store only about 359 kilobytes of information per station.

File names were devised which would clearly identify the station location of the trucks, lane location, and bridge being tested. The VIEWDAC[®] software would then automatically increment the station number and channel number as the data were stored. With the exception of the first Northbound test, the basic file name structure was the bridge code, followed by the test number, a dash, the station number, the letters "CH", and the channel number. Careful record keeping during testing made deciphering the file names possible. Table 3.1.1 summarizes the file names associated with each static test.

Table 3.1.1: File Names for the Northbound and Southbound Static Tests.

File Name	Bridge	Lane(s)	Stations	Truck Positions	Setup	
N	Northbound	1	2-12	bumper-to-bumper	1	
N2-#CH#		2	2-12	bumper-to-bumper		
N4-#CH#		1 & 2	1-12	side-by-side		
N5-#CH#		Southbound	1	2-12	bumper-to-bumper	2
N6-#CH#			2	2-12	bumper-to-bumper	
N7-#CH#			1 & 2	1-12	side-by-side	
S1-#CH#			1	2-12	bumper-to-bumper	1
S2-#CH#	2	2-12	bumper-to-bumper			
S3-#CH#	1 & 2	1-12	side-by-side			
S4-#CH#	Southbound	1	2-12	bumper-to-bumper	2	
S5-#CH#		2	2-12	bumper-to-bumper		
S6-#CH#		1 & 2	1-12	side-by-side		
S7-#CH#		1	2-12	bumper-to-bumper	3	
S8-#CH#		2	2-12	bumper-to-bumper		
S9-#CH#	1 & 2	1-12	side-by-side			

A zero reading was always recorded prior to conducting each test, e.g., N2-1CH#.DAT. An illustration of the raw data contained in file N2-9CH32.DAT is given in Figure 3.1.1a (the complete record is not given for the sake of clarity).

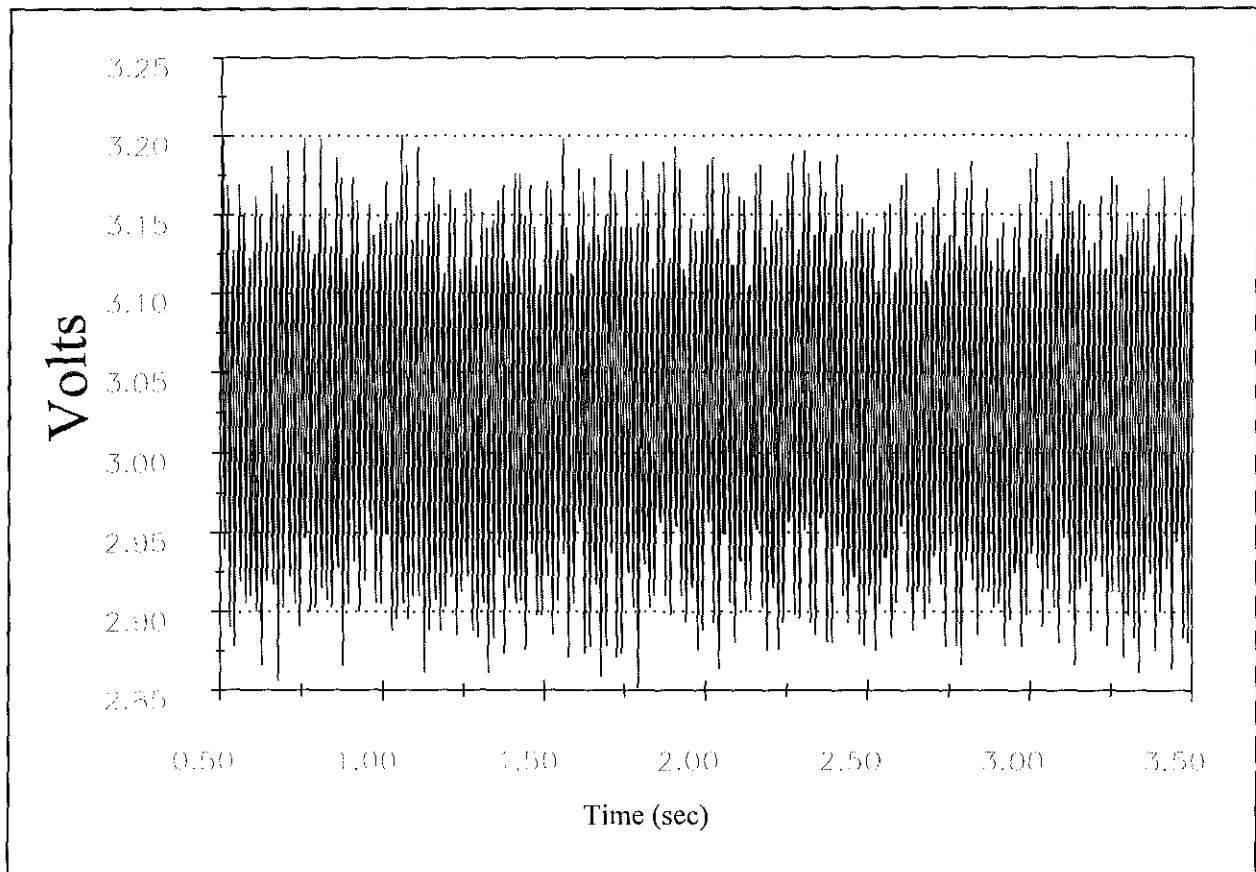


Figure 3.1.1a. Data Record N2-9CH32.DAT.

The computer program listed in Appendix B was written to process the static test data binary files and report the average and standard deviation values for data recorded on each channel number. Only the average value is necessary since change in strain with time was not measured and sufficient time for dynamic effects to dissipate was given before reading the gages. Figure 3.1.1b is an example of the output obtained from this computer program for the file set N2-9CH0.DAT through N2-9CH63.DAT. From this figure it can be seen that the average value of the data record in Figure 3.1.1a (N2-9CH32.DAT) is 3.028 volts with a standard deviation of 0.104 volts.

FILE NAME:	AVERAGE:	STD. DEV.:
DATA\STATIC\NORTH\N2\N2-9CH0.DAT	-0.1641736	0.05454
DATA\STATIC\NORTH\N2\N2-9CH1.DAT	1.133545E-02	1.304912E-02
DATA\STATIC\NORTH\N2\N2-9CH2.DAT	4.266846E-02	1.389659E-02
DATA\STATIC\NORTH\N2\N2-9CH3.DAT	7.763672E-03	1.345074E-02
DATA\STATIC\NORTH\N2\N2-9CH4.DAT	-0.6671948	0.0224626
DATA\STATIC\NORTH\N2\N2-9CH5.DAT	-5.0000000	0.0000000
DATA\STATIC\NORTH\N2\N2-9CH6.DAT	2.769775E-03	1.188653E-02
DATA\STATIC\NORTH\N2\N2-9CH7.DAT	-5.0000000	0.0000000
DATA\STATIC\NORTH\N2\N2-9CH8.DAT	-0.8883008	4.498872
DATA\STATIC\NORTH\N2\N2-9CH9.DAT	3.739748	2.169225
DATA\STATIC\NORTH\N2\N2-9CH10.DAT	4.997646	8.771611E-05
DATA\STATIC\NORTH\N2\N2-9CH11.DAT	-5.0000000	0.0000000
DATA\STATIC\NORTH\N2\N2-9CH12.DAT	-0.0171521	1.788705E-02
DATA\STATIC\NORTH\N2\N2-9CH13.DAT	1.519604	1.477306
DATA\STATIC\NORTH\N2\N2-9CH14.DAT	0.0231897	2.102361E-02
DATA\STATIC\NORTH\N2\N2-9CH15.DAT	4.997646	8.771611E-05
DATA\STATIC\NORTH\N2\N2-9CH16.DAT	-1.694092E-02	3.924331E-02
DATA\STATIC\NORTH\N2\N2-9CH17.DAT	-5.758301E-02	1.823875E-02
DATA\STATIC\NORTH\N2\N2-9CH18.DAT	-7.295044E-02	3.31558
DATA\STATIC\NORTH\N2\N2-9CH19.DAT	-0.0869519	3.346197
DATA\STATIC\NORTH\N2\N2-9CH20.DAT	-3.179199E-02	1.893407E-02
DATA\STATIC\NORTH\N2\N2-9CH21.DAT	-1.542603E-02	1.249486E-03
DATA\STATIC\NORTH\N2\N2-9CH22.DAT	-9.794922E-03	1.512229E-03
DATA\STATIC\NORTH\N2\N2-9CH23.DAT	-2.403565E-03	3.697833E-03
DATA\STATIC\NORTH\N2\N2-9CH24.DAT	-0.020802	1.546749E-03
DATA\STATIC\NORTH\N2\N2-9CH25.DAT	-6.64917E-03	3.681505E-03
DATA\STATIC\NORTH\N2\N2-9CH26.DAT	1.924667	3.251398E-03
DATA\STATIC\NORTH\N2\N2-9CH27.DAT	-2.634277E-02	1.953984E-03
DATA\STATIC\NORTH\N2\N2-9CH28.DAT	7.646484E-03	3.300573E-03
DATA\STATIC\NORTH\N2\N2-9CH29.DAT	2.351318E-02	3.450812E-03
DATA\STATIC\NORTH\N2\N2-9CH30.DAT	-1.401978E-02	1.124335E-03
DATA\STATIC\NORTH\N2\N2-9CH31.DAT	-0.1381702	1.429625E-03
DATA\STATIC\NORTH\N2\N2-9CH32.DAT	3.027546	0.1041275
DATA\STATIC\NORTH\N2\N2-9CH33.DAT	2.891602E-02	1.246926E-02
DATA\STATIC\NORTH\N2\N2-9CH40.DAT	4.997646	8.771611E-05
DATA\STATIC\NORTH\N2\N2-9CH41.DAT	1.660842	1.564495
DATA\STATIC\NORTH\N2\N2-9CH42.DAT	-0.3336414	4.363898E-03
DATA\STATIC\NORTH\N2\N2-9CH43.DAT	3.994264	8.750838E-03
DATA\STATIC\NORTH\N2\N2-9CH44.DAT	3.189515	7.559948E-03
DATA\STATIC\NORTH\N2\N2-9CH45.DAT	-1.70416	4.446297E-03
DATA\STATIC\NORTH\N2\N2-9CH48.DAT	-0.1005042	1.293349E-03
DATA\STATIC\NORTH\N2\N2-9CH49.DAT	-3.365112E-02	1.071253E-03
DATA\STATIC\NORTH\N2\N2-9CH56.DAT	-4.494263E-02	2.819753E-03
DATA\STATIC\NORTH\N2\N2-9CH57.DAT	-7.967529E-03	6.192624E-03

Figure 3.1.1b. Data File N2-9CH.SUM Obtained From Processing N2-9CH#.DAT Through the Computer Program of Appendix B.

3.1.2. DYNAMIC TESTING

The accelerometers were sampled at 1002 Hz for 29.94012 seconds to assure a complete, high resolution acceleration record. This led to data files of 30,000 points per channel per test. Data recording began with the truck approximately 100 ft (30.48 m) from the end of the bridge. Only 24 channels with simultaneous sample and hold capability were employed; three of these channels had no accelerometers connected and recorded insignificant data. Since wires from the accelerometers to the data acquisition system were not shielded from the overhead power lines by the bridge (as was the case during the static testing), several recordings were made without bridge excitation to assess the noise in each data set. The file naming system for the dynamic testing was not as complex as for the static testing. Only 21 instruments were involved in the dynamic testing, and each test setup did not require using different channels on the data acquisition board. Northbound dynamic test files had an "L" prefix, while Southbound files were written with a "K" prefix. Each prefix was then followed by the test number, the letters "CH", and the data channel recorded. Table 3.1.2 lists the dynamic test file names.

Table 3.1.2: File Names for the Northbound and Southbound Dynamic Tests.

File Name	Bridge	Test Setup	Accelerometer Locations (see Figure 2.3.1a)
L2CH#.DAT	Northbound	1	13W,12W,11W,10W,9W,8W,8E
L3CH#.DAT		2	7W,6W,5W,4W,3W,8W,8E
L4CH#.DAT		3	2W,1W,1E,2E,3E,8W,8E
L5CH#.DAT		4	4E,5E,6E,7E,9E,8W,8E
L6CH#.DAT		5	9E,10E,11E,12E,13E,8W,8E
K2CH#.DAT	Southbound	1	13W,12W,11W,10W,9W,8W,8E
K3CH#.DAT		2	7W,6W,5W,4W,3W,8W,8E
K4CH#.DAT		3	2W,1W,1E,2E,3E,8W,8E
K6CH#.DAT		4	4E,5E,6E,7E,9E,8W,8E
K7CH#.DAT		5	9E,10E,11E,12E,13E,8W,8E

An illustration of the raw data contained in file L2CH2.DAT is given in Figure 3.1.2. Only a portion of the data (1.75-9.75 seconds) is shown for clarity. This file contains the vertical acceleration measured at Station 8W during Test 1 on the Northbound bridge. A data point is located at every 0.000998 seconds (the reciprocal of 1002 Hz). The offset from zero acceleration observed in the graph is attributable to the "noise" within the data acquisition system and was corrected during the calibration phase.

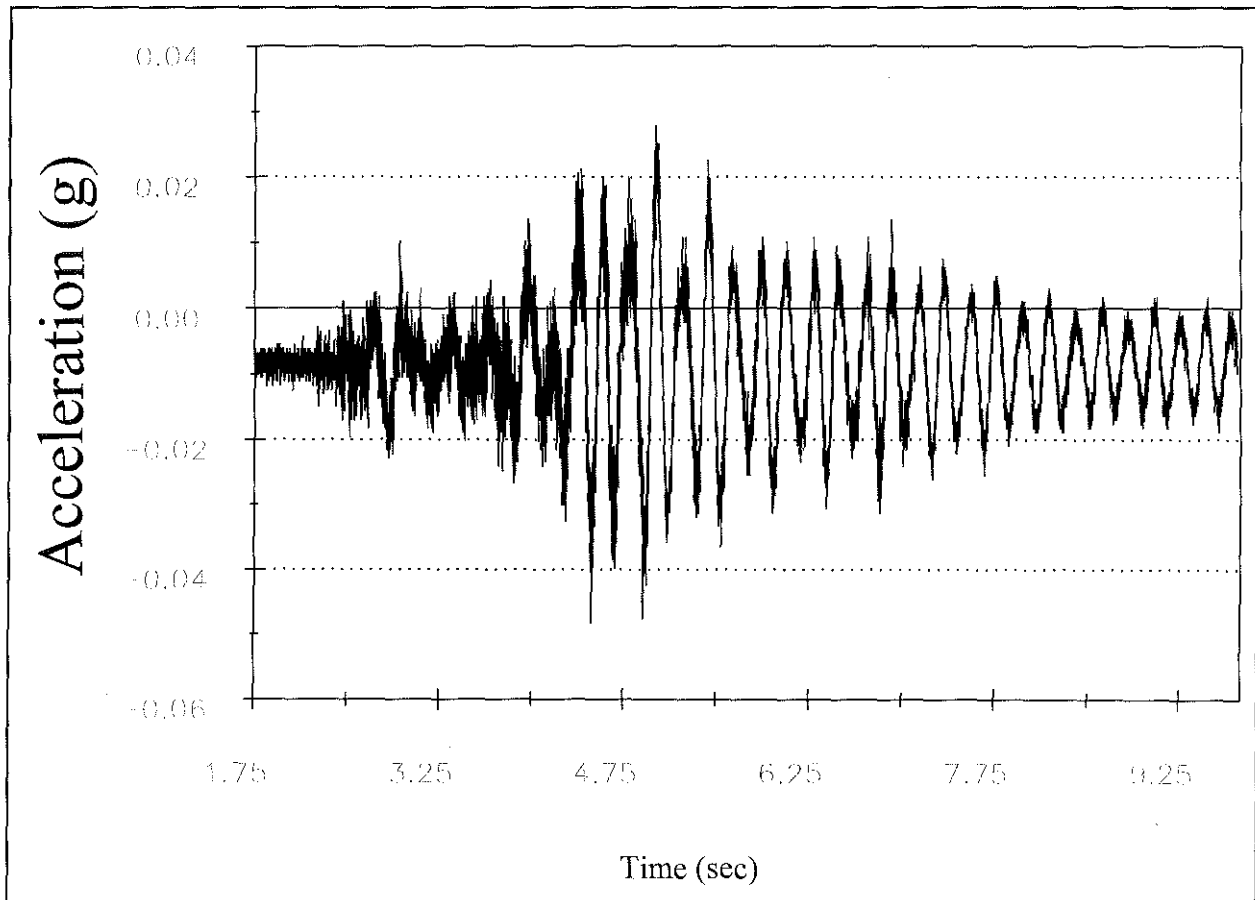


Figure 3.1.2. Data Record L2CH2.DAT.

3.2. CALIBRATION FACTORS

3.2.2. STATIC TESTING

Data obtained from the static testing were merely a reflection of a change in voltage read by the data acquisition board. In the case of the strain gages, the change in voltage output was due to a fluctuation in electrical resistance caused by the strain

on a particular gage. Voltage output on the LVDTs changed as the deflecting core altered the electric field within the instrument. Assessment of the strains and deflections associated with the static tests for each bridge required calibration factors to convert these voltage changes to quantities of microstrain ($1 \times 10^{-6} \epsilon$ or $\mu\epsilon$) or inches (millimeters).

Based on data reported by the manufacturer, Measurements Group, Inc., the calibration factor applied to the steel strain gages was 0.002 strain per volt for a voltage gain of 100 volts. During the static testing phase, differences in the signal conditioners required a voltage gain of 1,000 volts to be used on some gages. This led to a calibration factor of 0.0002 strain per volt for these steel strain gages. Manufacturer's data also were used to obtain the calibration factor associated with the LVDTs. Every one volt change in the LVDTs corresponded to 0.0498 in (1.27 mm) of deflection. Despite the fact that the reusable strain gages appeared to be the same, each had unique gage factors which led to different calibration factors. The calibration factors (for microstrain per volt) were calculated from the following equation:

$$C F = \frac{(G F) \times 1000}{(\text{excitation voltage}) \times (\text{voltage gain})} \quad (3.1)$$

Table 3.2.1 lists the calibration factors for each reusable strain gage based on a voltage gain of 100 volts.

Table 3.2.1: Reusable Strain Gage Calibration Factors.

Gage Number	321	322	323	324	325	326	327	328
Calibration Factor	726.1	630.8	680.5	683.6	656.7	652.2	702.4	709.6
Gage Number	329	330	331	332	333	334	335	290
Calibration Factor	611.9	634.6	693.0	662.6	666.3	611.3	656.4	617.0

Several of the data acquisition channels operated with a voltage gain of 200 volts. In these cases, the values listed in Table 3.2.1 were divided by two prior to applying the calibration factor to the data file. The static tests conducted on the diaphragms two months after the initial static tests employed a voltage gain of 1,000 volts, thereby

requiring these values to be divided by ten to obtain the calibrated strain readings on the face of the diaphragms.

3.2.2. DYNAMIC TESTING

Data recorded during the dynamic tests were calibrated in the field by the VIEWDAC[®] software to be in terms of the acceleration due to gravity. Therefore, no calibration factors were necessary to obtain a usable form of data.

3.3. EXPERIMENTAL RESULTS

3.3.1. STATIC TESTING

Throughout the discussion of the static test results, any mention of a station number or lane location is based upon the static test "lane" and "station" specification depicted in Figure 3.3.1a. The stations in Lane 2 were staggered relative to Lane 1 to account for the skew angle of the bridges. A significant portion of the strain and

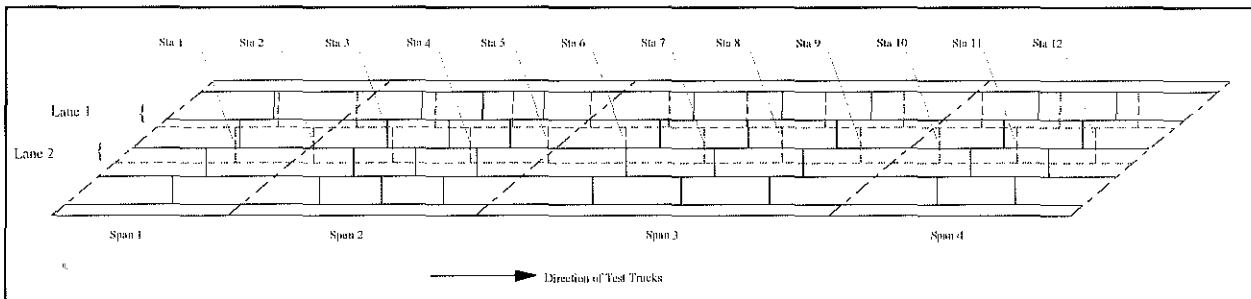


Figure 3.3.1a. Locations of Static Test Lanes and Stations on the US 23 Bridges.

deflection data obtained by the static tests was used to calibrate the finite element models of the US 23 bridges discussed in Chapter 4 of this research. However, much of the experimental data offers insight to the behavior of these two bridges when subjected to heavy coal truck loads without the need for extensive analytical studies. A summary of the experimental data obtained during the static testing phase is presented below with a comparison between Northbound and Southbound bridge values when appropriate. All of the experimental strain and deflection readings are included in Appendix C based on the average value results obtained from the computer program in Appendix B.

3.3.1.1. Instrumentation on the Transverse Reinforcement in the Deck

After applying the appropriate calibration factors and subtracting out the zero reading, strain values for the steel strain gages in the deck were obtained and tabulated for each test scenario. Any location codes referenced in the following paragraphs, figures, and/or tables correspond to those defined in Figures 3.3.1b and 3.3.1c for the Southbound (bridge with intermediate diaphragms) and Northbound (bridge without intermediate diaphragms) bridges, respectively. Strains in the

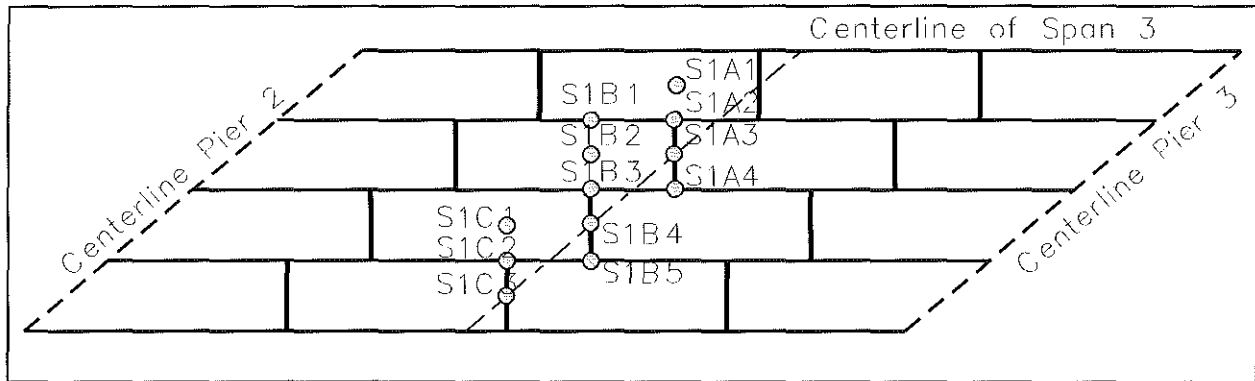


Figure 3.3.1b. Transverse Strain Gage Locations in the Southbound Deck (Bridge With Intermediate Diaphragms).

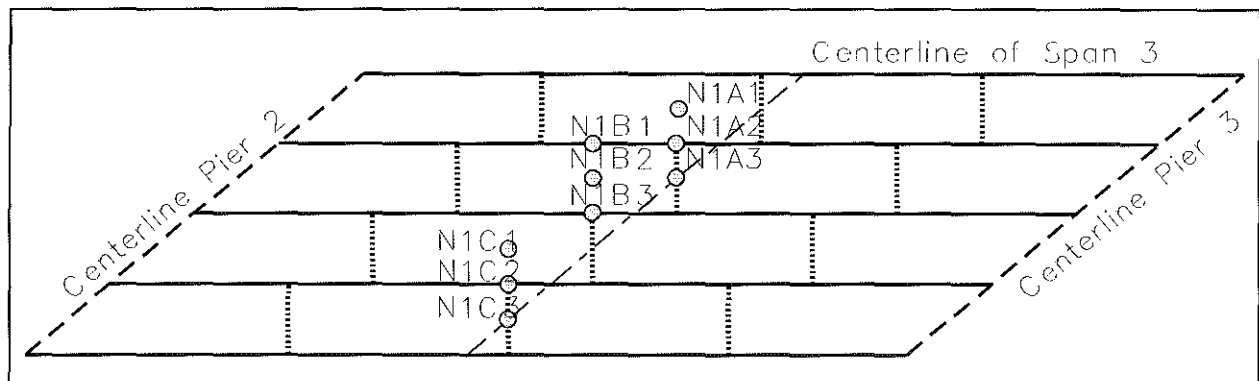


Figure 3.3.1c. Transverse Strain Gage Locations in the Northbound Deck (Bridge Without Intermediate Diaphragms).

transverse reinforcement bars of the Southbound bridge deck were observed to be fairly consistent and independent of the test truck positions. A slight rise in the magnitude of strain was noted when the trucks were directly over the transverse location considered. On the other hand, the strain in the transverse reinforcement bars of the Northbound bridge deck demonstrated a dependence on truck position.

Sharp rises in the strain data were recorded with the trucks directly above the transverse gage considered. An example of this observation is given in Figure 3.3.1d. Gages S1B3T and N1B3T are located close to Stations 6 and 7. It appears that the presence of intermediate diaphragms reduces the flexibility of the Southbound bridge deck, thereby causing less strain in the slab. However, the magnitude of strain experienced by the Northbound bridge deck should not cause alarm. With a concrete compressive strength of 4-ksi (27.58 MPa) and a steel yield strength of 60 ksi (413.70 MPa), the maximum compressive stresses in the bridge deck at location N1B3T illustrated in Figure 3.3.1d are 0.95 ksi (6.55 MPa) and 7.65 ksi (52.72 MPa) in the concrete and steel, respectively. Table 3.3.1a reports the maximum strain and stress values recorded for the static tests of both bridges.

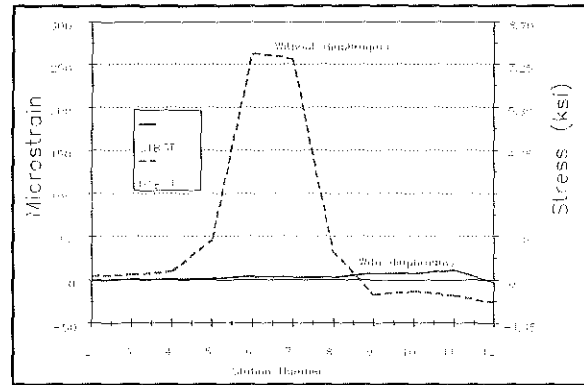


Figure 3.3.1d. Strain on the Top Transverse Rebar at Location S1B3T/N1B3T: Trucks Side-by-Side (Note: 1 ksi = 6.895 MPa).

Table 3.3.1a: Maximum Strain and Stress Values Encountered During Static Testing.

Bridge	Material	Compression		Tension	
		Micro-strain	Stress in ksi (MPa)	Micro-strain	Stress in ksi (MPa)
Northbound	concrete	267.87	0.97 (6.66)	78.08	0.28 (1.94)
	steel	267.87	7.77 (53.56)	78.08	2.26 (15.61)
Southbound	concrete	41.62	0.15 (1.04)	22.76	0.08 (0.57)
	steel	41.62	1.21 (8.32)	22.76	0.66 (4.55)

The maximum compressive strain measured on the transverse rebar in the Northbound bridge deck was 267.87 microstrain at location N1B3T with the trucks bumper-to-bumper in Lane 1 and Truck 1 at Station 7. Likewise, the maximum tensile strain recorded on the transverse rebar of the Northbound bridge deck was 78.08 microstrain at location N1B2B when the trucks were side-by-side in Lanes 1 and 2 with the trucks at Station 8. Comparable values for the Southbound bridge are: a

maximum compressive strain of 41.62 microstrain at location S1B2T when the trucks were bumper-to-bumper in Lane 2 with Truck 1 at Station 9 and a maximum tensile strain of 22.76 microstrain at location S1B3B when the trucks were bumper-to-bumper in Lane 2 with Truck 1 at Station 9.

Since the stress values at the transverse locations are within acceptable design criteria, the absence of intermediate diaphragms in the Northbound bridge does not pose a threat to the serviceability and load capacity of the deck in the transverse direction under the static test loads. Similarly, the presence of intermediate diaphragms does not impose excessive stresses on the Southbound bridge deck in the transverse direction. Table 3.3.1b compares strain and concrete stress values at various additional transverse locations in the Southbound and Northbound bridge decks.

Table 3.3.1b: Strain and Stress on Transverse Reinforcement Bars in the US 23 Bridge Decks.

Location ^a	Microstrain ^b	Stress in ksi (MPa)	Position of Test Trucks ^c
N1A2B	11.51 (T)	0.33 (2.30)	Bumper-to-bumper in Lane 1 with Truck 1 at Station 6
S1A2B	5.25 (T)	0.15 (1.05)	
N1B2T	48.72 (C)	1.41 (9.74)	Bumper-to-bumper in Lane 2 with Truck 1 at Station 8
S1B2T	36.16 (C)	1.05 (7.23)	
N1B3T	16.84 (C)	0.49 (3.37)	Side-by-side in Lanes 1 and 2 with Trucks at Station 9
S1B3T	7.97 (C)	0.23 (1.59)	

^a refer to Figures 3.3.1b and 3.3.1c.

^b "C" denotes compression and "T" denotes tension.

^c refer to Figure 3.3.1a for "lane" and "station" locations.

3.3.1.2. Instrumentation on the Longitudinal Reinforcement in the Deck

After applying the appropriate calibration factors and subtracting out the zero reading, strain values for the steel strain gages in the deck were obtained and tabulated for each test scenario. Any location codes referenced in the following paragraphs, figures, and/or tables correspond to those defined in Figures 3.3.1e and 3.3.1f for the Southbound (bridge with intermediate diaphragms) and Northbound (bridge without intermediate diaphragms) bridges, respectively.

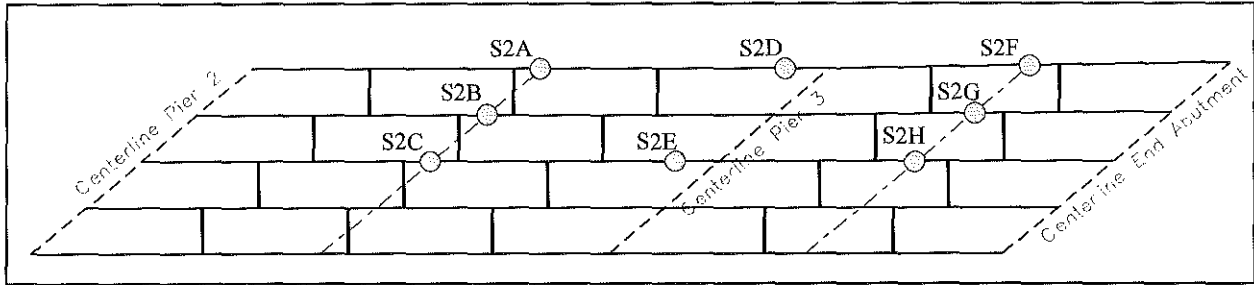


Figure 3.3.1e. Longitudinal Strain Gage Locations in the Southbound Deck (Bridge With Intermediate Diaphragms).

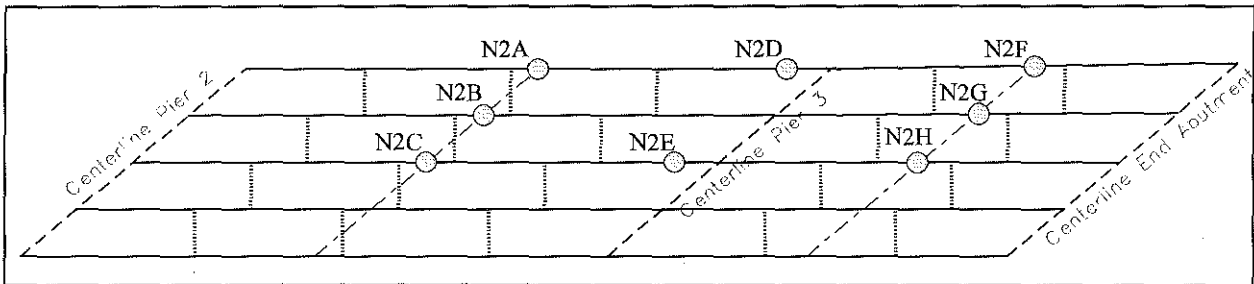


Figure 3.3.1f. Longitudinal Strain Gage Locations in the Northbound Deck (Bridge Without Intermediate Diaphragms).

An evaluation of the strain gage readings from the longitudinal reinforcement in the Northbound and Southbound bridge decks does not immediately lead to the same conclusions as observed above. The only striking example where a large difference between longitudinal bar strains in the two bridges exists is pictured in Figure 3.3.1g. In general, the Northbound bridge deck strains in the longitudinal direction do show added flexibility in the absence of intermediate diaphragms, but the effect is less pronounced than in the case of the transverse reinforcement. Strains on the longitudinal reinforcement seem to parallel each other when comparing values for the Northbound and Southbound bridges. In fact, the strain measured on the Southbound bridge deck bars were sometimes observed to be higher than comparable strains on the Northbound bridge deck. These cases were more often noted when strain values were compared at positions away from the location of the test trucks. This trend seems to indicate that the presence of the intermediate diaphragms assists in distributing the strain to adjacent girders. However, the differences in strain observed at these locations were not significant enough to warrant mandatory use of diaphragms. A further discussion of the strains in the longitudinal reinforcement bars in both the Northbound and Southbound bridge decks is given below when dealing with the strains obtained from the girder cross section. Table 3.3.1c compares strain readings on the longitudinal deck bars in both bridges at various locations.

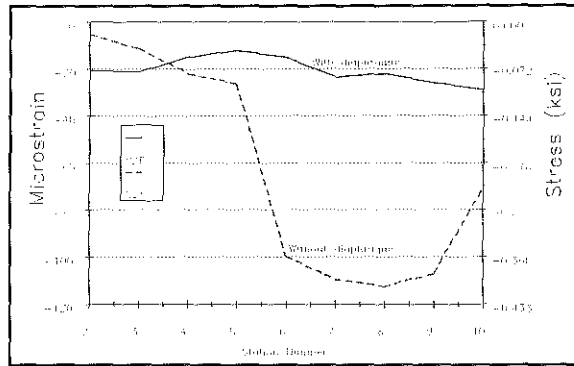


Figure 3.3.1g. Strain on the Longitudinal Rebar at Location S2F/N2F: Trucks Bumper-to-Bumper in Lane 1 (Note: 1 ksi = 6.895 MPa).

Table 3.3.1c: Strain and Stress on Longitudinal Reinforcement Bars in the US 23 Bridge Decks.

Location ^a	Micro-strain ^b	Stress in ksi (MPa)	Position of Test Trucks ^c
N2B	8.89 (C)	0.26 (1.78)	Bumper-to-bumper in Lane 1 with Truck 1 at Station 9
S2B	20.14 (C)	0.58 (4.03)	
N2E	25.42 (T)	0.74 (5.08)	Bumper-to-bumper in Lane 2 with Truck 1 at Station 7
S2E	23.30 (T)	0.68 (4.66)	
N2D	5.64 (T)	0.16 (1.13)	Side-by-side in Lanes 1 and 2 with trucks 1 at Station 7
S2D	1.10 (T)	0.03 (0.22)	

^a refer to Figures 3.3.1e and 3.3.1f.

^b "C" denotes compression and "T" denotes tension.

^c refer to Figure 3.3.1a for "lane" and "station" locations.

3.3.1.3. Instrumentation on the Girders - Displacements

After applying the appropriate calibration factors and subtracting out the zero reading, displacement values for the vertical and out-of-plane LVDTs on the girders were obtained and tabulated for each test scenario. Any location codes referenced in

the following paragraphs, figures, and/or tables correspond to those defined in Figures 3.3.1h and 3.3.1i for the Southbound (bridge with intermediate diaphragms) and Northbound (bridge without intermediate diaphragms) bridges, respectively.

An example of the variation of the out-of-plane displacement between the first and second girders as the trucks were positioned along Lane 1 is given in Figure 3.3.1j. Two conclusions can immediately be drawn from this illustration: 1) out-of-plane

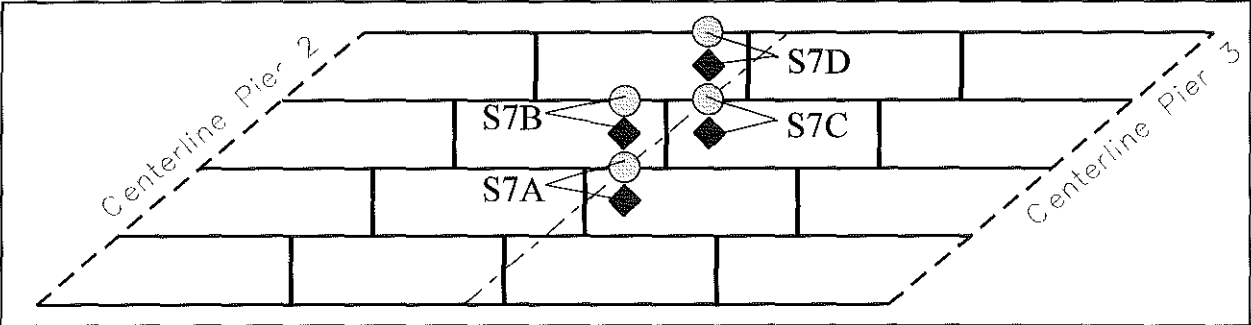


Figure 3.3.1h. Vertical (●) and Transverse (◆) LVDT Locations on Centerline of Southbound Span 3 (Bridge With Intermediate Diaphragms).

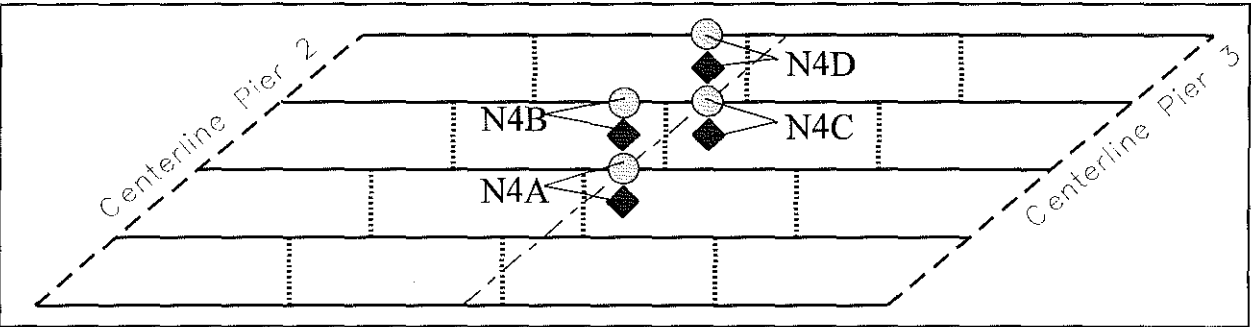


Figure 3.3.1i. Vertical (●) and Transverse (◆) LVDT Locations on Centerline of Northbound Span 3 (Bridge Without Intermediate Diaphragms).

displacements were prevalent only when the load was in the span where deflections were being measured and 2) although the absence of intermediate diaphragms leads to a large difference between out-of-plane displacements in the Southbound and Northbound bridges, the magnitude of the out-of-plane displacement is not sufficient to cause concern. In fact, the maximum out-of-plane displacement recorded in the Southbound and Northbound bridges was 0.04 in (1.11 mm) and 0.09 in (2.29 mm), respectively. Incidentally, these maximum values were recorded at the same location on each bridge with the test trucks in the same configuration. Additional out-of-plane displacement measurements were made at the base of a typical concrete intermediate

diaphragm and one that had been cut low, i.e., the reinforcement in the diaphragm did not extend into the deck. With a single truck straddling the centerline of the respective diaphragms, a 0.01 in (0.25 mm) difference in deflection was recorded. Under the static test loading, displacements obtained in the out-of-plane direction do not indicate that the intermediate diaphragms are very effective in transmitting load to adjacent girders. In other words, no large differences in deflections were observed.

Similar observations were made with the vertical displacements. In general, the Southbound bridge tended to deflect less than the Northbound bridge under the same static test loads. However, this difference was often minuscule. A maximum vertical displacement of 0.24 in (6.10 mm) was recorded for the Southbound bridge, and a maximum vertical displacement of 0.25 in (6.35 mm) was recorded for the Northbound bridge. It was observed in some instances that the vertical deflection in the Southbound bridge was larger than its counterpart in the Northbound bridge. An example of this phenomenon is illustrated in Figure 3.3.1k. These instances were noted at all locations where the positions of the test trucks were relatively far away from the point where the displacement was measured. This observation can be explained as follows using the location in Figure 3.3.1k as an example. In the Northbound bridge, the girder at point N4D (see Figure 3.3.1i) was allowed to deflect with only the slab acting to distribute some of the load. However, in the Southbound bridge, the presence of intermediate diaphragms allows for load distribution via the deck and diaphragms. The result is a reduction in the deflection of the girder at point S7D (see Figure 3.3.1h) with a subsequent increase in the displacement of the adjacent girder at point S7C. In this manner, intermediate diaphragms alter the bending behavior of the Southbound bridge since the reduction in the vertical displacement at S7D is only 0.01

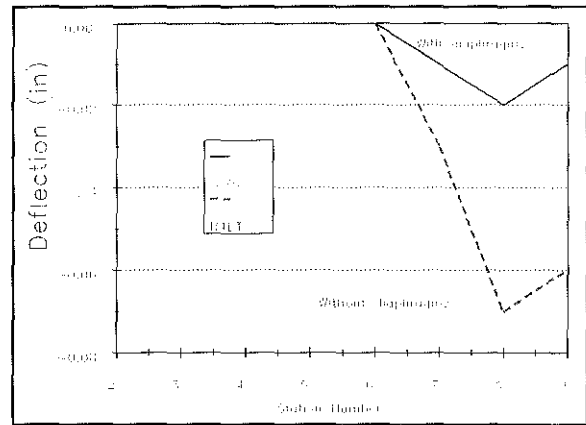


Figure 3.3.1j. Out-of-Plane Displacement at Location S7D/N4D: Trucks Bumper-to-Bumper in Lane 1 (Note: 1 in = 25.4 mm).

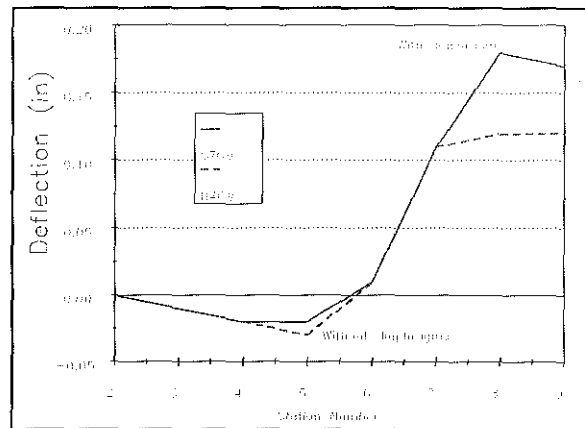


Figure 3.3.1k. Vertical Deflection at Location S7C/N4C: Trucks Bumper-to-Bumper in Lane 1 (Note: 1 in = 25.4 mm).

in (0.25 mm), but the increase at S7C is 0.05 in (1.27 mm) when compared to the vertical displacement counterparts in the Northbound bridge. Table 3.3.1d lists some of the displacements recorded in Span 3 of the Northbound and Southbound bridges.

Table 3.3.1d: Vertical and Out-of-Plane Displacements of the US 23 Bridge Girders.

Location ^a	Displacement in inches (mm)	Position of Test Trucks ^b
N4DV	0.25 (6.35)	Bumper-to-bumper in Lane 1 with Truck 1 at Station 9
S7DV	0.24 (6.10)	
N4BV	0.17 (4.32)	Bumper-to-bumper in Lane 2 with Truck 1 at Station 8
S7BV	0.14 (3.56)	
N4CT	0.02 (0.51)	Side-by-side in Lanes 1 and 2 with trucks at Station 7
S7CT	0.02 (0.51)	

^a refer to Figures 3.3.1h and 3.3.1i; V=vertical and T=transverse.

^b refer to Figure 3.3.1a for "lane" and "station" locations.

3.3.1.4. Instrumentation on the Girders - Strains

After applying the appropriate calibration factors and subtracting out the zero reading, strain values for the reusable strain gages on the girders were obtained and tabulated for each test scenario. Any location codes referenced in the following paragraphs, figures, and/or tables correspond to those defined in Figures 3.3.1j, 3.3.1m, and 3.3.1n for the Southbound (bridge with intermediate diaphragms) and Northbound (bridge without intermediate diaphragms) bridges, respectively.

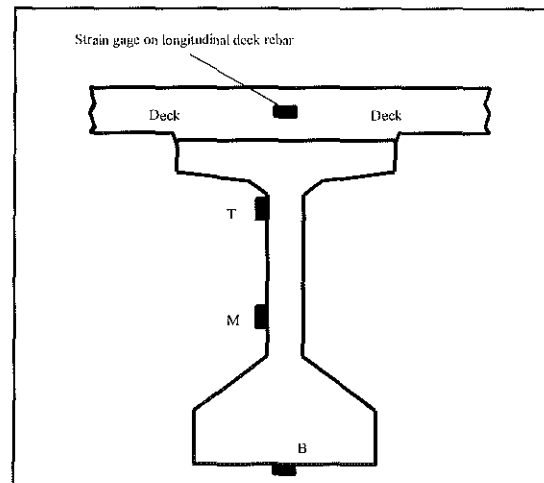


Figure 3.3.1j: Strain Gage Location on Girder Cross Section and Deck.

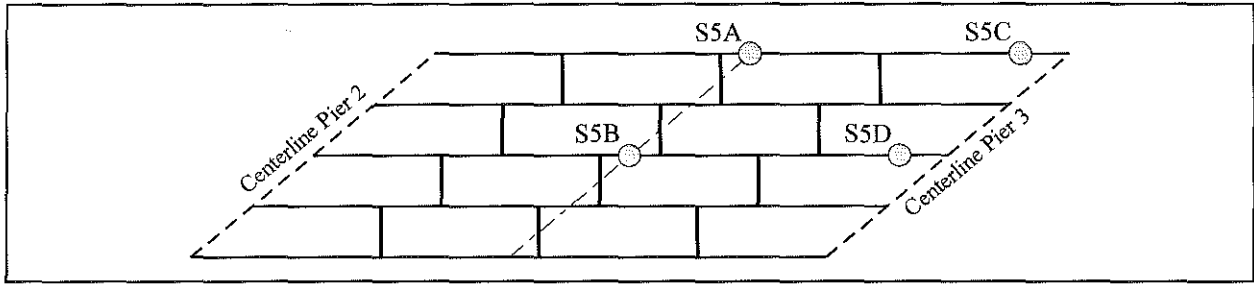


Figure 3.3.1m. Girder Strain Gage Locations in the Southbound Bridge (Bridge With Intermediate Diaphragms).

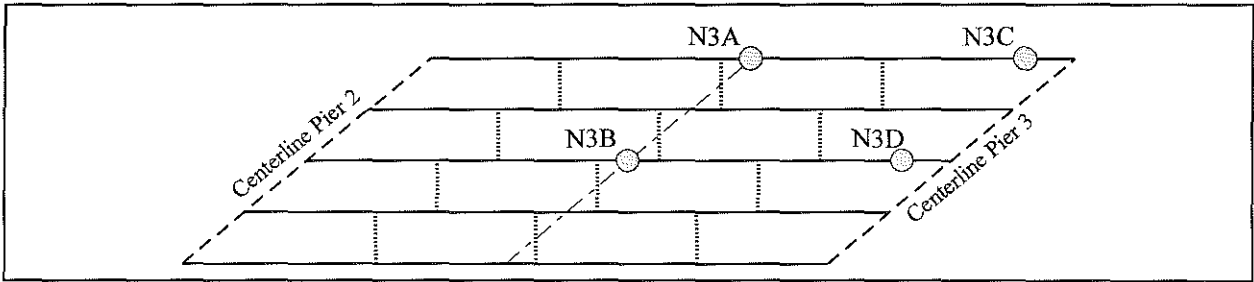


Figure 3.3.1n. Girder Strain Gage Locations in the Northbound Bridge (Bridge Without Intermediate Diaphragms).

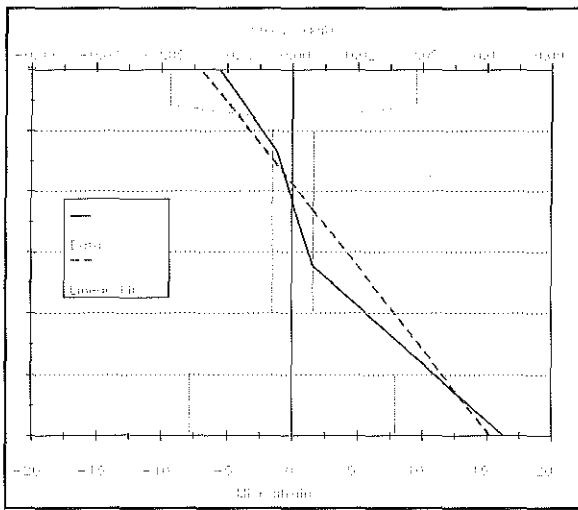


Figure 3.3.1o. Strain Across Girder Cross Section at Location S5C: Trucks Bumper-to-Bumper in Lane 1, Truck 1 at Station 9 (Note: 1 ksi = 6.895 MPa).

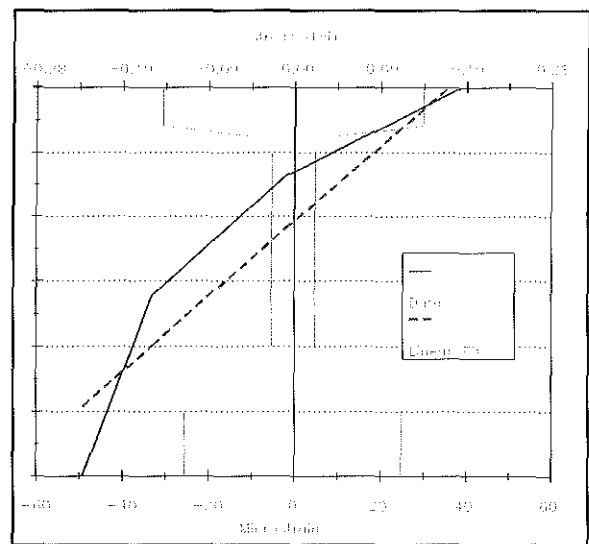


Figure 3.3.1p. Strain Across Girder Cross Section at Location N3A: Trucks Bumper-to-Bumper in Lane 1, Truck 1 at Station 9 (Note: 1 ksi = 6.895 MPa).

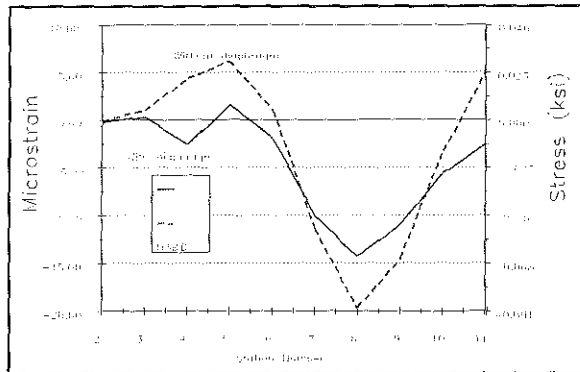


Figure 3.3.1q. Strain Along Bottom of Girder at Location S5B/N3B: Trucks Bumper-to-Bumper in Lane 1 (Note 1 ksi = 6.895 MPa).

The strains obtained from the gages on the longitudinal deck reinforcement were combined with the strains recorded along the cross section of the girder to determine the distribution of stress across the composite cross section. Using diagrams like Figures 3.3.1o and 3.3.1p (refer to Figure 3.3.1a for "lane" and "station" locations), the location of the neutral axis under the static test loads could also be readily obtained. Both figures plot the actual strain readings for all four gages (see Figure 3.3.1j) and a linear fit of that data across the girder cross section. In general the Southbound girder strains were more consistent with the linear fit than were

similar strains measured in the Northbound bridge. However, strain records for both bridges did demonstrate the trend of the neutral axis approaching the deck as the positions of the test truck approached the girder cross section considered. The neutral axis also appeared to be lower in the Southbound bridge when compared to similar cross section locations in the Northbound bridge. This would seem to indicate that the Southbound bridge did a better job of distributing the loads to adjacent girders than did the Northbound bridge. In other words, under the same static test load conditions, the girders in the Southbound bridge experienced less tensile stress on the bottom face of the girder than the girders in the Northbound bridge, a conclusion which is validated in Figure 3.3.1q (refer to Figure 3.3.1a for "lane" and "station" locations). The strain reported in this figure is obtained from the bottom gage on the center girder at midspan. An argument can be made, however, that the differences in the strain values at this location in the Southbound and Northbound bridge is insignificant. Figure 3.3.1q does show some influence by the intermediate diaphragms in distributing loads since the loading case reported in the graph is that of the test trucks positioned along the exterior girder. Again, the contribution observed tends to be minuscule.

Strains recorded across the composite cross section near the pier indicate a different trend, though. As illustrated in Figure 3.3.1r (refer to Figure 3.3.1a for "lane" and "station" locations), girder strains near the pier seem to parallel each other. In fact the presence of intermediate diaphragms appears to increase the compressive stress that the bottom face of the interior Southbound girder experiences under the static test loads. This condition was only noted when the test trucks were located in lanes opposite of the girder being considered, e.g., Figure 3.3.1r demonstrates the behavior of the center girder when loading was concentrated on the exterior girder.

When the test trucks were placed over the same girder under consideration, the same pattern of strain illustrated in Figure 3.3.1r was observed, but the magnitudes of strain were larger in the Northbound bridge than in the Southbound bridge. For example, at locations S5B and N3B (see Figures 3.3.1m and 3.3.1n) the strain on the bottom face of the Southbound girder was 10.07 microstrain while the strain on the Northbound girder was 13.25 microstrain when the trucks were positioned in Lane 2 with Truck 1 at Station 8. The maximum tensile stress experienced by any girder in the Southbound bridge was 0.30 ksi (2.05 MPa). Likewise, the maximum tensile stress experienced by any girder in the Northbound bridge was 0.35 ksi (2.40 MPa). The variation in position in which these maximum values were noted indicates that the absence of intermediate diaphragms leads to increased flexibility in the interior girders under the static test loads. However, this conclusion cannot be wholly substantiate since the exterior girder of the Northbound bridge experienced less tensile stress than the Southbound bridge when the test trucks were positioned directly above it. Table 3.3.1e lists some representative strain and stress values obtained on the girders of the Northbound and Southbound bridges.

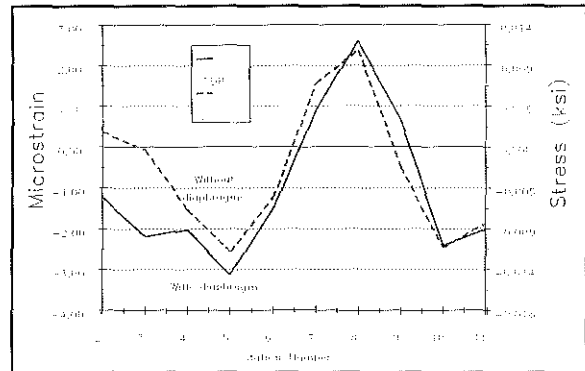


Figure 3.3.1r. Strain Along Bottom of Girder at Location S5D/N3D: Trucks Bumper-to-Bumper in Lane 1 (Note: 1 ksi = 6.895 MPa).

3.3.1.5. Instrumentation in the Diaphragm Region

After applying the appropriate calibration factors and subtracting out the zero reading, strain values for the steel strain gages and reusable strain gages in the diaphragm region were obtained and tabulated for each test scenario. Any location codes referenced in the following paragraphs correspond to those defined in Figures 3.3.1s, 3.3.1t, and 3.3.1u for the Southbound (bridge with intermediate diaphragms) and Northbound (bridge without intermediate diaphragms) bridges, respectively. Locations N3E and N3F on the Northbound bridge are comparable to locations S4A5 and S4B5, respectively, on the Southbound bridge and are denoted by the asterisk in Figures 3.3.1s and 3.3.1t.

Extensive instrumentation in the diaphragm region was used to define the state of stress on the diaphragm-girder interface. As Figure 3.3.1v (refer to Figure 3.3.1a for "lane" and "station" locations) depicts, small strains were generally recorded from the gages placed around the diaphragm on the girder as previously pictured in Figure

3.3.1s. In fact, the largest strain value recorded at the diaphragm-girder interface was 91.59 microstrain,

Table 3.3.1e: Strain and Stress Values Obtained From Girder Strain Gages.

Location ^a	Northbound Bridge		Southbound Bridge		Position of Test Trucks ^c
	Micro-strain ^b	Stress in ksi (MPa)	Micro-strain ^b	Stress in ksi (MPa)	
AB	49.77 (T)	0.23 (1.59)	64.16 (T)	0.30 (2.05)	Bumper-to-Bumper in Lane 1 with Truck 1 at Station 9
AM	32.03 (T)	0.15 (1.02)	30.18 (T)	0.14 (0.96)	
AT	2.43 (T)	0.01 (0.08)	3.41 (C)	0.02 (0.11)	
DB	13.04 (C)	0.06 (0.41)	4.60 (C)	0.02 (0.15)	Bumper-to-Bumper in Lane 2 with Truck 1 at Station 7
DM	7.10 (C)	0.03 (0.22)	4.36 (C)	0.02 (0.14)	
DT	3.60 (T)	0.02 (0.11)	0.29 (T)	0.00 (0.01)	

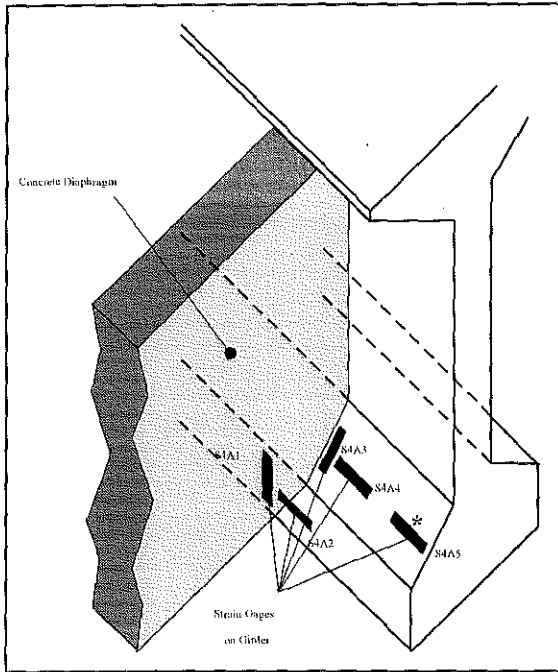
^a refer to Figures 3.3.1l, 3.3.1m, and 3.3.1n.

^b "C" denotes compression and "T" denotes tension.

^c refer to Figure 3.3.1a for "lane" and "station" locations.

corresponding to a tensile stress in the girder of 0.42 ksi (2.88 MPa). This maximum value occurred at location S4B2 when the trucks were bumper-to-bumper in Lane 2 with truck 1 at Station 9. These static test data alone, however, are insufficient to conclusively define what is causing the spalling around the diaphragm-girder interface. A more detailed investigation of the principal stresses in this region is required and will be discussed in a later chapter. In retrospect, instrumentation on the girder directly beneath the diaphragm, especially in the area around the diaphragm anchor bar, may have been helpful in determining a definitive cause to the concrete spalling.

Altering the configuration of the diaphragm, i.e., not extending the diaphragm reinforcement into the deck (cut low condition), served to reduce the strains on the



girder face with a subsequent increase in the strains on the diaphragm face. Figure 3.3.1w compares strain values at various locations in the gage rosette pattern considered in Figure 3.3.1u for the typical and cut low diaphragms. As was mentioned previously, these diaphragms were tested with a single truck that was positioned such that the passenger side, rear tires straddled the respective diaphragm. Despite the apparent advantages to using cut low diaphragms (strains on the face of the girder decreased while the increase in the diaphragm face strains were well within that allowable for concrete), consideration must be given to the ease in which this cut low diaphragm configuration can be constructed before they can be accepted as an alternative to the typical diaphragm.

Figure 3.3.1s. Strain Gages Located Near the Girder Flange-Diaphragm Interface.

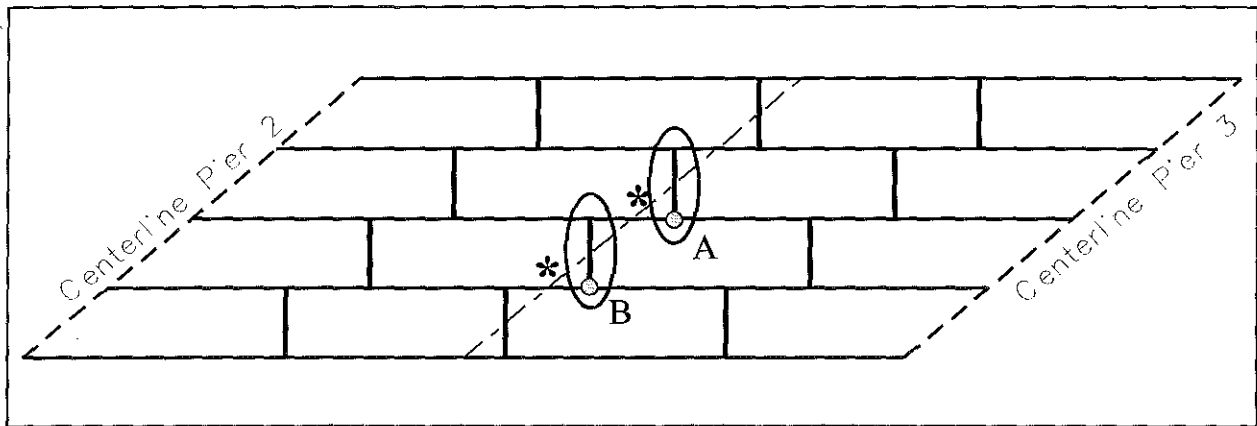


Figure 3.3.1t. Locations of Diaphragm Regions Instrumented With Strain Gages in Span 3 of the Southbound Bridge.

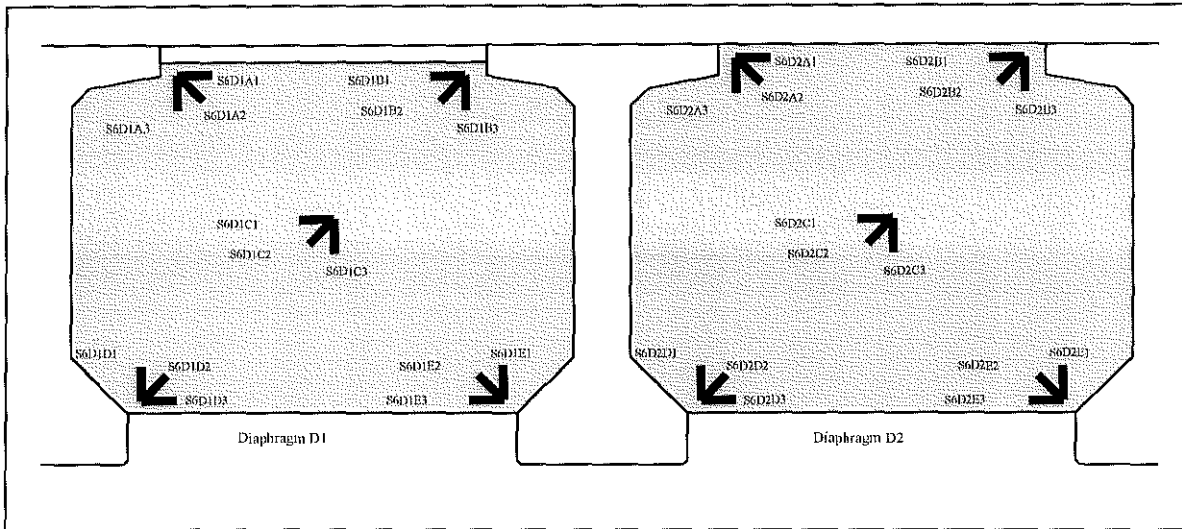


Figure 3.3.1u. Strain Gages on the Face of the Southbound Bridge Diaphragm D1 and Diaphragm D2.

Strain gages placed on comparable positions in the Southbound and Northbound bridges near the diaphragm region yielded expected results. As seen above and witnessed again in Figure 3.3.1x (refer to Figure 3.3.1a for "lane" and "station" locations), the Northbound bridge girders experience larger strains than do the Southbound bridge girders. However, the difference in the magnitude of strain/stress is not sufficient to suggest that intermediate diaphragms must always be included in

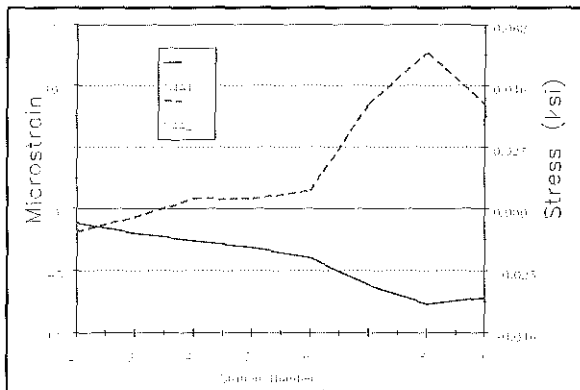


Figure 3.3.1v. Strain on Girder at Locations S4A1 and S4A2 of the Diaphragm-Girder Interface With Trucks Bumper-to-Bumper in Lane 1 (Note: 1 ksi = 6.895 MPa).

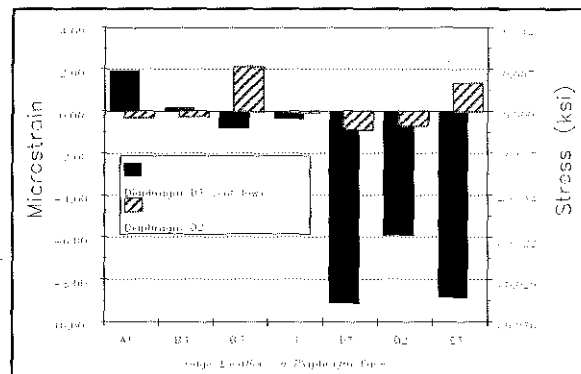


Figure 3.3.1w. Strain on Face of Diaphragms D1 and D2 With Truck Straddling Centerline of Diaphragm (Note: 1 ksi = 6.895 MPa).

bridges of prestressed concrete, slab-on-girder construction. Further support for this

conclusion comes from the marginally insignificant difference between the out-of-plane displacements in these areas, as discussed above.

3.3.2. DYNAMIC TESTING

Once the acceleration data were obtained, the Fast Fourier Transform (FFT) procedure was used to determine the vibrational frequencies of the structure. A FFT is a process by which acceleration records are transformed from the time domain to the frequency domain. As Nassif and Nowak (1995) reported, the FFT procedure can only be utilized assuming that the measured acceleration-time data can be represented as the sum of all contributions from all mode shapes.

The mode shapes were determined by plotting the ratios of the accelerometer FFT magnitudes to base station FFT magnitudes in three orthogonal directions

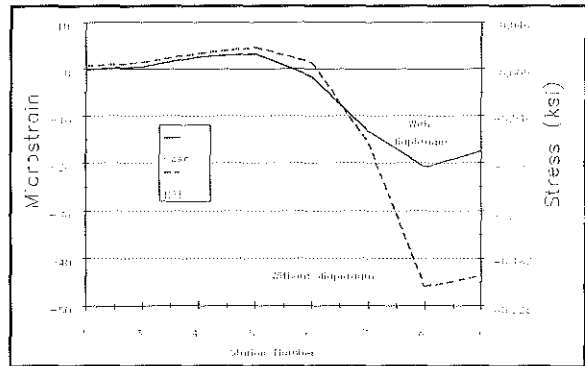


Figure 3.3.1x. Strain on Girder at Locations S4A5 and N3E With Trucks Bumper-to-Bumper in Lane 2
(Note: 1 ksi = 6.895 MPa).

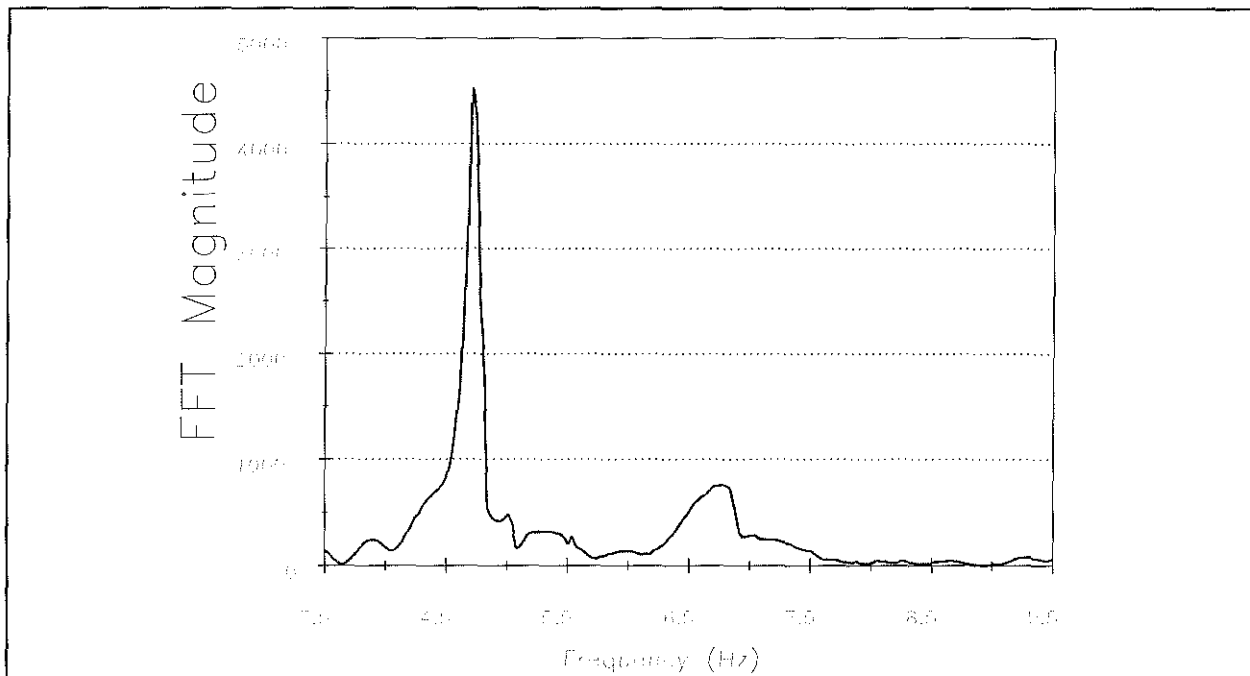


Figure 3.3.2a. Fast Fourier Transform of Acceleration Record L2CH2.DAT
(Note: Please See Figure 3.1.2 for Illustration of Raw Data Record).

(longitudinal, transverse, and vertical). Comparing the phase angle of an FFT to the base station FFT phase angle determined the sign of the magnitude to be plotted. Engineering judgment as well as results from an *a priori* finite element model were used to determine if the resulting mode shape was realistic and could be expected. Once the mode shapes were obtained, the contributing modes in the deflection of the bridges under traffic loading could be ascertained. Figure 3.3.2a illustrates a portion of a FFT of the vertical acceleration data from the base station accelerometer at Station 8W during the first dynamic test on the Northbound bridge (the acceleration record previously given in Figure 3.1.2). Results from plotting FFT magnitudes for the fundamental vertical frequency for the Northbound and Southbound bridges are demonstrated in Figures 3.3.2b and 3.3.2c. An isometric view has been provided to assist in observing the first vertical mode shape. It is obvious from Figure 3.3.2a that a peak exists at a frequency of 4.71 Hz, which corresponds to the mode shape plotted in Figure 3.3.2b.

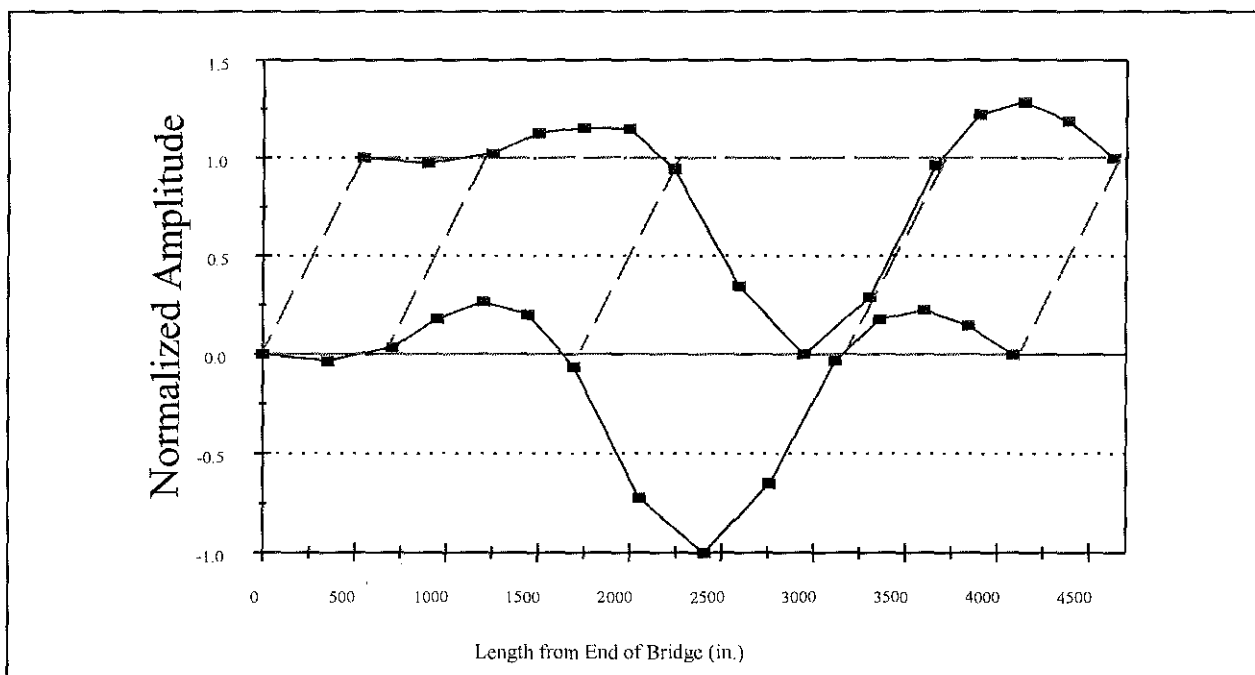


Figure 3.3.2b. Vertical Mode Shape of Northbound Bridge at 4.71 Hz Obtained from Experimental Data.

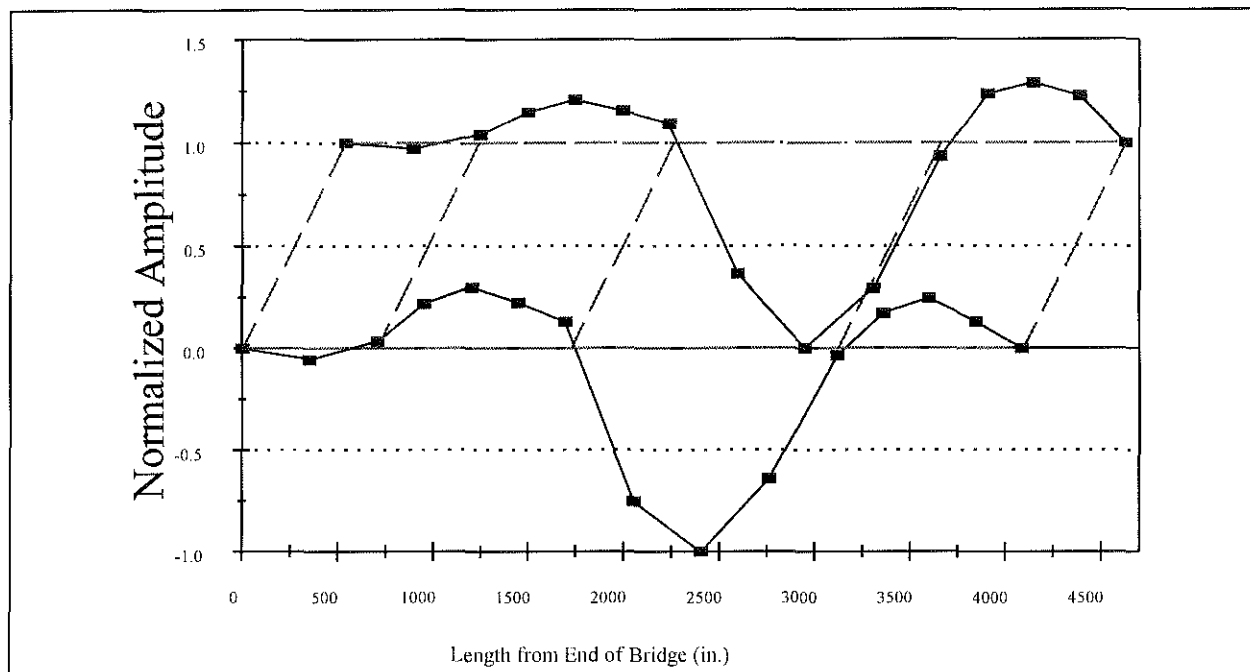


Figure 3.3.2c. Vertical Mode Shape of Southbound Bridge at 4.61 Hz Obtained from Experimental Data.

Table 3.3.2 lists the experimental frequencies associated with the Northbound and Southbound bridges for the first structurally significant modes. It was observed that mode 1 corresponds to the first transverse mode, mode 2 to the first longitudinal mode, mode 3 to the first vertical mode of bending, and mode 4 to the first torsional mode of bending.

In general, when comparing the vibrational frequencies, the Southbound bridge seems to be stiffer than the Northbound bridge. Two notable exceptions are evident, though, in modes 2 and 3. This discrepancy can be explained as follows. The vibrational frequency of a structure is related to the ratio of the structure stiffness to the structure mass. All other aspects being equal, the only difference between the two bridges is the presence of the 36 concrete intermediate diaphragms in the Southbound bridge. These obviously add some mass to the structure (approximately 5.5 percent of the total). The question then becomes whether or not the added stiffness from these diaphragms overcomes the contribution of the added mass. For mode 1, the contribution of the diaphragm stiffness in the transverse direction seems to outweigh the added mass and the pattern holds that the Southbound frequency is higher.

However, in modes 2 and 3, the mass of the diaphragms appears to negate any contribution to the stiffness of the structure provided by the diaphragms. Consequently, these frequencies are lower than their counterparts for the Northbound

bridge. In the higher modes, the diaphragms seem to contribute more to structure stiffness than to the overall mass of the structure. It should be noted that the presence of the loosened steel intermediate diaphragms in the Northbound bridge does not contribute to the structure stiffness, but does add to the overall structure mass (approximately one percent of the total). If this same bridge had all of the steel diaphragms removed, a slight increase in the vibrational frequencies of the structure could be expected.

Table 3.3.2: Frequencies of the Northbound and Southbound Bridges Identified by the Experimental Data

Frequencies (Hz)		Mode Shapes
Southbound Bridge (Bridge With Intermediate Diaphragms)	Northbound Bridge (Bridge Without Intermediate Diaphragms)	
2.1042	2.0374	1 st Transverse (half-sine)
2.7722	2.9058	1 st Longitudinal
4.6092	4.7094	1 st Vertical (half-sine all spans)
6.1456	5.9452	1 st Torsional (Span 3)
7.6486	6.9472	2 nd Torsional (Span 4) plus 2 nd Transverse (full-sine)
8.6172	8.0160	2 nd Vertical (full-sine Span 3)
9.1850	8.6506	3 rd Vertical (full-sine Span 4)
9.5524	9.3520	3 rd Torsional (Span 3)
10.4876	10.1870	4 th Torsional (Span 4) plus 2 nd Transverse (full-sine)
11.2558	10.7214	5 th Torsional (Span 2) plus 2 nd Transverse (full-sine)
13.3266	11.2224	6 th Torsional (Span 2)
14.1282	12.2578	4 th Vertical (full-sine Span 2)
19.1716	15.2304	3 rd Transverse
23.2464	21.4428	5 th Vertical (full-sine all spans)
27.0540	24.9498	4 th Transverse

3.3.3. REPEATABILITY OF TESTING

As with any experimental program, the reliability and validity of the test data is intertwined with the ability to repeat the tests and achieve similar results. For this particular research, the repeatability of the results from the static and dynamic tests were improved in large part by: 1) using the same truck(s) for every test, 2) using the same lane and station locations during each static test setup, and 3) using the same truck at the same speed along the same transverse location on the bridge during the dynamic tests. Figure 3.3.3a depicts two records of the vertical acceleration at a base station location during different dynamic tests. It is important to note the peaks in the FFT of the acceleration data occur at the same locations. As an additional means of comparison, several strain gages were read at the same location during more than one static test setup, thereby providing an opportunity to compare the results. An example of this is illustrated in Figure 3.3.3b.

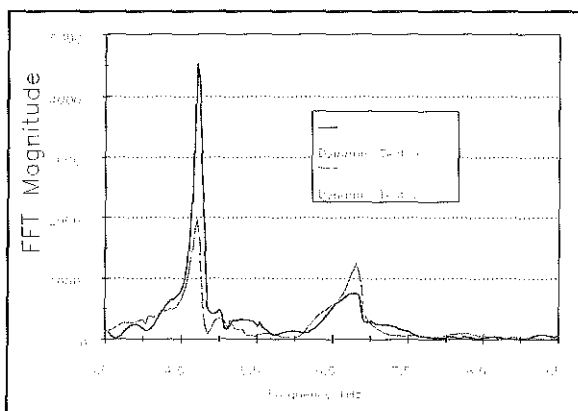


Figure 3.3.3a. Example of Dynamic Test Repeatability - Station 8E.

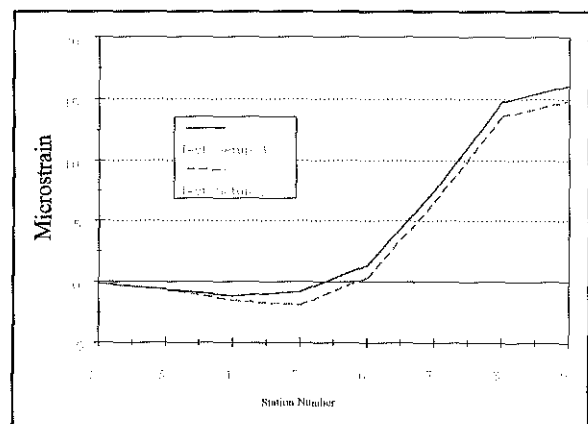


Figure 3.3.3b. Example of Static Test Repeatability - Gage N3CM.

CHAPTER 4

FINITE ELEMENT MODELING OF THE BRIDGES

4.1. INTRODUCTION

Having completed the static and dynamic test phase, finite element models of the US 23 bridges were constructed and calibrated to correlate with the experimentally measured data. Although modeling of any structure leads to approximations, a careful examination of geometric and material properties will enable the engineer to develop a practical model from which to begin. Refinement of the models, varying either geometric or material properties, is accomplished by evaluating the bridge response of the finite element models in comparison to the experimental data. Calibration, though, is a sensitive task. For example, if dynamic calibrations are assumed to be completed, i.e., the experimental and analytical frequencies match, subsequent static calibrations that incorporate adjustments in the elastic moduli will change the natural frequencies of the bridge model. Engineering judgment must be used to balance the manipulation of the geometric and/or material properties to achieve the "true" bridge model.

4.2. FINITE ELEMENT MODELS OF THE BRIDGES

As Chen and Aswad (1996) indicated, certain assumptions must be made when conducting a finite element analysis of a bridge. The assumptions used in formulating the finite element models of the US 23 bridges were as follows: 1) a small deflection theory was used, 2) linearly elastic behavior of materials was assumed, 3) the deck slab was assumed to have a constant thickness, and 4) the nodal loads were assumed to be statically equivalent to the actual point loads.

Since later analysis and research would center on very specific regions of the bridges, namely the diaphragm-girder interface, a detailed three-dimensional finite element model for each bridge was constructed. A three-dimensional representation of the bridges would also assist in the calibration of the models with experimental frequencies, mode shapes, and deflections. The models were analyzed using the packaged software SAP90[®] (Computers 1991). Table 4.2 summarizes the components of the two (Northbound and Southbound) bridge models. Due to a lack of symmetry in the longitudinal or transverse direction, it was necessary to model the entire length

and width of the bridges. The Northbound bridge model input file was 8,186 lines long. The Southbound bridge model input file was 9,975 lines long.

Table 4.2: Components of the Bridge Models.

Item	Northbound Bridge (Bridge Without Intermediate Diaphragms)	Southbound Bridge (Bridge With Intermediate Diaphragms)
Largest Joint Number	26,488	31,068
Frame Elements	288	288
Shell Elements	8,670	8,670
Solid Elements	10,370	12,098
Springs	50	50
Constraints	36	2,340
Total Degrees of Freedom	96,858	108,167

4.2.1. FRAME ELEMENTS

Frame elements with six degrees of freedom at each node were used to model the pier diaphragms. Each frame element was given a moment of inertia, I , and an elastic modulus, E , to simulate the rigid behavior between all of the girders and the deck over the pier cap. Similarly, the end bent diaphragm was assumed to rigidly connect the girders at the abutments. These "rigid links" connected the nodes over the centerline of the pier or abutment of adjacent girders. The total mass of the pier diaphragms was calculated and divided among the number of frame elements used to model this rigid link. The end bent diaphragm mass was incorporated into the models in the same manner. The lumped mass specified in both cases was 6.7899×10^{-5} k-s²/in (11.89 kg) per unit length of the frame element.

4.2.2. SHELL ELEMENTS

Four-node, isoparametric shell elements (membrane and plate bending behavior, i.e., six degrees of freedom at each node) were incorporated into the bridge models to

simulate the deck. The shell elements were placed at the geometric center (mid-thickness) of the slab. The skew in the slab was incorporated into the model by using the shell elements as parallelograms. The joint discretization was such to accommodate the transition between the shell elements of the deck and the solid elements used to model the girders and barrier walls. Consequently, three shell elements modeled the slab over the width of one girder. Two shell elements comprised the cantilevered portion of the slab directly beneath each barrier wall on both sides. Eight shell elements modeled the unstiffened portion of the deck between two adjacent girders. This mesh led to a total of 51 ($[2 \times 2] + [5 \times 3] + [4 \times 8]$) shell elements across the transverse (global X) section of the bridge. The longitudinal (global Y) section of the deck was broken up into 170 shell elements for a total of 8,670 (51×170) shell elements in the deck grid.

4.2.3. SOLID ELEMENTS

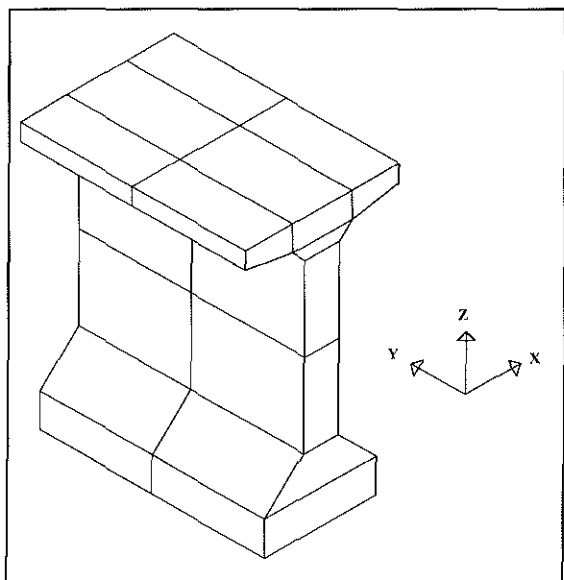


Figure 4.2.3a. Solid Element Model of the Modified AASHTO Type IV Girder.

Since one of the most important aspects of the current research was to investigate the effectiveness of diaphragms in a bridge subjected to coal truck loads, the interface between the P/C I-girders and diaphragms had to be highly detailed. Furthermore, because the three-dimensional state of stress for this region would be heavily examined, the elements chosen to model this area would have to have the capability to report such values. This necessitated the use of eight-node, isoparametric "brick" elements to model the girders, haunches, and barrier walls. Three translational degrees of freedom are available for this element, with all rotational degrees of freedom being restrained. The eight-node "brick" element formulation used in SAP90[®] includes nine incompatible bending modes (Computers 1991) as originally proposed by Wilson *et al.*

(Hughes 1987). Figure 4.2.3a illustrates the discretization of the P/C I-girder in both bridge models. Eighteen nodes define the geometry of the Modified AASHTO Type IV girder exactly. The incompatible bending modes were suppressed for the elements shaded in Figure 4.2.3b as recommended by Wilson due to the distortion of the element (Computers 1991). This eight element discretization represents a refinement of solid element models encountered in the literature (Abendroth *et al.* 1991, Abendroth *et al.* 1995).

However, before this cross-section mesh of elements could be used with confidence, a verification that the discretization would yield reliable and accurate answers was performed. A single P/C I-girder from Span 3 was modeled with fixed end conditions. Each element represented 1/60 of the total girder length. Analyses with a uniformly distributed load and a point load at the center of the span were conducted and compared to known results from beam formulas (AISC 1994). As Table 4.2.3 indicates, deflections and stresses matched within 1.88% for both load cases. Such a small error was determined to be satisfactory, so the bridge girders were modeled with the cross-section mesh described above.

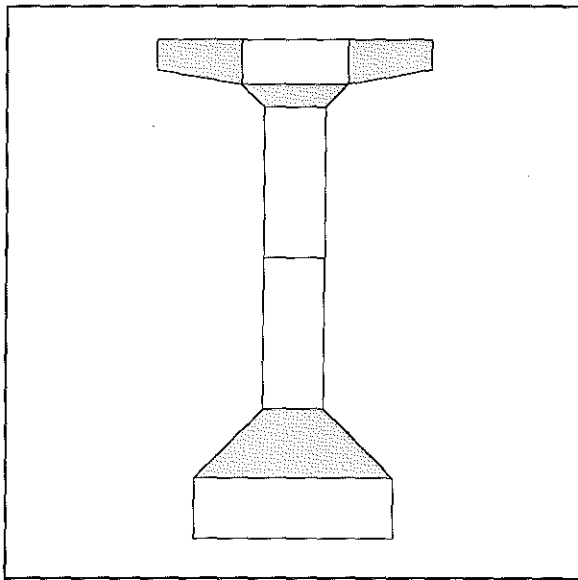


Figure 4.2.3b. Elements With Suppressed Incompatible Bending Modes.

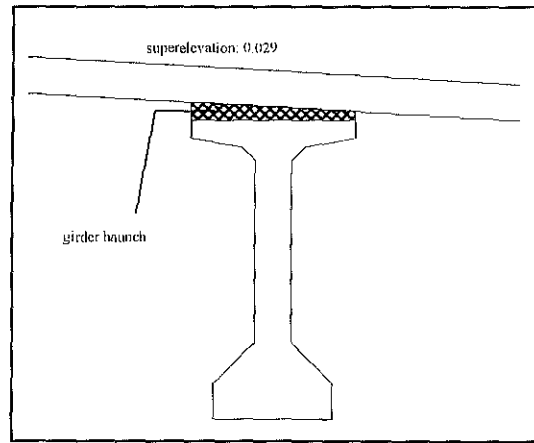


Figure 4.2.3c. Illustration of a Girder Haunch.

A girder haunch, pictured in Figure 4.2.3c, is common in bridges constructed with prestressed concrete girders since the process of prestressing a beam leads to camber. This camber is an integral portion of the design calculations and is often used to offset the expected deflections when the deck slab is poured (i.e., deflections due to the dead load of the wet concrete). However, the camber in a girder is seldom the value predicted by design calculations. Therefore, a haunch thickness of 1 in (25.4 mm) was assumed over the centerline of the girder. With the presence of the slab superelevation, the haunch varied from 0.48 in (12.14 mm) to 1.52 in (38.66 mm) across the width of the girder. The haunches were modeled with the eight-node

isoparametric elements and provided the composite connection between the girders and the deck. Special attention was made so that the mesh of the girders and the deck across the girders would be only three elements wide.

Table 4.2.3: Comparison of Solid Element Model of Girder With Beam Formulas.

Load Case	Item ^a	Solid Element Model ^b	Beam Formula ^b
Point Load at Center of Beam	Δ at 0.50L	0.07 in (1.75 mm)	0.07 in (1.75 mm)
	Δ at 0.25L	0.04 in (0.88 mm)	0.03 in (0.88 mm)
	σ_T at 0.50L	-0.11 ksi (-0.76 MPa)	-0.11 ksi (-0.76 MPa)
	σ_B at 0.50L	0.10 ksi (0.66 MPa)	0.10 ksi (0.66 MPa)
	σ_B at 0.25L	0.01 ksi (0.02 MPa)	0.01 ksi (0.02 MPa)
	σ_T at 0.00L	0.11 ksi (0.75 MPa)	0.11 ksi (0.76 MPa)
Uniformly Distributed Load on Beam	Δ at 0.50L	0.78 in (19.68 mm)	0.77 in (19.62 mm)
	Δ at 0.25L	0.44 in (11.24 mm)	0.44 in (11.19 mm)
	σ_T at 0.50L	-0.84 ksi (-5.77 MPa)	-0.85 ksi (-5.84 MPa)
	σ_B at 0.50L	0.74 ksi (5.07 MPa)	0.74 ksi (5.13 MPa)
	σ_B at 0.25L	0.15 ksi (1.02 MPa)	0.15 ksi (1.02 MPa)
	σ_T at 0.00L	1.61 ksi (11.10 MPa)	1.61 ksi (11.11 MPa)

^a Δ =vertical displacement, σ_T =top fiber stress along the longitudinal axis of the beam, and σ_B =bottom fiber stress along the longitudinal axis of the beam.

^b differences between seemingly equivalent values can be attributed to round off.

The barrier walls were also modeled using the eight-node, isoparametric "brick" element. Since the geometry was not complex, only three elements were needed to define the cross section of each wall. Although much of the literature indicated that the influence of parapets, curbs, etc., were negligible and their exclusion leads to conservative results, the barrier walls were included in the finite element models of both bridges. Two advantages exist in including the barrier walls: 1) the number of modeling assumptions/approximations was reduced and 2) the dynamic calibration could be accomplished easier without having to account for the absence of the extra mass and stiffness had the barriers been excluded.

The concrete intermediate diaphragms in the Southbound bridge were likewise modeled using the eight-node, isoparametric element. Each diaphragm was modeled as eight elements between the girders and six elements along the height of a girder. The 10 in (254 mm) thickness of the diaphragm was modeled as one element for a total of 48 (8 x 6 x 1) solid elements per diaphragm. Distortion in the elements due to the irregular surface of the girder was reduced towards the center of the diaphragm. Since specific concerns were to be investigated with regard to the diaphragm-girder interface, mesh grading was employed on the girder models near this region. Girder solid elements were graded to a 10 in (254 mm) thickness over a span of three elements on either side of the 10 in (254 mm) thick diaphragms. An illustration of the cross section of the Southbound bridge finite element model, including the girder haunches, intermediate diaphragms, and barrier wall, is given in Figure 4.2.3d. The cross section of the finite element model of the Northbound bridge is depicted in Figure 4.2.3e. The only difference between the two is the absence of intermediate diaphragms and the direction of superelevation in the Northbound bridge.

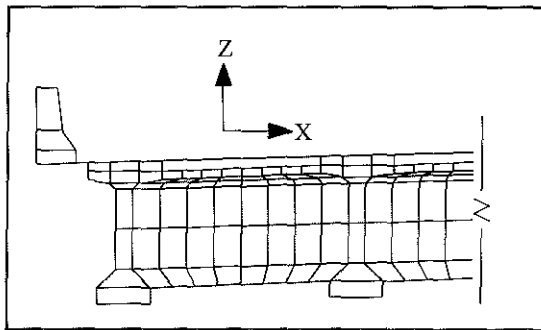


Figure 4.2.3d. Cross Section of the Southbound Bridge Finite Element Model.

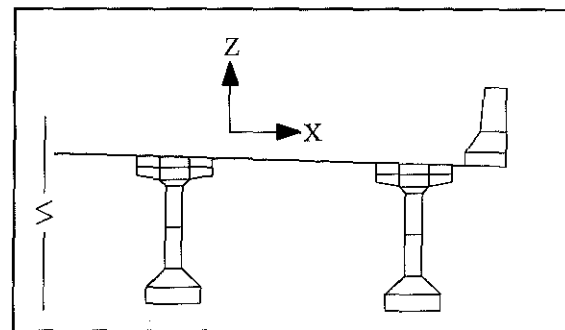


Figure 4.2.3e. Cross Section of the Northbound Bridge Finite Element Model.

4.2.4. SPRING SPECIFICATION

Due to the magnitude of elements and joints required to construct such a

complex model, some effort was made to reduce the parameters that needed to be included in the finite element analysis. Since the primary concern of this research was to investigate the effects of coal haul trucks on the bridge superstructure, an extensive model of the bridge substructure was not attempted. Therefore, the bridge piers and abutments were replaced by a series of linear springs.

Previous researchers have commented on the inability to accurately ascertain the end restraint condition at an abutment (Aktan *et al.* 1992). Additionally, support conditions at the abutment would ultimately be altered in order to calibrate the finite element models. No specific measures were used to determine the abutment spring stiffnesses in the original models. All abutment springs were assumed to approximate the restraint provided by the end bearing with an additional stiffness contribution provided by the expansion dam.

The spring stiffness of the piers was calculated directly through a finite element analysis of each three-bay structure (see Figure 4.2.4). The individual concrete pier columns, pier cap, and steel H-pilings were modeled with frame elements using the material and member properties listed in the construction drawings. The skew of the piers in relation to the bridge superstructure was maintained in the global sense. Linear springs were applied in directions perpendicular to the local axis of the pilings to simulate the soil conditions at the bridge site. The spring substitutes for the subsurface were calculated from the bearing capacity of the surrounding soil. Since pilings were driven to bedrock, a pinned-end condition was assumed at the tip of each piling.

Once the model was adequately defined, unit displacements in three orthogonal (transverse [global X], longitudinal [global Y], and vertical [global Z]) directions were applied to each model. After the analysis was completed, a spring stiffness in a global direction was obtained by dividing the resulting reaction force by the displacement:

$$K_i = \frac{\sum R_i}{\sum \Delta_i} \quad (4.1)$$

Different spring stiffnesses for each pier in the Northbound and Southbound bridges were calculated by using the appropriate pier column and piling lengths.

The spring stiffnesses calculated in this manner were divided by the number of girders distributed along the centerline of the respective pier. Dividing the spring stiffnesses as such is feasible since it was previously assumed that the pier and end bent diaphragms rigidly linked the girders. Rotational springs were not employed since the use of eight-noded solid elements required these degrees of freedom to be restrained. The pier spring stiffnesses obtained from the procedure described above

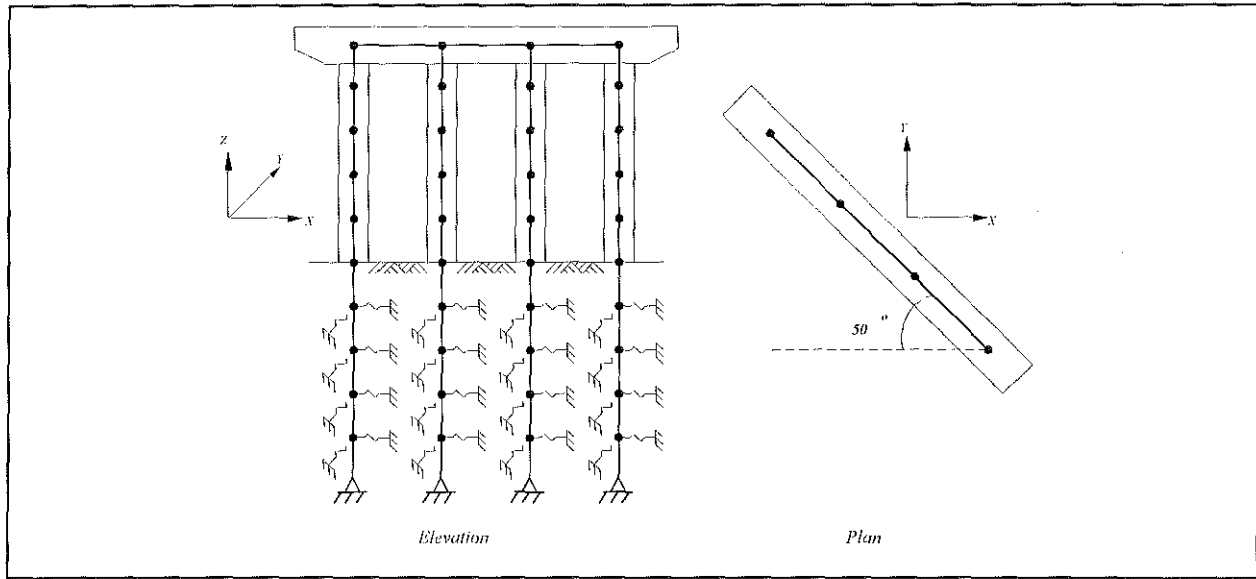


Figure 4.2.4. Finite Element Model of Pier Used to Obtain Spring Stiffnesses.

are listed in Table 4.2.4. The values reported in the table were divided by five when incorporated into the finite element model of the bridges.

Table 4.2.4: Spring Stiffness Substituted for the Piers in the Finite Element Models.

Bridge	Pier	Translational Spring Stiffness in kip/in (kN/mm)		
		Transverse	Longitudinal	Vertical
Northbound	1	29.16 (5.11)	31.10 (5.45)	14744.16 (2581.97)
	2	41.52 (7.27)	44.57 (7.81)	14068.34 (2463.62)
	3	35.60 (6.23)	38.42 (6.73)	21978.88 (3848.90)
Southbound	1	39.47 (6.91)	42.33 (7.41)	14373.62 (2517.08)
	2	44.65 (7.82)	48.09 (8.42)	15421.45 (2700.58)
	3	51.27 (8.98)	55.53 (9.72)	17074.08 (2989.98)

4.2.5. JOINT CONSTRAINT SPECIFICATION

Every attempt was made to make the finite element models of the bridges as accurate as possible. Therefore, special considerations as regards the connection of the intermediate diaphragms to the girders and the continuity of the barrier walls were warranted. The concrete intermediate diaphragms in the Southbound bridge were cast in place prior to the pouring of the deck. The continuity between the deck and the diaphragm was provided by reinforcing steel. However, the only connection that exists between the prestressed concrete girder and the diaphragm is two threaded diaphragm anchor bars. Friction between the diaphragm and the girder concrete was neglected as a valid restraint component. The anchor bars are located 4 in (101.6 mm) apart on the girder at the center of the diaphragm. An example of an anchor bar threaded into the girder prior to the pouring of the end bent diaphragm is given in Figure 4.2.5.

To model this condition, additional nodes were specified along the profile of the girder. These nodes coincided with those used to define the girder geometry, i.e., a double node scheme was employed. Using SAP90's constraint equation capabilities, the translational degrees of freedom in the top and bottom nodes of the diaphragm near the girder were constrained in the transverse (global X), longitudinal (global Y), and vertical (global Z) directions to the respective translational degrees of freedom in the girder nodes at these locations. This was done to approximate the connection by the anchor bars and the deck. The other nodes located along the girder diaphragm interface were constrained in the transverse (global X) and vertical (global Z) directions only. Although no connection is provided between the girder and diaphragm during construction outside of the anchor bar and friction between the surfaces, the transverse (global X) and vertical (global Z) directions were constrained in order to avoid modeling difficulties due to "contact" problems. Modeling the potential separation between the girder and the diaphragm would allow for the possibility of the two components overlapping in the model if two adjacent girders deflected towards each other. The longitudinal (global Y) direction displacement could remain free since "contact" problems would not be expected in this direction.

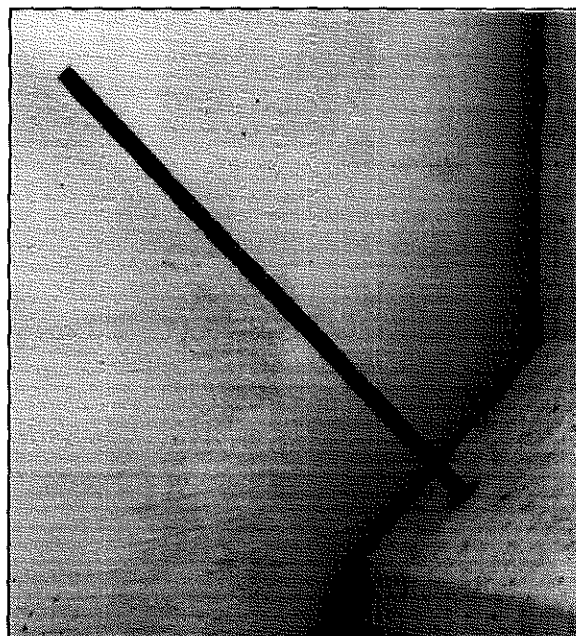


Figure 4.2.5. Diaphragm Anchor Bar in Place at the Abutment.

A similar approach was adopted to account for the expansion joints in the barrier walls. A double node scheme was again employed at the location of the expansion joint. Translational degrees of freedom in the longitudinal (global Y) direction were constrained for each double node, but the transverse (global X) and vertical (global Z) direction displacements were not. In this manner, the model reflected the barrier walls' ability to deflect outward in any span of the actual bridge, independent of the behavior of the barrier wall in an adjacent span, due to the presence of the expansion joint. Neither this case nor the diaphragm region required constraint equations for the rotational degrees of freedom since rotations are not available in the eight-node "brick" formulation.

4.2.6. MASS SPECIFICATION

Using linear springs as substitutes for the piers gives a good approximation of the stiffness but neglects the contribution to the structure mass that the piers provide. The absence of the pier mass in the bridge models would lead to higher vibrational frequencies than recorded in the field. Therefore, the total mass of the pier cap and pier columns were calculated and divided among each node where linear springs were specified on the girders. Table 4.2.6 lists the lumped mass specification used in the bridge models to account for the bridge piers. The mass values reported in this table were specified in the transverse (global X), longitudinal (global Y), and vertical (global Z) directions. Rotational mass moments of inertia could not be used since the girders were modeled with the eight-node "brick" element and the rotational degrees of freedom were restrained.

Table 4.2.6: Lumped Masses Used to Simulate the Presence of Bridge Piers.

Pier	Northbound Pier Mass in k-s ² /in (kg)	Southbound Pier Mass in k-s ² /in (kg)
1	0.0669 (11725)	0.0616 (10796)
2	0.0610 (10691)	0.0578 (10130)
3	0.0536 (9394)	0.0536 (9394)

As mentioned in Chapter 3, the Northbound bridge intermediate diaphragms were loosened, but were still connected to the girders. Consequently, the mass of the steel diaphragms needed to be included in the Northbound bridge finite element model. The total mass of a single Z-type diaphragm was calculated and divided among the four girder nodes closest to where the diaphragms were connected to the girders (see

Figure 4.2.6 - the dashed line represents the steel intermediate diaphragm). The mass defined at each node was $1.719 \times 10^{-4} \text{ k-s}^2/\text{in}$ (30.13 kg) and was specified for the transverse (global X), longitudinal (global Y), and vertical (global Z) translational directions. Again, mass moments of inertia were not specified since the rotational degrees of freedom were restrained because eight-node "brick" elements were used to model the girders. In retrospect, the total contribution to the overall structure mass by these steel diaphragms is small (approximately one percent of the total structure mass), but their inclusion leads to a more accurate and complete representation of the Northbound bridge.

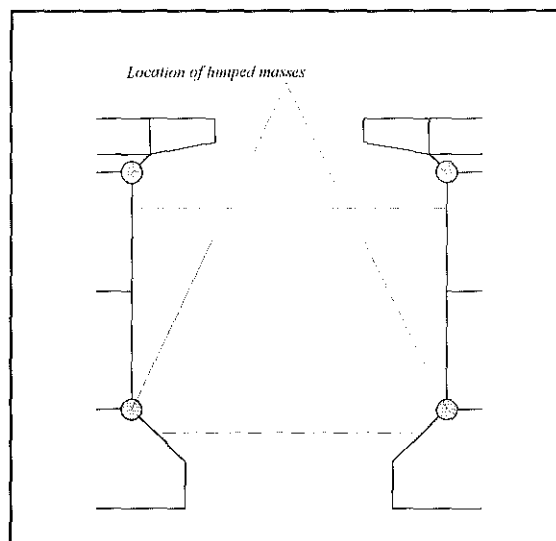


Figure 4.2.6. Lumped Mass Locations for Steel Diaphragms in Northbound Bridge Finite Element Model.

4.2.7. JOINT LOAD SPECIFICATION

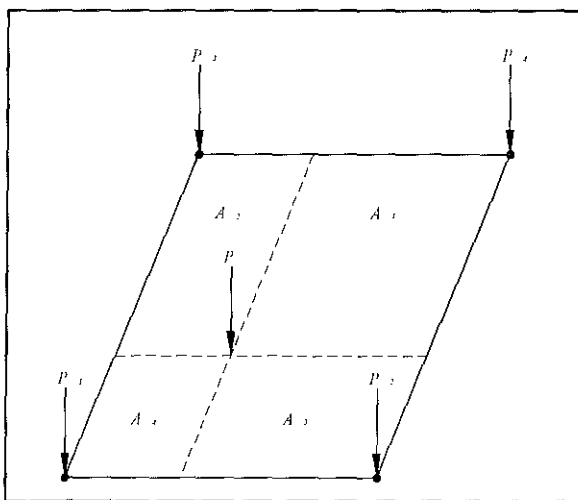


Figure 4.2.7. Determination of Equivalent Nodal Loads in a Parallelogram Element

After Chen (1995a).

$$P_i = P \left(\frac{A_i}{\sum A_i} \right)$$

(4.2)

The discretization adopted for the deck was chosen for modeling simplicity and continuity between elements rather than ease of locating the tire loads of the static test vehicles. Consequently, a procedure whereby the static truck loads could be applied to the adjacent shell element nodes (i.e., an equivalent static load method) was necessary. Chen (1995a) provided a very reasonable and easy method to calculate the equivalent nodal loads for a parallelogram element. Referring to Figure 4.2.7, contributions from the point load, P , to the element nodes are obtained from the following formula:

where A_i are the tributary areas and P_i are the equivalent nodal loads. It can be

readily observed that joint loads on four nodes are required to specify the equivalent loading of one truck tire.

4.3. CALIBRATION OF THE BRIDGE MODELS

As previously stated, the finite element models were calibrated with the experimental data obtained from static and dynamic field testing of the Northbound and Southbound US 23 bridges. The finite element models of the two bridges consist of several material and geometric parameters which could conceivably be varied during the calibration process. A careful selection of the parameters to be optimized is necessary. For example, altering the elastic modulus to calibrate a model with static test data will affect the dynamic calibration. With this understanding, the model components changed during the calibration process were: 1) the modulus of elasticity, E , of the frame, shell, and solid elements; 2) the translational spring stiffnesses substituted for the abutments; and 3) the mass of the individual structural elements. Using more elements would be an effective means to achieve better accuracy in the analytical frequencies, especially in the higher modes, but the maximum number of joints and elements allowed by SAP90[®] were nearly exhausted in the initial models.

4.3.1. DYNAMIC CALIBRATION

Once the initial bridge models were created, each was analyzed by a standard eigenvalue solution process in SAP90[®] in order to first calibrate the models for dynamic analysis. The analytical mode shapes and frequencies were examined for correlation to the experimental data. Realistically, a perfect match between the experimental and analytical results is not possible. Differences between the way the bridges were actually constructed and what was specified in the design drawings can lead to the variance between the experimental and analytical results. Since the finite element analysis would be conducted based upon the design drawings and would inherently involve a set of simplifications and assumptions, the "true" structure cannot be perfectly modeled. Therefore, for the purposes of calibrating the US 23 bridge models, the first three predominant vibrational modes identified from field testing were selected as the bench marks for correlation. Based upon preliminary finite element analyses, these three modes could be expected to have the greatest participation in the response of the bridges when subjected to traffic loading.

The bridge models were calibrated for dynamic analysis through a trial and adjustment process in which the first two predominant modes were matched with experimental data by altering the spring stiffnesses of the end abutments. The third predominant mode was then matched by varying the value of the elastic modulus for

each structural component by the same amount percentage-wise. Changes in the original elastic moduli are acceptable since the actual material properties in a bridge do not exactly correspond with the design specifications. This process required iteration since changes in E would subsequently alter the analytical frequencies associated with the first two predominant modes. Figure 4.3.1a demonstrates the iterative nature of calibrating the bridge models for dynamic analysis.

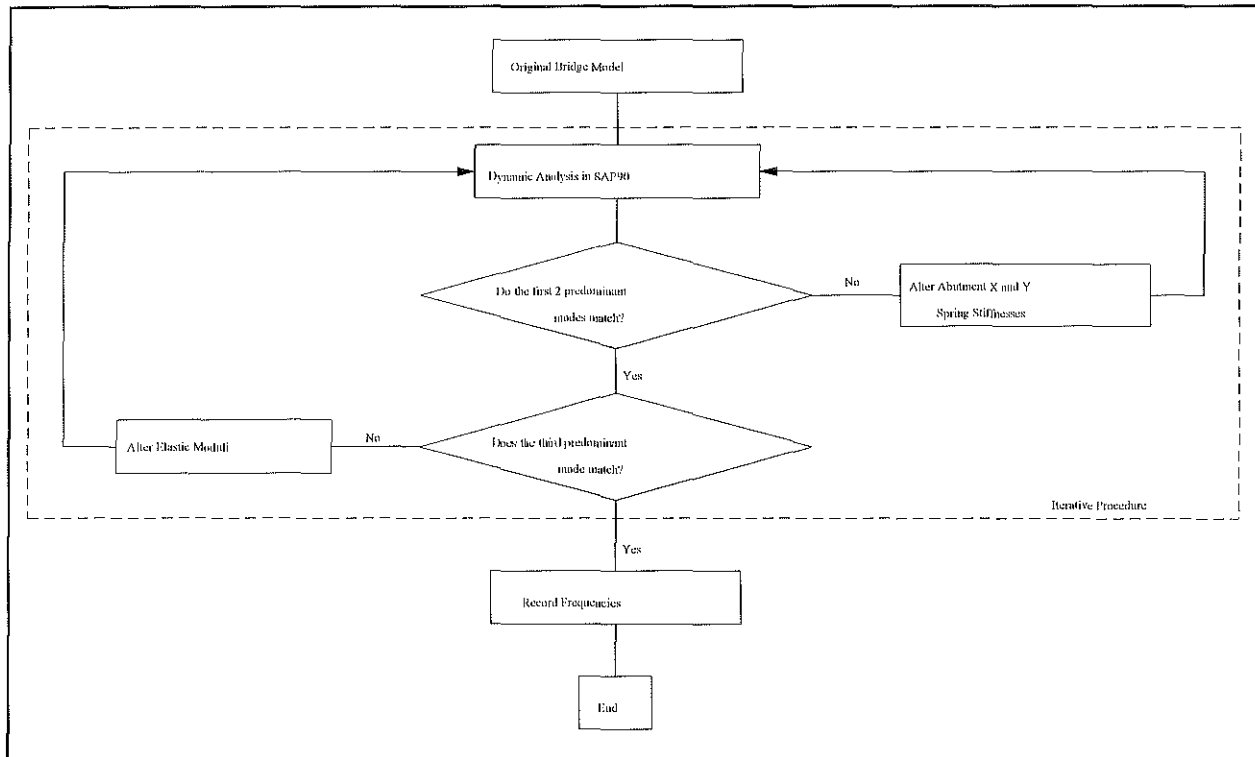


Figure 4.3.1a. Flow Chart of Iterative Procedure Used to Calibrate the US 23 Bridge Models With the Dynamic Test Data.

When analytical results were not matching experimental data as well as expected, a closer evaluation of the bridge model was required. It was noted that the use of solid elements in the barrier wall and girder haunches provided an overlap of materials since the bridge deck was modeled as 8 in (203.2 mm) thick. In the regions where the barrier walls and girder haunches connected to the deck, a duplication of the mass for this area was incorporated into the models. Therefore, calculations were made to reduce the solid element mass in these areas using the following formula:

$$\text{adjusted } W = \frac{A_{\text{actual}}}{A_{\text{total}}} W \quad (4.3)$$

where A_{actual} is the total area in this region (A_{total}) minus the overlapping area. With five girder haunches and two barrier walls, the reduction in the solid element mass for these components amounted to 55.87 percent of the original value specified. Figure 4.3.1b illustrates the regions where the overlapping area was encountered. Once the correction in mass specification was made for the girder haunches and barrier walls, higher analytical frequencies were obtained since the overall structure mass was reduced while the structure stiffness remained the same. The process of calibrating the models for dynamic analysis was then more efficient since the revised model better approximated the true structure.

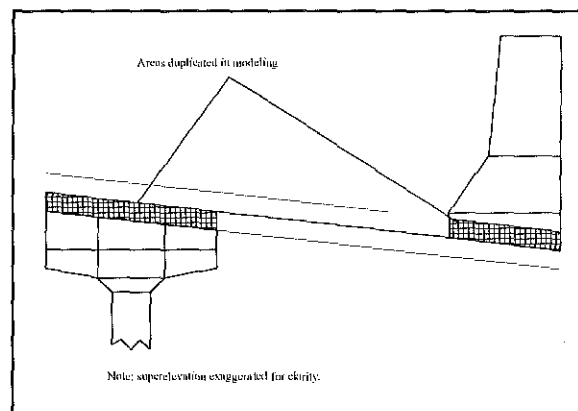


Figure 4.3.1b. Overlapping Regions Due to Solid Element Modeling of the Girder Haunches and Barrier Walls.

Figures 4.3.1c and 4.3.1d depict the first vertical and first torsional mode shapes obtained from the finite element analysis for free vibration of the Southbound and Northbound bridges. Most of the elements were eliminated for clarity. Tables 4.3.1a and 4.3.1b list the frequencies and mode shapes obtained from the eigenvalue solution of the Southbound and Northbound bridge models, respectively. As a means of comparison, the frequencies obtained from the experimental field test of both bridges are also reported in the table.

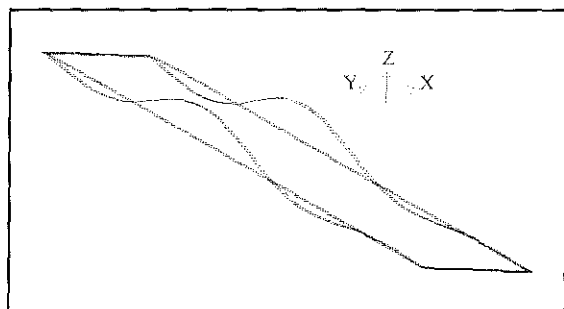


Figure 4.3.1c. Vertical Mode Shape of the Southbound Bridge (4.64 Hz) and Northbound Bridge (4.72 Hz).

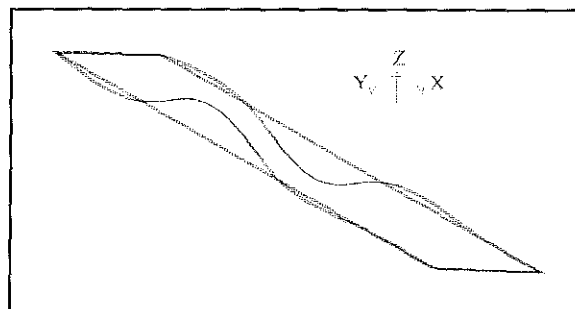


Figure 4.3.1d. Torsional Mode Shape of the Southbound Bridge (5.95 Hz) and Northbound Bridge (5.87 Hz).

Table 4.3.1a: Comparison of Experimental and Analytical Frequencies Obtained for the Southbound Bridge (Bridge With Intermediate Diaphragms).

Experimental Frequency (Hz)	Analytical Frequency (Hz)	Mode Shapes
2.10	2.09	1 st Transverse (half-sine)
2.77	2.78	1 st Longitudinal
4.61	4.64	1 st Vertical (half-sine all spans)
6.15	5.95	1 st Torsional (Span 3)
7.65	6.48	2 nd Torsional (Span 4) plus 2 nd Transverse (full-sine)
8.62	8.31	2 nd Vertical (full-sine Span 3)
9.19	8.88	3 rd Vertical (full-sine Span 4)
9.55	9.49	3 rd Torsional (Span 3)
10.49	10.30	4 th Torsional (Span 4) plus 2 nd Transverse (full-sine)
11.26	10.52	5 th Torsional (Span 2) plus 2 nd Transverse (full-sine)
13.33	10.89	6 th Torsional (Span 2)
14.13	13.06	4 th Vertical (full-sine Span 2)
19.17	15.92	3 rd Transverse
23.25	18.82	5 th Vertical (full-sine all spans)
27.05	24.92	4 th Transverse

Table 4.3.1b: Comparison of Experimental and Analytical Frequencies Obtained for the Northbound Bridge (Bridge Without Intermediate Diaphragms).

Experimental Frequency (Hz)	Analytical Frequency (Hz)	Mode Shapes
2.04	2.02	1 st Transverse (half-sine)
2.91	2.90	1 st Longitudinal
4.71	4.72	1 st Vertical (half-sine all spans)
5.95	5.87	1 st Torsional (Span 3)
6.95	6.42	2 nd Torsional (Span 4) plus 2 nd Transverse (full-sine)
8.02	7.56	2 nd Vertical (full-sine Span 3)
8.65	8.44	3 rd Vertical (full-sine Span 4)
9.35	9.02	3 rd Torsional (Span 3)
10.19	9.94	4 th Torsional (Span 4) plus 2 nd Transverse (full-sine)
10.72	10.41	5 th Torsional (Span 2) plus 2 nd Transverse (full-sine)
11.22	10.74	6 th Torsional (Span 2)
12.26	12.29	4 th Vertical (full-sine Span 2)
15.23	14.87	3 rd Transverse
21.44	17.26	5 th Vertical (full-sine all spans)
24.95	21.42	4 th Transverse

4.3.2. STATIC CALIBRATION

Static calibration involved careful optimization of the element elastic moduli and masses so that the dynamic calibration would not be discarded. Furthermore, steps were taken so that calibration factors were incorporated into the load block of the static analysis equations so that the vibrational characteristics of the bridge models would not be affected. For example, load factors were applied to the trucks in order to

correlate the experimental and finite element analysis results. As a measure of calibrating the models, an error analysis was completed on the displacement and stress results from each static analysis of the individual bridge models.

4.3.2.1. Error Analysis Function

After each static analysis of a bridge model, the displacement and stress values at a particular point were evaluated for error based upon the following formula:

$$E (\%) = 100 \% \left(\frac{\Phi_a - \Phi_e}{w_i \Phi_e} \right) \quad (4.4)$$

where Φ_a is a deflection or stress value obtained from the finite element analysis and Φ_e is a deflection or stress value obtained from field testing. The total error was balanced (over-predicting *versus* under-predicting) by applying a weighing factor associated with the magnitude of the field test value of the parameter under consideration and taking an average of the result:

$$E_r = \frac{\sum E_i w_i \Phi_i}{\sum w_i \Phi_i} \quad (4.5)$$

This method seemed to lead to quick convergence on balancing the error.

4.3.2.2. Static Calibration Load Factors

Once the error was minimized and balanced (e.g., under-predicting stresses *versus* over-predicting stresses), load calibration factors were obtained for three parameters: vertical deflection, out-of-plane displacements, and girder stresses. These load factors were subsequently associated with the dimensionless calibration factors necessary to correlate the static analysis results with the field test data. Table 4.3.2a lists the static calibration factors associated with the Southbound and Northbound bridges. These factors were incorporated into the load vector in subsequent finite element analyses.

In most cases, deflections (vertical and out-of-plane) were easier to match than strains. Kathol *et al.* (1995) recorded similar difficulties when correlating experimental and analytical results. In Kathol *et al.* (1995), deflections were noted to represent the global response of a structure and generally demonstrated better agreement between analytical results and field test data than did the stress results.

It was noted that stresses tended to reflect a more local response of a particular structure. Comparisons between the analytical and field test results of the displacements and stresses at representative points in the calibrated Southbound and Northbound bridge models are given in Tables 4.3.2b and 4.3.2c, respectively.

Table 4.3.2a: Static Calibration Factors for the US 23 Bridge Models.

Parameter	Southbound Bridge (Bridge With Intermediate Diaphragms)	Northbound Bridge (Bridge Without Intermediate Diaphragms)
Vertical Deflection	1.120	1.092
Out-of-Plane Displacement	1.210	1.000
Girder Stresses	0.500	0.600

Table 4.3.2b: Comparison of the Experimental and Analytical Results for Deflections and Stresses in the Southbound Bridge (Bridge With Intermediate Diaphragms).

Parameter ^{a,b}	Values From Field Testing	Values From FE Analysis	Position of Test Trucks ^c
Vertical Deflection at S7D	0.24 in (5.99 mm)	0.24 in (6.02 mm)	Bumper-to-Bumper in Lane 1 With Truck 1 at Station 8
Out-of-Plane Displacement at S7D	0.02 in (0.46 mm)	0.01 in (0.25 mm)	
Stress at S5AT	0.08 ksi (0.54 MPa)	0.06 ksi (0.44 MPa)	
Vertical Deflection at S7C	0.14 in (3.48 mm)	0.14 in (3.63 mm)	Bumper-to-Bumper in Lane 2 With Truck 1 at Station 8
Out-of-Plane Displacement at S7C	0.03 in (0.81 mm)	0.01 in (0.33 mm)	
Stress at S5BT	0.05 ksi (0.33 MPa)	0.05 ksi (0.31 MPa)	
Vertical Deflection at S7B	0.18 in (4.52 mm)	0.17 in (4.37 mm)	Side-by-Side in Lanes 1 and 2 With Trucks at Station 8
Out-of-Plane Displacement at S7B	0.02 in (0.61 mm)	0.02 in (0.50 mm)	
Stress at S5BB	0.14 ksi (0.97 MPa)	0.10 ksi (0.70 MPa)	
Vertical Deflection at S7A	0.11 in (2.72 mm)	0.11 in (2.86 mm)	Side-by-Side in Lanes 1 and 2 With Trucks at Station 8
Out-of-Plane Displacement at S7B	0.01 in (0.36 mm)	0.02 in (0.42 mm)	
Stress at S5AB	0.12 ksi (0.85 MPa)	0.07 ksi (0.47 MPa)	

^a refer to Figures 3.3.1h and 3.3.1m for deflection and stress locations, respectively.

^b stresses reported are along the longitudinal axis of the girder.

^c refer to Figure 3.3.1a for the definition of static test "lanes" and "stations."

Table 4.3.2c: Comparison of the Experimental and Analytical Results for Deflections and Stresses in the Northbound Bridge (Bridge Without Intermediate Diaphragms).

Parameter ^{a,b}	Values From Field Testing	Values From FE Analysis	Position of Test Trucks ^c
Vertical Deflection at N4D	0.25 in (6.27 mm)	0.25 in (6.28 mm)	Bumper-to-Bumper in Lane 1 With Truck 1 at Station 8
Out-of-Plane Displacement at N4D	0.07 in (1.80 mm)	0.07 in (1.73 mm)	
Stress at N3AT	0.07 ksi (0.47 MPa)	0.08 ksi (0.53 MPa)	
Vertical Deflection at N4C	0.16 in (4.01 mm)	0.18 in (4.46 mm)	Bumper-to-Bumper in Lane 2 With Truck 1 at Station 8
Out-of-Plane Displacement at N4C	0.08 in (2.01 mm)	0.09 in (2.16 mm)	
Stress at N3BT	0.06 ksi (0.42 MPa)	0.07 ksi (0.50 MPa)	
Vertical Deflection at N4B	0.20 in (5.11 mm)	0.20 in (5.08 mm)	Side-by-Side in Lanes 1 and 2 With Trucks at Station 8
Out-of-Plane Displacement at N4B	0.05 in (1.25 mm)	0.05 in (1.31 mm)	
Stress at N3BB	0.25 ksi (1.74 MPa)	0.14 ksi (0.99 MPa)	
Vertical Deflection at N4A	0.13 in (3.18 mm)	0.13 in (3.17 mm)	Side-by-Side in Lanes 1 and 2 With Trucks at Station 8
Out-of-Plane Displacement at N4B	0.03 in (0.74 mm)	0.03 in (0.78 mm)	
Stress at N3AB	0.10 ksi (0.68 MPa)	0.08 ksi (0.55 MPa)	

^a refer to Figures 3.3.1i and 3.3.1n for deflection and stress locations, respectively.

^b stresses reported are along the longitudinal axis of the girder.

^c refer to Figure 3.3.1a for the definition of static test "lanes" and "stations."

CHAPTER 5

ANALYSIS OF DIAPHRAGM EFFECTIVENESS

5.1. TRUCK LOADING

Having conducted the experimental testing and calibrated the finite element models based on the field data, further finite element analyses were necessary to determine the effectiveness of intermediate diaphragms on prestressed concrete I-girder bridges. The analyses, however, could not proceed without a proper identification of the truck loads to be used. The trucks selected would have to account for the type of traffic the bridges would normally experience.

5.1.1. AASHTO TRUCKS

In the design of simple and continuous span bridges, AASHTO requires that consideration be given to truck and lane loads. These lane loads were derived from the truck train loadings of the 1935 Specifications of AASHTO (AASHTO 1996). The equivalent lane loadings are pictured in Figure 5.1.1a. Axle weights and footprints of the H and HS group of trucks AASHTO considers in design are illustrated in Figure 5.1.1b (the HS group is a tractor-trailer configuration). The gross weights of the H and

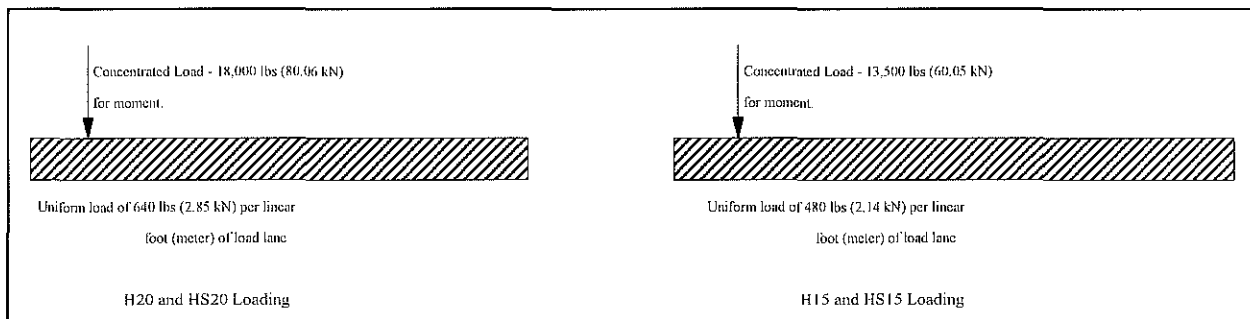


Figure 5.1.1a. Equivalent Lane Loadings Substituted for the Truck Trains of the 1935 AASHTO Specifications (AASHTO 1996).

HS truck groups are 40,000 lbs (178 kN) and 72,000 lbs (320 kN), respectively. In the current specification, all loads (truck or lane) are required to be positioned such that

the maximum stress within a span is produced. Section 3.5 provides guidelines for the application of an overload; however, the specification only requires the overload to be in a single lane with no concurrent loading in any other lane (AASHTO 1996).

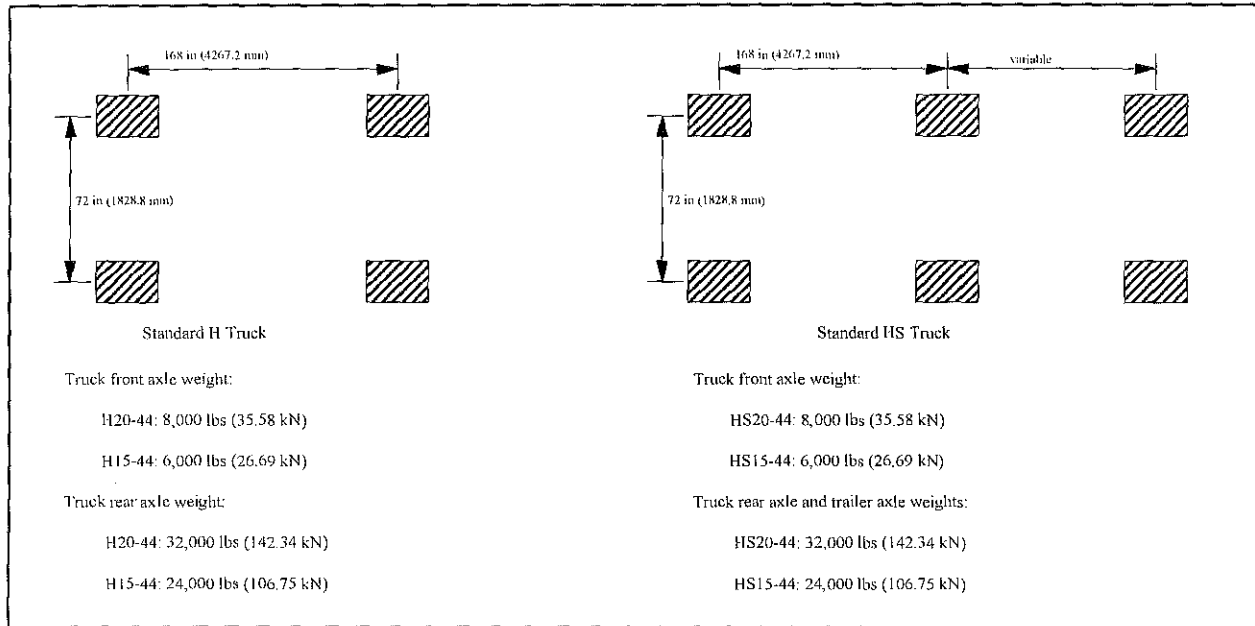


Figure 5.1.1b. Footprint of the AASHTO H and HS Trucks (AASHTO 1996).

Consequently, the design loads used per AASHTO's recommendation do not compare to the coal truck loading that the US 23 bridges can be expected to experience. For this reason, the finite element analyses discussed in this chapter used the coal truck loads described below as means to assess the behavior of the bridge in response to the normal coal truck loading. Testing the validity of the design using AASHTO trucks in the analyses was not a goal of this research. Rather, the main objective was to ascertain the response of the structure under normal traffic conditions, i.e., coal truck loading.

5.1.2. COAL TRUCKS

Actual coal trucks were used to conduct the static testing, therefore the dimensions for the standard tandem (two rear axles) and tridem (three rear axles) dump trucks were on file (during the static testing, the tridem retracted the third rear axle, thereby making the vehicle a tandem dump truck). The dimensions of the respective vehicles and the corresponding axle weights are illustrated in Figure 5.1.2a.

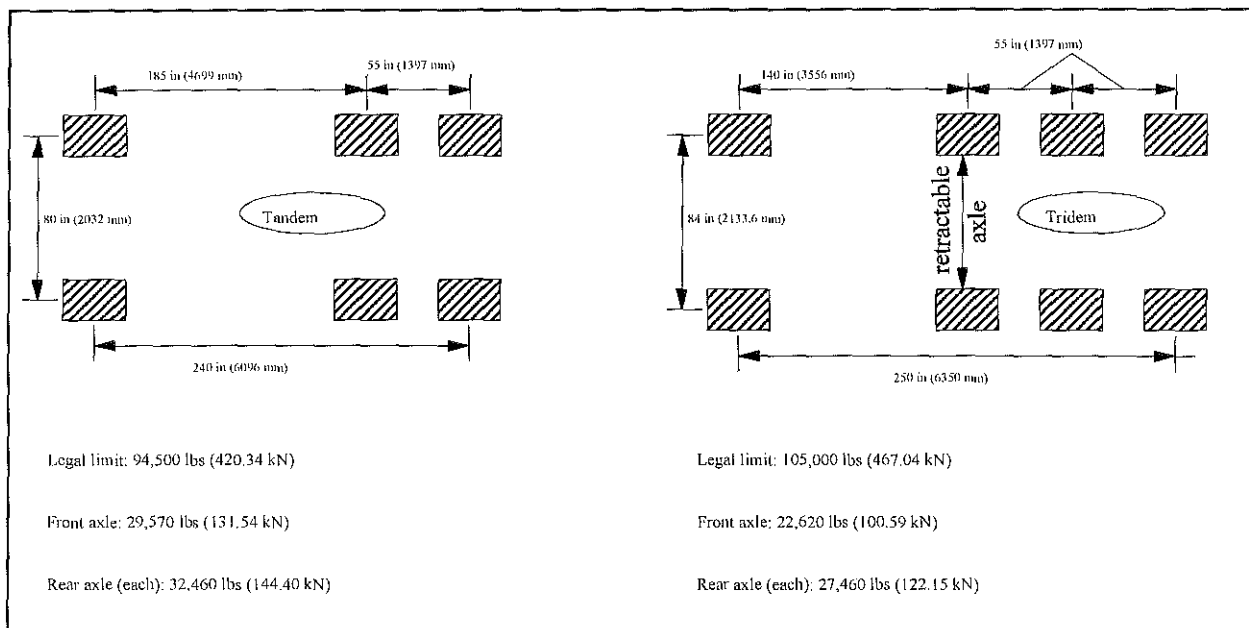


Figure 5.1.2a. Footprint of Tandem and Tridem Coal Haul Trucks.

As has been previously mentioned, coal trucks in Kentucky are allowed to exceed the regular 80,000 lbs (355.84 kN) weight limit if permits are obtained. Under the Kentucky extended-weight coal haul road system, three-axle dump trucks (tandems) may haul 94,500 lbs (420.34 kN) and four-axle dump trucks (tridems) may haul 105,000 lbs (467.04 kN) (Associated Press 1995, Breed 1995b). However, citations issued to overweight coal trucks in Johnson County between January 1993 and May 1996 indicate an average overweight of 53,588 lbs (238.36 kN) (Breed and Bridis 1996). Naturally, this average overweight would be skewed by the five- and six-axle tractor-trailers which could conceivably haul a greater load. The average overweight values for the tandem and tridem vehicles were obtained by determining a dimensionless multiplication factor which would account for the individual truck weight *versus* the total weight of the three truck configurations (tandem, tridem, and tractor-trailer). In this manner, the average overweight assigned to each truck was proportional to the legal weight limit corresponding to that truck. Since the total combined legal gross weight of the three truck configurations (tandem, tridem, and tractor-trailer) was 325,500 lbs (1,447.82 kN), the dimensionless multiplication factor was obtained as follows:

$$F_{\text{over}} = 1 + \frac{3 (53,588)}{325,500} = 1.494 \quad (5.1)$$

Thus, the average overweight associated with a tandem truck was 46,650 lbs (207.49

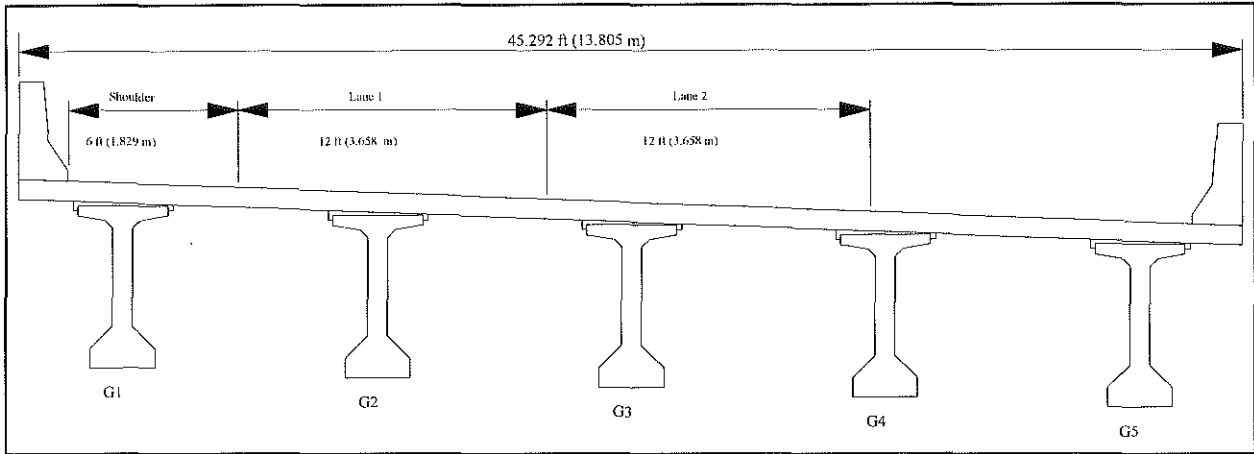


Figure 5.1.2b. Cross Section of Northbound US 23 Bridge (Bridge Without Intermediate Diaphragms) Illustrating Location of Traffic Lanes and Girder Number.

kN) and the average overweight associated with a tridem truck was 51,830 lbs (230.54 kN). These overweight loads led to truck gross weights of 141,150 lbs (627.82 kN) and 156,830 lbs (697.80 kN), respectively. The axle weights given in Figure 5.1.2a were multiplied by the 1.494 factor to obtain the axle weights for the overweight trucks.

Once the axle weights and dimensions for the tandem and tridem vehicles were determined, equivalent nodal loads were calculated after the process given by Chen (1995a). This process was outlined previously in Chapter 4. Since the bridges had two traffic lanes (see Figures 5.1.2b and 5.1.2c) and four spans, 16 sets of equivalent nodal loads were required to define each truck at the midspan of each span in both lanes.

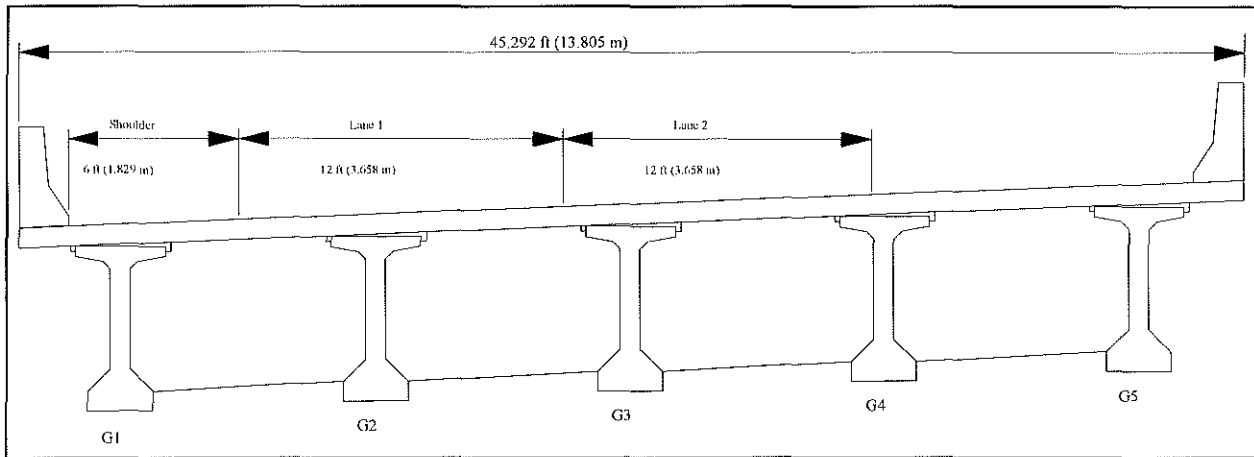


Figure 5.1.2c. Cross Section of Southbound US 23 Bridge (Bridge With Intermediate Diaphragms) Illustrating Location of Traffic Lanes and Girder Number.

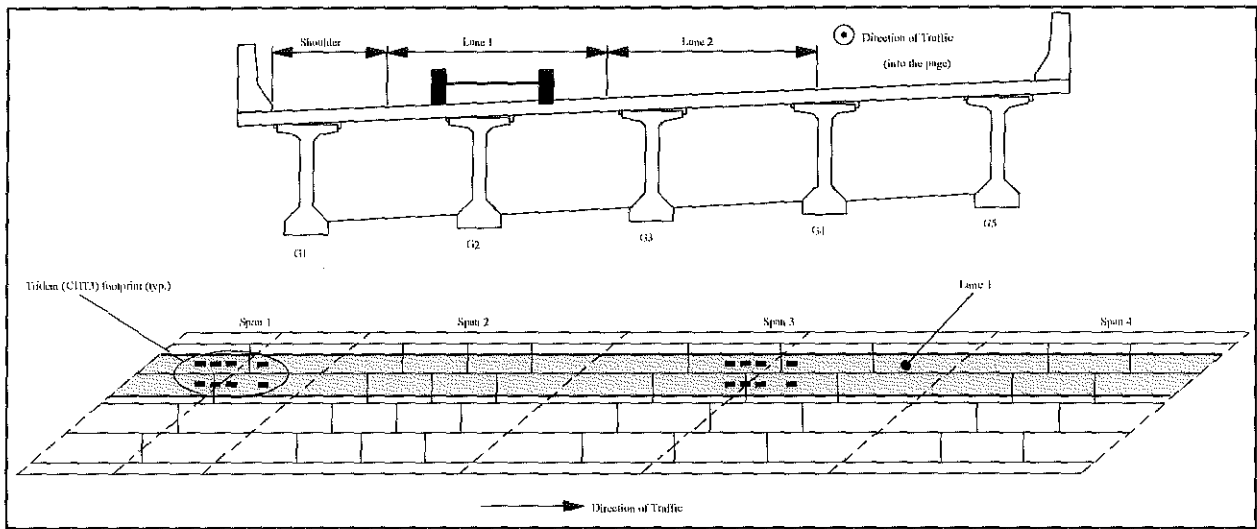


Figure 5.1.2d. Orientation of Tridem Coal Trucks in Load Case 1 (See Table 5.1a).

As Figure 5.1.2c indicates the traffic lanes in the Southbound bridge were positioned such that they were identical to those in the Northbound. The midspan was chosen for the placement of the coal trucks in order to induce the maximum deflection and stress response in the bridge finite element models. By using the load combination feature of SAP90[®], though, these 16 sets could be positioned on the bridges such that a total of 48 load conditions could be analyzed. The 48 permutations of truck position based on truck type, lane number, and span number are listed in Table 5.1a for single lane combinations and Table 5.1b for the two lane combinations. Figure 5.1.2d illustrates the orientation of the coal trucks for Load Case 1. All other load cases follow the same pattern of vehicle direction and positioning within the center of the lane considered.

Based upon safe trailing distances and the author's personal observations, loaded coal trucks rarely follow each other at such a distance that would allow for more than one truck to occupy a single lane within a span of the US 23 bridges. Consequently, a combination where, for instance, two trucks were positioned for maximum effect in each lane of Span 3 (for a total of four trucks in Span 3) was not considered.

Table 5.1a: Load Combinations Applied to Finite Element Models in Single Lane.

Load Case	Trucks in Midspan of Spans 1 and 3^a	Load Case	Trucks in Midspan of Spans 2 and 4^a
Lane 1			
1	CHT3, CHT3	5	CHT3, CHT3
2	CHT3, CHT2	6	CHT3, CHT2
3	CHT2, CHT3	7	CHT2, CHT3
4	CHT2, CHT2	8	CHT2, CHT2
Lane 2			
9	CHT3, CHT3	13	CHT3, CHT3
10	CHT3, CHT2	14	CHT3, CHT2
11	CHT2, CHT3	15	CHT2, CHT3
12	CHT2, CHT2	16	CHT2, CHT2

^a CHT2=tandem coal truck, CHT3=tridem coal truck.

Table 5.1b: Load Combinations Applied to Finite Element Models in Both Lanes.

Load Case	Trucks in Midspan of Spans 1 and 3 ^a	Load Case	Trucks in Midspan of Spans 2 and 4 ^a
17	CHT3, CHT3, CHT3, CHT3	33	CHT3, CHT3, CHT3, CHT3
18	CHT3, CHT3, CHT3, CHT2	34	CHT3, CHT3, CHT3, CHT2
19	CHT3, CHT3, CHT2, CHT3	35	CHT3, CHT3, CHT2, CHT3
20	CHT3, CHT3, CHT2, CHT2	36	CHT3, CHT3, CHT2, CHT2
21	CHT3, CHT2, CHT3, CHT3	37	CHT3, CHT2, CHT3, CHT3
22	CHT3, CHT2, CHT3, CHT2	38	CHT3, CHT2, CHT3, CHT2
23	CHT3, CHT2, CHT2, CHT3	39	CHT3, CHT2, CHT2, CHT3
24	CHT3, CHT2, CHT2, CHT2	40	CHT3, CHT2, CHT2, CHT2
25	CHT2, CHT3, CHT3, CHT3	41	CHT2, CHT3, CHT3, CHT3
26	CHT2, CHT3, CHT3, CHT2	42	CHT2, CHT3, CHT3, CHT2
27	CHT2, CHT3, CHT2, CHT3	43	CHT2, CHT3, CHT2, CHT3
28	CHT2, CHT3, CHT2, CHT2	44	CHT2, CHT3, CHT2, CHT2
29	CHT2, CHT2, CHT3, CHT3	45	CHT2, CHT2, CHT3, CHT3
30	CHT2, CHT2, CHT3, CHT2	46	CHT2, CHT2, CHT3, CHT2
31	CHT2, CHT2, CHT2, CHT3	47	CHT2, CHT2, CHT2, CHT3
32	CHT2, CHT2, CHT2, CHT2	48	CHT2, CHT2, CHT2, CHT2

^a CHT2=tandem coal truck, CHT3=tridem coal truck.

5.2. PARAMETRIC STUDY

In order to assess the effectiveness of intermediate diaphragms in distributing load in prestressed concrete I-girder bridges, a parametric study was completed using the calibrated finite element models of Chapter 4. The variables used in the parametric study were truck type and truck position (based upon the 48 load combinations discussed above), span length, and the presence of intermediate diaphragms as well as their location. Naturally, the results from the Southbound bridge (bridge with intermediate diaphragms) would be compared to the results from the Northbound bridge (bridge without intermediate diaphragms). Vertical and out-of-plane displacements of the girders as well as bottom flange stresses at midspan were chosen as the parameters to examine in the study.

Span lengths and diaphragm locations other than what was found in the US 23 bridges were not considered in the parametric study. The reason for this is the fact that no experimental (i.e., field test) data would be available to calibrate finite element models incorporating these variances in span lengths and diaphragm locations. Table 5.2 summarizes the span lengths of the US 23 bridges in addition to reporting whether the diaphragm locations in the Southbound bridge meet or exceed the AASHTO and Kentucky code requirements for inclusion of intermediate diaphragms.

Table 5.2: Summary of Span Length and Diaphragm Location on the US 23 Bridges.

Northbound and Southbound Bridges		Southbound Bridge Only			
Span Number	Span Length in ft (m)	Number of Diaphragms	Diaphragm Location	AASHTO Code	Kentucky Code
1	58.875 (17.95)	4	midspan	OK	OK
2	82.50 (25.15)	12	quarter points	exceeds	exceeds
3	118.50 (36.12)	12	quarter points	exceeds	exceeds
4	80.625 (24.58)	8	third points	exceeds	OK

5.3. ANALYSIS RESULTS

5.3.1. MIDSPAN VERTICAL DEFLECTIONS

Typical variations of girder vertical deflections at midspan are pictured in Figures 5.3.1a and 5.3.1b for the Southbound and Northbound bridges subjected to

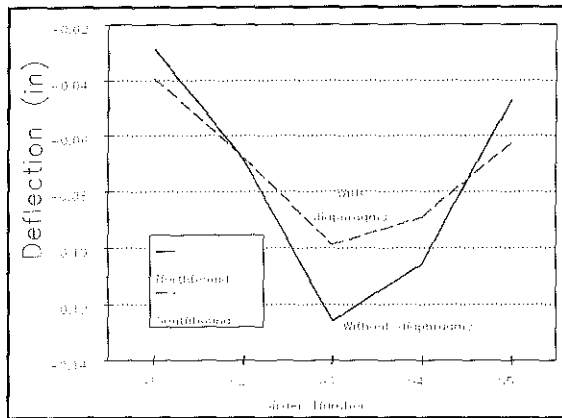


Figure 5.3.1a. Vertical Deflection at Midspan of Span 3 - Load Case 10. Positive Value Denotes Upward Deflection (Note 1 in = 25.4 mm).

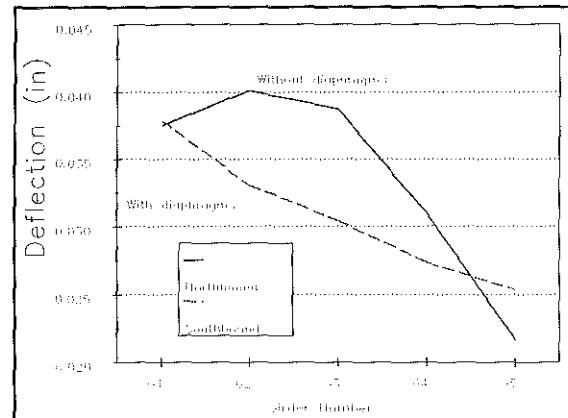


Figure 5.3.1b. Vertical Deflection at Midspan of Span 2 - Load Case 31. Positive Value Denotes Upward Deflection (Note 1 in = 25.4 mm).

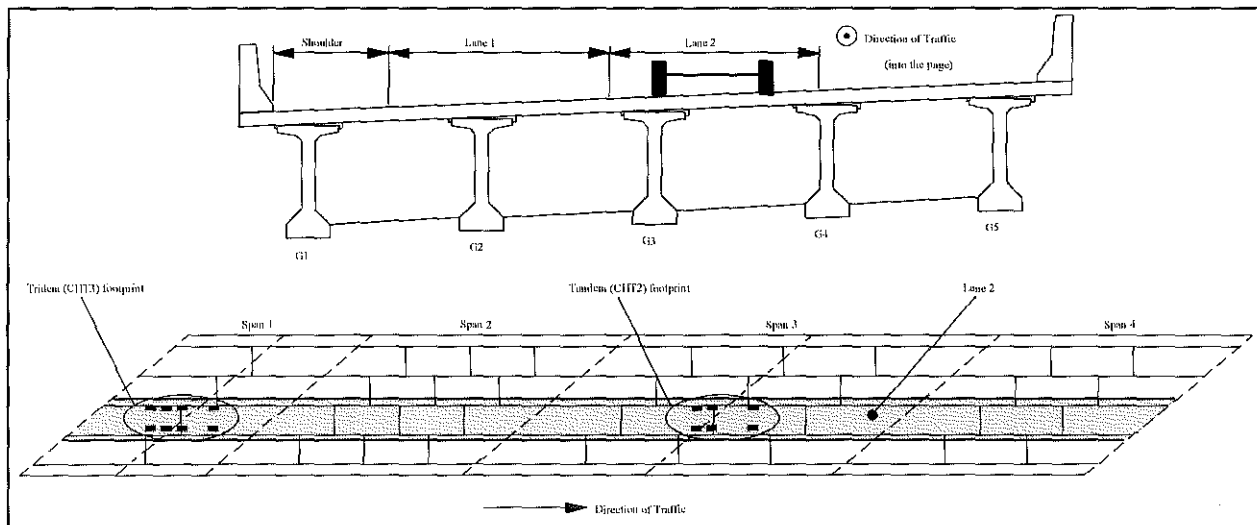


Figure 5.3.1c. Orientation of Coal Trucks in Load Case 10 (See Table 5.1a).

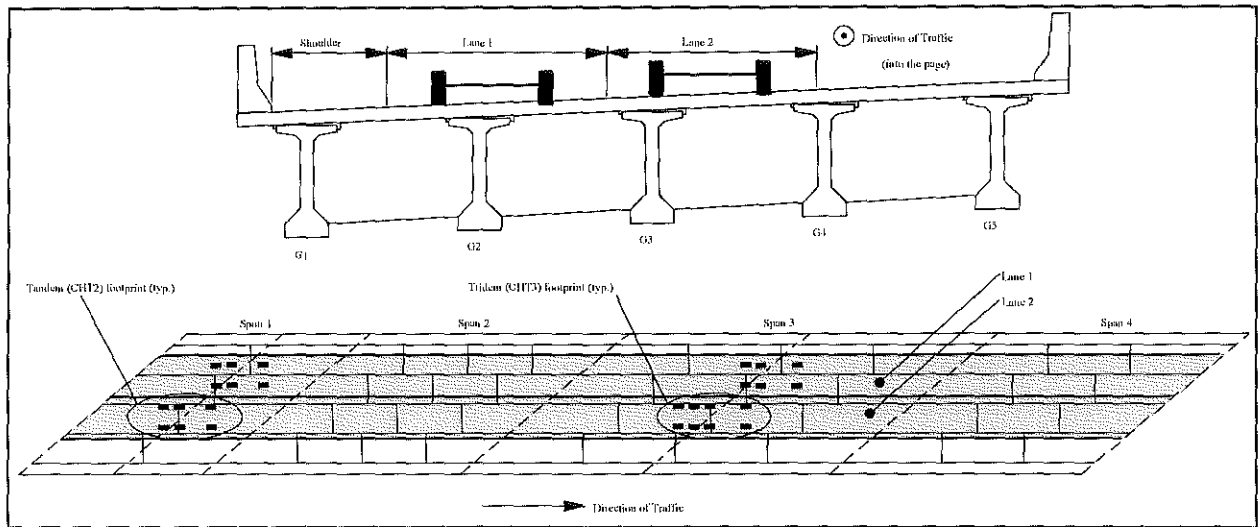


Figure 5.3.1d. Orientation of Coal Trucks in Load Case 31 (See Table 5.1b).

legal weight coal trucks. Figures 5.3.1c and 5.3.1d illustrate Load Cases 10 and 31, respectively. In general, girder deflections in the Northbound bridge (bridge without intermediate diaphragms) demonstrate a contribution from the deck in distributing the load. Vertical deflections of the girders tend to rise in proximity of the load. On the other hand, vertical deflections in the girders of the Southbound bridge (bridge with intermediate diaphragms) indicate the intermediate diaphragms do play a role in distributing the load. Vertical deflections in proximity of the load are reduced (a peak is still noted), while the vertical deflections of adjacent girders are increased. However, the difference observed between these vertical deflections in the Southbound and Northbound bridge are insufficient to require intermediate diaphragms. All deflections calculated in the static analyses were within the AASHTO limitation of $L/800$ given in Section 9.11.3.1 (AASHTO 1996) where L is the clear span length. This criterion leads to deflection limits of 1.19-in (30.10 mm) and 1.73 in (43.82 mm) for Spans 2 and 3, respectively.

The Northbound bridge does not seem to experience any detrimental effects caused by large vertical displacements in the absence of intermediate diaphragms when considering static analysis. The bridge, though, is new and some consideration should be given to evaluating the fatigue resistance of both bridges before a definitive statement can be made on the impact of cyclic, moving loads. It is very likely the bridges will experience the one million cycles of loading necessary to warrant a fatigue analysis. The other criterion would be a stress range of 20 ksi (137.90 MPa), but such a large range of stress is highly unlikely, as a later section in this chapter will demonstrate.

The maximum response observed for vertical deflections in each lane loading condition were as follows (see Tables 5.1 and 5.2 for the definition of "load cases"). With the trucks in Lane 1 only, Load Case 5 produced the largest vertical deflections of the girders. The largest vertical deflections in the girders with loading in only Lane 2 was produced by Load Case 15. With the trucks in both Lanes 1 and 2, Load Case 35 produced the largest vertical deflections in the girders (illustrated in Figure 5.3.1e). The maximum girder deflection experienced by any girder using legal weight coal trucks occurred in Span 3 and was 0.85 in (21.63 mm) in the Southbound bridge (bridge with intermediate diaphragms) compared to 0.87 in (22.19 mm) in the Northbound bridge (bridge without intermediate diaphragms). Despite the presence of intermediate diaphragms, the maximum deflection in the Southbound bridge was only 2.3 percent lower (within the accuracy of the experimentally correlated analytical results) than the maximum deflection in the Northbound bridge. This suggests that intermediate diaphragms may be ineffective at higher load levels as was considered in Load Case 35 using legal weight coal haul trucks. Figure 5.3.1f illustrates the orientation of the coal trucks in Load Case 35.

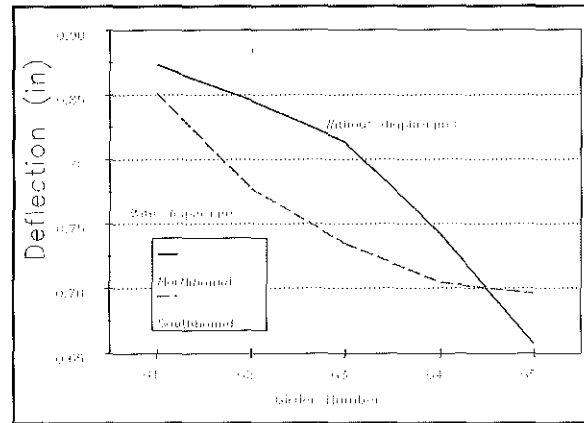


Figure 5.3.1e. Maximum Vertical Deflection at Midspan of Span 3 Load Case 35. Positive Value Denotes Upward Deflection (Note 1 in = 25.4 mm).

The same trends discussed above were noted in the analyses performed using

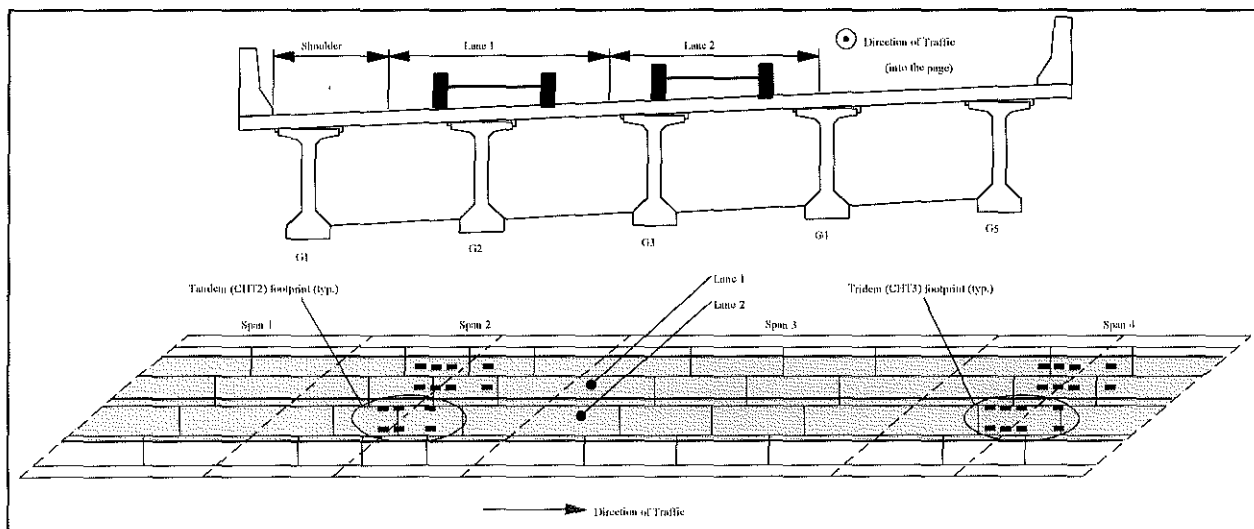


Figure 5.3.1f. Orientation of Coal Trucks in Load Case 35 (See Table 5.1b).

the overweight coal trucks (i.e., the truck gross weight exceeds the allowable permit load). This is a realistic response since the finite element models are assumed to react in the linearly elastic range and therefore conform to the principle of superposition. Maximum vertical deflections observed in any girder using overweight coal trucks occurred in Span 3 and were 1.27 in (32.30 mm) in the Southbound bridge (bridge with intermediate diaphragms) and 1.30 in (33.14 mm) in the Northbound bridge (bridge without intermediate diaphragms). These displacements are within the AASHTO deflection limitation of L/800 (where L is the clear span length), which for Span 3 is 1.73 in (43.82 mm). The maximum vertical deflections experienced by any girder in the finite element analyses are summarized in Table 5.3.1.

Based on these results, a significant advantage in structural response is not noted due to the presence of intermediate diaphragms. Recommendations for their inclusion or exclusion will be reserved until after an examination of the girder stresses is completed (see Section 5.3.3).

Table 5.3.1: Maximum Vertical Deflections of the US 23 Bridges.

Bridge	Load	Maximum Vertical Deflection in Span 3 in inches (mm)	AASHTO Deflection Limitation in inches (mm)
Southbound (Bridge With Intermediate Diaphragms)	legal	0.85 (21.63)	1.73 (43.82)
	overweight	1.27 (32.30)	
Northbound (Bridge Without Intermediate Diaphragms)	legal	0.87 (22.19)	
	overweight	1.30 (33.14)	

5.3.2. MIDSPAN OUT-OF-LANE DISPLACEMENTS

Typical variations of girder out-of-plane displacements at midspan are pictured in Figures 5.3.2a and 5.3.2b for the Southbound and Northbound bridges subjected to legal weight coal trucks (Load Cases 10 and 31 are illustrated in Figures 5.3.2c and 5.3.2d). In general, out-of-plane displacements in the Northbound bridge (bridge

without intermediate diaphragms) tend to be larger than comparable displacements in the Southbound bridge (bridge with intermediate diaphragms). The sharp rise in the Northbound bridge results in contrast to the Southbound bridge results indicate the intermediate diaphragms do play a role in restraining lateral movement of the girders. Out-of-plane deflections of the girders in proximity of the load are in the Southbound bridge (bridge with intermediate diaphragms). The sharp rise in the Northbound bridge results in contrast to the Southbound bridge results indicate the

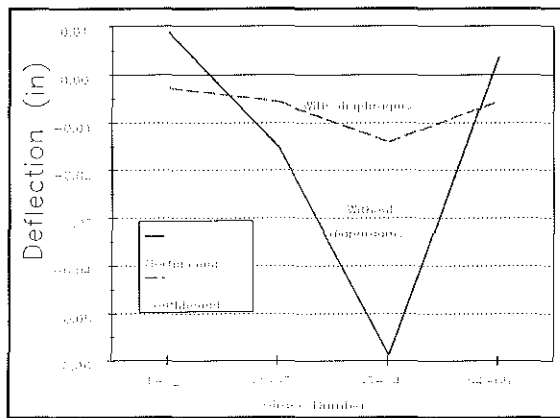


Figure 5.3.2a. Out-of-Plane Displacement at Midspan of Span 3 - Load Case 10. Negative Value Denotes Girder Separation (Note 1 in = 25.4 mm).

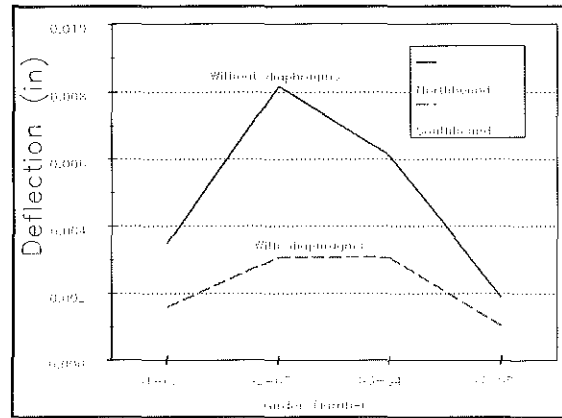


Figure 5.3.2b. Out-of-Plane Displacement at Midspan of Span 2 - Load Case 31. Negative Value Denotes Girder Separation (Note 1 in = 25.4 mm).

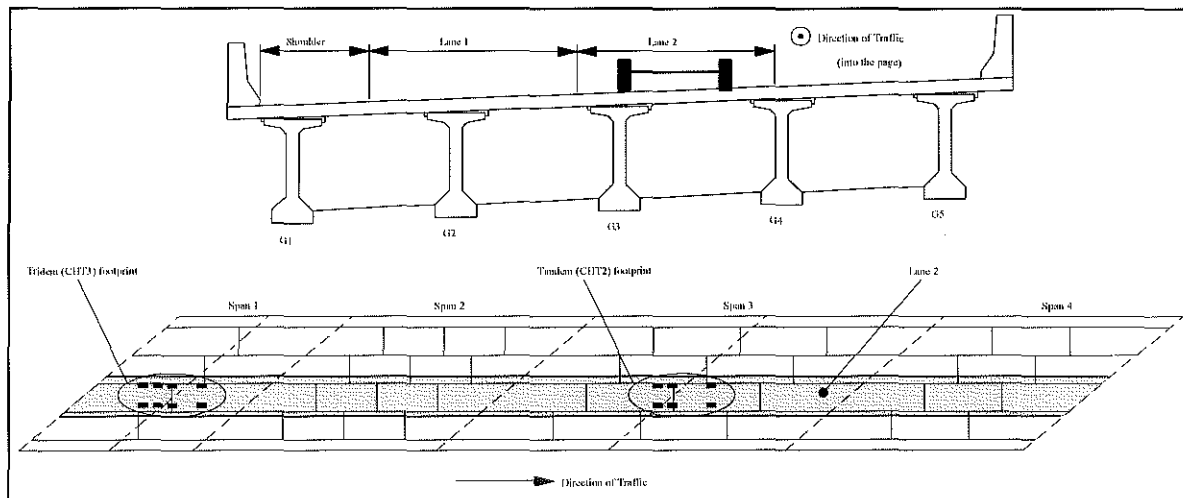


Figure 5.3.2c. Orientation of Coal Trucks in Load Case 10 (See Table 5.1a).

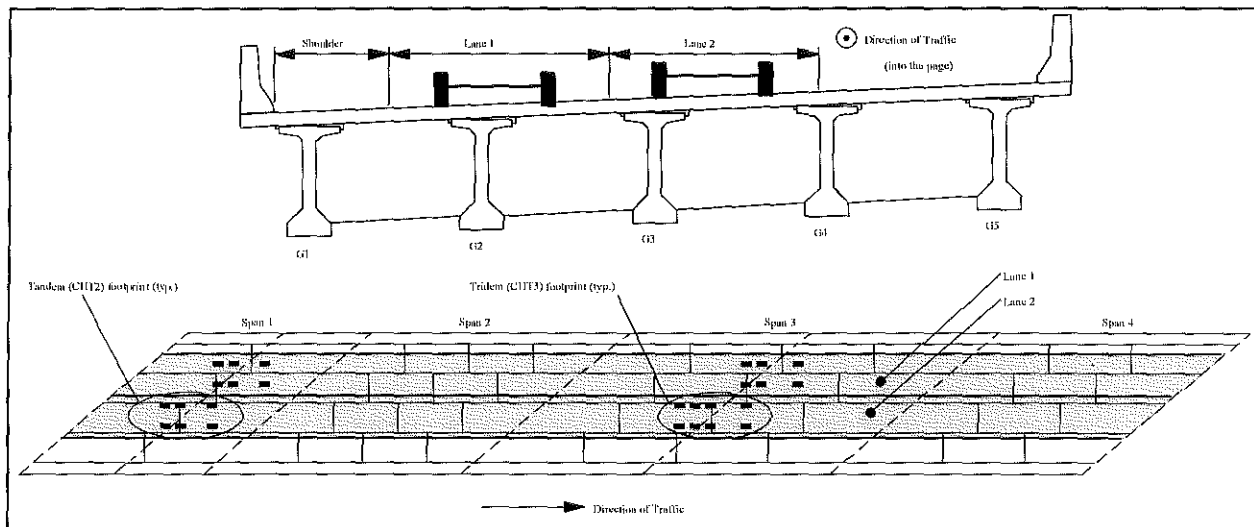


Figure 5.3.2d. Orientation of Coal Trucks in Load Case 31 (See Table 5.1b).

intermediate diaphragms do play a role in restraining lateral movement of the girders. Out-of-plane deflections of the girders in proximity of the load are reduced (a peak is still noted), while those of adjacent girders are increased. However, the difference observed between the out-of-plane movement of the girders in the Southbound and Northbound bridges are insufficient to require intermediate diaphragms.

The maximum response observed for girder out-of-plane displacements in each lane loading condition was as follows (see Tables 5.1 and 5.2 for the definition of "load case"). With the trucks in Lane 1 only, Load Case 5 produced the largest out-of-plane movement between the girders. The largest out-of-plane displacement in the girders with loading in only Lane 2 was produced by Load Case 15. With the trucks in both Lanes 1 and 2, Load Case 35 produced the largest out-of-plane displacement between the girders. The maximum out-of-plane girder deflection experienced by any girder using legal weight coal trucks was 0.03 in (0.71 mm) in the Southbound bridge (bridge with intermediate diaphragms) and 0.08 in (1.92 mm) in the Northbound bridge (bridge without intermediate diaphragms).

The same trends discussed above were noted in the analyses performed using the overweight coal trucks. This is a realistic response since the finite element models are assumed to react in the linearly elastic range and therefore conform to the principle of superposition. Maximum out-of-plane displacements observed in any girder using overweight coal trucks were 0.04 in (1.06 mm) in the Southbound bridge (bridge with intermediate diaphragms) and 0.11 in (2.87 mm) in the Northbound bridge (bridge without intermediate diaphragms). The corresponding maximum values obtained from the static testing were 0.04 in (1.02 mm) and 0.09 in (2.29 mm),

respectively. Since the vertical deflections experienced much larger differences in magnitude between the experimental field test data and the finite element analyses results, it can be deduced that the out-of-plane movements of girders are relatively insensitive to the magnitude of load beyond a certain value. This conclusion is more prevalent in the Northbound bridge where diaphragms are not present to restrain out-of-plane displacements. The maximum out-of-plane displacements experienced by the girders in the finite element analyses are summarized in Table 5.3.2.

Table 5.3.2: Maximum Out-of-Plane Displacements of the US 23 Bridges.

Bridge	Load	Maximum Out-of-Plane Displacements in Span 3 in inches (mm)
Southbound (Bridge With Intermediate Diaphragms)	legal	0.03 (0.71)
	overweight	0.04 (1.06)
Northbound (Bridge Without Intermediate Diaphragms)	legal	0.08 (1.92)
	overweight	0.11 (2.87)

Based on these results, a significant advantage in structural response is not noted due to the presence of intermediate diaphragms. Recommendations for their inclusion or exclusion will be reserved until after an examination of the girder stresses is completed (see Section 5.3.3).

5.3.3. MIDSPAN BOTTOM FLANGE STRESSES

An evaluation of the stresses experienced by the girders under various load and diaphragm conditions is perhaps the best judge of the effectiveness of diaphragms in load distribution in a bridge. Since stresses are directly related to moments, the flexural behavior of the bridges can also be ascertained. Typical variations of longitudinal stresses on the bottom flange of the girders at midspan are pictured in Figures 5.3.3a and 5.3.3b for

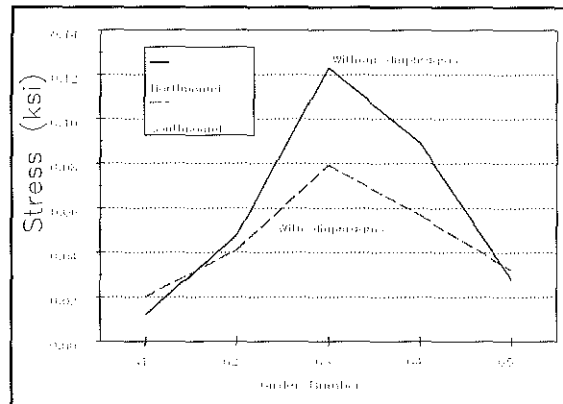


Figure 5.3.3a. Bottom Flange Girder Stress at Midspan of Span 3 - Load Case 10. Positive Value Denotes Tension (Note 1 ksi = 6.895 MPa).

the Southbound and Northbound bridges when subjected to legal weight coal trucks (Load Cases 10 and 31 are illustrated in Figures 5.3.3c and 5.3.3d). In general, the longitudinal stress on the bottom face of the girders in the Southbound bridge (bridge with intermediate diaphragms) tends to be lower and more evenly distributed than the longitudinal stress on the bottom face of the girders in the Northbound bridge (bridge without intermediate diaphragms). This supports the idea that intermediate diaphragms provide a mechanism whereby load is distributed to adjacent girders. The trend pictured in Figure 5.3.3b would even

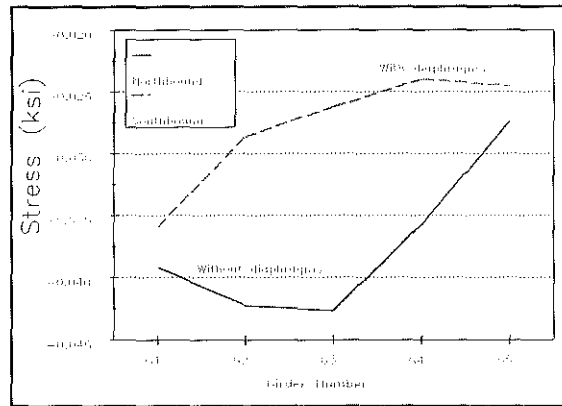


Figure 5.3.3b. Bottom Flange Girder Stress at Midspan of Span 2 - Load Case 31. Positive Value Denotes Tension (Note 1 ksi = 6.895 MPa).

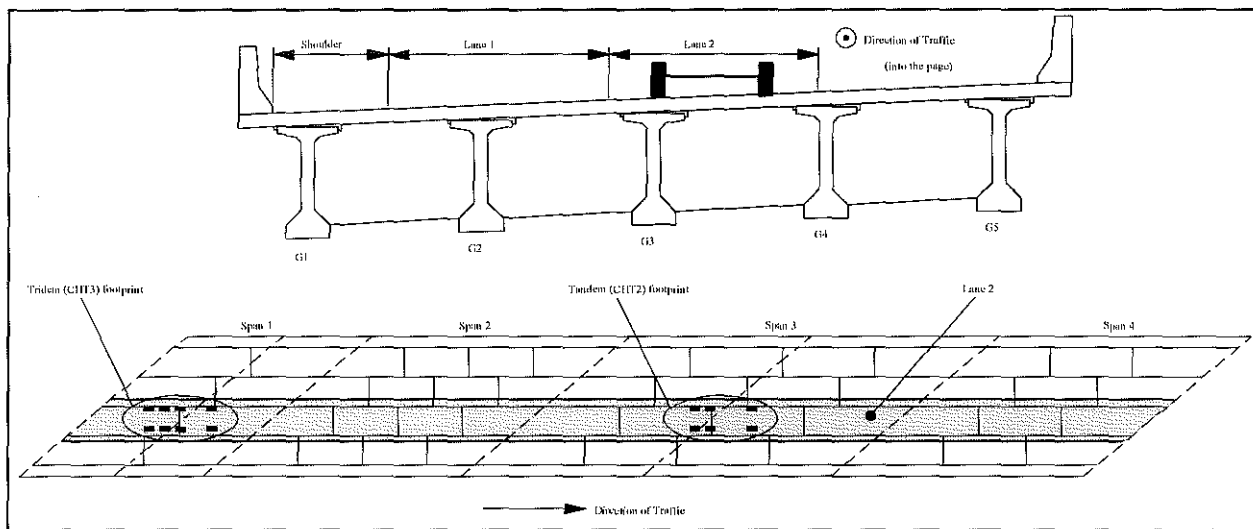


Figure 5.3.3c. Orientation of Coal Trucks in Load Case 10 (See Table 5.1a).

suggest that the diaphragms are more effective in distributing tensile stresses in the girder bottom flange to the exterior girders than they are in distributing compression stresses. Stress results near the piers were approximately one-fourth that observed at midspan, and, therefore, are not reported herein.

The maximum response observed for girder stresses in each lane loading condition occurred at the midspan of Span 3 and were as follows (see Tables 5.1a and 5.1b for the definition of "load case"). With the trucks in Lane 1 only, Load Case 1 and Load Case 5 produced the largest tensile and compressive stresses, respectively, in the

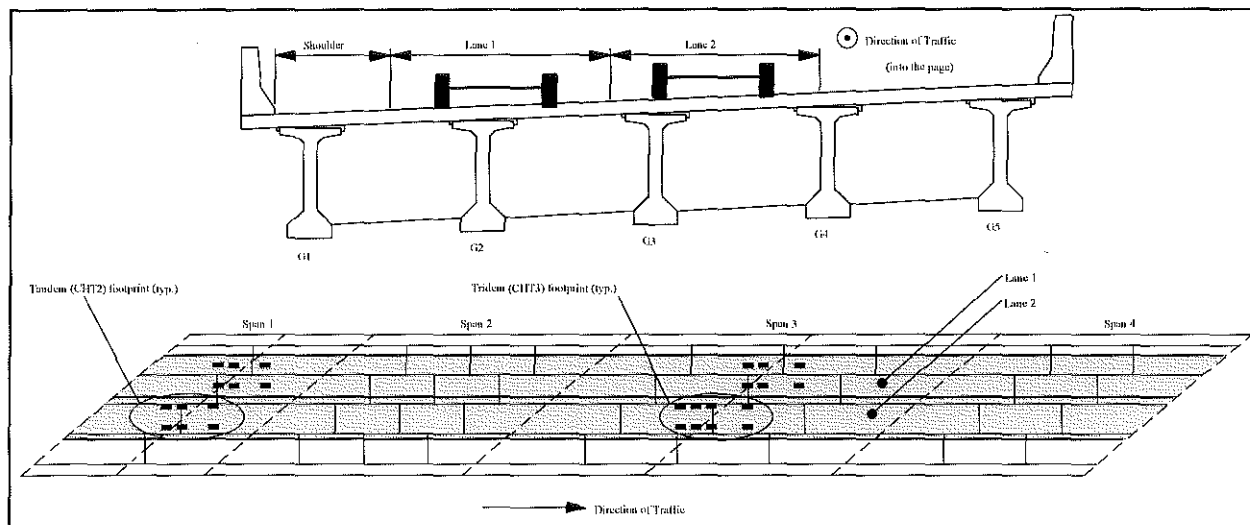


Figure 5.3.3d. Orientation of Coal Trucks in Load Case 31 (See Table 5.1b).

bottom flange of the girders. The largest compressive stresses in the girders with loading in only Lane 2 were produced by Load Case 15 while the largest tensile stresses induced in the girders by only Lane 2 loading were caused by Load Case 9. With the trucks in both Lanes 1 and 2, Load Case 17 produced the largest tensile stresses in the girders while Load Case 35 generated the largest compressive stresses.

The maximum tensile stress experienced by any girder using legal weight coal trucks in the finite element analyses was 0.21 ksi (1.44 MPa) in the Southbound bridge (bridge with intermediate diaphragms) and 0.33 ksi (2.30 MPa) in the Northbound bridge (bridge without intermediate diaphragms). These maximum tensile stresses satisfy the American Concrete Institute (ACI) and AASHTO design requirements for rupture stress, f_r , as given in ACI Section 18.4.2 (ACI 1995) and AASHTO Section 9.15.2.2 (AASHTO 1996) by:

$$f_r = 6 \sqrt{f'_c} \quad (5.2)$$

where f'_c is the concrete compressive stress. The rupture stresses for girders in Span 3 are 0.49 ksi (3.36 MPa) for G1 and G2 and 0.48 ksi (3.31 MPa) for G3 through G5.

The maximum compressive stress experienced by any girder using legal weight coal trucks in the finite element analyses was 0.41 ksi (2.83 MPa) in the Southbound bridge (bridge with intermediate diaphragms) and 0.46 ksi (3.15 MPa) in the Northbound bridge (bridge without intermediate diaphragms). These maximum stresses are within those allowed by ACI Section 18.4.2 (ACI 1995) for extreme fibers in compression ($0.45f'_c$): 2.97 ksi (20.48 MPa) for G1 and G2 and 2.88 ksi (19.86 MPa)

for G3 through G5 in Span 3. AASHTO Section 9.15.2.2 allows a compressive stress of $0.60f_c'$. The variation of the girder stresses when the maximum tensile and compressive stresses occurred are pictured in Figures 5.3.3e and 5.3.3f, respectively, for the Southbound bridge (bridge with intermediate diaphragms) and the Northbound bridge (bridge without intermediate diaphragms) subjected to legal (permit) coal tuck loads.

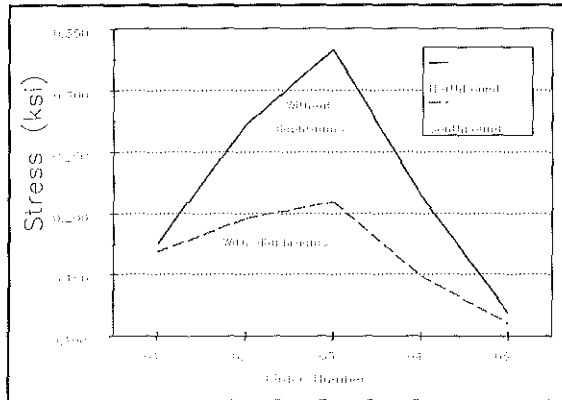


Figure 5.3.3e. Maximum Girder Tensile Stresses
(Note 1 ksi = 6.895 MPa).

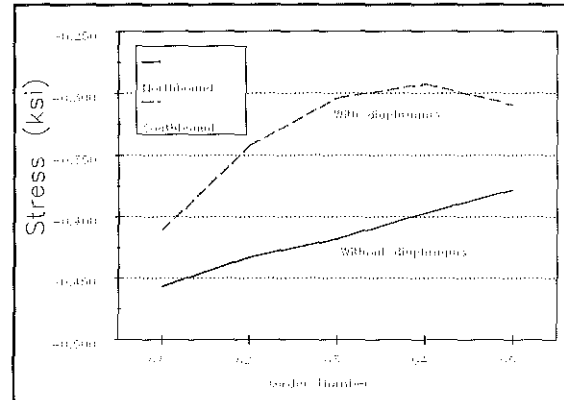


Figure 5.3.3f. Maximum Girder Compressive Stresses
(Note 1 ksi = 6.895 MPa).

The same trends discussed above were noted in the analyses performed using the overweight coal trucks. This is a realistic response since the finite element models are assumed to react in the linearly elastic range and therefore conform to the principle of superposition. Maximum compressive stress in any girder using overweight coal trucks in the finite element analyses were 0.61 ksi (4.23 MPa) in the Southbound bridge (bridge with intermediate diaphragms) and 0.68 ksi (4.71 MPa) in the Northbound bridge (bridge without intermediate diaphragms). The relatively small difference in the maximum compressive stresses experienced in the two bridges, whether subjected to legal weight coal trucks or overweight coal trucks, indicates that intermediate diaphragms do not provide a significant reduction in compressive stresses compared to the cost of their inclusion. In the case of the US 23 bridges, the most affected girder received only a 0.07 ksi (0.48 MPa) reduction (ten percent reduction) in maximum compressive stress under the worst loading considered (i.e., four overweight coal trucks positioned in the two traffic lanes in such a way as to cause the highest negative moment possible in Span 3).

The same cannot be said of the case where the maximum tensile stress is induced. The maximum tensile stress in any girder using overweight coal trucks in the finite element analyses was 0.31 ksi (2.16 MPa) in the Southbound bridge (bridge with intermediate diaphragms) and 0.50 ksi (3.43 MPa) in the Northbound bridge (bridge without intermediate diaphragms). This tensile stress in the Northbound bridge

slightly exceeds the ACI and AASHTO criteria for rupture stress (as given in Equation 5.2) of 0.48 ksi (3.31 MPa). Cracking in the girder concrete, therefore, might be expected. Generally, this minute difference would not be of concern to an engineer since the code limitations tend to be conservative. However, if cracking is assumed to occur, the use of a finite element model assuming linearly elastic behavior is invalid. Whether or not this cracking is a cause for concern would then best be analyzed by a finite element model which could incorporate nonlinear effects. Based upon a comparison of the tensile stresses, though, it is reasonable to conclude that a significant advantage is gained by the presence of the intermediate diaphragms. In the case of the US 23 bridges, the most affected girder on the Southbound bridge (bridge with intermediate diaphragms) received a 37 percent reduction in maximum tensile stress under the worst loading combination considered. The maximum longitudinal stresses experienced by the bottom flanges of the girders in the finite element analyses are summarized in Table 5.3.3.

Table 5.3.3: Maximum Longitudinal Stresses in the Bottom Flanges of the Girders in the US 23 Bridges.

Bridge	Load	Stress Type	Maximum Longitudinal Stresses in Span 3 in ksi (MPa)
Southbound (Bridge With Intermediate Diaphragms)	legal	tension	0.21 (1.44)
		compression	0.41 (2.83)
	overweight	tension	0.31 (2.16)
		compression	0.61 (4.23)
Northbound (Bridge Without Intermediate Diaphragms)	legal	tension	0.33 (2.30)
		compression	0.46 (3.15)
	overweight	tension	0.50 (3.43)
		compression	0.68 (4.71)

5.4. CONCLUSIONS

Based on the results presented above for vertical deflections, out-of-plane displacements, and girder stresses, a significant advantage in structural response is generally not noted due to the presence of intermediate diaphragms. Analyses

completed using legal weight coal trucks suggest the Northbound bridge (bridge without intermediate diaphragms) will experience displacements and stresses well within the design parameters outlined by AASHTO and ACI. The single exception to this statement was noted in the load case where overweight tridem coal trucks were located at the midspan of Spans 1 and 3 in both traffic lanes. A nonlinear finite element and/or fatigue analysis would better ascertain whether or not the Northbound bridge would experience any detrimental effects when subjected to this particular combination of overweight coal trucks. The reduction in displacements and stresses of the Southbound bridge (bridge with intermediate diaphragms) seemed to be advantageous percentage-wise, but the magnitudes of these two parameters were insufficient to suggest mandatory use of intermediate diaphragms.

On the whole, intermediate diaphragms do provide some load distribution among the adjacent girders, but the cost of construction and maintenance of this type of diaphragm outweighs the gain. The total elimination of intermediate diaphragms, though, is not feasible since they are required during the construction phase (prior to the placement of the deck) and if the deck is to be replaced ("re-decking"). Therefore, the use of steel diaphragms, such as the Z-type bracing mentioned previously, is recommended as substitutes for the concrete intermediate diaphragms. The steel diaphragms could be loosened after the deck and girders have achieved composite action (i.e., after the deck has cured).

CHAPTER 6

ANALYSIS OF DIAPHRAGM-GIRDER INTERFACE

6.1. DIAPHRAGM-GIRDER INTERFACE

Bridges of prestressed concrete I-girder construction that carry coal truck traffic in Southeastern Kentucky have experienced unusual concrete spalling at the interface of the concrete intermediate diaphragms and the bottom flange of the girders. An example of the spalled region at the diaphragm-girder interface is depicted in Figure 6.1. As is evident from the illustration, the concrete spalling has exposed the diaphragm anchor bars. It is interesting to note that bridges of similar design subjected to only normal traffic loading (i.e., vehicles operating below the 80,000 lbs [355.84 MPa] weight limit) do not seem to incur the same damage. In the case of coal truck loading (overloads), the concrete intermediate diaphragms appear to be contributing to the deterioration and damage witnessed in the prestressed concrete I-girders. Based on the results from the analyses on the calibrated model of the Southbound bridge (bridge with intermediate diaphragms), a smaller, more refined model of the diaphragm-girder interface was constructed and analyzed to determine the cause of the concrete spalling.

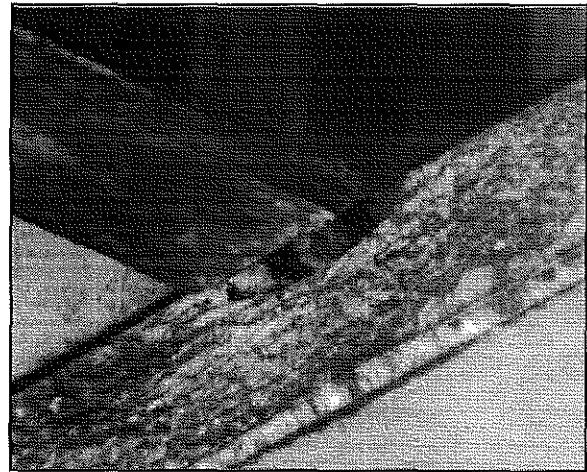


Figure 6.1. Concrete Spalling at Diaphragm-Girder Interface.

6.2. FINITE ELEMENT MODEL

A three-dimensional representation of a single diaphragm and two girders was modeled to analyze the interface region in order to determine the cause of concrete spalling. The model was analyzed using the packaged software SAP90[®] (Computers 1991). Table 6.1 summarizes the components of this new finite element model. The girders were modeled as one diaphragm thickness (10 in [254 mm]) on either side of the diaphragm for a total of 30 in (762 mm) as is pictured in Figure 6.2. Results from

the larger bridge model of Chapter 5 indicated the stress concentration in the interface region dissipated within this length. The girders were also modeled as full-depth for completeness, but the deck was not incorporated into this finite element analysis. Boundary conditions based on the results from Chapter 5 were used to replace the deck and remaining length of the girders.

Table 6.1: Components of the Girder-Diaphragm Model.

Item	Girders	Diaphragm
Joint Numbers	1,001-2,946 (G1) 3,001-4,946 (G2)	5,001-8,836
Solid Elements	1,908	2,322
Constraints	922	36
Total Degrees of Freedom	17,354	

6.2.1. SOLID ELEMENTS

A detailed finite element model of the interface between two prestressed concrete I-girders and a single diaphragm was constructed to evaluate the cause of concrete spalling in this region. Since the three-dimensional state of stress for this region would be heavily examined, the elements chosen to model this area would need to have the capability to report such values. This necessitated the use of eight-node, isoparametric "brick" elements to model the girders and diaphragm. Three translational degrees of freedom are available for this element, with all rotational degrees of freedom being restrained. The eight-node "brick" element formulation used in SAP90[®] includes nine incompatible bending modes (Computers 1991) as originally proposed by Wilson *et al.* (Hughes 1987). Figure 6.2.1a illustrates the discretization of the prestressed concrete I-girder in the interface region model. One-hundred and thirty-nine nodes define the geometry of the Modified AASHTO Type

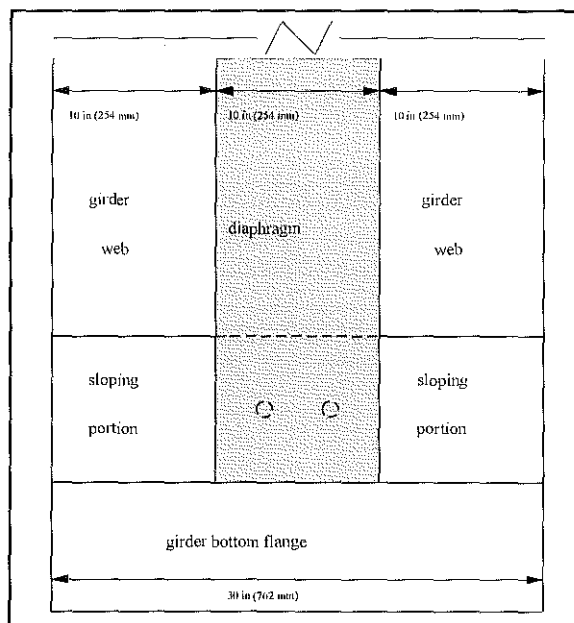


Figure 6.2. Longitudinal Dimensions of Diaphragm-Girder Interface Model.

IV girder exactly for this discretization. However, 146 nodes were used per girder slice in the actual model. The presence of the extra seven nodes is explained below.

The concrete intermediate diaphragm was likewise modeled using the eight-node, isoparametric element. The diaphragm was modeled as 43 elements between the girders and 18 elements along the height of a girder. The 10 in (254 mm) thickness of the diaphragm was modeled as three elements for a total of 2,322 ($43 \times 18 \times 3$) solid elements in the diaphragm. Distortion in the elements due to the irregular surface of the girder was reduced towards the center of the diaphragm. An illustration of the cross section of the diaphragm-girder finite element model is given in Figure 6.2.1b.

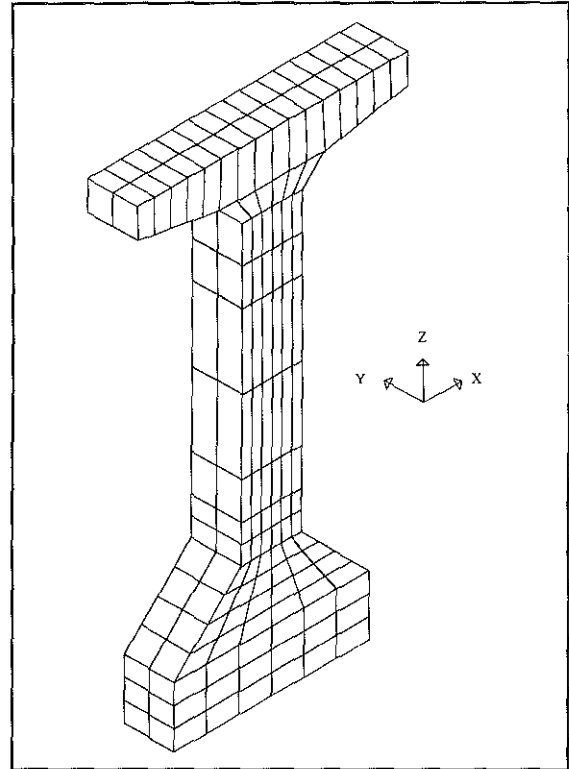


Figure 6.2.1a. Solid Element Model of the Modified AASHTO Type IV Girder.

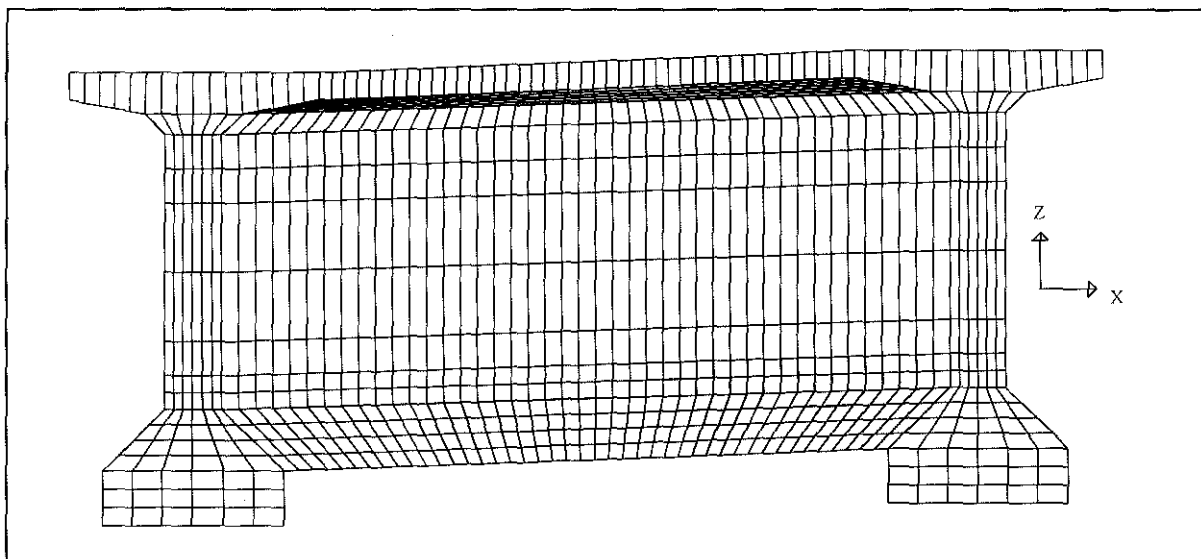


Figure 6.2.1b. Cross Section of Diaphragm-Girder Finite Element Model.

6.2.2. JOINT CONSTRAINT SPECIFICATION

Every attempt was made to make the finite element model of the diaphragm-girder interface region as accurate as possible. Therefore, special considerations as regards the connection of the intermediate diaphragms to the girders, continuity with the bridge deck, and presence of the insert for the threaded anchor bar were warranted.

The concrete intermediate diaphragms in the Southbound bridge were cast-in-place prior to the pouring of the deck. The continuity between the deck and the diaphragm was provided by reinforcing steel. However, the only connection that exists between the prestressed concrete girder and the diaphragm is two threaded diaphragm anchor bars. The anchor bars are located 4 in (101.6 mm) apart on the girder at the center of the diaphragm (see Figure 6.2.2a). An example of an anchor bar threaded into the girder prior to the pouring of the end bent diaphragm is given in Figure 6.2.2b.

To model this condition, additional nodes were specified along the profile of the girder. These nodes coincided with those used to define the girder geometry, i.e., a double node scheme was employed. Using SAP90's constraint equation capabilities, the translational degrees of freedom in the top nodes of the diaphragm near the girder were constrained in the transverse (global X), longitudinal (global Y), and vertical (global Z) directions to the respective translational degrees of freedom in the girder nodes at these locations. This was done to provide the continuity between the two members without having to incorporate the bridge deck into the model. The diaphragm nodes at the location of the anchor bars were also constrained in the transverse (global X), longitudinal (global Y), and vertical (global Z) directions to the respective translational degrees of freedom in the girder nodes. This simulated the connection between the diaphragm and girder through the anchor bar. The other nodes located along the girder diaphragm interface were not constrained about any degree of freedom. Modeling difficulties due to "contact" problems were avoided by selecting the proper displacement parameters from the results of the bridge models.

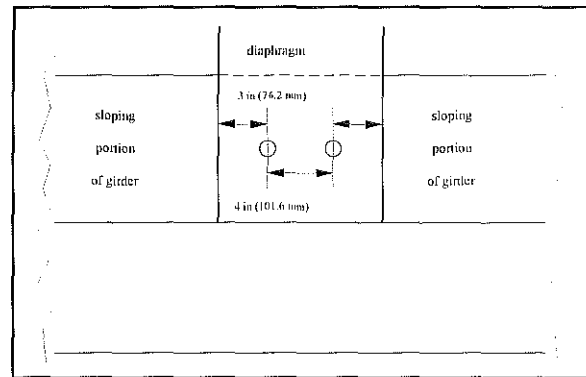


Figure 6.2.2a. Location of Diaphragm Anchor Bars on Actual Girder.

A similar approach was adopted to account for the insert into which the diaphragm anchor bars would be threaded in the prestressed concrete I-girders. A double node scheme was again employed within the girder model, as illustrated in

Figure 6.2.2c. This led to the seven extra nodes mentioned above. Translational degrees of freedom in the transverse (global X), longitudinal (global Y), and vertical (global Z) directions were constrained for each double node, except at the location of the insert. Here, only the longitudinal (global Y) degree of freedom was constrained to the node below. In this manner the model reflected the absence of bond between the insert and the girder concrete (i.e., the insert could not transfer a tensile stress to the girder concrete). This is a valid assumption given the problem witnessed in Figure 6.1, otherwise spalling would have been observed above the anchor bars. Therefore, the results would only show the distribution of compressive stress on the face of the girder. Neither the additional girder nodes or the diaphragm

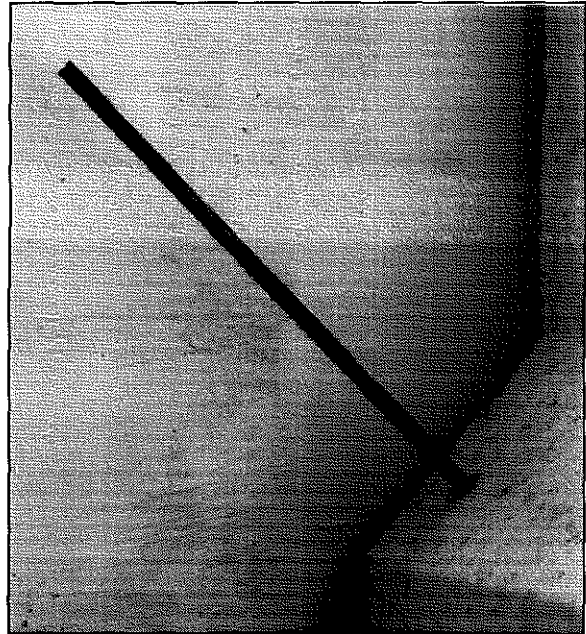


Figure 6.2.2b. Diaphragm Anchor Bar in Place at the Abutment.

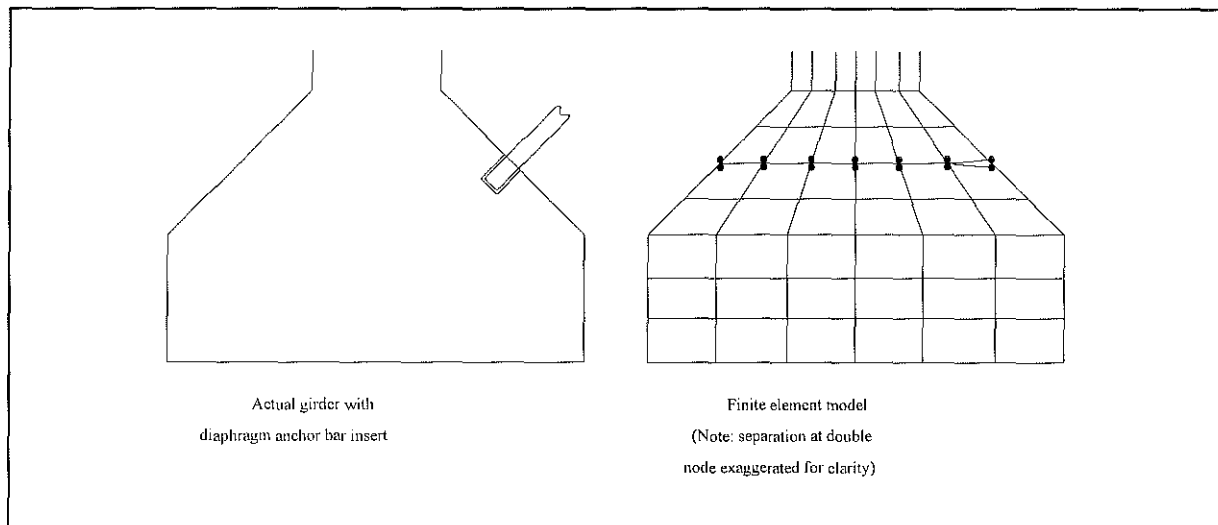


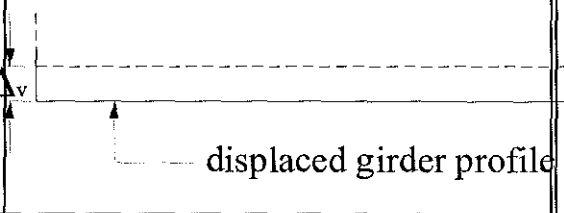
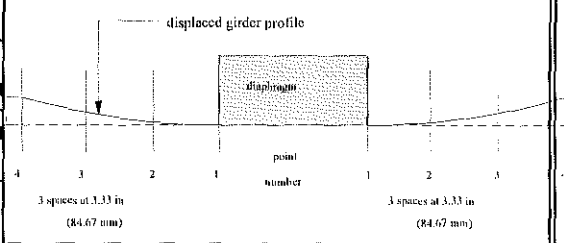
Figure 6.2.2c. Illustration of Double Node Scheme Employed at Location of Diaphragm Anchor Bar Insert.

nodes required constraint equations for the rotational degrees of freedom since rotations are not available in the eight-node "brick" formulation.

6.2.3. DISPLACEMENT SPECIFICATION

Based upon results obtained from the analyses of the entire bridge model (see Chapter 5), the diaphragm-girder interface model was subjected to an out-of-plane displacement between the girders and a relative vertical deflection of one girder to induce stress in the members. The values for the two displacement quantities were taken directly from the analysis of the Southbound bridge under Load Case 35 using legal weight coal trucks. The relative vertical deflection of one girder as opposed to the other was specified as a uniform 0.043 in (1.092 mm). The out-of-plane displacement was taken to vary parabolically on either side of the diaphragm, making use of the fact that there was no girder separation at the interface of the diaphragm and the girder. The maximum separation at the boundary of the interface model was specified as 0.010 in (0.254 mm). Table 6.2 summarizes the deflection conditions imposed on the diaphragm-girder interface model.

Table 6.2: Nodal Deflections Imposed on Diaphragm-Girder Interface Model.

Direction	Location	Displacement in inches (mm)	Orientation
Vertical	bottom face	0.043 (1.092)	
Out-of-Plane	point 1	0.001 (0.016)	
	point 2	0.003 (0.064)	
	point 3	0.006 (0.143)	
	point 4	0.010 (0.254)	

6.3. ANALYSIS RESULTS

The analysis of the diaphragm-girder interface region yielded normal stresses in three orthogonal directions (σ_x , σ_y , and σ_z) and shear stresses in three orthogonal planes (τ_{xy} , τ_{xz} , and τ_{yz}). More importantly, though, principal stresses (σ_1 , σ_2 , and σ_3) as well as direction cosines were also reported. As mentioned previously, tension in

this area is not a consideration due to the lack of bond between the anchor bar insert and the girder concrete. The main concern is then focused on whether the concrete compressive strength is exceeded. Figure 6.3a depicts the stress distribution for the three orthogonal normal (σ_x , σ_y , and σ_z) stresses and the largest principal stress (σ_1)

along a line that runs through the center of the diaphragm anchor bars and is parallel to the longitudinal axis of the girder (see Figure 6.3b). Figure 6.3c demonstrates the orientation of the coal trucks in Load Case 35. As Figure 6.3a illustrates, no individual normal stress exceeded the concrete compressive strength of 6.4 ksi (44.13 MPa) in the prestressed concrete I-girder. However, the principal stress (σ_1) does exceed the concrete compressive stress in the region around the diaphragm anchor bars. This would suggest that concrete spalling would occur on the girder near the diaphragm anchor bars.

The variation of the principal stress along a line normal to the bottom flange of the girder is pictured in Figure 6.3d. In contrast, if the bridge was only subjected to the normal legal limit of 80,000 lbs (355.84 kN), the maximum principal stress would have been 5.11 ksi (35.20 MPa) and the girder concrete might not have spalled.

On the other hand, the diaphragm itself does not experience spalling on its face. This can be explained as follows. First, the anchor bars are within confined concrete whereas the anchor bar inserts in the girder are not. Second, the diaphragm anchor bar is smooth and is embedded in the diaphragm a distance of 22.5 in (571.5 mm) which is less than the minimum required development length of 28.13 in (714.38 mm). Therefore, minimal bond with the concrete can be expected. This leads to slippage between the diaphragm and anchor bar which relieves some of the stress concentration in this region. Conversely, the anchor bar is threaded into the girder

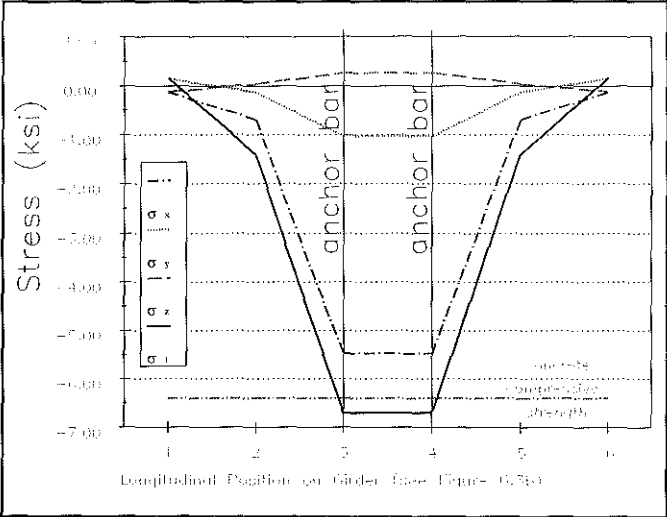


Figure 6.3a. Stress Distribution at Diaphragm-Girder Interface - Load Case 35 (Legal Weight). Positive Value Denotes Tension (Note 1 ksi = 6.896 MPa).

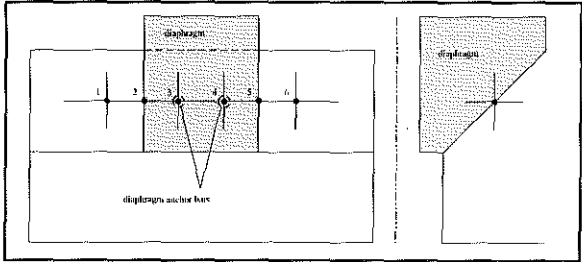


Figure 6.3b. Girder Locations Reported in Figure 6.3a.

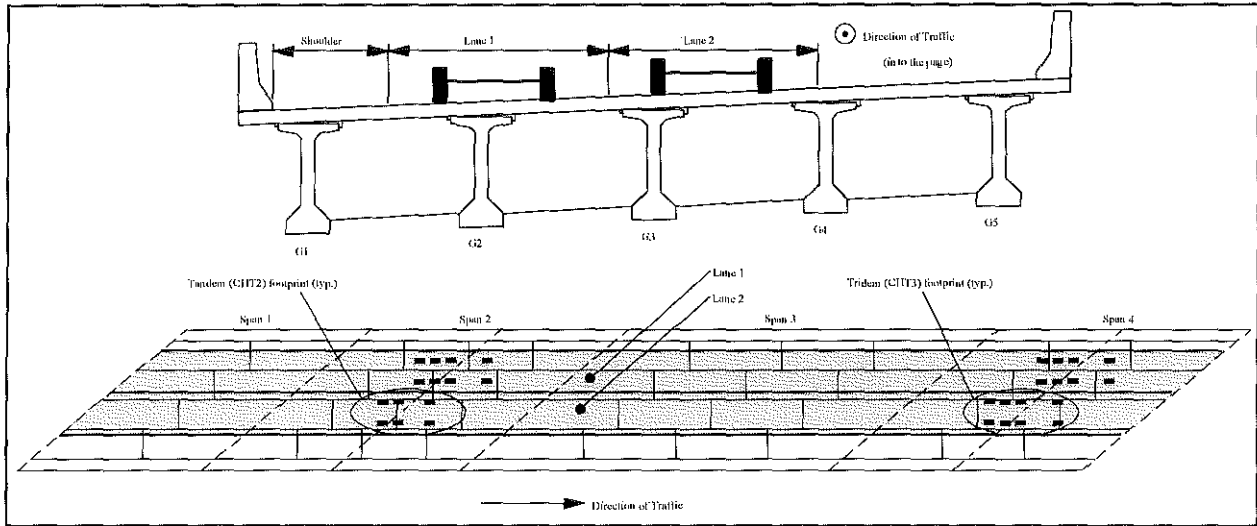


Figure 6.3c. Orientation of Coal Trucks in Load Case 35.

insert and no slippage occurs. Thus, a stress concentration develops in the vicinity of the insert.

Figures 6.3e and 6.3f illustrate the same stress diagrams for Load Case 35 considering overweight coal trucks. It is interesting to note that the overweight load case leads to a transverse stress (σ_x) which exceeds the compressive strength of the girder concrete. From this set of graphs, the area of spalled concrete observed in Figure 6.1 is clearly defined across the lower half of the sloping portion of the girder and across almost the entire width of the diaphragm (i.e., the region where the girder

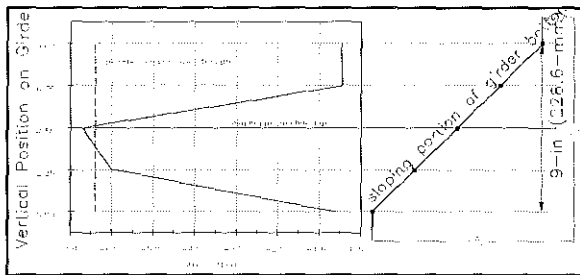


Figure 6.3d. Principal Stress Distribution at Diaphragm-Girder Interface - Load Case 35 (Legal Weight). Positive Value Denotes Tension (Note 1 ksi = 6.896 MPa).

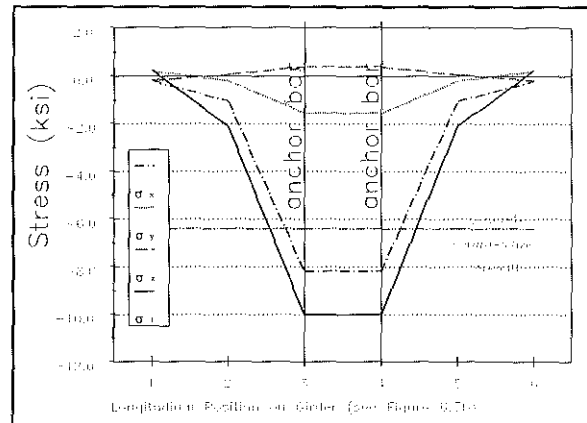


Figure 6.3e. Stress Distribution at Diaphragm-Girder Interface - Load Case 35 (Overweight). Positive Value Denotes Tension (Note 1 ksi = 6.896 MPa).

principal stress exceeds the concrete compressive stress).

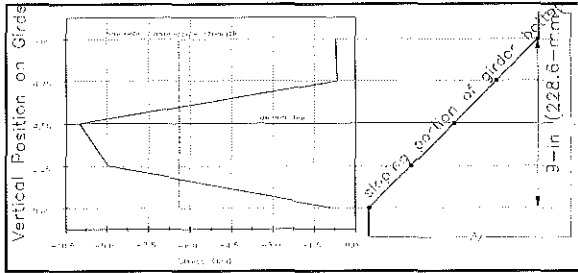


Figure 6.3f. Principal Stress Distribution at Diaphragm-Girder Interface - Load Case 35 (Overweight). Positive Value Denotes Tension (Note 1 ksi = 6.896 MPa).

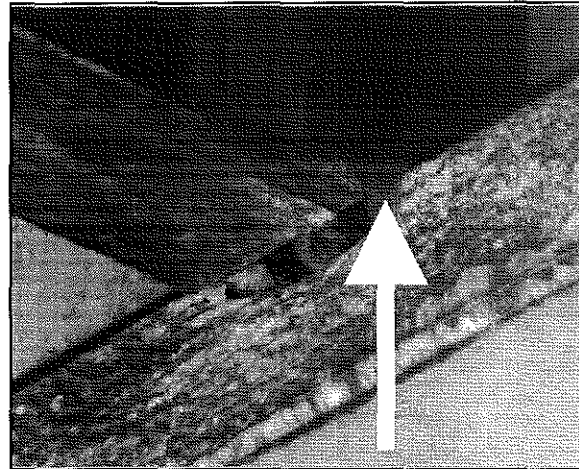


Figure 6.3g. Concrete Spalling at Diaphragm-Girder Interface.

Concrete spalling is not observed, though, in the portion of the girder flange above the anchor bar insert (see Figure 6.3g), as could be expected if the girders displaced toward each other laterally. This is because no stress concentration is created in the anchor bar region for this case. As the girders move toward each other, the entire height and thickness of the diaphragm acts in bearing against the girder. This phenomenon is noted regardless of the relative vertical displacement between the two girders. The damage to the girder concrete in the diaphragm-girder interface region can, therefore, be attributed to the tendency of the girders to separate under loading and the inability of the girder concrete to withstand the force transmitted through the diaphragm anchor bar and insert.

6.4. CONCLUSIONS

A finite element analysis focusing on the diaphragm-girder interface region has demonstrated that the concrete spalling witnessed in these locations is a result of excessive girder compressive stresses (i.e., greater than the concrete compressive strength). The cause appeared to be the tendency of the girders to separate as the bridge is loaded. Other mitigating factors were the presence of the diaphragm anchor bars and the fact the bridge is subjected to the heavy loads of coal trucks. Analyses with regular trucks indicated that the normal and principal stresses in this interface region would be insufficient to cause failure. Given the problems associated with concrete intermediate diaphragms (see Figure 6.1) in bridges subjected to overloads, an alternative course of action seems advisable. Intermediate diaphragms do provide some load distribution among the adjacent girders, as discussed in Chapter 5, but the cost of construction and maintenance of the concrete "full-depth" type of diaphragm outweighs the gain. However, the total elimination of intermediate diaphragms is not

recommended since they are required during the construction phase (prior to the placement of the deck) and if the deck is to be replaced ("re-decking"). It is, therefore, recommended to use steel diaphragms, such as the Z-type bracing mentioned previously, as substitutes for the concrete intermediate diaphragms. The diaphragms could be loosened after the girders and deck have achieved composite action (i.e., after the deck has cured).

CHAPTER 7

CONCLUSIONS AND RECOMMENDATIONS

7.1. GENERAL SUMMARY

7.1.1. COAL TRUCK LOADING

The extended-weight coal haul road system created by Kentucky's General Assembly in 1986 allows trucks hauling coal to weigh a great deal more than the normal 80,000 lbs (355.84 kN) limit if a permit is obtained. Under this system, three-axle (tandem) dump trucks may haul 94,500 lbs (420.34 kN), four-axle (tridem) dump trucks may haul 105,000 lbs (467.04 kN), and the five to six-axle tractor-trailers may haul 126,000 lbs (560.45 kN) (Associated Press 1995, Breed 1995b). These limits, however, are rarely followed. State records have indicated an average overweight in Johnson County between January 1993 and May 1996 of 53,588 lbs (238.36 kN) when citations were issued for exceeding the legal, permit weight limit (Breed and Bridis 1996). When designing a bridge in coal regions of the United States, engineers must be aware of the potential for these tremendous overloads - even if that overload is 206,000 lbs (916.29 kN) on a tractor-trailer configuration as was measured in Pike County, Kentucky (Breed 1995b). The legal weight tandem and tridem coal trucks are 2.36 and 2.63 times greater, respectively, than the AASHTO H20 Group of trucks. Even the tractor-trailer permit load is 1.75 times greater than the AASHTO HS20 Group of trucks.

7.1.2. RESEARCH OBJECTIVES

Bridges of prestressed concrete I-girder design along coal haul routes have been experiencing unusual distress (concrete spalling) at the interface of the diaphragms and the bottom flange of the girders. The intermediate diaphragms appear to be contributing more to the increased rate of deterioration and damage than reducing the moment coefficient and distributing the traffic loads as expected. The objectives of this study were as follows: 1) to complete three-dimensional, static and dynamic finite element analyses of both bridges, 2) to conduct field testing on both bridges, 3) to calibrate the finite element models with the field test data, and 4) to analyze the influence of intermediate diaphragms on load distribution in prestressed concrete I-girder bridges subjected to vehicle overload common among coal haul trucks.

7.1.3. RESEARCH SIGNIFICANCE

Previously, AASHTO recommended the use of diaphragms at points of maximum moment for spans greater than 40 ft (12.19 m). Kentucky exceeds the AASHTO guidelines by specifying diaphragms at points of maximum moment for spans between 40 and 80 ft (12.19 and 24.38 m) and diaphragms at third points for spans greater than 80 ft (24.38 m). The US 23 bridges investigated in this research study exceed even the Kentucky requirements since diaphragms are located at the quarter points in Spans 2 and 3 (see Figure 7.1.3).

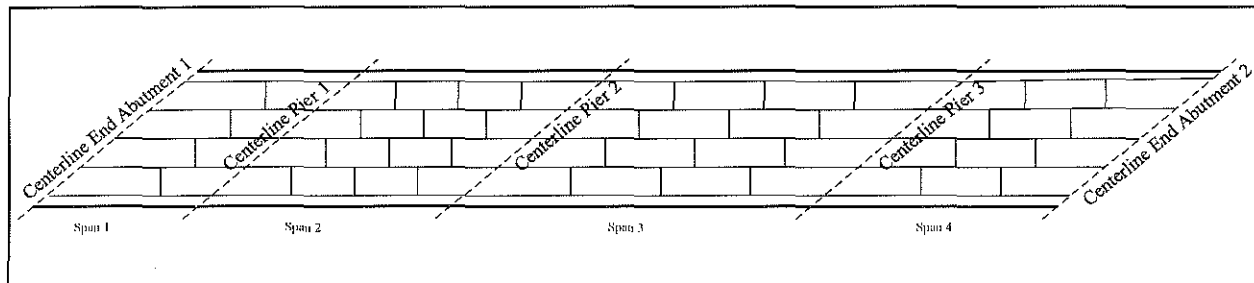


Figure 7.1.3. Span and Diaphragm Locations in the Southbound US 23 Bridge.

It should be noted that Section 9.10.1 of the *Standard Specifications for Highway Bridges* (AASHTO 1996) allows for diaphragms to be omitted when adequate strength is determined through testing or structural analysis. By investigating the load distribution and the relative transverse displacement (or twisting) between the prestressed concrete girders, it was possible to ascertain whether or not the intermediate diaphragms are performing as intended in bridges subjected to the severe overload of coal trucks. This research was the first study to address the issues of coal truck loading and the influence of intermediate diaphragms in bridges with and without diaphragms by using finite element models calibrated with static and dynamic experimental test data.

7.1.4. EXPERIMENTAL TESTING

An instrumentation plan was prepared to conduct complete and comprehensive dynamic and static testing on the US 23 bridges over KY 40. Since the greatest response to loading could be expected in the longest span, Span 3, only this section had extensive instrumentation during the static testing phase. All of the spans were instrumented during the dynamic testing phase in order to determine the global dynamic response of the structure.

Instrumentation for static testing was placed on the girders and on the

transverse and longitudinal reinforcement bars in the deck of both bridges. Instrumentation was also placed on the intermediate diaphragms of the Southbound bridge. Foil strain gages were used on the steel reinforcement while reusable strain gages were used on the faces of the diaphragms as well as on the girders at midspan and near the pier. Linear Variable Differentiable Transducers (LVDTs) were used to measure the vertical deflection of the girders and out-of-plane displacement between adjacent girders at midspan. Accelerometers arranged in a triaxial setup were used to conduct the dynamic testing on the two bridges. The instrumentation was the same for both bridges so that a comparison could be made between the structural response of bridges with and without diaphragms. The details of the instrumentation used in the static and dynamic testing of both bridges were given previously in Chapter 2.

Static testing was accomplished by using two fully-loaded, tandem coal haul trucks to induce the displacements and strains on the Southbound and Northbound bridges. The gross weights of the two trucks were 95,500 lbs (424.8 kN) and 85,800 lbs (381.6 kN). Test lanes and stations were marked along the length of the bridge to fully initiate response in the instrumentation. Trucks were positioned such that they were either bumper-to-bumper in Lane 1, bumper-to-bumper in Lane 2, or side-by-side in Lanes 1 and 2 (Truck 1 was in Lane 1 while Truck 2 was staggered in Lane 2 to account for the skew angle of the bridges). All data acquisition channels were read for seven seconds using a sampling rate of 200 Hz while the trucks were positioned at these locations. Subsequent data readings were made by incrementing the truck positions to the next station.

Dynamic testing was accomplished by using a single fully-loaded, tandem coal haul truck. The truck passed over the two bridges traveling along the centerline of the bridge. For each test the truck speed was 52 mph (83.7 km per hour). Due to the construction of the approach roadway, the driver did not have enough space to reach 55 mph (88.514 km per hour) with a fully-loaded truck. However, there was enough roadway so that the driver did not have to decelerate until the truck was clear of the bridge. The accelerometers used in the dynamic testing were sampled at 1002 Hz for 29.94012 seconds to assure a complete, high resolution acceleration record. Data recording began with the truck approximately 100 ft (30.5 m) from the end of the bridge and continued for the 29.94012-second duration.

Static testing provided an opportunity to determine the deflections and stresses induced by normal traffic and coal truck loading. Dynamic testing provided an opportunity for the natural frequencies and mode shapes of the structures to be determined. The results from each test were used to calibrate finite element models of the US 23 bridges.

7.1.5. EXPERIMENTAL RESULTS

7.1.5.1. Strains Recorded in the Deck

Strains in the transverse reinforcement bars of the Southbound bridge (bridge with intermediate diaphragms) deck were observed to be fairly consistent and independent of the test truck positions. A slight rise in the magnitude of strain was noted when the trucks were directly over the transverse location considered. On the other hand, the strain in the transverse reinforcement bars in the deck of the Northbound bridge (bridge without intermediate diaphragms) demonstrated a dependence on truck position. Sharp rises in the strain data were recorded with the trucks directly above the transverse gage considered. It appears that the presence of intermediate diaphragms reduces the flexibility in the deck of the Southbound bridge, thereby causing less strain in the slab. However, the magnitude of strain observed should not cause alarm. The maximum concrete stresses in the Northbound bridge deck were 0.97 ksi (6.66 MPa) in compression and 0.28 ksi (1.94 MPa) in tension. Comparable maximum concrete stress values in the Southbound bridge deck were 0.15 ksi (1.21 MPa) in compression and 0.08 ksi (0.57 MPa) in tension. Since the stress values at the transverse locations are within acceptable design criteria, the absence of intermediate diaphragms in the Northbound bridge does not seem to pose a threat to the serviceability and load capacity of the deck in the transverse direction under the static test loads. Similarly, the presence of intermediate diaphragms does not seem to impose excessive stresses on the Southbound bridge deck in the transverse direction.

An evaluation of the strain gage readings from the longitudinal reinforcement in the Northbound and Southbound bridge decks does not immediately lead to the same conclusions. In general, the Northbound bridge deck strains in the longitudinal direction do show added flexibility in the absence of intermediate diaphragms, but the effect is less pronounced than in the case of the transverse reinforcement. Strains on the longitudinal reinforcement seem to parallel each other when comparing values for the Northbound and Southbound bridges. In fact, the strain measured on the Southbound bridge deck bars were sometimes observed to be higher than comparable strains on the Northbound bridge deck. These cases were more often noted when strain values were compared at positions away from the location of the test trucks. This trend seems to indicate that the presence of the intermediate diaphragms assists in distributing the strain to adjacent girders. However, the differences in strain observed at these locations were not significant enough to warrant the use of diaphragms.

7.1.5.2. Displacements Recorded on the Girders

Two conclusions were drawn from the experimental results of the girder out-of-

plane displacements: 1) out-of-plane displacements were prevalent only when the load was in the span where deflections were being measured and 2) although the absence of intermediate diaphragms leads to a large difference between out-of-plane displacements in the Southbound and Northbound bridges percentage-wise, the magnitude of the out-of-plane displacement is not sufficient to cause concern. In fact the maximum out-of-plane displacement recorded in the Southbound and Northbound bridges was 0.04 in (1.11 mm) and 0.09 in (2.29 mm), respectively. Additional out-of-plane displacement measurements were made at the base of a typical intermediate diaphragm and one that had been cut low, i.e., the reinforcement in the diaphragm did not extend into the deck. With a single truck straddling the centerline of the respective diaphragms, a 0.01 in (0.25 mm) difference in deflection was recorded. Under the static test loading, displacements obtained in the out-of-plane direction do not indicate that the intermediate diaphragms are very effective in transmitting load to adjacent girders. In other words, no large differences in deflections were observed.

Similar observations were made with the vertical displacements recorded on the bottom face of the girders at the midspan of Span 3. In general, the Southbound bridge tended to deflect less than the Northbound bridge under the same static test loads. However, this difference was often minuscule. A maximum vertical displacement of 0.24 in (6.10 mm) was recorded for the Southbound bridge, and a maximum vertical displacement of 0.25 in (6.35 mm) was recorded for the Northbound bridge.

7.1.5.3. Strains Recorded on the Girders

The strains obtained from the gages on the longitudinal deck reinforcement were combined with the strains recorded along the cross section of the girder to determine the distribution of stress across the composite cross section. The location of the neutral axis under the static test loads could also be readily obtained. Strain records for both bridges did demonstrate the trend that the neutral axis approaches the deck as the positions of the test truck approached the girder cross section considered. The neutral axis also appeared to be lower in the Southbound bridge (bridge with intermediate diaphragms) when compared to similar cross section locations in the Northbound bridge (bridge without intermediate diaphragms). Consequently, under the same static test load conditions, the girders in the Southbound bridge experienced less tensile stress on the bottom face of the girder than the girders in the Northbound bridge. However, the tensile stresses obtained from static testing were not sufficient enough to induce cracking in the deck or girders.

Strains recorded across the composite cross section near the pier indicate a different trend, though, and indeed seem to parallel each other. In fact the presence of intermediate diaphragms appears to increase the compressive stresses that the bottom faces of the interior Southbound girders experience under the static test loads.

This condition was only noted when the test trucks were located in lanes opposite to the girder being considered. The maximum tensile stress experienced by any girder in the Southbound bridge was 0.30 ksi (2.05 MPa). Likewise, the maximum tensile stress experienced by any girder in the Northbound bridge was 0.35 ksi (2.39 MPa).

Small strains were generally recorded from the gages placed around the diaphragm on the girder. In fact, the largest strain value recorded at the diaphragm-girder interface was 91.59 microstrain, corresponding to a tensile stress in the girder of 0.417 ksi (2.880 MPa). A more detailed investigation of the principal stresses in this region was required and was presented in Chapter 6. The details of the experimental results obtained from the static and dynamic field testing of both US 23 bridges were given in Chapter 3.

7.1.6. FINITE ELEMENT MODEL

Having completed the static and dynamic test phases, finite element models of the US 23 bridges were constructed and calibrated to correlate with the experimentally measured data. Refinement of the models, varying either geometric or material properties, was accomplished by evaluating the bridge response of the finite element models in comparison to the field test data.

Since later analysis and research centered on very specific regions of the bridges, namely the diaphragm-girder interface, a detailed three-dimensional finite element model for each bridge was constructed. Due to a lack of symmetry in the longitudinal or transverse direction, it was necessary to model the entire length and width of the bridges. The complete, calibrated finite element models, as described previously in Chapter 4, were used to evaluate the global response of the structure to anticipated coal truck loadings.

Local responses in the form of stresses around the diaphragm-girder interface were examined through the use of a smaller, more refined three-dimensional finite element model as presented in Chapter 6. This smaller model was highly detailed (more refined mesh) and used the material and geometric properties obtained from the calibrated larger model. The response from the larger model was used to define displacement and stress boundary conditions for the two girders and single diaphragm represented in the small model.

7.2. EFFECTIVENESS OF INTERMEDIATE DIAPHRAGMS

Based on the results presented in Chapter 5 for vertical deflections, out-of-plane

displacements, and girder stresses, a significant advantage in structural response is generally not noted due to the presence of intermediate diaphragms. Analyses completed using legal weight coal trucks suggests the Northbound bridge (bridge without intermediate diaphragms) will experience displacements and stresses well within the design parameters outlined by AASHTO and ACI. The single exception to this statement was noted in the load case where a tridem coal truck was located at the midspan of Spans 1 and 3 in both traffic lanes. A nonlinear finite element analysis would better ascertain whether or not the Northbound bridge would experience any detrimental effects when subjected to this particular combination of overweight coal trucks. Furthermore, a fatigue analysis would be beneficial in ascertaining the long-term response of the Northbound bridge to the repeated coal truck loading it will experience. The reduction in displacements and stresses of the Southbound bridge (bridge with intermediate diaphragms) seemed to be advantageous percentage-wise, but the magnitudes of these two parameters were insufficient to suggest mandatory use of intermediate diaphragms.

Finite element analyses (detailed in Chapter 6) focusing on the diaphragm-girder interface region demonstrated that the concrete spalling witnessed in these locations was a result of girder stresses in excess of the concrete compressive strength. The tendency of the girders to separate as the bridge was loaded played a large role in generating these high stress concentrations. Other mitigating factors were the presence of the diaphragm anchor bars and the fact the bridge is subjected to the heavy loads of coal trucks. Given the spalling associated with the presence of concrete intermediate diaphragms in bridges subjected to overloads, an alternative course of action seems advisable. Intermediate diaphragms on the whole do provide some load distribution among the adjacent girders, as discussed in Chapter 5, but the cost of construction and maintenance of this type of diaphragm outweighs the gain. However, the total elimination of intermediate diaphragms is not recommended since they are required during the construction phase (prior to the placement of the deck) and if the deck is to be replaced ("re-decking"). Therefore, the use of steel diaphragms, such as the Z-type bracing mentioned previously, is recommended as substitutes for the concrete intermediate diaphragms. The steel diaphragms could be loosened after the deck and girders have achieved composite action (i.e., after the deck has cured).

7.3. FUTURE RESEARCH NEEDS

Although this research attempted to be a comprehensive investigation of the influence of intermediate diaphragms in bridges subjected to coal truck loads (overloads), several areas exist which could merit further research. These items are listed below.

7.3.1. ALTERNATE DIAPHRAGM TYPES

The US 23 bridges investigated in this research had either concrete intermediate diaphragms (Southbound bridge) or no intermediate diaphragms (Northbound bridge). The experimental and analytical results seem to indicate that full-depth, concrete intermediate diaphragms do play a functional role, however, their return *versus* cost (cost of construction plus cost of repair once the spalling occurs) may not be advantageous. A review of the previous literature indicated that extensive research has been conducted on different types of diaphragms/cross-frames in steel girder bridges, but not prestressed concrete I-girder bridges. In light of the concrete spalling that occurs at the interface of concrete diaphragms and the girders, alternate forms of intermediate diaphragms (e.g., Z-bracing) could be investigated for those instances where the engineer or state agencies requires their inclusion and significant overloads, such as coal trucks, could be expected.

7.3.2. SKEWED *VERSUS* NON-SKEWED BRIDGES

The US 23 bridges were highly skewed (50 degrees) structures, and as such were not representative of a much larger class of slab-on-girder bridges constructed with prestressed concrete I-girders. Future research should concentrate on experimental testing and analytical modeling of bridges with no skew (right bridges) and bridges with small skew (less than 30 degrees) to examine the influence of intermediate diaphragms in bridges subjected to coal truck loads. Only then can a definitive answer as to whether or not intermediate diaphragms should always be incorporated into bridge design be ascertained. Additionally, comparisons between right bridges and bridges with small skew could also be beneficial in evaluating the increase/decrease of stress around the diaphragm-girder interface as the bridge parameters vary.

7.3.3. BRIDGES OF VARIOUS CONSTRUCTION

The present research study has investigated and attempted to solve a real problem associated with many of the prestressed concrete I-girder bridges in Kentucky that are subjected to coal truck loading. However, before recommendations can be made to change the AASHTO code, a variety of bridge types that will be subjected to this type of overload must be considered in order to form a general statement about the inclusion (or exclusion) of intermediate diaphragms. Suggested types to study and compare are steel slab-on-girder bridges, reinforced concrete slab-on-girder bridges, and prestressed concrete slab-on-girder bridges. Of interest to any future research in this area may be the difference in response between these bridges if they are considered composite and non-composite.

7.3.4. OTHER ANALYSIS TECHNIQUES

Finite element analyses on the Northbound bridge using overweight coal trucks and assuming linear elastic response indicated that cracking may occur on the bottom flange of the prestressed concrete I-girders of Span 3. In such loading cases as this cracking may occur, a nonlinear finite element analysis would be advantageous. The long-term effect of the non-linear behavior of the girders would be beneficial in ascertaining whether or not intermediate diaphragms are necessary later in the bridge's operating life. Furthermore, a fatigue analysis would be assist in determining the long-term response of the US 23 bridges to the repeated coal truck loading that they will experience. Again, this would be a measure of evaluating the long-term behavior of bridges with and without intermediate diaphragms.

BIBLIOGRAPHY

- AASHTO. (1994). *Load Resistance Factor Design Bridge Design Specifications*. First Edition. American Association of State Highway and Transportation Officials: Washington, D.C.
- AASHTO. (1996). *Standard Specifications for Highway Bridges*. Sixteenth Edition. American Association of State Highway and Transportation Officials: Washington, D.C.
- AASHTO Subcommittee on Bridges and Structures. (1994). *Guide Specifications for Distribution of Loads for Highway Bridges*. American Association of State Highway and Transportation Officials: Washington, D.C.
- ACI. (1995). *Building Code Requirements for Reinforced Concrete (ACI 318-95) and Commentary (ACI 318R-95)*. American Concrete Institute: Detroit.
- AISC. (1994). *Manual of Steel Construction: Load and Resistance Factor Design Volume I*. Second Edition. American Institute of Steel Construction, Inc.: Chicago.
- Abdalla, H. and Kennedy, J.B. (1995). "Dynamic Analysis of Prestressed Concrete Beams With Openings." *ASCE Journal of Structural Engineering*. Vol. 121, No. 7, 1058-1038.
- Abendroth, R.E., Klaiber, F.W., and Shafer, M.W. (1991). "Lateral Load Resistance of Diaphragms in Prestressed Concrete Girder Bridges." *Research Report ISU-ERI-Ames-92076, Iowa DOT Project HR-319*, College of Engineering, Department of Civil and Construction Engineering, Iowa State University of Science and Technology.
- Abendroth, R.E., Klaiber, F.W., and Shafer, M.W. (1995). "Diaphragm Effectiveness in Prestressed-Concrete Girder Bridges." *ASCE Journal of Structural Engineering*. Vol. 121, No. 9, 1362-1369.
- Adeli, H. and Zhang, J. (1995). "Fully Nonlinear Analysis of Composite Girder Cable-Stayed Bridges." *Computers & Structures*. Vol. 54, No. 2, 267-277.
- Ahlborn, T.M., French, C.W., and Leon, R.T. (1995). "Applications of High-Strength

Concrete to Long-Span Prestressed Bridge Girders." *Transportation Research Board, 74th Annual Meeting, Preprint Paper No. 950400*. Transportation Research Board: Washington, D.C.

Aktan, A.E., Miller, R., Shahrooz, B., Zwick, M., Heckenmueller, M., Ho, I., Hrinko, W., and Toksoy, T. (1992). "Nondestructive and Destructive Testing of a Reinforced Concrete Slab Bridge and Associated Analytical Studies." *Report FHWA/OH-93/017*, FHWA, U.S. Department of Transportation, Washington, D.C., December 1992.

Aktan, A.E., Farhey, D.N., and Dalal, V. (1995). "Issues in Rating Steel-Stringer Bridges." *Transportation Research Board, 74th Annual Meeting, Preprint Paper No. 950674*. Transportation Research Board: Washington, D.C.

Associated Press. (1995). "Kentucky permits some allowances for heavy trucks." *Lexington Herald-Leader*. September 3, 1995, page B4.

Associated Press. (1996). "Higher fines for heavy trucks doubtful." *Lexington Herald-Leader*. September 4, 1996, page B3.

Azizinamini, A., Kathol, S., and Beacham, M.W. (1995). "Influence of Cross Frames on Load Resisting Capacity of Steel Girder Bridges." *Engineering Journal*. Third Quarter, 107-116.

Baker, W.E., Spivey, K.H., and Baker, Q.A. (1992). "Energy-Balance Methods for Structural Response and Damage Analysis Under Transient Loads." *Structural Design for Hazardous Loads*. E & FN Spon: London, 229-237.

Bakht, B. and Jaeger, L.G. (1985). *Bridge Analysis Simplified*. McGraw-Hill Book Company: New York.

Bakht, B. (1988). "Analysis of Some Skew Bridges as Right Bridges." *ASCE Journal of Structural Engineering*. Vol. 114, No. 10, 2307-2322.

Barker, M.G. (1995a). "Load Rating and Ultimate Capacity Evaluation of Compact Steel Girder Bridges." *Transportation Research Record, No. 1476*. National Academy Press: Washington, D.C., 1-7.

Barker, M.G. (1995b). "Guide Specification Strength Capacity Rating of Existing Girder Bridges." *Transportation Research Record, No. 1476*. National Academy Press: Washington, D.C., 98-105.

- Barker, M.G., Bergson, P.M., French, C.E., Leon, R.T., Galambos, T.V., and Klaiber, F.W. (1996). "Shakedown Tests of One-Third-Scale Composite Bridge." *Journal of Bridge Engineering*. Vol. 1, No. 1, 2-9.
- Bathe, K.-J. (1996). *Finite Element Procedures*. Prentice Hall: Englewood Cliffs, New Jersey.
- Boresi, A.P., Schmidt, R.J., and Sidebottom, O.M. (1993). *Advanced Mechanics of Materials*, fifth edition. John Wiley & Sons, Inc.: New York.
- Breed, A.G. (1995a). "Letcher man crusading for coal-truck safety." *Lexington Herald-Leader*. September 3, 1995, page B1.
- Breed, A.G. (1995b). "Engineer points to dangers." *Lexington Herald-Leader*. September 3, 1995, page B1.
- Breed, A.G. and Bridis, T. (1996). "Overweight trucks burden state roads." *Lexington Herald-Leader*. September 1, 1996, page B1.
- Breed, A.G. (1996a). "Coal truckers say heavy loads needed for profit." *Lexington Herald-Leader*. September 2, 1996, page C1.
- Breed, A.G. (1996b). "Hauling fines higher in Boyd County than in Pike." *Lexington Herald-Leader*. September 2, 1996, page C4.
- Breed, A.G. (1996c). "Study favors heavier trucks, fewer of them." *Lexington Herald-Leader*. September 3, 1996, page B1.
- Bridis, T. (1996a). "State records on load citations incomplete, could be inaccurate." *Lexington Herald-Leader*. September 2, 1996, page C4.
- Bridis, T. (1996b). "Kentucky's 16 weigh stations monitor trucks." *Lexington Herald-Leader*. September 3, 1996, page B3.
- Buchanan, J.A. (1927). "Impact Forces Exerted by the Motor Truck on the Highway." *Proceedings of Sixth Annual Meeting of the Highway Research Board*. Highway Research Board: Washington, D.C., 175-184.
- Burdette, E.G. and Goodpasture, D.W. (1988). "Correlation of Bridge Load Capacity With Test Data." *National Cooperative Highway Research Program Report No. 306*. Transportation Research Board: Washington, D.C.

- Burke, M.P. (1994). "Semi-Integral Bridges: Movements and Forces." *Transportation Research Record, No. 1460*. National Academy Press: Washington, D.C., 1-7.
- Casas, J.R. (1995). "Dynamic Modeling of Bridges: Observations from Field Testing." *Transportation Research Record, No. 1476*. National Academy Press: Washington, D.C., 59-68.
- Chan, T.H.T., and O'Connor, C. (1990a). "Wheel Loads from Highway Bridge Strains: Field Studies." *ASCE Journal of Structural Engineering*. Vol. 116, No. 7, 1751-1771.
- Chan, T.H.T., and O'Connor, C. (1990b). "Vehicle Model for Highway Bridge Impact." *ASCE Journal of Structural Engineering*. Vol. 116, No. 7, 1772-1793.
- Chatterjee, P.K. and Datta, T.K. (1995). "Dynamic Analysis of Arch Bridges Under Traveling Loads." *International Journal of Solids and Structures*. Vol. 32, No. 11, 1585-1594.
- Chen, Y. and Aswad, A. (1994). "Efficient Design Using Refined Methods of Lateral Distribution for Prestressed Bridges." *IBC Paper No. 94-33*. 1994 International Bridge Conference Proceedings, 240-246.
- Chen, Y. (1995a). "Prediction of Lateral Distribution of Vehicular Live Loads on Bridges With Unequally Spaced Girders." *Computers & Structures*. Vol. 54, No. 4, 609-620.
- Chen, Y. (1995b). "Refined and Simplified Methods of Lateral Load Distribution for Bridges With Unequally Spaced Girders: I. Theory." *Computers & Structures*. Vol. 55, No. 1, 1-15.
- Chen, Y. (1995c). "Refined and Simplified Methods of Lateral Load Distribution for Bridges With Unequally Spaced Girders: II. Applications." *Computers & Structures*. Vol. 55, No. 1, 17-32.
- Chen, Y. and Aswad, A. (1996). "Stretching Span Capability of Prestressed Concrete Bridges Under AASHTO LRFD." *ASCE Journal of Bridge Engineering*. Vol. 1, No. 3, 112-120.
- Cheung, M.S., Jategaonkar, R., and Jaeger, L.G. (1986). "Effects of Intermediate Diaphragms in Distributing Live Loads in Beam-and-Slab Bridges." *Canadian Journal of Civil Engineering*. Vol. 13, 278-292.

- Cheung, M.S., Akhras, G., and Li, W. (1994). "Combined Boundary Element/Finite Strip Analysis of Bridges." *ASCE Journal of Structural Engineering*. Vol. 120, No. 3, 716-727.
- Chompooming, K. and Yener, M. (1995). "The Influence of Roadway Surface Irregularities and Vehicle Deceleration on Bridge Dynamics Using the Method of Lines." *Journal of Sound and Vibration*. Vol. 183, No. 4, 567-589.
- Chopra, A.K. (1995). *Dynamics of Structures: Theory and Applications to Earthquake Engineering*. Prentice Hall: Englewood Cliffs, NJ.
- Computers and Structures, Inc. (1991). *SAP90 Manual*. University of California at Berkeley: Berkeley, CA.
- Cook, R.A., Fagundo, F.E., Rozen, A.D., and Mayer, H. (1993). "Service, Fatigue, and Ultimate Load Evaluation of a Continuous Prestressed Flat-Slab Bridge System." *Transportation Research Record, No. 1393*. National Academy Press: Washington, D.C., 104-111.
- Craig, R.J., Gill, S.L., Everett, A.G., Vasquez, G.D., and Brooten, L.A. (1994). "Static and Dynamic Load Testing of 15 Chester County Bridges." *IBC Paper No. 94-31*. 1994 International Bridge Conference Proceedings, 219-226.
- Culham, G.A. and Ghali, A. (1977). "Distribution of Wheel Loads on Bridge Girders." *Canadian Journal of Civil Engineering*. Vol. 4, 57-65.
- Daniel, I.M., and Ishai, O. (1994). *Engineering Mechanics of Composite Materials*. Oxford University Press: New York.
- Dicleli, M. and Bruneau, M. (1995). "Fatigue-Based Methodology for Managing Impact of Heavy-Permit Trucks on Steel Highway Bridges." *ASCE Journal of Structural Engineering*. Vol. 121, No. 11, 1651-1659.
- Dunncliff, John. (1993). *Geotechnical Instrumentation for Monitoring Field Performance*. John Wiley & Sons, Inc.: New York.
- Dusseau, R.A. and Dubaisi, H.N. (1993). "Natural Frequencies of Concrete Bridges in the Pacific Northwest." *Transportation Research Record, No. 1393*. National Academy Press: Washington, D.C., 119-132.
- Easterling, W.S. and Porter, M.L. (1994a). "Steel Deck Reinforced Concrete Diaphragms I." *ASCE Journal of Structural Engineering*. Vol. 120, No. 2, 560-

- Easterling, W.S. and Porter, M.L. (1994b). "Steel Deck Reinforced Concrete Diaphragms II." *ASCE Journal of Structural Engineering*. Vol. 120, No. 2, 577-596.
- Ebeido, T. and Kennedy, J.B. (1996a). "Girder Moments in Continuous Skew Composite Bridges." *ASCE Journal of Bridge Engineering*. Vol. 1, No. 1, 37-45.
- Ebeido, T. and Kennedy, J.B. (1996b). "Shear and Reaction Distributions in Continuous Skew Composite Bridges." *ASCE Journal of Bridge Engineering*. Vol. 1, No. 4, 155-165.
- Federal Highway Administration. (1981). *Bridge Gross Weight Formula*. Pamphlet HTO-30/5-81(30M). U.S. Government Printing Office: Washington, D.C.
- Fenske, T.E., Yener, M., Liu, D., and Fenske, S.M. (1995). "Computationally Efficient Method for Inclusion of Nonprismatic Member Properties in a Practical Bridge Analysis Procedure." *Transportation Research Record*, No. 1476. National Academy Press: Washington, D.C., 171-179.
- Fu, C.C., Elhelbawey, M., Sahin, M.A., and Schelling, D.R. (1996). "Lateral Distribution Factor from Bridge Field Testing." *ASCE Journal of Structural Engineering*. Vol. 122, No. 9, 1106-1109.
- Fu, G. and Hag-Elsafi O. (1996). "New Safety-Based Checking Procedure for Overloads on Highway Bridges." *Transportation Research Record*, No. 1541. National Academy Press: Washington, D.C., 22-28.
- Galambos, T.V., Leon, R.T., French, C.W., Barker, M., and Dishongh, B. (1993). "Inelastic Rating Procedures for Steel Beam and Girder Bridges." *National Cooperative Highway Research Program Report No. 352*. National Academy Press: Washington, D.C.
- Gbadeyan, J.A. and Oni, S.T. (1995). "Dynamic Behavior of Beams and Rectangular Plates Under Moving Loads." *Journal of Sound and Vibration*. Vol. 182, No. 5, 677-695.
- Ghali, A. (1967). "Analysis of Continuous Skew Concrete Girder Bridges." *ACI Publication SP-23, Paper SP 23-9*. American Concrete Institute: Detroit.
- Ghosn, M. and Moses, F. (1996). "Redundancy of Prestressed Concrete I-Beam

- Bridges." *Proceedings of Structures Congress XIV: Building an International Community of Structural Engineers*, Volume 2. American Society of Civil Engineers: New York, 688-695.
- Green, R. (1994). "A Code for Ontario Bridge Substructures." *Transportation Research Board, 73rd Annual Meeting, Preprint Paper No. 940406*. Transportation Research Board: Washington, D.C.
- Hays, C.O., Sessions, L.M., and Berry, A.J. (1986). "Further Studies on Lateral Load Distribution Using a Finite Element Method." *Transportation Research Record, No. 1072*. Transportation Research Board: Washington, D.C., 6-14.
- Helba, A. and Kennedy, J.B. (1995). "Skew Composite Bridges - Analyses for Ultimate Load." *Canadian Journal of Civil Engineering*. Vol. 22, No. 6, 1092-1103.
- Huang, D.Z., Wang, T.L., and Shahawy, M. (1992). "Impact Analysis of Continuous Multigirder Bridges Due to Moving Vehicles." *ASCE Journal of Structural Engineering*. Vol. 118, No. 12, 3427-3443.
- Huang, D.Z., Wang, T.L., and Shahawy, M. (1993). "Impact Studies of Multigirder Concrete Bridges." *ASCE Journal of Structural Engineering*. Vol. 119, No. 8, 2387-2402.
- Huang, D.Z., Wang, T.L., and Shahawy, M. (1994). "Dynamic Loading of a Rigid Frame Bridge." *Proceedings of Structures Congress XII, Volume 2*. American Society of Civil Engineers: New York, 85-90.
- Huang, D.Z., Wang, T.L., and Shahawy, M. (1995). "Vibration of Thin-Walled Box-Girder Bridges Excited by Vehicles." *ASCE Journal of Structural Engineering*. Vol. 121, No. 9, 1330-1337.
- Hughes, T.J.R. (1987). *The Finite Element Method - Linear Static and Dynamic Finite Element Analysis*. Prentice Hall: Englewood Cliffs, New Jersey.
- Hughes, T.J.R. (1976). "Stability, Convergence, and Growth and Decay of Energy of the Average Acceleration Method in Nonlinear Structural Dynamics." *Computers & Structures*. Vol. 6, 313-324.
- Hulsey, J.L. and Delaney, D.K. (1993). "Static Live Load Tests on a Cable-Stayed Bridge." *Transportation Research Record, No. 1393*. National Academy Press: Washington, D.C., 162-174.

- Jaeger, L.G. and Bakht, B. (1982). "The Grillage Analogy in Bridge Analysis." *Canadian Journal of Civil Engineering*. Vol. 9, 224-235.
- Jones, R.M. (1975). *Mechanics of Composite Materials*. Hemisphere Publishing Company: New York.
- Kankam, J.A. and Habib, J.D. (1995). "Nonlinear FE Analyses of RC Skewed Slab Bridges." *ASCE Journal of Structural Engineering*. Vol. 121, No. 9, 1338-1345.
- Kathol, S., Azizinamini, A., and Luedke, J. (1995). "Strength Capacity of Steel Girder Bridges." *NDOR Research Project Number RES1(0099) P469*. Department of Civil Engineering, University of Nebraska-Lincoln.
- Kennedy, J.B. and Soliman, M. (1982). "Ultimate Loads of Continuous Composite Bridges." *ASCE Journal of Structural Engineering*. Vol. 118, No. 9, 2610-2623.
- Kentucky Transportation Cabinet. (1994). *Kentucky's Official Coal Haul Highway System 1994*. Highway Systems Section, Division of Planning, Department of Highways, Kentucky Transportation Cabinet: Frankfort, KY.
- Khaleel, M.A. and Itani, R.Y. (1993). "Effect of Alternative Truck Configurations and Weights on the Fatigue Life of Bridges." *Transportation Research Record, No. 1393*. National Academy Press: Washington, D.C., 112-118.
- Kim, S., Sokolik, A.F., and Nowak, A.S. (1996). "Measurement of Truck Load on Bridges in Detroit, Michigan, Area." *Transportation Research Record, No. 1541*. National Academy Press: Washington, D.C., 58-63.
- Klaiber, F.W., Dunker, K.F., Wipf, T.J., and Sanders, W.W. (1987). "Methods of Strengthening Existing Highway Bridges." *National Cooperative Highway Research Program Report No. 293*. Transportation Research Board: Washington, D.C.
- Kostem, C.N. (1979). "Effects of Diaphragms on Lateral Load Distribution in Beam-Slab Bridges." *Transportation Research Record, No. 645*. Transportation Research Board: Washington, D.C., 6-9.
- Kou, J.-W. and DeWolf, J.T. (1997). "Vibrational Behavior of Continuous Span Highway Bridge - Influencing Variables." *ASCE Journal of Structural Engineering*. Vol. 123, No. 3, 333-344.
- Laman, J.A. (1995). "Load Spectra for Girder Bridges." *Fourth International Bridge*

Engineering Conference. August 28-30, 1995, 314-323.

- Law, S.S., Ward, H.S., Shi, G.B., Chen, R.Z., Waldron, P., and Taylor, C. (1995a). "Dynamic Assessment of Bridge Load-Carrying Capacities I." *ASCE Journal of Structural Engineering*. Vol. 121, No. 3, 478-487.
- Law, S.S., Ward, H.S., Shi, G.B., Chen, R.Z., Waldron, P., and Taylor, C. (1995b). "Dynamic Assessment of Bridge Load-Carrying Capacities II." *ASCE Journal of Structural Engineering*. Vol. 121, No. 3, 488-495.
- Lee, H.P. (1995). "Dynamic Response of a Multi-Span Beam on One-Sided Point Constraints Subject to a Moving Load." *Computers & Structures*. Vol. 55, No. 4, 615-623.
- Lieh, J. and Qi, W. (1995). "Simulation of Dynamic Truck Loading on Pavements Using Measured Road Roughness." *Transportation Research Board, 74th Annual Meeting, Preprint Paper No. 950747*. Transportation Research Board: Washington, D.C.
- Lin, J., Yu, J., Lewis, F.L., and Huang, T. (1994). "Dynamic Modeling for Bridge Vibration Control." *Transportation Research Board, 73rd Annual Meeting, Preprint Paper No. 940849*. Transportation Research Board: Washington, D.C.
- Lu, Y. and Madanat, S. (1994). "Bayesian Updating of Infrastructure Deterioration Models." *Transportation Research Board, 73rd Annual Meeting, Preprint Paper No. 940044*. Transportation Research Board: Washington, D.C.
- Miller, R.A. and Parekh, K. (1994). "Destructive Testing of a Deteriorated Prestressed Box Bridge Beam." *Transportation Research Board, 73rd Annual Meeting, Preprint Paper No. 940468*. Transportation Research Board: Washington, D.C.
- Moses, F. (1992). "Truck Weight Effects on Bridge Costs." *Report No. FHWA/OH-93/001*. Department of Civil Engineering, Case Western Reserve University: Cleveland.
- Moses, F. and Verma, D. (1987). "Load Capacity Evaluation of Existing Bridges." *National Cooperative Highway Research Program Report No. 301*. Transportation Research Board: Washington, D.C.
- Mufti, A.A., Tadros, G., and Agarwal, A.C. (1994). "On the Use of Finite Element Programs in Structural Evaluation and Development of Design Charts." *Canadian Journal of Civil Engineering*. Vol. 21, 797-804.

- Muller, J.F. and Dux, P.F. (1992). "Prestressed Concrete Railway Bridge Live Load Strains." *ASCE Journal of Structural Engineering*. Vol. 118, No. 2, 359-376.
- Nassif, H.H. and Nowak, A.S. (1995). "Dynamic Load Spectra for Girder Bridges." *Transportation Research Record, No. 1476*. National Academy Press: Washington, D.C., 69-83.
- Newmark, N.M. (1959). "A Method of Computation for Structural Dynamics." *ASCE Journal of Engineering Mechanics*. Vol. 85, No. EM 3, 67-94.
- Ng, S.F. and Chen, X. (1995). "Analysis of Arbitrary Mindlin Plates or Bridge Decks by Spline Finite Strip Method." *Computers & Structures*. Vol. 54, No. 1, 111-118.
- Nowak, A.S., Nassif, H.H., and Frank, K.H. (1993a). "Fatigue Load Spectra for a Steel Girder Bridge." *Transportation Research Record, No. 1393*. National Academy Press: Washington, D.C., 154-161.
- Nowak, A.S., Nassif, H.H., and DeFrain, L. (1993b). "Effect of Truck Loads on Bridges." *ASCE Journal of Transportation Engineering*. Vol. 119, No. 6, 853-867.
- Oesterle, R.G., Glikin, J.D., and Larson, S.C. (1989). "Design of Precast Prestressed Bridge Girders Made Continuous." *National Cooperative Highway Research Program Report No. 322*. Transportation Research Board: Washington, D.C.
- Paultre, P., Proulx, J., and Talbot, M. (1995). "Dynamic Testing Procedures for Highway Bridges Using Traffic Loads." *ASCE Journal of Structural Engineering*. Vol. 121, No. 2, 362-376.
- Pentas, H.A., Avent, R.R., Gopu, V.K.A., and Rebello, K.J. (1995). "Field Study of Longitudinal Movements in Composite Bridges." *Transportation Research Record, No. 1476*. National Academy Press: Washington, D.C., 117-128.
- Petrou, M.F., Perdikaris, P.C., and Wang, A. (1994). "Fatigue Behavior of Non-Composite Reinforced Concrete Bridge Deck Models - Stationary Pulsating Versus Moving Constant Wheel Load and AASHTO Versus OHBDC Design." *Transportation Research Board, 73rd Annual Meeting, Preprint Paper No. 940498*. Transportation Research Board: Washington, D.C.
- Robson, B.N. and Harik, I.E. (1996). "Field Testing of a Seismically Isolated, Skewed, P/C Girder Bridge." *IBC Paper No. 96-48*. 1996 International Bridge

Conference Proceedings, 240-245.

- Roschke, P.N. (1995). "Dynamic Vehicle Loading on a Slab Bridge Using Multiple Actuators." *Transportation Research Record, No. 1476*. National Academy Press: Washington, D.C., 31-36.
- Rösler, M. (1994). "Dynamic Interaction Between Bridge and Vehicle." *Transportation Research Record, No. 1460*. National Academy Press: Washington, D.C., 81-86.
- Sanders, W.W. and Elleby, H.A. (1970). "Distribution of Wheel Loads on Highway Bridges." *National Cooperative Highway Research Program Report No. 83*. Highway Research Board: Washington, D.C.
- Saraf, V., Sokolik, A.F., and Nowak, A.S. (1996). "Proof Load Testing of Highway Bridges." *Transportation Research Record, No. 1541*. National Academy Press: Washington, D.C., 51-57.
- Shahrooz, B.M., Miller, R.A., Saraf, V.K., and Godbole, B. (1994). "Behavior of RC Slab Bridges During and After Repair." *Transportation Research Board, 73rd Annual Meeting, Preprint Paper No. 940469*. Transportation Research Board: Washington, D.C.
- Shanafelt, G.O. and Horn, W.B. (1980). "Damage Evaluation and Repair Methods for Prestressed Concrete Bridge Members." *National Cooperative Highway Research Program Report No. 226*. Transportation Research Board: Washington, D.C.
- Sithichaikasem, S. and Gamble, W.L. (1972). "Effects of Diaphragms in Bridges With Prestressed Concrete I-Section Girders." *Structural Research Series No. 383*. Illinois Cooperative Highway Research Program, Series No. 128: University of Illinois.
- Spiegel, M.R. (1974). *Fourier Analysis With Applications to Boundary Value Problems*. Schaum's Outline Series, McGraw-Hill Book Company: New York.
- Stallings, J.M. and Yoo, C.H. (1993a). "Tests and Ratings of Short-Span Steel Bridges." *ASCE Journal of Structural Engineering*. Vol. 119, No. 7, 2150-2168.
- Stallings, J.M., Cousins, T.E., and Rutland, S.K. (1993b). "Evaluation of Fatigue Cracking in I-65 Mobile Delta Crossing Bridges Volume III: Floortruss-Girder Connections." *Project Number ST 2019-16*. Highway Research Center: Auburn

University.

- Stallings, J.M., Cousins, T.E., and Stafford, T.E. (1996a). "Effects of Removing Diaphragms From a Steel Girder Bridge." *Transportation Research Record*, No. 1541. Transportation Research Board: Washington, D.C., 183-188.
- Stallings, J.M., Cousins, T.E., and Tedesco, J.W. (1996b). "Fatigue of Diaphragm-Girder Connections." *Project Number RP 930-307*. Highway Research Center: Auburn University.
- Stanton, J.F. and Mattock, A.H. (1986). "Load Distribution and Connection Design for Precast Stemmed Multibeam Bridge Superstructures." *National Cooperative Highway Research Program Report No. 287*. Transportation Research Board: Washington, D.C.
- Su, X. and Zhu, B. (1994). "Algorithm for Hysteresis Analysis of Prestressed Concrete Frames." *ASCE Journal of Structural Engineering*. Vol. 120, No. 6, 1732-1744.
- Tabsh, S.W. (1994). "Simple Live Load Distribution Factors for Girder Bridges." *Proceedings of Structures Congress XII*, Volume 2. American Society of Civil Engineers: New York, 497-502.
- Tarhini, K.M. and Frederick, G.R. (1995). "Lateral Load Distribution in I-Girder Bridges, Technical Note." *Computers & Structures*. Vol. 54, No. 2, 351-354.
- Tedesco, J.W., Stallings, J.M., and Tow, D.R. (1995). "Finite Element Method Analysis of Bridge Girder-Diaphragm Interaction." *Computers & Structures*. Vol. 56, No. 2/3, 461-473.
- Walsh, D.P., Simon, S., and Bsu, T.K. (1994). "Evaluation of Vibrating Webs on the Silas N. Pearman Bridge Charleston, South Carolina." *IBC Paper No. 94-25*. 1994 International Bridge Conference Proceedings, 160-170.
- Wang, T.L., Shahawy, M., and Huang, D.Z. (1992). "Impact in Highway Prestressed Concrete Bridges." *Computers & Structures*. Vol. 44, No. 3, 525-534.
- Wang, T.L., Huang, D.Z., and Shahawy, M. (1993). "Vibration and Impact in Multigirder Steel Bridges." *Transportation Research Record*, No. 1393. National Academy Press: Washington, D.C., 96-103.
- Wilson, E.L. (1996). *Three Dimensional Dynamic Analysis of Structures With Emphasis on Earthquake Engineering*. Computers and Structures, Inc.:

Berkeley, CA.

- Yang, Y. and Lin, B. (1995a). "Vehicle-Bridge Interaction Analysis by Dynamic Condensation Method." *ASCE Journal of Structural Engineering*. Vol. 121, No. 11, 1636-1643.
- Yang, Y., Liao, S., and Lin, B. (1995b). "Impact Formulas for Vehicles Moving Over Simple and Continuous Beams." *ASCE Journal of Structural Engineering*. Vol. 121, No. 11, 1644-1650.
- Zienkiewicz, O.C. and Taylor, R.L. (1989). *The Finite Element Method Volume 1: Basic Formulation and Linear Problems*. Fourth Edition. McGraw-Hill Book Company: New York.
- Zwerneman, F.J., West, A.B., and Lim, K.S. (1993). "Fatigue Damage to Steel Bridge Diaphragms." *ASCE Journal of Performance of Constructed Facilities*. Vol. 7, No. 4, 207-224.

APPENDIX A: STATIC TEST INSTRUMENTATION

All steel bars with test instruments were fitted with electrical resistance strain gages from Measurements Group, Inc. The strain gages were 0.25 in (6.35 mm) in length and had a nominal resistance of 350 ohms. The rebars were ground flat with minimal diameter loss and polished with a Dremel tool (Figures A.1 and A.2). The strain gage was then applied in a four-step process. First, the smooth steel surface was degreased and cleaned with an acidic solution (M-Prep Conditioner A). The acid was

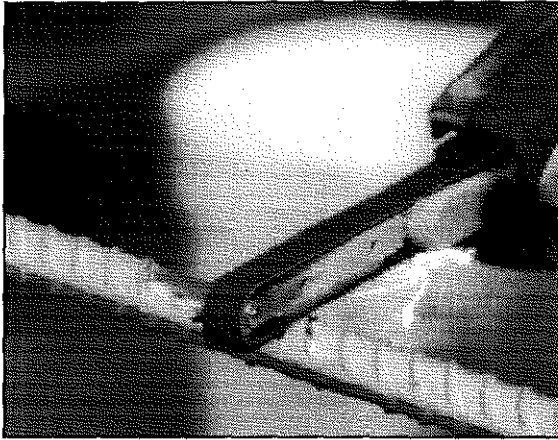


Figure A.1. Grinding of Rebar.

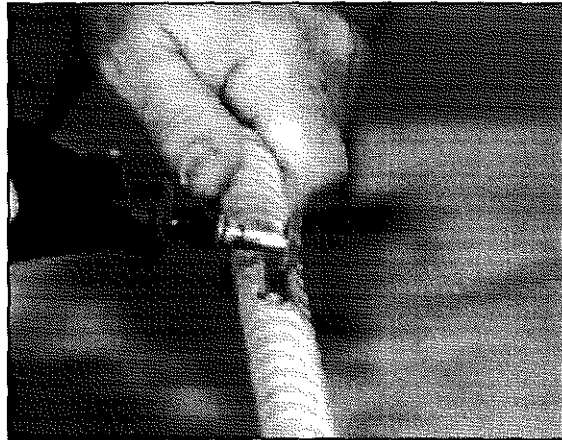


Figure A.2. Polishing of Rebar.

subsequently neutralized with a base (M-Prep Neutralizer 5A). Second, a strain gage on cellophane tape was fastened to the rebar with the strain gage manufacturer's adhesive (M-Bond 200 adhesive). A catalyst

(M-Bond 200 catalyst) was used to insure proper application and rapid curing. Third, once the adhesive was sufficiently cured and wire leads were soldered, a rubber compound (M-Coat B Nitrile Rubber) was spread over the strain gage and exposed wires to protect the strain gage against the final step. These materials are shown in Figure A.3. Finally, Teflon tape was cut to blanket the strain gage system and a polysulfide liquid polymer (M-Coat J - shown applied on an epoxy coated steel bar in Figure A.4) was applied to seal the system against the chemical and thermal reactions of curing concrete. All steel bars

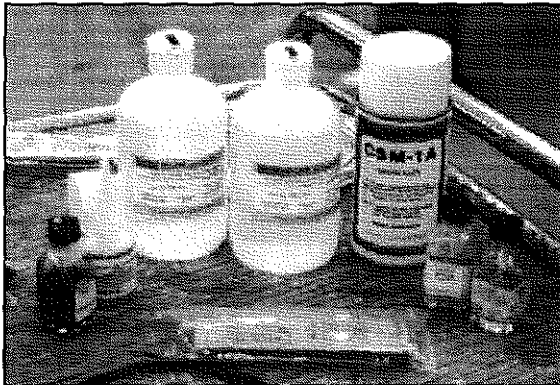


Figure A.3. Surface Preparation and Strain Gage Mounting Materials.

were instrumented with strain gages in the laboratory prior to placement in the respective bridge decks.

In order to minimize the time required to mount concrete strain gages in the field, reusable strain gages manufactured by Bridge Diagnostics, Inc., were used to complete the testing of the two bridges. These gages required little surface preparation and could be easily moved to different locations, thus preventing the need to use an inordinate amount of the typical "glue-on" gages. The gages have holes at either end, spaced 3 in (76.2 mm) apart, through which the threaded posts of the mounting tabs pass.

A mounting template was constructed in the laboratory to expedite the placement of the mounting tabs on the bridge girders. Once locations were identified and marked, the surface was cleaned of any loose materials with a wire brush and sandpaper. The tabs were inserted into the template and glued to the girders with an industrial strength adhesive. A catalyst was once again used to reduce the adhesive curing time. The process of mounting the strain gages was then just a matter of placing the gage on the tabs and tightening the nut on the threaded post. Figure A.5 shows two reusable strain gages mounted to a girder. Mounting tabs were left in place after the testing in the event future studies were considered.

The tables which follow outlined the color coding and location of the strain gages as described in the text and figures of Chapter 2 (Tables A.1 through A.5) and indicate the sequence in which these gages were read during the static testing of the Southbound (Table A.6) and Northbound bridges (Table A.7). The last table, Table A.8, records the location of the accelerometers during each setup of the dynamic testing of the two bridges.

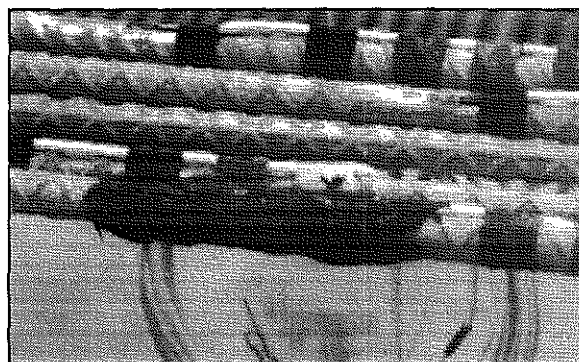


Figure A.4. Liquid Polymer Protective Coating.

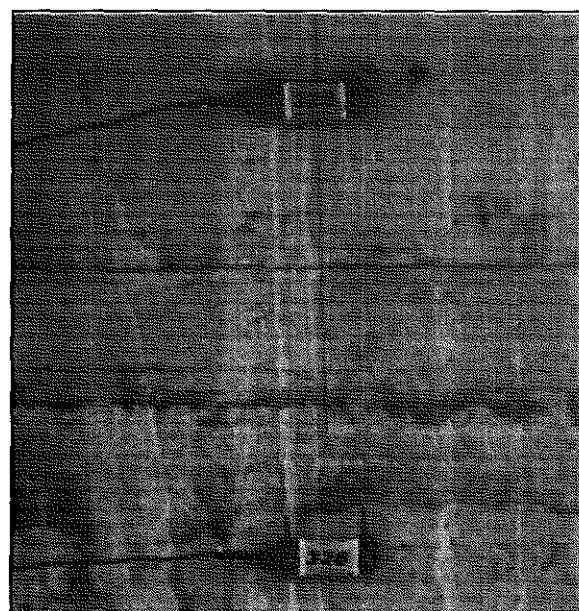


Figure A.5. Reusable Strain Gages Mounted on the Side of a Bridge Girder.

Table A.1: Transverse Bar Color Coding and Placement in the Southbound Bridge.

Location		Designation	Bar Size	Bar Color Coding	Top of Girder to \perp Rebar
1A1	bottom	S1A1B	6	BrBY	2.5 in/63.5 mm
	top	S1A1T	6	GBY	6.25 in/158.75 mm
1A2	bottom	S1A2B	6	BrRY	2.5 in/63.5 mm
	top	S1A2T	6	GRY	6.25 in/158.75 mm
1A3	bottom	S1A3B	6	BrYY	2.5 in/63.5 mm
	top	S1A3T	6	GYY	6.25 in/158.75 mm
1A4	bottom	S1A4B	6	BrB/	2.5 in/63.5 mm
1B1	bottom	S1B1B	6	BrBR	2.5 in/63.5 mm
	top	S1B1T	6	GBR	6.25 in/158.75 mm
1B2	bottom	S1B2B	6	BrRR	2.5 in/63.5 mm
	top	S1B2T	6	GRR	6.25 in/158.75 mm
1B3	bottom	S1B3B	6	BrYR	2.5 in/63.5 mm
	top	S1B3T	6	GYR	6.25 in/158.75 mm
1B4	bottom	S1B4B	6	BrY	2.5 in/63.5 mm
1B5	bottom	S1B5B	6	RY	2.5 in/63.5 mm
1C1	bottom	S1C1B	6	BrBB	2.5 in/63.5 mm
	top	S1C1T	6	GBB	6.25 in/158.75 mm
1C2	bottom	S1C2B	6	BrRB	2.5 in/63.5 mm
	top	S1C2T	6	GRB	6.25 in/158.75 mm
1C3	bottom	S1C3B	6	BrYB	2.5 in/63.5 mm
	top	S1C3T	6	GYB	6.25 in/158.75 mm

Table A.2: Transverse Bar Color Coding and Placement in the Northbound Bridge.

Location		Designation	Bar Size	Bar Color Coding	Top of Girder to \bar{c} Rebar
1A1	bottom	N1A1B	5	BrBY	2.5 in/63.5 mm
	top	N1A1T	5	GBY	6.25 in/158.75 mm
1A2	bottom	N1A2B	5	BrRY	2.5 in/63.5 mm
	top	N1A2T	5	GRY	6.25 in/158.75 mm
1A3	bottom	N1A3B	5	BrYY	2.5 in/63.5 mm
	top	N1A3T	5	GY Y	6.25 in/158.75 mm
1B1	bottom	N1B1B	6	BrBR	2.5 in/63.5 mm
	top	N1B1T	5	GBR	6.25 in/158.75 mm
1B2	bottom	N1B2B	6	BrRR	2.5 in/63.5 mm
	top	N1B2T	5	GRR	6.25 in/158.75 mm
1B3	bottom	N1B3B	6	BrYR	2.5 in/63.5 mm
	top	N1B3T	5	GYR	6.25 in/158.75 mm
1C1	bottom	N1C1B	5	BrBB	2.5 in/63.5 mm
	top	N1C1T	5	GBB	6.25 in/158.75 mm
1C2	bottom	N1C2B	5	BrRB	2.5 in/63.5 mm
	top	N1C2T	5	GRB	6.25 in/158.75 mm
1C3	bottom	N1C3B	5	BrYB	2.5 in/63.5 mm
	top	N1C3T	5	GYB	6.25 in/158.75 mm

Table A.3: Longitudinal Bar Color Coding and Placement in the Southbound Bridge.

Location	Designation	Bar Size	Bar Color Coding	Top of Girder to ϕ Rebar
2A	S2A	6	BrR	3.25 in/82.55 mm
2B	S2B	6	RB/	3.25 in/82.55 mm
2C	S2C	6	GB/	3.25 in/82.55 mm
2D	S2D	6	GY	3.25 in/82.55 mm
2E	S2E	6	GB	3.25 in/82.55 mm
2F	S2F	6	GR	3.25 in/82.55 mm
2G	S2G	6	BrB	3.25 in/82.55 mm
2H	S2H	6	GBr	3.25 in/82.55 mm

Table A.4: Longitudinal Bar Color Coding and Placement in the Northbound Bridge.

Location	Designation	Bar Size	Bar Color Coding	Top of Girder to ϕ Rebar
2A	N2A	6	GR	3.25 in/82.55 mm
2B	N2B	6	RY	3.25 in/82.55 mm
2C	N2C	6	RB	3.25 in/82.55 mm
2D	N2D	6	RB/	3.25 in/82.55 mm
2E	N2E	6	GBr	3.25 in/82.55 mm
2F	N2F	6	BrB/	3.25 in/82.55 mm
2G	N2G	6	BrB	3.25 in/82.55 mm
2H	N2H	6	GY	3.25 in/82.55 mm

Table A.5: Anchor Bar Color Coding and Orientation in the Southbound Bridge.

Location	Designation	Orientation (Angle to Vertical)	Color of Wire on Gage
3A	S3A	0°	Red
3B	S3B	90°	Blue
3C	S3C	0°	Red
3D	S3D	90°	Blue
3E	S3E	0°	Red

3F	S3F	90°	Blue
3G	S3G	0°	Red
3H	S3H	90°	Blue
3J	S3J	0°	Red
3K	S3K	90°	Blue
3L	S3L	0°	Red
3M	S3F	90°	Blue

Table A.6: Southbound Bridge Static Testing Schedule.

Item	Gage No.	Test SS1		Test SS2		Test SS3	
		Code	Color	Code	Color	Code	Color
Foil Strain Gages on Steel Rebar	1	S2A	BrR	S2A	BrR	S1A1B	BrBY
	2	S2B	RBl	S2B	RBl	S1A1T	GBY
	3	S2C	GBl	S2C	GBl	S1A2B	BrRY
	4	S2D	GY	S2D	GY	S1A2T	GRY
	5	S2E	GB	S2E	GB	S1A3B	BrYY
	6	S2F	GR	S2F	GR	S1A3T	GYG
	7	S2G	BrB	S2G	BrB	S1A4B	BrBl
	8	S2H	GBr	S2H	GBr	S1B1B	BrBR
	9					S1B1T	GBR
	10	S3A	R	S3A	R	S1B2B	BrRR
	11	S3B	B	S3B	B	S1B2T	GRR
	12	S3C	R	S3C	R	S1B3B	BrYR
	13	S3D	B	S3D	B	S1B3T	GYR
	14	S3E	R	S3E	R	S1B4B	BrY
	15	S3F	B	S3F	B	S1B5B	RY
	16	S3G	R	S3G	R	S1C1B	BrBB
	17	S3H	B	S3H	B	S1C1T	GBB
	18	S3J	R	S3J	R	S1C2B	BrRB
	19	S3K	B	S3K	B	S1C2T	GRB
	20	S3L	R	S3L	R	S1C3B	BrYB
	21	S3M	B	S3M	B	S1C3T	GYB

Table A.6 (cont'd): Southbound Bridge Static Testing Schedule.

Item	Gage No.	Test SS1	Test SS2	Test SS3
Reusable Strain Gages	321	S5AB	S4A1	S6D1E3
	322	S5AM	S4A2	S6D1C1
	323	S5AT	S4A3	S6D1B1
	324	S5BB	S4A4	S6D1A1
	325	S5BM	S4A5	S6D1D3
	326	S5BT	S4B1	S6D2A1
	335	S5CB	S4B2	S6D2D3
	290	S5CM	S4B3	S6D2C1
	329	S5CT	S4B4	S6D2E3
	330	S5DB	S4B5	S6D2B1
	331	S5DM		
	332	S5DT		
	LVDT	42	S7AV	S7CV
43		S7BT	S7DT	
44		S7AT	S7CT	
45		S7BV	S7DV	

Table A.6 (cont'd): Southbound Bridge Static Testing Schedule.

Item	Gage No.	Test SS4	Test SS5
Reusable Strain Gages	328	S6D1A1	S6D2A1
	290	S6D1A2	S6D2A2
	----	S6D1A3	S6D2A3
	332	S6D1B1	S6D2B1
	331	S6D1B2	S6D2B2
	330	S6D1B3	S6D2B3
	335	S6D1C1	S6D2C1
	334	S6D1C2	S6D2C2
	333	S6D1C3	S6D2C3
	325	S6D1D1	S6D2D1
	324	S6D1D2	S6D2D2
	323	S6D1D3	S6D2D3
	329	S6D1E1	S6D2E1
	322	S6D1E2	S6D2E2
	321	S6D1E3	S6D2E3
LVDT	20	S6D1F	S6D2F

Table A.7: Northbound Bridge Static Testing Schedule.

Item	Gage No.	Test NS1		Test NS2	
		Code	Color	Code	Color
Foil Strain Gages on Steel Rebar	1	N1A1B	BrBY	N2A	GR
	2	N1A1T	GBY	N2B	RY
	3	N1A2B	BrRY	N2C	RB
	4	N1A2T	GRY	N2D	RB/
	5	N1A3B	BrYY	N2E	GBr
	6	N1A3T	GYY	N2F	BrB/
	7	N1B1B	BrBR	N2G	BrB
	8	N1B1T	GBR	N2H	GY
	9	N1B2B	BrRR		
	10	N1B2T	GRR		
	11	N1B3B	BrYR		
	12	N1B3T	GYR		
	13	N1C1B	BrBB		
	14	N1C1T	GBB		
	15	N1C2B	BrRB		
	16	N1C2T	GRB		
	17	N1C3B	BrYB		
	18	N1C3T	GYB		

Table A.7 (cont'd): Northbound Bridge Static Testing Schedule.

Instrument	Gage No.	Test NS1	Test NS2
Reusable Strain Gages	321	N3AB	N3AB
	322	N3AM	N3AM
	323	N3AT	N3AT
	324	N3BB	N3BB
	325	N3BM	N3BM
	326	N3BT	N3BT
	335	N3CB	N3CB
	290	N3CM	N3CM
	329	N3CT	N3CT
	330	N3DB	N3DB
	331	N3DM	N3DM
	332	N3DT	N3DT
	333	N3E	N3E
	334	N3F	N3F
LVDT	42	N4AT	N4DT
	43	N4AV	N4BV
	44	N4CV	N4DV
	45	N4BT	N4CT

Table A.8: Southbound and Northbound Bridge Dynamic Testing Schedule.

Accel. No. ⁰	SD1/ND1		SD2/ND2		SD3/ND3		SD4/ND4		SD5/ND5	
	Code	Color	Code	Color	Code	Color	Code	Color	Code	Color
1H	8E	B	8E	B	8E	B	8E	B	8E	B
1T										
1V										
2H	8W	Bl	8W	Bl	8W	Bl	8W	Bl	8W	Bl
2T										
2V										
3H	13W	Y	7W	G	2W	G	4E	Y	9E	G
3T										
3V										
4H	12W	W	6W	O	1W	O	5E	W	10E	O
4T										
4V										
5H	11W	R	5W	R	1E	Y	6E	R	11E	R
5T										
5V										
6H	10W	O	4W	W	2E	W	7E	O	12E	W
6T										
6V										
7H	9W	G	3W	Y	3E	R	9E	G	13E	Y
7T										
7V										

⁰Accelerometers 1 and 2 are the base station accelerometers (L=longitudinal, T=transverse, V=vertical).

APPENDIX B: COMPUTER PROGRAM TO PROCESS STATIC TEST FILES

```

DECLARE SUB DIAPHRAGM ()
DECLARE SUB NORTHPASS ()
DECLARE SUB SOUTHPASS ()
DECLARE SUB STATION ()
DECLARE SUB TITLE ()
REM
DIM d(15000), avg(100), std(100)
COMMON SHARED file$, stat$
REM
REM*****
REM*
REM*      *
REM* Binary File Conversion to ASCII format of US23 Bridges Test Data *
REM* (reports average and standard deviation values for all channels) *
REM*      *
REM* Written by:      Jeff Griffin      *
REM*      Kentucky Transportation Center      *
REM*      University of Kentucky      *
REM*      February 7, 1997      *
REM*      *
REM* Any person using this program must realize filenames and data paths *
REM* are specific to the US 23 project and the author's personal files *
REM*      *
REM*****
REM
CLS
REM
10 CLS
SCREEN 12
CALL TITLE
REM
LOCATE 17, 10: INPUT "What bridge test do you wish to consider (e.g., N=NORTH)"; brdg$
bridge$ = UCASE$(brdg$)
COLOR 9
IF bridge$ = "N" THEN
LOCATE 18, 21: PRINT "Path = D:\GRIFFIN\BRIDGE23.40\DATA\STATIC\NORTH\"
CALL NORTHPASS
ELSEIF bridge$ = "S" THEN
LOCATE 18, 21: PRINT "Path = D:\GRIFFIN\BRIDGE23.40\DATA\STATIC\SOUTH\"
CALL SOUTHPASS
ELSEIF bridge$ = "D" THEN
LOCATE 18, 21: PRINT "Path = D:\GRIFFIN\BRIDGE23.40\DATA\STATIC\DIAPHR~1\"
CALL DIAPHRAGM
ELSE
GOTO 30
END IF
REM

```

```

CALL STATION
COLOR 15
LOCATE 26, 22: INPUT "Do you wish to change anything"; ans$
ans$ = UCASE$(ans$)
IF ans$ = "Y" THEN
    GOTO 10
ELSE
    GOTO 20
END IF
REM
20 CLS
filesum$ = file$ + ".sum"
OPEN filesum$ FOR OUTPUT AS #1
FOR i = 1 TO 58
    IF i > 34 AND i < 41 THEN
        GOTO 25
    ELSEIF i = 47 THEN
        GOTO 25
    ELSEIF i = 48 THEN
        GOTO 25
    ELSEIF i > 50 AND i < 57 THEN
        GOTO 25
    END IF
    chnum$ = LTRIM$(RTRIM$(STR$(i - 1)))
    filein$ = file$ + chnum$ + ".DAT"
    PRINT TAB(10); "Processing channel no. ";
    COLOR 9
    PRINT chnum$
REM
    sum = 0
    avg(i) = 0
    sumstd = 0
    sumnoc = 0
    std(i) = 0
    j = 1
REM
    OPEN filein$ FOR BINARY AS #2
    DO WHILE NOT EOF(2)
        GET #2, , d(j)
        sum = sum + d(j)
        j = j + 1
    LOOP
    avg(i) = sum / (j - 2)
    COLOR 10
    FOR k = 1 TO (j - 2)
        sumstd = (avg(i) - d(k)) ^ 2
        sumnoc = sumnoc + sumstd
    NEXT k
    std(i) = (sumnoc / k) ^ .5
    COLOR 15
    CLOSE #2

```



```

    PRINT #1, filein$; ","; i - 1; ","; avg(i); ","; std(i)
25 NEXT i
    CLOSE #1
REM
30 CALL TITLE
    BEEP
    LOCATE 20, 19: INPUT "Do you wish to analyze another file set"; ans$
    ans$ = UCASE$(ans$)
    IF ans$ = "Y" THEN
        GOTO 10
    ELSE
        COLOR 11
        LOCATE 23, 25: PRINT "Thank you and have a good day."
40 END
    END IF

SUB DIAPHRAGM
    COLOR 15
    LOCATE 19, 10: INPUT "What test no. do you wish to consider (e.g., 1, 2, etc.)"; pass$
    COLOR 9
    IF pass$ = "1" THEN
        file$ = UCASE$("d:\griffin\bridge23.40\data\static\diaphr~1\d1\")
        LOCATE 20, 15: PRINT "Path = D:\GRIFFIN\BRIDGE23.40\DATA\STATIC\DIAPHR~1\D1\"
    ELSEIF pass$ = "2" THEN
        file$ = UCASE$("d:\griffin\bridge23.40\data\static\diaphr~1\d2\")
        LOCATE 20, 15: PRINT "Path = D:\GRIFFIN\BRIDGE23.40\DATA\STATIC\DIAPHR~1\D2\"
    END IF
END SUB

SUB NORTHPASS
    COLOR 15
    LOCATE 19, 10: INPUT "What test no. do you wish to consider (e.g., 1, 2, etc.)"; pass$
    COLOR 9
    IF pass$ = "1" THEN
        file$ = UCASE$("d:\griffin\bridge23.40\data\static\north\n1\")
        LOCATE 20, 18: PRINT "Path = D:\GRIFFIN\BRIDGE23.40\DATA\STATIC\NORTH\N1\"
    ELSEIF pass$ = "2" THEN
        file$ = UCASE$("d:\griffin\bridge23.40\data\static\north\n2\")
        LOCATE 20, 18: PRINT "Path = D:\GRIFFIN\BRIDGE23.40\DATA\STATIC\NORTH\N2\"
    ELSEIF pass$ = "4" THEN
        file$ = UCASE$("d:\griffin\bridge23.40\data\static\north\n4\")
        LOCATE 20, 18: PRINT "Path = D:\GRIFFIN\BRIDGE23.40\DATA\STATIC\NORTH\N4\"
    ELSEIF pass$ = "5" THEN
        file$ = UCASE$("d:\griffin\bridge23.40\data\static\north\n5\")
        LOCATE 20, 18: PRINT "Path = D:\GRIFFIN\BRIDGE23.40\DATA\STATIC\NORTH\N5\"
    ELSEIF pass$ = "6" THEN
        file$ = UCASE$("d:\griffin\bridge23.40\data\static\north\n6\")
        LOCATE 20, 18: PRINT "Path = D:\GRIFFIN\BRIDGE23.40\DATA\STATIC\NORTH\N6\"
    ELSEIF pass$ = "7" THEN
        file$ = UCASE$("d:\griffin\bridge23.40\data\static\north\n7\")
        LOCATE 20, 18: PRINT "Path = D:\GRIFFIN\BRIDGE23.40\DATA\STATIC\NORTH\N7\"

```

```
END IF
END SUB
```

```
SUB SOUTHPASS
```

```
  COLOR 15
```

```
  LOCATE 19, 10: INPUT "What test no. do you wish to consider (e.g., 1, 2, etc.)"; pass$
```

```
  COLOR 9
```

```
  IF pass$ = "1" THEN
```

```
    file$ = UCASE$("d:\griffin\bridge23.40\data\static\south\s1\")
```

```
    LOCATE 20, 18: PRINT "Path = D:\GRIFFIN\BRIDGE23.40\DATA\STATIC\SOUTH\S1\"
```

```
  ELSEIF pass$ = "2" THEN
```

```
    file$ = UCASE$("d:\griffin\bridge23.40\data\static\south\s2\")
```

```
    LOCATE 20, 18: PRINT "Path = D:\GRIFFIN\BRIDGE23.40\DATA\STATIC\SOUTH\S2\"
```

```
  ELSEIF pass$ = "3" THEN
```

```
    file$ = UCASE$("d:\griffin\bridge23.40\data\static\south\s3\")
```

```
    LOCATE 20, 18: PRINT "Path = D:\GRIFFIN\BRIDGE23.40\DATA\STATIC\SOUTH\S3\"
```

```
  ELSEIF pass$ = "4" THEN
```

```
    file$ = UCASE$("d:\griffin\bridge23.40\data\static\south\s4\")
```

```
    LOCATE 20, 18: PRINT "Path = D:\GRIFFIN\BRIDGE23.40\DATA\STATIC\SOUTH\S4\"
```

```
  ELSEIF pass$ = "5" THEN
```

```
    file$ = UCASE$("d:\griffin\bridge23.40\data\static\south\s5\")
```

```
    LOCATE 20, 18: PRINT "Path = D:\GRIFFIN\BRIDGE23.40\DATA\STATIC\SOUTH\S5\"
```

```
  ELSEIF pass$ = "6" THEN
```

```
    file$ = UCASE$("d:\griffin\bridge23.40\data\static\south\s6\")
```

```
    LOCATE 20, 18: PRINT "Path = D:\GRIFFIN\BRIDGE23.40\DATA\STATIC\SOUTH\S6\"
```

```
  ELSEIF pass$ = "7" THEN
```

```
    file$ = UCASE$("d:\griffin\bridge23.40\data\static\south\s7\")
```

```
    LOCATE 20, 18: PRINT "Path = D:\GRIFFIN\BRIDGE23.40\DATA\STATIC\SOUTH\S7\"
```

```
  ELSEIF pass$ = "8" THEN
```

```
    file$ = UCASE$("d:\griffin\bridge23.40\data\static\south\s8\")
```

```
    LOCATE 20, 18: PRINT "Path = D:\GRIFFIN\BRIDGE23.40\DATA\STATIC\SOUTH\S8\"
```

```
  ELSEIF pass$ = "9" THEN
```

```
    file$ = UCASE$("d:\griffin\bridge23.40\data\static\south\s9\")
```

```
    LOCATE 20, 18: PRINT "Path = D:\GRIFFIN\BRIDGE23.40\DATA\STATIC\SOUTH\S9\"
```

```
  END IF
```

```
END SUB
```

```
SUB STATION
```

```
  COLOR 15
```

```
  LOCATE 21, 10: INPUT "What file set do you wish to consider (e.g., N1-1, etc.)"; stat$
```

```
  stat$ = UCASE$(stat$)
```

```
  file$ = file$ + stat$ + "CH"
```

```
  COLOR 9
```

```
  LOCATE 22, 6: PRINT "Files = "; file$ + "*.DAT"
```

```
END SUB
```

```
SUB TITLE
```

```
  CLS
```

```
  COLOR 9
```

```
  PRINT "    ***      ***      *****      *****      *****"
```

```
  PRINT "    ***      ***      *****      *****      *****"
```

```

PRINT "   ***   ***   ***           ***   ****"
PRINT "   ***   ***   ***           ***   ****"
PRINT "   ***   ***   ****             ***   ****"
PRINT "   ***   ***   ****             ***   ****"
PRINT "   ***   ***           ***   ***   ****"
PRINT "   ***   ***           ***   ***   ****"
PRINT " ***** ***** ***** ***** *****"
PRINT " ***** ***** ***** ***** *****"
PRINT
LINE (0, 165)-(700, 165), 10
COLOR 14
PRINT "   Binary File Conversion to ASCII format of US23 Bridges Test Data"
PRINT "   (reports average and standard deviation values at the end of file)"
LINE (0, 215)-(700, 215), 10
COLOR 15
END SUB

```

APPENDIX C: STATIC TEST EXPERIMENTAL RESULTS

Northbound Bridge

Setup No. 1 - Bumper to Bumper Trucks in Lane 1

ch no.	sta 2	sta 3	sta 4	sta 5	sta 6	sta 7	sta 8	sta 9	sta 10	sta 11	sta 12	description
0	-552.40	-133.52	-121.19	-318.57	-328.18	-345.66	-396.16	-410.77	-267.07	-232.07	-458.14	microstrain at transverse steel gage, location N1A1B
1	-1.83	-3.04	-3.71	-4.45	-2.14	5.23	10.88	6.38	1.66	0.07	0.41	microstrain at transverse steel gage, location N1A1T
2	3.71	3.67	5.47	5.15	11.51	10.49	13.44	9.69	11.90	14.89	11.76	microstrain at transverse steel gage, location N1A2B
3	0.89	0.63	0.12	-0.01	0.47	0.15	0.54	0.06	2.96	2.94	2.51	microstrain at transverse steel gage, location N1A2T
4	-86.02	-193.93	-24.03	-46.65	-54.22	-46.15	-167.51	-79.69	-270.97	-77.40	-507.50	microstrain at transverse steel gage, location N1A3B
5	0.00	0.00	0.00	0.00	0.00	0.00	0.00	0.00	-5000.00	-5000.00	-5000.00	microstrain at transverse steel gage, location N1A3T
6	-1.43	-2.49	-3.68	-5.44	8.52	5.53	3.26	3.86	6.25	5.13	4.36	microstrain at transverse steel gage, location N1B1B
7	0.00	0.00	0.00	0.00	0.00	0.00	0.00	0.00	-5000.00	-5000.00	-5000.00	microstrain at transverse steel gage, location N1B1T
8	0.18	3.22	2.97	-1.66	-29.88	-48.44	-28.14	6.45	-54.94	-54.95	-57.00	microstrain at transverse steel gage, location N1B3B
9	5.52	6.03	12.69	30.83	205.90	267.87	200.91	41.61	307.80	316.37	314.60	microstrain at transverse steel gage, location N1B3T
10	0.00	0.00	0.00	0.00	0.00	0.00	0.00	0.00	499.78	499.78	499.78	microstrain at transverse steel gage, location N1C1B
11	0.00	0.00	0.00	0.00	0.00	0.00	0.00	0.00	-500.00	-500.00	-500.00	microstrain at transverse steel gage, location N1C1T
12	3.74	4.19	7.62	6.60	-20.44	-21.46	-20.02	-19.26	-19.90	-21.62	-21.91	microstrain at transverse steel gage, location N1C2B
13	14.35	20.59	38.04	66.66	135.48	145.87	92.61	90.68	199.35	209.06	205.88	microstrain at transverse steel gage, location N1C2T
14	1.21	0.66	-0.74	-1.48	-1.80	-1.01	-1.31	-7.01	-10.85	-15.17	-17.23	microstrain at transverse steel gage, location N1C3B
15	0.00	0.00	0.00	0.00	0.00	0.00	0.00	0.00	499.78	499.78	499.78	microstrain at transverse steel gage, location N1C3T
21	-0.51	0.46	2.85	4.72	-0.16	-18.19	-45.99	-49.77	-22.58	1.72	8.49	microstrain at girder cross section, location N3AB
22	0.27	1.10	3.04	4.88	1.66	-10.13	-28.57	-32.03	-14.85	1.64	6.50	microstrain at girder cross section, location N3AM
23	0.22	0.19	0.34	0.81	0.53	-0.41	-1.42	-2.43	-0.56	1.56	1.97	microstrain at girder cross section, location N3AT
24	-0.40	-0.84	-1.12	-1.14	-0.49	1.38	2.18	0.97	-0.14	-0.23	-0.32	microstrain at girder cross section, location N3BT
25	0.17	-0.28	-1.57	-2.21	0.08	6.45	14.00	16.07	8.45	5.39	10.11	microstrain at girder cross section, location N3CB
27	-0.65	-0.83	-0.78	-0.41	-0.45	-0.94	-1.79	-2.34	-1.70	-0.98	0.18	microstrain at girder cross section, location N3CT
28	0.39	-0.07	-1.52	-2.56	-1.23	1.56	2.39	-0.49	-2.45	-1.86	-1.06	microstrain at girder cross section, location N3DB
29	-0.17	-0.50	-0.85	-0.63	0.47	2.69	4.17	3.21	1.94	1.70	1.51	microstrain at girder cross section, location N3DM
30	-0.44	-0.51	-0.27	0.15	0.14	-0.13	-0.39	0.46	1.10	0.48	-0.73	microstrain at girder cross section, location N3DT
31	-0.48	0.09	2.03	3.18	-0.24	-7.52	-12.81	-10.92	-4.67	1.40	3.36	microstrain at girder cross section, location N3E
32	0.00	0.00	0.00	-0.13	0.00	0.00	0.00	0.00	986.22	999.23	999.31	microstrain at transverse steel gage, location N1B2B
33	-0.42	-1.52	-2.48	-2.57	-6.02	-9.03	-8.87	-7.78	-4.10	-4.35	-4.43	microstrain at transverse steel gage, location N1B2T
40	0.00	0.00	0.00	0.00	0.00	0.00	0.00	0.00	499.78	499.78	499.78	microstrain at transverse steel gage, location N1A1B
41	12.05	18.19	33.22	64.27	147.95	158.52	91.32	84.94	209.67	218.64	216.95	microstrain at transverse steel gage, location N1A1T
42	0.00	0.00	0.00	0.00	0.00	0.02	0.03	0.02	0.01	0.01	0.00	displacement between girders, location N4AT
43	-0.00	-0.01	-0.02	-0.02	0.00	0.06	0.09	0.08	0.04	0.00	-0.01	vertical displacement of girders, location N4AV
44	-0.00	-0.01	-0.02	-0.03	0.01	0.11	0.12	0.12	0.09	0.01	-0.02	vertical displacement of girders, location N4CV
45	0.00	0.00	0.00	0.00	0.00	0.00	0.01	0.01	0.01	0.01	0.00	displacement between girders, location N4BT
48	-0.11	1.04	4.38	6.20	1.05	-11.37	-19.65	-14.56	-3.30	5.11	7.73	microstrain at girder cross section, location N3BB
49	-0.32	-0.22	0.36	0.87	-0.22	-3.09	-5.05	-4.41	-1.36	1.26	2.15	microstrain at girder cross section, location N3BM
56	-0.35	-0.18	0.72	1.22	0.52	-0.49	-1.22	-1.11	-0.22	0.97	1.20	microstrain at girder cross section, location N3F
57	-0.13	-0.63	-1.19	-0.82	1.37	7.51	14.76	16.12	8.54	7.12	13.45	microstrain at girder cross section, location N3CM

Northbound Bridge

Setup No. 1 - Bumper to Bumper Trucks in Lane 2

ch no.	sta 2	sta 3	sta 4	sta 5	sta 6	sta 7	sta 8	sta 9	sta 10	sta 11	sta 12	description
0	22.48	-262.64	-39.39	-107.01	-345.16	-309.76	-345.18	-146.78	-144.64	105.16	-58.42	microstrain at transverse steel gage, location N1A1B
1	1.68	5.86	7.27	9.81	12.67	9.98	15.85	-6.82	-6.82	-6.82	-6.82	microstrain at transverse steel gage, location N1A1T
2	-5.34	10.04	12.39	17.48	30.19	34.00	50.74	-34.60	-34.60	-34.60	-34.60	microstrain at transverse steel gage, location N1A2B
3	0.96	1.10	1.94	1.49	3.37	3.09	7.56	-7.97	-7.97	-7.97	-7.97	microstrain at transverse steel gage, location N1A2T
4	-35.20	62.78	-119.54	37.82	-63.91	-25.14	-156.96	1177.43	1177.43	1177.43	1177.43	microstrain at transverse steel gage, location N1A3B
5	0.00	0.00	0.00	0.00	0.00	0.00	-7500.00	2500.00	2500.00	2500.00	2500.00	microstrain at transverse steel gage, location N1A3T
6	0.39	3.59	4.20	5.98	6.72	3.50	7.13	1.59	1.59	1.59	1.59	microstrain at transverse steel gage, location N1B1B
7	0.00	0.00	0.00	0.00	0.00	0.00	-7500.00	-7500.00	-7500.00	-7500.00	-7500.00	microstrain at transverse steel gage, location N1B1T
8	-3.43	-9.17	-9.66	-10.27	-4.26	-5.19	-137.59	-118.68	-110.09	-111.96	-110.16	microstrain at transverse steel gage, location N1B3B
9	3.01	9.51	10.42	13.96	52.32	47.62	616.32	558.11	531.59	520.99	515.93	microstrain at transverse steel gage, location N1B3T
10	0.00	0.00	0.00	0.00	0.00	0.00	749.65	-249.88	-249.88	-249.88	-249.88	microstrain at transverse steel gage, location N1C1B
11	0.00	0.00	0.00	0.00	0.00	0.00	-750.00	250.00	250.00	250.00	250.00	microstrain at transverse steel gage, location N1C1T
12	0.26	-0.27	0.13	2.00	14.26	14.58	14.84	18.27	18.27	18.27	18.27	microstrain at transverse steel gage, location N1C2B
13	-12.88	-22.45	-26.13	-19.19	73.52	61.45	220.30	-83.62	-83.62	-83.62	-83.62	microstrain at transverse steel gage, location N1C2T
14	-5.16	-5.58	-5.60	-4.61	16.74	18.09	19.24	14.60	14.60	14.60	14.60	microstrain at transverse steel gage, location N1C3B
15	0.00	0.00	0.00	0.00	0.00	0.00	749.65	-249.88	-249.88	-249.88	-249.88	microstrain at transverse steel gage, location N1C3T
21	-0.79	-1.18	-0.91	-2.57	-7.95	-13.53	-11.40	-0.20	-0.20	-0.20	-0.20	microstrain at girder cross section, location N3AB
22	-0.82	-3.92	-3.85	-4.63	-7.34	-9.43	-8.25	-2.07	-2.07	-2.07	-2.07	microstrain at girder cross section, location N3AM
23	-1.36	-4.22	-4.42	-4.36	-3.83	-2.04	-1.00	0.63	0.63	0.63	0.63	microstrain at girder cross section, location N3AT
24	-1.01	-2.67	-2.67	-2.77	-2.96	-2.36	-3.53	3.26	3.26	3.26	3.26	microstrain at girder cross section, location N3BT
25	-0.19	-0.69	-1.00	-0.72	0.09	0.56	1.11	3.29	3.29	3.29	3.29	microstrain at girder cross section, location N3CB
27	-0.52	-1.61	-1.70	-2.03	-3.24	-4.81	-4.52	3.54	3.54	3.54	3.54	microstrain at girder cross section, location N3CT
28	-1.34	-1.88	-2.17	-0.46	5.41	13.04	13.25	10.83	10.83	10.83	10.83	microstrain at girder cross section, location N3DB
29	-0.54	-2.46	-2.80	-1.69	2.05	7.10	6.95	7.13	-2.38	-2.37	3.40	microstrain at girder cross section, location N3DM
30	-0.70	-2.14	-2.18	-2.40	-2.93	-3.60	-3.65	0.99	0.99	0.99	0.99	microstrain at girder cross section, location N3DT
31	-0.74	-0.30	0.68	-2.95	-19.99	-50.12	-50.66	-4.63	-4.63	-4.63	-4.63	microstrain at girder cross section, location N3E
32	0.00	0.00	0.00	0.00	0.00	0.00	3556.27	-2498.82	-2498.82	-2498.82	-2498.82	microstrain at transverse steel gage, location N1B2B
33	3.33	5.56	6.07	10.19	26.90	40.38	48.72	-9.11	-9.11	-9.11	-9.11	microstrain at transverse steel gage, location N1B2T
40	0.00	0.00	0.00	0.00	0.00	0.00	749.65	-249.88	-249.88	-249.88	-249.88	microstrain at transverse steel gage, location N1A1B
41	-11.31	-14.69	-18.47	-11.44	75.70	62.02	247.80	-84.37	-84.37	-84.37	-84.37	microstrain at transverse steel gage, location N1A1T
42	-0.00	0.00	0.00	-0.00	-0.02	-0.03	-0.03	-0.02	-0.02	-0.02	-0.02	displacement between girders, location N4AT
43	-0.00	-0.01	-0.01	0.00	0.02	0.02	0.20	0.00	0.00	0.00	0.00	vertical displacement of girders, location N4AV
44	-0.00	-0.00	-0.01	0.00	0.01	0.01	0.16	-0.00	-0.00	-0.00	-0.00	vertical displacement of girders, location N4CV
45	0.00	0.00	0.00	-0.00	-0.04	-0.07	-0.09	-0.01	-0.01	-0.01	-0.01	displacement between girders, location N4BT
48	-0.65	-1.52	-0.18	-5.50	-29.67	-75.79	-76.11	-7.41	-7.41	-7.41	-7.41	microstrain at girder cross section, location N3BB
49	-0.54	-0.65	-0.27	-2.21	-10.28	-23.38	-22.68	-19.92	-7.23	-1.71	0.00	microstrain at girder cross section, location N3BM
56	-0.31	-0.21	0.16	-3.12	-11.20	-16.75	-16.61	-2.88	-2.88	-2.88	-2.88	microstrain at girder cross section, location N3F
57	0.07	-1.38	-1.72	-1.82	-2.14	-2.81	-2.41	0.05	0.05	0.05	0.05	microstrain at girder cross section, location N3CM

Northbound Bridge

Setup No. 1 - Side by Side Trucks in Lanes 1 and 2

ch no.	sta 1	sta 2	sta 3	sta 4	sta 5	sta 6	sta 7	sta 8	sta 9	sta 10	sta 11	sta 12	description
0	148.17	-412.44	-422.00	-120.92	-299.51	-423.21	-105.14	-353.80	-469.77	-181.88	-667.05	-234.38	microstrain at transverse steel gage, location N1A1B
1	0.92	1.30	1.70	2.73	2.24	3.23	9.12	6.84	-15.65	-15.65	-15.65	-15.65	microstrain at transverse steel gage, location N1A1T
2	1.30	1.31	0.64	2.84	3.34	3.89	-2.50	-3.59	-113.20	-113.20	-113.20	-113.20	microstrain at transverse steel gage, location N1A2B
3	0.06	0.39	0.14	0.30	0.72	-9.75	-12.38	-12.43	-29.93	-29.93	-29.93	-29.93	microstrain at transverse steel gage, location N1A2T
4	-88.08	97.21	-14.43	-125.99	1.81	-328.41	-313.15	-327.78	1258.97	1258.97	1258.97	1258.97	microstrain at transverse steel gage, location N1A3B
5	0.00	0.00	0.00	0.00	0.00	0.00	0.00	0.00	10000.00	10000.00	10000.00	10000.00	microstrain at transverse steel gage, location N1A3T
6	1.32	0.35	0.41	2.03	1.71	0.14	-3.74	-3.97	-22.46	-22.46	-22.46	-22.46	microstrain at transverse steel gage, location N1B1B
7	0.00	0.00	0.00	0.00	0.00	0.00	0.00	0.00	0.00	0.00	0.00	0.00	microstrain at transverse steel gage, location N1B1T
8	-9.06	-13.59	-18.57	-20.86	-35.78	-113.47	-119.07	-54.75	-48.50	-45.72	-45.60	-49.81	microstrain at transverse steel gage, location N1B3B
9	0.65	4.89	5.88	9.62	46.51	263.68	256.86	33.23	-16.84	-12.89	-17.69	-25.61	microstrain at transverse steel gage, location N1B3T
10	0.00	0.00	0.00	0.00	0.00	0.00	0.00	0.00	-999.51	-999.51	-999.51	-999.51	microstrain at transverse steel gage, location N1C1B
11	0.00	0.00	0.00	0.00	0.00	0.00	0.00	0.00	1000.00	1000.00	1000.00	1000.00	microstrain at transverse steel gage, location N1C1T
12	-1.69	-1.91	-2.88	-1.51	-2.58	-5.83	-7.96	-8.52	-15.56	-15.56	-15.56	-15.56	microstrain at transverse steel gage, location N1C2B
13	-29.38	-32.90	-46.62	-49.51	-67.46	-108.44	-125.49	-143.22	-234.96	-234.96	-234.96	-234.96	microstrain at transverse steel gage, location N1C2T
14	-281.11	73.35	-392.56	-575.99	72.30	35.91	54.15	23.06	167.32	167.32	167.32	167.32	microstrain at transverse steel gage, location N1C3B
15	0.00	0.00	0.00	0.00	0.00	0.00	0.00	0.00	-999.51	-999.51	-999.51	-999.51	microstrain at transverse steel gage, location N1C3T
21	-0.36	-0.36	1.22	2.99	2.86	-3.89	-21.33	-39.83	3.04	3.04	3.04	3.04	microstrain at girder cross section, location N3AB
22	0.38	0.40	1.25	1.89	1.94	-1.66	-12.53	-23.28	2.27	2.27	2.27	2.27	microstrain at girder cross section, location N3AM
23	0.14	0.14	-0.06	-0.66	-0.65	-0.72	-0.89	-0.03	7.93	7.93	7.93	7.93	microstrain at girder cross section, location N3AT
24	-0.06	-0.19	-0.26	-0.75	-0.70	0.04	1.26	1.87	6.38	6.38	6.38	6.38	microstrain at girder cross section, location N3BT
25	-0.15	-0.38	-0.82	-2.11	-2.12	0.63	6.23	9.73	7.24	7.24	7.24	7.24	microstrain at girder cross section, location N3CB
27	0.25	0.07	-0.11	-0.65	-0.74	-0.54	-1.18	-1.91	9.81	9.81	9.81	9.81	microstrain at girder cross section, location N3CT
28	-0.53	-0.93	-1.26	-2.36	-2.31	-0.25	3.54	5.32	18.23	18.23	18.23	18.23	microstrain at girder cross section, location N3DB
29	0.43	0.16	-0.24	-0.95	-0.78	1.14	3.98	5.54	2.73	-3.14	2.29	2.03	microstrain at girder cross section, location N3DM
30	0.26	0.13	0.10	-0.25	-0.36	-0.56	-1.21	-1.72	7.87	7.87	7.87	7.87	microstrain at girder cross section, location N3DT
31	0.22	0.37	1.97	3.86	3.49	-2.55	-19.71	-36.37	-1.26	-1.26	-1.26	-1.26	microstrain at girder cross section, location N3E
32	24.92	30.68	24.67	44.03	65.40	68.70	58.53	78.08	-6186.97	-6186.97	-6186.97	-6186.97	microstrain at transverse steel gage, location N1B2B
33	2.35	2.81	2.45	4.24	3.49	7.07	12.86	21.33	-33.90	-33.90	-33.90	-33.90	microstrain at transverse steel gage, location N1B2T
40	0.00	0.00	0.00	0.00	0.00	0.00	0.00	0.00	-999.51	-999.51	-999.51	-999.51	microstrain at transverse steel gage, location N1A1B
41	-28.39	-30.33	-43.93	-47.56	-67.98	-107.08	-123.13	-142.60	-269.61	-269.61	-269.61	-269.61	microstrain at transverse steel gage, location N1A1T
42	0.00	0.00	0.00	0.00	0.00	0.00	0.00	0.01	-0.01	-0.01	-0.01	-0.01	displacement between girders, location N4AT
43	-0.00	-0.00	-0.01	-0.03	-0.02	0.03	0.13	0.16	0.00	0.00	0.00	0.00	vertical displacement of girders, location N4AV
44	0.00	0.00	-0.01	-0.03	-0.02	0.04	0.15	0.21	0.00	0.00	0.00	0.00	vertical displacement of girders, location N4CV
45	0.00	0.00	0.00	0.00	0.00	-0.01	-0.03	-0.05	-0.01	-0.01	-0.01	-0.01	displacement between girders, location N4BT
48	0.61	1.32	3.79	6.60	6.31	-3.09	-28.87	-55.38	-5.65	-5.65	-5.65	-5.65	microstrain at girder cross section, location N3BB
49	-0.14	-0.11	0.93	1.45	1.30	-1.45	-8.83	-15.48	-7.05	-1.34	0.88	1.09	microstrain at girder cross section, location N3BM
56	0.03	0.04	0.85	1.39	1.07	-2.23	-7.11	-8.37	0.04	0.04	0.04	0.04	microstrain at girder cross section, location N3F
57	1.04	0.79	0.31	-0.95	-0.81	2.32	7.39	10.58	-0.02	-0.02	-0.02	-0.02	microstrain at girder cross section, location N3CM

Northbound Bridge

Setup No. 2 - Bumper to Bumper Trucks in Lane 1

ch no.	sta 2	sta 3	sta 4	sta 5	sta 6	sta 7	sta 8	sta 9	sta 10	sta 11	sta 12	description
0	-63.61	-8.30	-107.86	6.00	-75.18	-150.20	-213.43	-52.03	-108.95	-185.32	28.98	microstrain at longitudinal steel gage, location N2A
1	-1.36	-1.61	-1.67	-0.93	-24.11	-18.97	-4.24	-8.89	-7.10	-7.10	-7.10	microstrain at longitudinal steel gage, location N2B
2	-24.74	0.91	3.34	26.94	58.74	60.89	61.84	63.04	-257.95	-257.95	-257.95	microstrain at longitudinal steel gage, location N2C
3	-2.80	-0.93	0.15	-1.02	-14.92	-20.06	-24.72	-24.67	-5.69	-5.69	-5.69	microstrain at longitudinal steel gage, location N2D
4	-261.68	-346.56	-208.37	-220.47	-145.15	-64.40	-161.83	-261.98	-466.48	-466.48	-466.48	microstrain at longitudinal steel gage, location N2E
5	-4.98	-11.20	-21.81	-26.33	-99.78	-109.19	-112.28	-107.14	-70.47	-70.47	-70.47	microstrain at longitudinal steel gage, location N2F
6	0.44	1.76	2.92	4.49	-39.66	-50.30	-52.62	-55.49	-3.00	-3.00	-3.00	microstrain at longitudinal steel gage, location N2G
7	0.00	0.00	0.00	0.00	0.00	0.00	0.00	0.00	0.00	0.00	0.00	microstrain at longitudinal steel gage, location N2H
21	-0.03	1.00	4.00	5.65	0.54	-17.93	-46.11	-49.28	-3.75	-3.75	-3.75	microstrain at girder cross section, location N3AB
22	0.37	0.81	3.08	4.23	0.70	-11.45	-29.79	-33.07	-2.73	-2.73	-2.73	microstrain at girder cross section, location N3AM
23	0.42	0.54	0.85	1.14	0.89	-0.00	-1.01	-2.05	-1.65	-1.65	-1.65	microstrain at girder cross section, location N3AT
24	0.26	0.21	0.01	0.05	0.72	2.50	3.38	2.04	0.19	0.19	0.19	microstrain at girder cross section, location N3BT
25	0.21	-0.46	-1.51	-1.94	0.42	7.00	14.53	16.47	-0.71	-0.71	-0.71	microstrain at girder cross section, location N3CB
27	-0.10	-0.36	-0.33	-0.35	-0.47	-0.89	-1.34	-1.63	2.01	2.01	2.01	microstrain at girder cross section, location N3CT
28	0.18	-0.05	-0.99	-1.13	0.01	2.02	2.79	0.41	-3.75	-3.75	-3.75	microstrain at girder cross section, location N3DB
29	-0.24	-0.72	-1.04	-1.15	-0.35	0.94	2.04	1.25	0.18	-0.14	-0.10	microstrain at girder cross section, location N3DM
30	-0.12	-0.31	-0.22	-0.30	-0.67	-1.51	-1.78	-0.83	1.98	1.98	1.98	microstrain at girder cross section, location N3DT
31	-0.05	0.93	2.78	3.57	-0.31	-8.58	-13.96	-12.24	5.44	5.44	5.44	microstrain at girder cross section, location N3E
42	-0.00	-0.00	0.00	0.00	-0.00	-0.03	-0.07	-0.06	0.02	0.02	0.02	displacement between girders, location N4DT
43	0.00	-0.01	-0.02	-0.03	0.01	0.12	0.19	0.16	-0.00	-0.00	-0.00	displacement of girders, location N4BV
44	-0.00	-0.01	-0.02	-0.03	0.01	0.13	0.25	0.25	0.01	0.01	0.01	displacement of girders, location N4DV
45	0.00	0.00	0.00	0.00	-0.00	-0.00	-0.00	0.01	0.01	-0.00	-0.00	displacement between girders, location N4CT
48	-0.00	1.04	4.12	5.27	-0.61	-14.99	-23.56	-18.76	-3.15	-3.15	-3.15	microstrain at girder cross section, location N3BB
49	0.05	0.35	1.19	1.49	0.36	-2.82	-4.92	-4.34	-1.47	0.68	1.50	microstrain at girder cross section, location N3BM
56	0.11	0.53	1.20	1.51	0.47	-0.86	-1.79	-1.93	1.79	1.79	1.79	microstrain at girder cross section, location N3F
57	-0.10	-0.66	-1.51	-1.90	0.33	6.59	13.58	14.89	7.89	7.89	7.89	microstrain at girder cross section, location N3CM

Northbound Bridge

Setup No. 2 - Bumper to Bumber Trucks in Lane 2

ch no.	sta 2	sta 3	sta 4	sta 5	sta 6	sta 7	sta 8	sta 9	sta 10	sta 11	sta 12	description
0	41.18	116.59	-34.53	53.87	373.46	47.27	233.09	210.71	82.00	195.50	215.63	microstrain at longitudinal steel gage, location N2A
1	-7.83	-9.21	-6.72	-13.01	-9.24	-11.29	3.14	11.99	10.33	10.33	10.33	microstrain at longitudinal steel gage, location N2B
2	2.23	5.70	3.73	1.91	5.41	5.67	11.48	16.88	-328.34	-328.34	-328.34	microstrain at longitudinal steel gage, location N2C
3	-10.20	-10.98	-9.32	-16.08	-11.34	-17.94	-13.96	-10.52	-0.88	-0.88	-0.88	microstrain at longitudinal steel gage, location N2D
4	135.70	132.32	298.21	202.75	165.51	125.42	63.36	-31.62	-436.47	-436.47	-436.47	microstrain at longitudinal steel gage, location N2E
5	11.75	11.87	-11.30	-26.05	9.79	-5.44	-1.74	12.03	17.21	17.21	17.21	microstrain at longitudinal steel gage, location N2F
6	6.84	7.52	11.18	12.84	6.04	-9.72	-4.21	13.09	40.27	40.27	40.27	microstrain at longitudinal steel gage, location N2G
7	0.00	0.00	0.00	0.00	0.00	0.00	0.00	0.00	0.00	0.00	0.00	microstrain at longitudinal steel gage, location N2H
21	0.32	0.57	1.48	2.19	0.29	-4.34	-9.82	-10.23	-5.99	-5.99	-5.99	microstrain at girder cross section, location N3AB
22	0.43	0.60	1.18	1.51	1.07	-1.31	-2.91	-1.99	-6.14	-6.14	-6.14	microstrain at girder cross section, location N3AM
23	-0.32	-0.53	-0.71	-1.03	-0.30	0.41	2.38	4.07	-4.37	-4.37	-4.37	microstrain at girder cross section, location N3AT
24	0.36	0.18	0.24	0.38	0.44	0.31	0.52	-1.26	-1.92	-1.92	-1.92	microstrain at girder cross section, location N3BT
25	-0.23	-0.42	-0.73	-1.43	-0.65	0.35	0.80	0.30	-0.31	-0.31	-0.31	microstrain at girder cross section, location N3CB
27	-0.03	-0.12	-0.05	0.03	-0.07	-0.90	-2.25	-2.72	1.77	1.77	1.77	microstrain at girder cross section, location N3CT
28	0.38	-0.22	-1.04	-1.36	0.06	4.39	11.21	12.25	-1.18	-1.18	-1.18	microstrain at girder cross section, location N3DB
29	0.36	0.15	-0.16	-0.12	0.97	4.15	8.51	8.45	-0.59	0.19	6.16	microstrain at girder cross section, location N3DM
30	0.20	0.16	0.27	0.38	0.25	-0.26	-1.05	-2.34	2.29	2.29	2.29	microstrain at girder cross section, location N3DT
31	0.68	1.47	3.45	4.73	1.34	-15.74	-46.03	-43.51	2.72	2.72	2.72	microstrain at girder cross section, location N3E
42	0.00	-0.00	0.00	0.00	-0.00	-0.01	-0.00	-0.00	0.03	0.03	0.03	displacement between girders, location N4DT
43	-0.00	-0.00	-0.02	-0.02	0.01	0.09	0.17	0.16	-0.01	-0.01	-0.01	displacement of girders, location N4BV
44	-0.00	-0.00	-0.01	-0.01	0.00	0.03	0.07	0.07	0.01	0.01	0.01	displacement of girders, location N4DV
45	0.00	0.00	0.00	0.00	-0.00	-0.03	-0.08	-0.09	0.00	0.00	0.00	displacement between girders, location N4CT
48	0.54	1.33	4.29	5.85	1.22	-22.60	-68.17	-58.82	-7.46	-7.46	-7.46	microstrain at girder cross section, location N3BB
49	0.56	0.72	1.76	2.40	0.93	-6.86	-19.99	-17.58	-4.55	1.05	2.80	microstrain at girder cross section, location N3BM
56	-0.46	0.17	1.57	1.58	-1.12	-8.89	-14.40	-12.34	-0.86	-0.86	-0.86	microstrain at girder cross section, location N3F
57	-1.56	-1.75	-1.87	-2.94	-1.48	-1.35	-1.71	-2.47	4.36	4.36	4.36	microstrain at girder cross section, location N3CM

Northbound Bridge

Setup No. 2 - Side by Side Trucks in Lanes 1 and 2

ch no.	sta 1	sta 2	sta 3	sta 4	sta 5	sta 6	sta 7	sta 8	sta 9	sta 10	sta 11	sta 12	description
0	163.09	247.13	249.03	324.85	317.64	360.48	384.92	423.04	575.73	361.34	241.64	276.76	microstrain at longitudinal steel gage, location N2A
1	-2.34	-1.25	-2.80	-1.52	-2.99	0.03	11.01	24.90	16.65	16.65	16.65	16.65	microstrain at longitudinal steel gage, location N2B
2	7.42	2.22	4.87	5.36	5.42	4.14	4.62	8.78	-358.82	-358.82	-358.82	-358.82	microstrain at longitudinal steel gage, location N2C
3	-2.87	-4.40	-1.63	0.43	-2.83	-2.05	-5.64	-5.60	5.10	5.10	5.10	5.10	microstrain at longitudinal steel gage, location N2D
4	37.93	-206.39	-84.23	-139.70	-234.98	-29.80	-222.83	-158.06	-459.15	-459.15	-459.15	-459.15	microstrain at longitudinal steel gage, location N2E
5	24.13	25.66	33.98	35.09	34.71	54.77	37.07	36.70	13.30	13.30	13.30	13.30	microstrain at longitudinal steel gage, location N2F
6	11.34	15.59	19.42	20.01	14.54	13.39	13.84	14.22	31.90	31.90	31.90	31.90	microstrain at longitudinal steel gage, location N2G
7	0.00	0.00	0.00	0.00	0.00	0.00	0.00	0.00	0.00	0.00	0.00	0.00	microstrain at longitudinal steel gage, location N2H
21	-0.51	-0.37	1.14	3.53	3.37	-3.53	-20.64	-39.85	-7.10	-7.10	-7.10	-7.10	microstrain at girder cross section, location N3AB
22	-0.07	0.06	1.16	2.59	2.52	-1.85	-12.30	-23.03	-10.40	-10.40	-10.40	-10.40	microstrain at girder cross section, location N3AM
23	0.18	0.32	0.24	0.22	0.19	0.02	-0.16	0.66	-6.38	-6.38	-6.38	-6.38	microstrain at girder cross section, location N3AT
24	0.05	0.08	-0.02	-0.21	-0.22	0.36	1.62	2.30	-3.56	-3.56	-3.56	-3.56	microstrain at girder cross section, location N3BT
25	0.04	-0.16	-0.67	-1.62	-1.74	0.98	6.11	9.76	1.02	1.02	1.02	1.02	microstrain at girder cross section, location N3CB
27	0.05	0.01	0.10	0.09	0.07	0.10	-0.56	-1.37	1.26	1.26	1.26	1.26	microstrain at girder cross section, location N3CT
28	-0.15	-0.32	-0.88	-1.57	-1.37	0.84	5.00	7.48	1.63	1.63	1.63	1.63	microstrain at girder cross section, location N3DB
29	0.05	-0.05	-0.31	-0.60	-0.38	1.14	4.04	5.68	2.72	-3.15	2.77	2.46	microstrain at girder cross section, location N3DM
30	0.13	0.11	0.31	0.49	0.43	0.12	-0.61	-1.28	1.55	1.55	1.55	1.55	microstrain at girder cross section, location N3DT
31	0.05	0.28	1.91	4.15	3.79	-2.86	-19.86	-37.22	-0.78	-0.78	-0.78	-0.78	microstrain at girder cross section, location N3E
42	0.00	0.00	0.00	0.00	0.00	-0.00	-0.03	-0.04	0.02	0.02	0.02	0.02	displacement between girders, location N4DT
43	0.00	0.00	-0.01	-0.03	-0.02	0.04	0.16	0.20	-0.02	-0.02	-0.02	-0.02	displacement of girders, location N4BV
44	0.00	0.00	-0.01	-0.02	-0.02	0.03	0.14	0.20	0.01	0.01	0.01	0.01	displacement of girders, location N4DV
45	0.00	0.00	0.00	0.00	0.00	-0.00	-0.02	-0.04	-0.00	-0.00	-0.00	-0.00	displacement between girders, location N4CT
48	-0.14	0.35	2.68	6.30	5.58	-4.65	-29.84	-56.45	-11.66	-11.66	-11.66	-11.66	microstrain at girder cross section, location N3BB
49	0.06	0.37	0.93	1.99	1.63	-1.22	-8.32	-14.75	-6.13	-0.47	1.71	1.80	microstrain at girder cross section, location N3BM
56	-0.16	0.06	1.10	2.26	1.84	-1.66	-6.66	-7.93	-2.29	-2.29	-2.29	-2.29	microstrain at girder cross section, location N3F
57	0.02	0.11	-0.12	-0.99	-0.76	1.94	6.53	9.44	3.72	3.72	3.72	3.72	microstrain at girder cross section, location N3CM

Southbound Bridge

Setup No. 1 - Bumper to Bumber Trucks in Lane 1

ch no.	sta 2	sta 3	sta 4	sta 5	sta 6	sta 7	sta 8	sta 9	sta 10	sta 11	sta 12	description
0	0.00	0.00	10000.00	0.00	0.00	0.00	0.00	0.00	0.00	0.00	0.00	microstrain at longitudinal steel gage, location S2A
1	-1.45	-2.66	-5.70	-3.44	-0.31	13.22	25.09	20.14	9.11	-5.70	-5.70	microstrain at longitudinal steel gage, location S2B
2	-64.29	-63.72	-61.44	-55.82	-50.18	-41.06	-36.60	-38.40	-45.05	-61.44	-61.44	microstrain at longitudinal steel gage, location S2C
3	-1.25	-1.20	-5.58	-0.75	-1.81	-2.38	-4.45	-6.98	-3.07	-5.58	-5.58	microstrain at longitudinal steel gage, location S2D
4	-685.15	-676.36	-737.08	-613.82	-605.66	-557.19	-557.74	-540.16	-529.20	-737.08	-737.08	microstrain at longitudinal steel gage, location S2E
5	-20.45	-21.28	-15.09	-12.12	-15.08	-23.42	-22.02	-26.09	-29.03	-15.09	-15.09	microstrain at longitudinal steel gage, location S2F
6	-1.06	0.86	-22.86	11.22	10.29	9.10	7.51	2.24	6.78	-22.86	-22.86	microstrain at longitudinal steel gage, location S2G
7	-2.25	-1.00	-21.24	10.09	11.24	10.86	8.06	7.05	9.96	17.99	22.03	microstrain at longitudinal steel gage, location S2H
8	0.00	0.00	1000.00	0.00	0.00	0.00	0.00	0.00	0.00	0.00	0.00	microstrain at diaphragm bar steel gage, location S3C
9	-154.62	-150.63	-161.02	-202.97	-192.08	-126.53	-45.16	-46.15	-191.13	-191.18	-181.74	microstrain at diaphragm bar steel gage, location S3D
10	-37.72	-36.67	-50.43	-89.85	-58.48	-4.68	13.69	-27.81	-89.11	-50.43	-50.43	microstrain at diaphragm bar steel gage, location S3E
11	-171.70	-144.37	-184.95	-137.29	-171.10	-206.29	-130.80	-67.14	-61.80	-184.95	-184.95	microstrain at diaphragm bar steel gage, location S3F
12	-38.75	-42.83	-53.11	-100.50	-84.93	-71.17	-72.05	-87.75	-95.52	-53.11	-53.11	microstrain at diaphragm bar steel gage, location S3G
13	-77.92	-73.19	-80.51	-106.07	-89.72	-35.79	-28.98	-35.86	-40.43	-80.51	-80.51	microstrain at diaphragm bar steel gage, location S3H
14	-65.75	-65.40	-65.69	-117.26	-141.09	-183.48	-184.20	-185.61	-190.02	-65.69	-65.69	microstrain at diaphragm bar steel gage, location S3J
15	-71.66	-93.17	-9.78	-141.83	-71.78	216.61	250.16	248.19	231.57	-9.78	-9.78	microstrain at diaphragm bar steel gage, location S3K
17	-2.23	-2.92	-0.38	-3.71	-2.51	-1.38	1.63	1.58	-1.89	-0.38	-0.38	microstrain at girder cross section, location S5CB
18	0.15	-0.38	-1.70	-0.20	-0.25	1.09	1.51	0.80	0.20	-1.70	-1.70	microstrain at girder cross section, location S5BT
21	0.55	1.35	-3.06	7.63	0.05	-23.09	-62.07	-64.16	-28.22	-3.06	-3.06	microstrain at girder cross section, location S5AB
22	1.15	1.07	-1.95	4.47	0.26	-11.15	-28.46	-30.18	-13.11	-1.95	-1.95	microstrain at girder cross section, location S5AM
23	1.40	0.94	-1.29	1.95	0.95	1.55	2.72	3.41	3.44	-1.29	-1.29	microstrain at girder cross section, location S5AT
27	1.16	0.91	-3.02	1.40	0.88	0.90	0.06	-1.12	-1.69	-3.02	-3.02	microstrain at girder cross section, location S5CT
28	-1.21	-2.19	2.02	-3.13	-1.49	0.92	2.61	0.65	-2.40	2.02	2.02	microstrain at girder cross section, location S5DB
29	-0.64	-1.02	-3.67	-1.14	0.26	5.19	8.32	7.07	3.01	1.38	1.57	microstrain at girder cross section, location S5DM
30	0.36	0.27	-3.19	0.48	0.46	0.76	1.26	1.98	1.90	-3.19	-3.19	microstrain at girder cross section, location S5DT
32	-39.89	-55.23	-6.23	-116.46	-107.51	-173.72	-170.81	-176.97	-171.99	-6.23	-6.23	microstrain at diaphragm bar steel gage, location S3A
33	-7.70	-11.75	-3.35	-6.41	-3.15	25.55	149.36	129.90	16.58	-3.35	-3.35	microstrain at diaphragm bar steel gage, location S3B
40	-11.47	-7.41	-59.36	74.90	67.22	43.37	54.93	43.39	31.20	-59.36	-59.36	microstrain at diaphragm bar steel gage, location S3L
41	-93.25	-90.93	-85.72	-144.57	-118.40	-87.99	-85.76	-95.34	-102.73	-85.72	-85.72	microstrain at diaphragm bar steel gage, location S3M
42	0.00	-0.01	0.00	-0.02	0.01	0.06	0.09	0.08	0.04	0.00	0.00	displacement of girders, location S7AV
43	0.00	0.00	-0.03	0.00	0.00	0.00	0.01	0.01	0.01	-0.03	-0.03	displacement between girders, location S7BT
44	0.00	0.00	0.00	0.00	0.00	0.01	0.02	0.02	0.02	0.00	0.00	displacement between girders, location S7AT
45	0.00	-0.01	-0.00	-0.03	0.02	0.12	0.18	0.15	0.08	-0.00	-0.00	displacement of girders, location S7BV
48	-0.18	0.32	-2.55	1.59	-1.88	-10.02	-14.26	-10.92	-5.60	-2.55	-2.55	microstrain at girder cross section, location S5BB
49	0.86	0.54	-1.72	2.86	-0.27	-5.91	-9.93	-7.41	-2.71	1.46	3.48	microstrain at girder cross section, location S5BM
57	1.91	1.44	-1.89	0.81	2.75	9.74	16.74	16.30	7.11	-1.89	-1.89	microstrain at girder cross section, location S5CM

Southbound Bridge

Setup No. 1 - Bumper Trucks in Lane 2

ch no.	sta 2	sta 3	sta 4	sta 5	sta 6	sta 7	sta 8	sta 9	sta 10	sta 11	sta 12	description
0	0.00	0.00	0.00	0.00	0.00	0.00	0.00	0.00	0.00	0.00	0.00	microstrain at longitudinal steel gage, location S2A
1	0.09	0.39	0.71	-0.91	0.80	4.84	14.54	18.54	-11.27	-11.27	-11.27	microstrain at longitudinal steel gage, location S2B
2	2.03	2.70	1.36	1.89	3.79	10.76	25.92	24.73	-19.15	-19.15	-19.15	microstrain at longitudinal steel gage, location S2C
3	1.41	1.80	2.13	1.53	1.99	1.16	0.72	-0.20	-6.52	-6.52	-6.52	microstrain at longitudinal steel gage, location S2D
4	8.80	12.88	20.42	21.81	20.39	23.30	33.26	34.40	-298.20	-298.20	-298.20	microstrain at longitudinal steel gage, location S2E
5	-5.37	-5.22	-2.51	-4.79	-7.49	-9.05	-8.88	-8.70	19.87	19.87	19.87	microstrain at longitudinal steel gage, location S2F
6	0.59	1.06	2.19	0.56	0.80	0.32	-0.77	-1.44	-36.28	-36.28	-36.28	microstrain at longitudinal steel gage, location S2G
7	-0.65	0.18	0.07	0.73	0.79	-0.47	-2.63	-2.41	-0.52	6.76	21.01	microstrain at longitudinal steel gage, location S2H
8	0.00	0.00	0.00	0.00	0.00	0.00	0.00	0.00	0.00	0.00	0.00	microstrain at diaphragm bar steel gage, location S3C
9	104.95	100.48	91.69	91.89	93.81	84.19	48.38	-28.63	33.90	80.62	82.76	microstrain at diaphragm bar steel gage, location S3D
10	6.25	5.09	-1.14	-11.61	19.77	-12.16	-187.97	-170.40	44.19	44.19	44.19	microstrain at diaphragm bar steel gage, location S3E
11	15.25	20.81	39.52	53.29	-2.77	-605.90	-570.61	-501.45	-108.21	-108.21	-108.21	microstrain at diaphragm bar steel gage, location S3F
12	0.91	-0.57	-5.51	-10.05	12.08	26.46	178.52	156.02	48.03	48.03	48.03	microstrain at diaphragm bar steel gage, location S3G
13	-1.55	1.50	2.10	2.27	-1.74	-15.11	0.91	-2.57	-35.06	-35.06	-35.06	microstrain at diaphragm bar steel gage, location S3H
14	-2.31	-3.02	-3.95	-5.90	-3.39	107.64	107.20	128.16	104.79	104.79	104.79	microstrain at diaphragm bar steel gage, location S3J
15	0.29	1.54	6.21	8.14	-29.88	-412.55	-721.48	-585.04	182.38	182.38	182.38	microstrain at diaphragm bar steel gage, location S3K
17	-0.62	-0.78	-1.23	-1.41	-1.21	-0.56	0.07	0.06	5.39	5.39	5.39	microstrain at girder cross section, location S5CB
18	-0.24	-0.39	-0.58	-0.73	-0.94	-1.04	-2.89	-3.98	-1.85	-1.85	-1.85	microstrain at girder cross section, location S5BT
21	-0.06	0.04	1.19	1.81	-0.23	-7.77	-17.53	-20.48	-3.58	-3.58	-3.58	microstrain at girder cross section, location S5AB
22	-0.27	-0.42	-0.03	-0.00	-1.36	-4.63	-7.90	-8.20	-3.03	-3.03	-3.03	microstrain at girder cross section, location S5AM
23	-0.28	-0.44	-0.67	-0.93	-1.11	-0.96	0.66	2.52	-3.54	-3.54	-3.54	microstrain at girder cross section, location S5AT
27	-0.09	-0.03	0.06	-0.07	-0.47	-1.41	-2.80	-3.68	-3.65	-3.65	-3.65	microstrain at girder cross section, location S5CT
28	-0.09	-0.49	-0.99	-1.30	0.13	4.60	10.07	11.11	6.11	6.11	6.11	microstrain at girder cross section, location S5DB
29	-0.14	-0.50	-1.00	-1.42	-0.20	4.36	10.32	11.14	0.09	-0.51	6.51	microstrain at girder cross section, location S5DM
30	-0.05	-0.14	-0.06	-0.07	-0.23	-0.29	-0.67	-1.67	-3.54	-3.54	-3.54	microstrain at girder cross section, location S5DT
32	-4.35	-7.80	-12.49	-7.35	-13.74	-11.66	-14.21	-17.72	170.31	170.31	170.31	microstrain at diaphragm bar steel gage, location S3A
33	5.85	4.63	2.33	1.09	17.52	46.48	81.20	61.72	10.85	10.85	10.85	microstrain at diaphragm bar steel gage, location S3B
40	-27.49	-22.18	-18.39	-13.12	-36.42	-655.51	-667.19	-833.04	-79.51	-79.51	-79.51	microstrain at diaphragm bar steel gage, location S3L
41	0.91	2.69	5.47	4.62	4.24	-83.44	-148.91	-170.77	13.11	13.11	13.11	microstrain at diaphragm bar steel gage, location S3M
42	0.00	-0.00	-0.02	-0.02	0.01	0.08	0.16	0.16	0.00	0.00	0.00	displacement of girders, location S7AV
43	0.00	0.00	0.00	0.00	-0.00	-0.02	-0.04	-0.04	-0.03	-0.03	-0.03	displacement between girders, location S7BT
44	-0.00	-0.00	-0.00	-0.00	-0.00	-0.01	-0.02	-0.02	-0.01	-0.01	-0.01	displacement between girders, location S7AT
45	0.00	-0.00	-0.01	-0.02	0.00	0.07	0.14	0.15	-0.01	-0.01	-0.01	displacement of girders, location S7BV
48	-0.18	0.43	1.77	2.25	0.55	-11.28	-35.60	-31.22	-1.14	-1.14	-1.14	microstrain at girder cross section, location S5BB
49	-0.39	-0.27	0.45	1.22	-0.35	-8.42	-26.61	-23.48	-6.47	-0.95	0.11	microstrain at girder cross section, location S5BM
57	0.09	0.07	-0.26	-0.54	-0.38	0.15	0.20	-0.73	-4.05	-4.05	-4.05	microstrain at girder cross section, location S5CM

Southbound Bridge

Setup No. 1 - Side by Side Trucks in Lanes 1 and 2

ch no.	sta 1	sta 2	sta 3	sta 4	sta 5	sta 6	sta 7	sta 8	sta 9	sta 10	sta 11	sta 12	description
0	0.00	0.00	0.00	0.00	0.00	0.00	0.00	0.00	0.00	0.00	0.00	0.00	microstrain at longitudinal steel gage, location S2A
1	0.36	0.69	0.19	-1.90	-1.20	3.43	15.46	27.12	-18.01	-18.01	-18.01	-18.01	microstrain at longitudinal steel gage, location S2B
2	2.79	3.90	2.46	2.32	3.89	10.33	20.42	28.44	-34.45	-34.45	-34.45	-34.45	microstrain at longitudinal steel gage, location S2C
3	0.11	0.27	0.97	0.92	-0.18	-0.99	-1.10	-2.81	-10.71	-10.71	-10.71	-10.71	microstrain at longitudinal steel gage, location S2D
4	-22.62	-22.13	-21.95	-21.96	-30.73	-40.09	-41.66	-46.55	-370.50	-370.50	-370.50	-370.50	microstrain at longitudinal steel gage, location S2E
5	-0.35	0.95	1.60	5.14	-0.34	-2.03	-2.36	-4.89	30.27	30.27	30.27	30.27	microstrain at longitudinal steel gage, location S2F
6	-0.43	-0.06	-0.68	-0.07	-12.96	-10.43	-11.69	-13.88	-39.76	-39.76	-39.76	-39.76	microstrain at longitudinal steel gage, location S2G
7	1.76	1.98	1.72	3.25	1.64	3.30	1.90	-0.65	-1.29	1.76	13.16	16.83	microstrain at longitudinal steel gage, location S2H
8	0.00	0.00	0.00	0.00	0.00	0.00	0.00	0.00	0.00	0.00	0.00	0.00	microstrain at diaphragm bar steel gage, location S3C
9	26.38	1.45	19.38	-30.38	20.24	44.46	100.19	280.37	0.90	36.99	42.81	45.18	microstrain at diaphragm bar steel gage, location S3D
10	45.77	57.90	63.64	49.87	62.18	136.20	133.98	27.06	263.12	263.12	263.12	263.12	microstrain at diaphragm bar steel gage, location S3E
11	-3.34	5.00	11.25	39.03	33.34	-70.00	-1072.57	-1017.12	-587.05	-587.05	-587.05	-587.05	microstrain at diaphragm bar steel gage, location S3F
12	-0.75	0.75	-1.23	-8.39	-14.10	16.72	17.22	61.71	7.34	7.34	7.34	7.34	microstrain at diaphragm bar steel gage, location S3G
13	-3.30	-1.58	-2.87	-1.38	-4.27	-4.74	5.67	10.58	-23.56	-23.56	-23.56	-23.56	microstrain at diaphragm bar steel gage, location S3H
14	0.98	1.50	2.41	-5.53	-5.87	-12.44	16.44	28.08	77.07	77.07	77.07	77.07	microstrain at diaphragm bar steel gage, location S3J
15	0.00	0.00	0.00	0.00	0.00	0.00	0.00	0.00	1000.00	1000.00	1000.00	1000.00	microstrain at diaphragm bar steel gage, location S3K
17	-0.05	-0.61	-1.18	-1.62	-1.52	-0.39	1.91	3.68	8.39	8.39	8.39	8.39	microstrain at girder cross section, location S5CB
18	-0.18	-0.12	0.20	0.08	0.11	0.60	1.41	0.81	-1.61	-1.61	-1.61	-1.61	microstrain at girder cross section, location S5BT
21	-1.08	-0.54	1.84	5.07	4.96	-3.57	-26.52	-54.34	-5.39	-5.39	-5.39	-5.39	microstrain at girder cross section, location S5AB
22	-0.69	-0.22	0.31	1.94	1.81	-1.75	-12.67	-24.23	-3.07	-3.07	-3.07	-3.07	microstrain at girder cross section, location S5AM
23	-0.32	0.01	0.19	0.17	0.12	0.09	0.42	2.33	-3.30	-3.30	-3.30	-3.30	microstrain at girder cross section, location S5AT
27	-0.20	-0.08	0.16	0.26	0.12	-0.25	-1.05	-2.20	-3.19	-3.19	-3.19	-3.19	microstrain at girder cross section, location S5CT
28	-0.23	-0.45	-0.96	-1.81	-1.36	1.22	5.99	8.23	7.65	7.65	7.65	7.65	microstrain at girder cross section, location S5DB
29	-0.24	-0.28	-0.71	-1.47	-1.34	1.61	7.13	10.47	6.84	-3.30	3.87	4.08	microstrain at girder cross section, location S5DM
30	-0.28	-0.43	-0.34	-0.28	-0.40	-0.37	-0.08	-0.00	-2.76	-2.76	-2.76	-2.76	microstrain at girder cross section, location S5DT
32	5.86	2.70	9.42	-2.91	-2.99	-57.30	-93.10	-78.07	115.66	115.66	115.66	115.66	microstrain at diaphragm bar steel gage, location S3A
33	2.72	3.86	0.29	-1.51	5.93	32.32	58.69	182.90	-14.38	-14.38	-14.38	-14.38	microstrain at diaphragm bar steel gage, location S3B
40	26.08	36.06	42.41	26.83	36.78	28.54	-302.80	-703.12	-619.74	-619.74	-619.74	-619.74	microstrain at diaphragm bar steel gage, location S3L
41	1.70	4.19	6.55	7.21	7.80	11.61	27.45	23.17	-4.73	-4.73	-4.73	-4.73	microstrain at diaphragm bar steel gage, location S3M
42	0.00	0.00	-0.01	-0.02	-0.02	0.03	0.11	0.14	-0.00	-0.00	-0.00	-0.00	displacement of girders, location S7AV
43	0.00	0.00	0.00	0.00	0.00	-0.00	-0.01	-0.02	-0.03	-0.03	-0.03	-0.03	displacement between girders, location S7BT
44	0.00	-0.00	0.00	0.00	0.00	0.00	-0.00	-0.00	-0.00	-0.00	-0.00	-0.00	displacement between girders, location S7AT
45	0.00	0.00	-0.01	-0.02	-0.02	0.04	0.14	0.18	-0.01	-0.01	-0.01	-0.01	displacement of girders, location S7BV
48	-0.51	-0.58	0.84	2.01	1.59	-3.73	-17.05	-30.86	-0.30	-0.30	-0.30	-0.30	microstrain at girder cross section, location S5BB
49	-0.61	-0.22	1.37	2.61	2.59	-0.91	-9.99	-20.40	-5.62	0.86	3.44	3.95	microstrain at girder cross section, location S5BM
57	0.01	0.17	-0.22	-0.83	-0.60	1.85	6.54	9.47	-4.21	-4.21	-4.21	-4.21	microstrain at girder cross section, location S5CM

Southbound Bridge

Setup No. 2 - Bumper to Bumber Trucks in Lane 1

ch no.	sta 2	sta 3	sta 4	sta 5	sta 6	sta 7	sta 8	sta 9	sta 10	sta 11	sta 12	description
0	0.00	0.00	0.00	0.00	0.00	0.00	0.00	0.00	0.00	0.00	0.00	microstrain at longitudinal steel gage, location S2A
1	27.65	58.08	56.12	123.10	154.78	162.42	173.97	169.05	29.39	29.39	29.39	microstrain at longitudinal steel gage, location S2B
2	2.80	2.72	2.51	2.40	4.42	12.77	16.40	14.01	-11.82	-11.82	-11.82	microstrain at longitudinal steel gage, location S2C
3	0.35	0.84	0.90	-0.82	-0.60	-3.18	-5.50	-6.70	-7.57	-7.57	-7.57	microstrain at longitudinal steel gage, location S2D
4	-17.45	-36.68	-33.38	-14.04	-6.19	-14.74	-32.19	-32.48	154.22	154.22	154.22	microstrain at longitudinal steel gage, location S2E
5	3.24	3.96	4.04	3.34	4.19	1.73	-0.54	-2.81	-10.40	-10.40	-10.40	microstrain at longitudinal steel gage, location S2F
6	1.45	1.82	2.48	9.17	3.51	1.59	-0.86	-1.86	-4.63	-4.63	-4.63	microstrain at longitudinal steel gage, location S2G
7	2.81	5.11	6.07	-6.65	-3.03	-4.90	-7.89	-8.57	-5.02	1.67	6.29	microstrain at longitudinal steel gage, location S2H
8	0.00	0.00	0.00	0.00	0.00	0.00	0.00	0.00	0.00	0.00	0.00	microstrain at diaphragm bar steel gage, location S3C
9	3.28	2.23	1.54	-2.00	5.25	58.53	192.79	164.93	32.35	14.62	8.89	microstrain at diaphragm bar steel gage, location S3D
10	-11.86	-16.64	-19.63	-20.32	-5.09	65.62	109.37	76.50	-6.13	-6.13	-6.13	microstrain at diaphragm bar steel gage, location S3E
11	-0.92	4.17	15.16	19.17	1.28	-22.55	10.45	50.55	-13.46	-13.46	-13.46	microstrain at diaphragm bar steel gage, location S3F
12	-24.23	-46.52	-43.08	-44.75	-12.08	6.45	7.28	-3.85	-1.42	-1.42	-1.42	microstrain at diaphragm bar steel gage, location S3G
13	3.04	3.62	5.15	-4.06	5.73	18.14	19.66	12.01	-1.32	-1.32	-1.32	microstrain at diaphragm bar steel gage, location S3H
14	-4.96	-6.16	-5.37	-8.54	-13.80	-20.17	-19.19	-22.51	6.41	6.41	6.41	microstrain at diaphragm bar steel gage, location S3J
15	0.00	0.00	0.00	0.00	0.00	0.00	0.00	0.00	1000.00	1000.00	1000.00	microstrain at diaphragm bar steel gage, location S3K
17	-1.79	-0.28	2.27	2.42	-2.36	-0.89	5.39	5.19	0.50	0.50	0.50	microstrain at girder cross section, location S4B2
18	-0.75	-1.26	-1.96	-2.15	-1.33	-3.73	-7.04	-5.97	-2.63	-2.63	-2.63	microstrain at girder cross section, location S4B1
21	-1.13	-1.95	-2.61	-3.15	-3.95	-6.14	-7.68	-7.18	10.49	10.49	10.49	microstrain at girder cross section, location S4A1
22	-1.87	-0.70	0.85	0.83	1.46	8.49	12.71	8.48	8.41	8.41	8.41	microstrain at girder cross section, location S4A2
23	3.58	5.97	7.92	10.17	13.91	17.76	27.08	405.13	-9.37	-9.37	-9.37	microstrain at girder cross section, location S4A3
27	-1.22	-0.38	1.17	1.30	-2.58	-5.67	-5.10	-4.22	1.31	1.31	1.31	microstrain at girder cross section, location S4B4
28	-1.27	-0.45	1.00	1.04	-3.14	-8.80	-11.19	-9.30	4.37	4.37	4.37	microstrain at girder cross section, location S4B5
32	-6.46	-9.25	-16.64	-21.24	-16.16	-18.87	-13.69	-9.21	-25.32	-25.32	-25.32	microstrain at diaphragm bar steel gage, location S3A
33	0.40	0.31	0.47	-0.51	1.73	62.97	231.87	178.51	-11.13	-11.13	-11.13	microstrain at diaphragm bar steel gage, location S3B
40	-4.68	-1.17	-2.24	-6.63	-0.71	55.75	59.79	48.33	13.80	13.80	13.80	microstrain at diaphragm bar steel gage, location S3L
41	0.79	3.78	3.25	3.61	11.77	19.82	19.39	14.82	-0.79	-0.79	-0.79	microstrain at diaphragm bar steel gage, location S3M
42	0.00	-0.01	-0.02	-0.02	0.01	0.11	0.18	0.17	-0.00	-0.00	-0.00	displacement of girders, location S7CV
43	-0.00	-0.00	0.00	0.00	-0.00	-0.01	-0.02	-0.01	-0.00	-0.00	-0.00	displacement between girders, location S7DT
44	0.00	0.00	0.00	0.00	0.00	0.00	0.00	0.00	0.01	0.01	0.01	displacement between girders, location S7CT
45	0.00	-0.01	-0.03	-0.03	0.02	0.15	0.24	0.24	-0.01	-0.01	-0.01	displacement of girders, location S7DV
48	-1.17	-0.58	0.62	0.60	0.03	2.01	4.12	1.79	-1.70	-1.70	-1.70	microstrain at girder cross section, location S4A4
49	-1.05	-0.56	0.77	0.88	-0.54	-0.71	-0.64	-1.39	-2.11	-1.69	-1.68	microstrain at girder cross section, location S4A5
57	-0.44	-0.51	-0.84	-0.82	-0.23	0.79	1.41	1.25	-0.11	-0.11	-0.11	microstrain at girder cross section, location S4B3

Southbound Bridge

Setup No. 2 - Bumper to Bumper Trucks in Lane 2

ch no.	sta 2	sta 3	sta 4	sta 5	sta 6	sta 7	sta 8	sta 9	sta 10	sta 11	sta 12	description
0	0.00	0.00	0.00	0.00	0.00	0.00	0.00	0.00	0.00	0.00	0.00	microstrain at longitudinal steel gage, location S2A
1	-1.05	-1.86	-2.74	-3.16	-1.63	2.52	11.50	13.94	-125.02	-125.02	-125.02	microstrain at longitudinal steel gage, location S2B
2	0.27	0.18	0.80	0.30	0.55	7.09	21.89	18.92	-28.06	-28.06	-28.06	microstrain at longitudinal steel gage, location S2C
3	-0.28	-0.22	1.55	1.83	1.45	-1.66	-5.51	-7.81	-19.57	-19.57	-19.57	microstrain at longitudinal steel gage, location S2D
4	-17.97	-0.42	20.81	38.39	41.56	25.25	33.25	27.01	325.55	325.55	325.55	microstrain at longitudinal steel gage, location S2E
5	-0.75	-0.38	1.49	0.74	-1.06	-3.42	-6.50	-5.05	-35.80	-35.80	-35.80	microstrain at longitudinal steel gage, location S2F
6	0.06	0.28	2.02	2.39	1.44	1.21	-0.28	-0.74	-18.46	-18.46	-18.46	microstrain at longitudinal steel gage, location S2G
7	-0.82	-1.02	0.55	0.68	0.88	-0.59	-2.49	-4.38	-2.93	5.10	19.07	microstrain at longitudinal steel gage, location S2H
8	0.00	0.00	0.00	0.00	0.00	0.00	0.00	0.00	0.00	0.00	0.00	microstrain at diaphragm bar steel gage, location S3C
9	2.14	1.42	1.65	5.96	4.47	13.17	-9.33	-63.87	-43.05	-8.45	-5.35	microstrain at diaphragm bar steel gage, location S3D
10	23.15	28.24	31.27	30.10	47.97	138.78	-102.74	-110.12	59.92	59.92	59.92	microstrain at diaphragm bar steel gage, location S3E
11	7.57	13.01	27.41	22.68	-13.25	-915.80	-915.80	-915.80	84.20	84.20	84.20	microstrain at diaphragm bar steel gage, location S3F
12	1.46	1.97	1.04	-0.32	6.74	5.86	150.23	136.11	7.19	7.19	7.19	microstrain at diaphragm bar steel gage, location S3G
13	-3.05	-1.43	2.38	1.11	-1.86	-36.45	-24.62	-25.95	-16.42	-16.42	-16.42	microstrain at diaphragm bar steel gage, location S3H
14	-78.19	-128.58	-103.24	-101.46	-124.32	-39.89	-87.77	-56.41	62.19	62.19	62.19	microstrain at diaphragm bar steel gage, location S3J
15	0.00	0.00	0.00	0.00	0.00	0.00	0.00	0.00	1000.00	1000.00	1000.00	microstrain at diaphragm bar steel gage, location S3K
17	-0.42	0.55	3.81	5.60	-2.61	-31.11	-87.55	-91.59	3.72	3.72	3.72	microstrain at girder cross section, location S4B2
18	0.13	-0.51	-2.21	-2.81	0.81	11.97	44.68	46.71	-0.36	-0.36	-0.36	microstrain at girder cross section, location S4B1
21	-0.97	-1.50	-2.61	-3.32	-2.12	2.42	4.81	3.02	22.34	22.34	22.34	microstrain at girder cross section, location S4A1
22	-0.55	0.72	3.73	4.42	-5.16	-25.04	-37.41	-32.03	11.58	11.58	11.58	microstrain at girder cross section, location S4A2
23	2.23	2.58	2.92	3.40	4.80	6.10	7.40	8.00	-463.64	-463.64	-463.64	microstrain at girder cross section, location S4A3
27	-0.13	0.53	2.62	3.78	-0.69	-17.72	-51.32	-52.99	4.35	4.35	4.35	microstrain at girder cross section, location S4B4
28	-0.52	0.01	1.68	2.57	-0.75	-15.32	-43.68	-43.11	8.65	8.65	8.65	microstrain at girder cross section, location S4B5
32	-9.17	0.27	-8.81	-4.46	-6.94	-14.47	-20.78	-15.14	-12.27	-12.27	-12.27	microstrain at diaphragm bar steel gage, location S3A
33	1.82	1.86	1.34	-0.17	5.19	50.90	74.91	68.50	-7.22	-7.22	-7.22	microstrain at diaphragm bar steel gage, location S3B
40	-0.80	2.34	4.85	4.74	-5.73	-789.16	-902.86	-902.86	97.14	97.14	97.14	microstrain at diaphragm bar steel gage, location S3L
41	-0.32	2.14	4.02	4.24	3.37	-94.28	-135.52	-153.27	-17.63	-17.63	-17.63	microstrain at diaphragm bar steel gage, location S3M
42	-0.00	-0.00	-0.01	-0.02	0.00	0.06	0.14	0.15	0.17	0.17	0.17	displacement of girders, location S7CV
43	0.00	0.00	0.00	0.00	0.00	-0.00	-0.01	-0.01	0.00	0.00	0.00	displacement between girders, location S7DT
44	0.00	0.00	0.00	0.00	0.00	-0.01	-0.03	-0.04	0.01	0.01	0.01	displacement between girders, location S7CT
45	-0.00	-0.00	-0.01	-0.02	-0.00	0.04	0.08	0.09	0.22	0.22	0.22	displacement of girders, location S7DV
48	-0.15	0.76	3.07	3.74	-2.42	-15.76	-24.37	-20.63	1.36	1.36	1.36	microstrain at girder cross section, location S4A4
49	-0.12	0.52	2.58	3.27	-1.62	-13.16	-20.91	-17.43	-7.57	1.07	3.81	microstrain at girder cross section, location S4A5
57	0.39	0.15	0.05	-0.03	0.97	3.78	5.37	5.46	-0.26	-0.26	-0.26	microstrain at girder cross section, location S4B3

Southbound Bridge

Setup No. 2 - Side by Side Trucks in Lanes 1 and 2

ch no.	sta 2	sta 3	sta 4	sta 5	sta 6	sta 7	sta 8	sta 9	sta 10	sta 11	sta 12	description	
0	0.00	0.00	0.00	-10000.00		-10000.00		-10000.00		-10000.00		-10000.00	
.00	-10000.00											-10000.00	
1	-1.37	0.99	0.49	8.17	13.64	25.42	136.11	136.11	136.11	136.11	136.11	136.11	microstrain at longitudinal steel gage, location S2A
2	2.05	0.78	0.64	5.63	10.37	19.76	-30.13	-30.13	-30.13	-30.13	-30.13	-30.13	microstrain at longitudinal steel gage, location S2B
3	-1.97	1.19	1.76	4.02	1.86	-4.47	-38.69	-38.69	-38.69	-38.69	-38.69	-38.69	microstrain at longitudinal steel gage, location S2C
4	4.45	1.65	34.83	33.23	40.83	0.64	237.26	237.26	237.26	237.26	237.26	237.26	microstrain at longitudinal steel gage, location S2D
5	-1.98	1.89	1.72	6.47	5.87	4.39	-23.58	-23.58	-23.58	-23.58	-23.58	-23.58	microstrain at longitudinal steel gage, location S2E
6	2.69	0.35	1.52	7.90	6.96	5.74	-36.21	-36.21	-36.21	-36.21	-36.21	-36.21	microstrain at longitudinal steel gage, location S2F
7	-2.51	1.49	1.87	8.15	7.78	6.28	4.28	4.39	9.01	17.98	25.74	16.15	microstrain at longitudinal steel gage, location S2G
8	0.00	0.00	0.00	-1000.00	-1000.00	-1000.00	-1000.00	-1000.00	-1000.00	-1000.00	-1000.00	-1000.00	microstrain at longitudinal steel gage, location S2H
9	7.36	8.99	3.84	10.82	14.71	86.25	314.49	10.86	24.43	24.35	26.78	24.12	microstrain at diaphragm bar steel gage, location S3C
10	37.81	48.94	56.29	72.63	147.04	185.66	174.31	174.31	174.31	174.31	174.31	174.31	microstrain at diaphragm bar steel gage, location S3D
11	-1.54	-6.24	-8.16	-9.18	-97.47	-1021.02	111.62	111.62	111.62	111.62	111.62	111.62	microstrain at diaphragm bar steel gage, location S3E
12	1.75	1.36	-0.48	-5.21	32.89	44.29	-41.01	-41.01	-41.01	-41.01	-41.01	-41.01	microstrain at diaphragm bar steel gage, location S3F
13	-12.52	-19.84	-21.01	-22.40	-30.36	-52.97	-9.83	-9.83	-9.83	-9.83	-9.83	-9.83	microstrain at diaphragm bar steel gage, location S3G
14	12.85	19.18	22.15	47.26	58.24	96.94	110.40	110.40	110.40	110.40	110.40	110.40	microstrain at diaphragm bar steel gage, location S3H
15	0.00	0.00	0.00	-1000.00	-1000.00	-1000.00	1000.00	1000.00	1000.00	1000.00	1000.00	1000.00	microstrain at diaphragm bar steel gage, location S3I
17	-2.00	-2.44	-0.35	2.42	-8.77	-29.82	5.05	5.05	5.05	5.05	5.05	5.05	microstrain at diaphragm bar steel gage, location S3J
18	-0.70	-1.29	-2.36	-1.53	1.70	7.61	2.82	2.82	2.82	2.82	2.82	2.82	microstrain at diaphragm bar steel gage, location S3K
21	-0.57	-1.04	-2.00	-1.52	-0.84	0.53	33.38	33.38	33.38	33.38	33.38	33.38	microstrain at girder cross section, location S4B1
22	-2.17	-2.54	-0.81	1.41	-6.32	-14.27	11.26	11.26	11.26	11.26	11.26	11.26	microstrain at girder cross section, location S4A1
23	0.72	0.57	0.47	2.06	3.14	4.63	-473.85	-473.85	-473.85	-473.85	-473.85	-473.85	microstrain at girder cross section, location S4A2
27	-0.89	-1.16	0.22	1.69	-5.57	-21.06	4.97	4.97	4.97	4.97	4.97	4.97	microstrain at girder cross section, location S4A3
28	-0.77	-1.25	-0.02	1.42	-5.26	-20.07	11.82	11.82	11.82	11.82	11.82	11.82	microstrain at girder cross section, location S4B4
32	10.53	5.26	11.64	18.30	9.36	16.04	3.01	3.01	3.01	3.01	3.01	3.01	microstrain at girder cross section, location S4B5
33	-0.24	1.26	1.50	4.13	21.37	173.47	-12.25	-12.25	-12.25	-12.25	-12.25	-12.25	microstrain at diaphragm bar steel gage, location S3A
40	28.67	32.02	41.16	62.36	47.05	-363.59	58.37	58.37	58.37	58.37	58.37	58.37	microstrain at diaphragm bar steel gage, location S3B
41	-0.23	-0.10	-1.07	-1.98	3.33	-10.30	-23.77	-23.77	-23.77	-23.77	-23.77	-23.77	microstrain at diaphragm bar steel gage, location S3L
42	0.00	0.00	-0.01	-0.02	0.03	0.14	0.17	0.17	0.17	0.17	0.17	0.17	microstrain at diaphragm bar steel gage, location S3M
43	-0.00	-0.00	-0.00	-0.00	-0.00	-0.01	0.01	0.01	0.01	0.01	0.01	0.01	displacement of girders, location S7CV
44	0.00	0.00	0.00	0.00	0.00	-0.01	0.02	0.02	0.02	0.02	0.02	0.02	displacement between girders, location S7DT
45	0.00	-0.00	-0.01	-0.02	0.04	0.15	0.22	0.22	0.22	0.22	0.22	0.22	displacement between girders, location S7CT
48	-0.65	-0.94	0.09	2.01	-2.60	-10.30	1.43	1.43	1.43	1.43	1.43	1.43	displacement of girders, location S7DV
49	-1.00	-1.20	-0.14	1.91	-2.86	-10.83	-11.80	-8.29	-2.60	-1.31	-2.05	-13.75	microstrain at girder cross section, location S4A4
57	-0.46	-0.48	-0.92	-0.82	0.44	3.42	-2.98	-2.98	-2.98	-2.98	-2.98	-2.98	microstrain at girder cross section, location S4A5
													microstrain at girder cross section, location S4B3

Southbound Bridge

Setup No. 3 - Bumper to Bumper Trucks in Lane 1

ch no.	sta 2	sta 3	sta 4	sta 5	sta 6	sta 7	sta 8	sta 9	sta 10	sta 11	sta 12	description
0	90.50	124.02	119.00	83.05	81.48	67.35	77.86	96.58	106.62	114.03	92.20	microstrain at transverse steel gage, location S1A1B
1	-4.14	7.94	8.23	3.52	3.25	-4.14	-4.14	-4.14	-4.14	-4.14	-4.14	microstrain at transverse steel gage, location S1A1T
2	7.83	2.37	3.48	5.44	5.25	7.83	7.83	7.83	7.83	7.83	7.83	microstrain at transverse steel gage, location S1A2B
3	-14.83	-6.22	-6.23	-6.51	-6.73	-14.83	-14.83	-14.83	-14.83	-14.83	-14.83	microstrain at transverse steel gage, location S1A2T
4	-7.60	9.33	26.85	59.61	55.47	-7.60	-7.60	-7.60	-7.60	-7.60	-7.60	microstrain at transverse steel gage, location S1A3B
5	-9994.19	-4996.63	-4996.63	-4996.63	-4996.63	-9994.19	-9994.19	-9994.19	-9994.19	-9994.19	-9994.19	microstrain at transverse steel gage, location S1A3T
6	-1.84	-7.19	-6.01	-5.40	-6.83	-1.84	-1.84	-1.84	-1.84	-1.84	-1.84	microstrain at transverse steel gage, location S1A4B
7	12.40	8.46	9.01	13.58	11.63	8.72	8.11	11.61	11.43	12.12	12.39	microstrain at transverse steel gage, location S1B1B
8	23.30	6.16	10.78	22.34	24.86	22.25	22.50	24.74	19.06	19.37	17.04	microstrain at transverse steel gage, location S1B3B
9	69.77	42.12	44.05	50.09	31.80	45.01	50.07	57.39	59.94	59.57	63.13	microstrain at transverse steel gage, location S1B3T
10	-2.28	12.93	13.22	14.59	13.57	-2.28	-2.28	-2.28	-2.28	-2.28	-2.28	microstrain at transverse steel gage, location S1B4B
11	-0.88	18.34	10.98	25.86	25.52	-0.88	-0.88	-0.88	-0.88	-0.88	-0.88	microstrain at transverse steel gage, location S1B5B
12	0.50	12.62	13.48	13.14	12.73	0.50	0.50	0.50	0.50	0.50	0.50	microstrain at transverse steel gage, location S1C1B
13	-7.72	20.96	21.05	23.88	24.75	-7.72	-7.72	-7.72	-7.72	-7.72	-7.72	microstrain at transverse steel gage, location S1C1T
14	-5.51	15.87	17.06	19.21	18.30	-5.51	-5.51	-5.51	-5.51	-5.51	-5.51	microstrain at transverse steel gage, location S1C2B
15	1000.00	500.00	500.00	500.00	500.00	1000.00	1000.00	1000.00	1000.00	1000.00	1000.00	microstrain at transverse steel gage, location S1C2T
17	-2.58	-2.76	-2.70	-2.75	-2.78	-2.58	-2.58	-2.58	-2.58	-2.58	-2.58	microstrain on diaphragm face, location S6D2D3
18	-2.24	-3.34	-3.44	-3.68	-3.78	-2.24	-2.24	-2.24	-2.24	-2.24	-2.24	microstrain on diaphragm face, location S6D2A1
21	-2.77	-3.47	-3.48	-3.87	-2.93	-2.77	-2.77	-2.77	-2.77	-2.77	-2.77	microstrain on diaphragm face, location S6D1E3
22	-1.72	-3.15	-3.21	-3.59	-3.20	-1.72	-1.72	-1.72	-1.72	-1.72	-1.72	microstrain on diaphragm face, location S6D1C1
23	6.57	-14.14	-14.49	-15.31	-15.69	6.57	6.57	6.57	6.57	6.57	6.57	microstrain on diaphragm face, location S6D1B1
27	-4.04	-1.92	-1.71	-1.42	-2.37	-4.04	-4.04	-4.04	-4.04	-4.04	-4.04	microstrain on diaphragm face, location S6D2E3
28	-0.52	-1.84	-1.75	-1.78	-1.66	-0.52	-0.52	-0.52	-0.52	-0.52	-0.52	microstrain on diaphragm face, location S6D2B1
32	-15.37	-3.15	-2.77	-2.22	-1.30	-15.37	-15.37	-15.37	-15.37	-15.37	-15.37	microstrain at transverse steel gage, location S1B2B
33	-5.68	-0.29	0.86	2.91	1.51	-5.68	-5.68	-5.68	-5.68	-5.68	-5.68	microstrain at transverse steel gage, location S1B2T
40	-45.64	1.81	2.18	6.05	6.78	-45.64	-45.64	-45.64	-45.64	-45.64	-45.64	microstrain at transverse steel gage, location S1C3B
41	0.26	1.24	1.97	6.04	6.23	0.26	0.26	0.26	0.26	0.26	0.26	microstrain at transverse steel gage, location S1C3T
48	-3.51	-0.66	-0.88	-0.97	-1.14	-3.51	-3.51	-3.51	-3.51	-3.51	-3.51	microstrain on diaphragm face, location S6D1A1
49	-3.86	-2.61	-2.67	-2.93	-1.59	1.73	1.23	-1.03	-2.44	-3.58	-3.81	microstrain on diaphragm face, location S6D1D3
57	-3.23	-2.17	-2.09	-2.02	-2.37	-3.23	-3.23	-3.23	-3.23	-3.23	-3.23	microstrain on diaphragm face, location S6D2C1

Southbound Bridge

Setup No. 3 - Bumper to Bumper Trucks in Lane 2

ch no.	sta 2	sta 3	sta 4	sta 5	sta 6	sta 7	sta 8	sta 9	sta 10	sta 11	sta 12	description
0	46.14	-22.70	-11.38	-40.00	-37.29	11.27	-21.93	-16.13	23.26	69.18	56.02	microstrain at transverse steel gage, location S1A1B
1	-11.13	-2.65	-2.65	-2.44	-2.45	-3.26	-7.05	-6.01	-11.13	-11.13	-11.13	microstrain at transverse steel gage, location S1A1T
2	-2.12	2.86	3.10	4.16	2.65	1.47	-2.56	-1.92	-2.12	-2.12	-2.12	microstrain at transverse steel gage, location S1A2B
3	-7.50	-2.52	-2.80	-2.59	-2.62	-3.01	-3.39	-3.18	-7.50	-7.50	-7.50	microstrain at transverse steel gage, location S1A2T
4	-110.77	67.79	62.87	64.32	87.11	77.49	86.96	97.79	-110.77	-110.77	-110.77	microstrain at transverse steel gage, location S1A3B
5	-4997.56	-2498.78	-2498.78	-2498.78	-2498.78	-2498.78	-2498.78	-2498.78	-4997.56	-4997.56	-4997.56	microstrain at transverse steel gage, location S1A3T
6	4.71	0.77	1.62	1.69	1.76	0.12	-4.24	-4.21	4.71	4.71	4.71	microstrain at transverse steel gage, location S1A4B
7	-0.22	-0.56	0.27	0.19	0.22	-1.94	-5.26	-3.42	0.22	0.63	0.89	microstrain at transverse steel gage, location S1B1B
8	9.51	6.06	0.84	3.39	5.43	12.46	22.53	22.76	11.78	10.37	10.05	microstrain at transverse steel gage, location S1B3B
9	40.89	33.32	33.99	35.25	34.21	36.16	32.98	34.84	39.00	37.52	39.78	microstrain at transverse steel gage, location S1B3T
10	-18.46	-0.88	-0.89	-1.24	-0.07	1.70	0.88	-0.22	-18.46	-18.46	-18.46	microstrain at transverse steel gage, location S1B4B
11	-36.78	5.53	6.96	8.28	10.07	3.28	1.44	6.53	-36.78	-36.78	-36.78	microstrain at transverse steel gage, location S1B5B
12	-15.39	-0.20	0.23	0.46	0.69	-1.68	-3.26	-2.43	-15.39	-15.39	-15.39	microstrain at transverse steel gage, location S1C1B
13	-38.81	1.28	3.26	3.63	3.19	-0.85	-1.04	2.29	-38.81	-38.81	-38.81	microstrain at transverse steel gage, location S1C1T
14	-29.02	0.68	1.33	1.25	3.58	4.51	6.39	7.51	-29.02	-29.02	-29.02	microstrain at transverse steel gage, location S1C2B
15	500.00	250.00	250.00	250.00	250.00	250.00	250.00	250.00	500.00	500.00	500.00	microstrain at transverse steel gage, location S1C2T
17	1.84	3.68	4.24	4.42	2.46	-1.40	-9.50	-7.96	1.84	1.84	1.84	microstrain on diaphragm face, location S6D2D3
18	3.46	0.90	0.99	1.00	1.12	0.73	1.31	1.21	3.46	3.46	3.46	microstrain on diaphragm face, location S6D2A1
21	1.40	1.22	1.55	1.51	-0.97	-4.98	-7.86	-5.08	1.40	1.40	1.40	microstrain on diaphragm face, location S6D1E3
22	2.02	0.70	0.74	0.70	0.37	0.18	1.09	1.35	2.02	2.02	2.02	microstrain on diaphragm face, location S6D1C1
23	24.86	-3.19	-3.43	-3.58	-3.21	-1.54	4.17	1.21	24.86	24.86	24.86	microstrain on diaphragm face, location S6D1B1
27	-1.23	1.49	2.00	2.19	0.56	-2.58	-8.27	-7.58	-1.23	-1.23	-1.23	microstrain on diaphragm face, location S6D2E3
28	1.71	-0.38	-0.21	-0.17	-0.54	-0.33	0.30	0.24	1.71	1.71	1.71	microstrain on diaphragm face, location S6D2B1
32	-13.04	-4.21	-4.07	-4.22	-4.46	-6.02	-11.55	-10.10	-13.04	-13.04	-13.04	microstrain at transverse steel gage, location S1B2B
33	-9.35	0.11	1.15	1.35	-1.35	-16.87	-41.62	-36.16	-9.35	-9.35	-9.35	microstrain at transverse steel gage, location S1B2T
40	-52.44	-1.60	-0.69	-0.96	-4.20	-12.32	-17.11	-12.77	-52.44	-52.44	-52.44	microstrain at transverse steel gage, location S1C3B
41	-11.26	2.53	1.30	0.40	2.03	-0.81	-2.51	0.56	-11.26	-11.26	-11.26	microstrain at transverse steel gage, location S1C3T
48	-2.17	1.70	1.32	1.46	2.24	3.75	5.36	5.08	-2.17	-2.17	-2.17	microstrain on diaphragm face, location S6D1A1
49	5.19	3.85	4.07	4.19	1.68	-2.21	-5.21	-3.20	1.35	5.06	6.18	microstrain on diaphragm face, location S6D1D3
57	0.10	1.06	1.41	1.51	0.56	-2.59	-9.72	-6.79	0.10	0.10	0.10	microstrain on diaphragm face, location S6D2C1

Southbound Bridge

Setup No. 3 - Side by Side Trucks in Lanes 1 and 2

ch no.	sta 1	sta 2	sta 3	sta 4	sta 5	sta 6	sta 7	sta 8	sta 9	sta 10	sta 11	sta 12	description
0	-22.95	-52.02	-50.54	-45.77	-61.63	-51.67	-46.13	-2.22	26.77	38.93	51.45	8.28	microstrain at transverse steel gage, location S1A1B
1	3.74	3.95	4.56	5.31	4.17	4.51	-7.41	-7.41	-7.41	-7.41	-7.41	-7.41	microstrain at transverse steel gage, location S1A1T
2	0.47	0.34	0.77	1.68	1.51	1.35	-7.16	-7.16	-7.16	-7.16	-7.16	-7.16	microstrain at transverse steel gage, location S1A2B
3	-0.06	0.01	-0.01	-0.00	-0.17	0.05	-4.35	-4.35	-4.35	-4.35	-4.35	-4.35	microstrain at transverse steel gage, location S1A2T
4	101.91	110.67	107.79	108.46	110.52	116.87	-137.61	-137.61	-137.61	-137.61	-137.61	-137.61	microstrain at transverse steel gage, location S1A3B
5	0.00	0.00	0.00	0.00	0.00	0.00	-2498.78	-2498.78	-2498.78	-2498.78	-2498.78	-2498.78	microstrain at transverse steel gage, location S1A3T
6	0.27	0.08	1.01	1.57	1.28	0.12	0.84	0.84	0.84	0.84	0.84	0.84	microstrain at transverse steel gage, location S1A4B
7	-0.30	-0.56	-0.08	0.73	0.82	-0.10	-3.21	-2.56	0.62	1.36	1.53	2.10	microstrain at transverse steel gage, location S1B1B
8	-10.98	-15.75	-7.92	-3.22	192.16	192.16	192.16	192.16	192.16	192.16	192.16	192.16	microstrain at transverse steel gage, location S1B3B
9	0.41	-0.33	1.22	1.40	1.94	4.37	3.36	3.32	7.97	7.42	11.40	-2.74	microstrain at transverse steel gage, location S1B3T
10	4.06	4.05	4.22	4.66	5.01	4.93	-16.27	-16.27	-16.27	-16.27	-16.27	-16.27	microstrain at transverse steel gage, location S1B4B
11	25.34	27.27	30.82	32.42	32.04	29.87	-38.32	-38.32	-38.32	-38.32	-38.32	-38.32	microstrain at transverse steel gage, location S1B5B
12	0.37	0.12	0.53	1.17	1.39	0.81	-16.04	-16.04	-16.04	-16.04	-16.04	-16.04	microstrain at transverse steel gage, location S1C1B
13	6.62	8.21	-32.02	2.01	5.24	4.21	-47.43	-47.43	-47.43	-47.43	-47.43	-47.43	microstrain at transverse steel gage, location S1C1T
14	4.72	3.96	5.39	6.76	9.11	11.14	-33.39	-33.39	-33.39	-33.39	-33.39	-33.39	microstrain at transverse steel gage, location S1C2B
15	0.00	0.00	0.00	0.00	0.00	0.00	250.00	250.00	250.00	250.00	250.00	250.00	microstrain at transverse steel gage, location S1C2T
17	-2.39	-2.69	-2.14	-2.32	-2.85	-4.36	-4.21	-4.21	-4.21	-4.21	-4.21	-4.21	microstrain on diaphragm face, location S6D2D3
18	-1.09	-1.37	-1.62	-1.77	-2.01	-2.59	0.85	0.85	0.85	0.85	0.85	0.85	microstrain on diaphragm face, location S6D2A1
21	-1.85	-1.99	-1.93	-1.85	-2.33	-2.38	-1.02	-1.02	-1.02	-1.02	-1.02	-1.02	microstrain on diaphragm face, location S6D1E3
22	-1.76	-1.87	-1.92	-1.97	-2.15	-1.74	0.68	0.68	0.68	0.68	0.68	0.68	microstrain on diaphragm face, location S6D1C1
23	-1.71	-1.81	-2.01	-2.11	-2.20	-1.93	30.03	30.03	30.03	30.03	30.03	30.03	microstrain on diaphragm face, location S6D1B1
27	-1.68	-1.84	-1.64	-1.27	-1.73	-3.88	-4.25	-4.25	-4.25	-4.25	-4.25	-4.25	microstrain on diaphragm face, location S6D2E3
28	-0.04	0.10	0.29	0.33	0.10	-0.12	1.98	1.98	1.98	1.98	1.98	1.98	microstrain on diaphragm face, location S6D2B1
32	3.08	3.05	3.08	3.57	3.94	4.48	-8.06	-8.06	-8.06	-8.06	-8.06	-8.06	microstrain at transverse steel gage, location S1B2B
33	1.27	1.20	1.81	3.24	3.12	-1.89	-9.67	-9.67	-9.67	-9.67	-9.67	-9.67	microstrain at transverse steel gage, location S1B2T
40	0.05	-0.04	0.02	0.88	0.38	-1.88	-46.87	-46.87	-46.87	-46.87	-46.87	-46.87	microstrain at transverse steel gage, location S1C3B
41	-0.58	-1.32	1.36	0.45	3.42	3.42	-8.82	-8.82	-8.82	-8.82	-8.82	-8.82	microstrain at transverse steel gage, location S1C3T
48	-0.06	-0.42	-0.71	-0.66	-0.68	-0.63	-5.88	-5.88	-5.88	-5.88	-5.88	-5.88	microstrain on diaphragm face, location S6D1A1
49	-1.95	-2.47	-2.46	-2.06	-2.59	-2.82	-2.45	-3.79	-4.93	-3.53	-2.80	-3.79	microstrain on diaphragm face, location S6D1D3
57	-1.33	-1.45	-1.35	-1.19	-1.71	-3.17	-2.48	-2.48	-2.48	-2.48	-2.48	-2.48	microstrain on diaphragm face, location S6D2C1

Southbound Bridge

Setup No. 4 - Diaphragm Test (D1 is CUT-LOW) With trucks Straddling Respective Diaphragm

ch. no.	D1	D2	description
0 -8.82	1.33		microstrain on diaphragm face, location S6E3
1 -3.26	0.00		microstrain on diaphragm face, location S6E2
2 -9.09	-0.87		microstrain on diaphragm face, location S6D3
3 -5.89	-0.68		microstrain on diaphragm face, location S6D2
4 -1.15	0.18		microstrain on diaphragm face, location S6D1
7 1.92	-0.29		microstrain on diaphragm face, location S6A1
8 -0.05	-0.11		microstrain on diaphragm face, location S6B2
9 0.17	-0.23		microstrain on diaphragm face, location S6B1
10	0.10	-0.17	microstrain on diaphragm face, location S6C3
11	-0.18	-0.02	microstrain on diaphragm face, location S6C2
12	-0.32	-0.06	microstrain on diaphragm face, location S6C1
13	-0.02	-0.06	microstrain on diaphragm face, location S6A2
20	-0.01	0.00	displacement between girders at base of diaphragm
32	0.00	0.00	microstrain on diaphragm face, location S6E1
33	-0.78	2.11	microstrain on diaphragm face, location S6B3